State-Specific Density Functional Theory for Computational Screening of Organic Optoelectronic Materials

Dissertation
zur
Erlangung des Doktorgrades (Dr. rer. nat.)
der
Mathematisch-Naturwissenschaftlichen Fakultät
der
Rheinischen Friedrich-Wilhelms-Universität Bonn

vorgelegt von
Lukas Kunze
aus
Langenfeld (Rhld.)

Bonn 2025

Angefertigt mit Genehmigung der Mathematisch-Naturwissenschaftlichen Fakultät der Rheinischen Friedrich-Wilhelms-Universität Bonn

Gutachter/Betreuer:	Prof. Dr. Stefan Grimme
Gutachter:	Prof. Dr. Thomas Bredow
Tag der Promotion:	04.12.2025
Erscheinungsjahr:	2025

Affirmation in Lieu of an Oath

I, Lukas Kunze, hereby declare that I am the sole author of this dissertation.

The doctoral thesis I submitted is my own work and was prepared without unauthorized outside assistance. I have not included text passages, graphics or other materials from third parties or my own examination papers without identifying them. Only the sources and resources that I have indicated were used. All verbatim and non-verbatim citations from other works are identified in accordance with the citation rules for academic writing. The thesis that I submitted has not yet been published, or has been published in full or in part other than the locations indicated. The thesis that I submitted has not yet been submitted in any form as part of an examination/qualification course. I prepared the doctoral thesis that I submitted in accordance with the principles of good research practice. I am aware of the significance and criminal consequences of a false affirmation in lieu of an oath.

My statements are true to the best of my knowledge and belief.

Publications

Parts of this thesis have been published in peer-reviewed journals.

1. L. Kunze, A. Hansen, S. Grimme, and J.-M. Mewes, *PCM-ROKS for the description of charge-transfer states in solution: Singlet-triplet gaps with chemical accuracy from open-shell Kohn-Sham reaction-field calculations*, J. Phys. Chem. Lett. **12** (2021) 8470, DOI: 10.1021/acs.jpclett.1c02299.

2. T. Froitzheim, L. Kunze, S. Grimme, J. M. Herbert, and J.-M. Mewes, *Benchmarking charge-transfer excited states in TADF emitters: ΔDFT outperforms TD-DFT for emission energies*, J. Phys. Chem. A **128** (2024) 6324, DOI: 10.1021/acs.jpca.4c03273.

3. L. Kunze, T. Froitzheim, A. Hansen, S. Grimme, and J.-M. Mewes, *ΔDFT predicts inverted singlet–triplet gaps with chemical accuracy at a fraction of the cost of wave function-based approaches*, J. Phys. Chem. Lett. **15** (2024) 8065, DOI: 10.1021/acs.jpclett.4c01649.

4. L. Kunze, A. Hansen, S. Grimme, and J.-M. Mewes, *The best of both worlds: ΔDFT describes multiresonance TADF emitters with wave-function accuracy at density-functional cost*, J. Phys. Chem. Lett. **16** (2025) 1114, DOI: 10.1021/acs.jpclett.4c03192.

For the following articles significant contributions have been made.

5. T. Jin, L. Kunze, S. Breimaier, M. Bolte, H.-W. Lerner, F. Jäkle, R. F. Winter, M. Braun, J.-M. Mewes, and M. Wagner, *Exploring structure–property relations of B, S-doped polycyclic aromatic hydrocarbons through the trinity of synthesis, spectroscopy, and theory*, J. Am. Chem. Soc. **144** (2022) 13704, DOI: 10.1021/jacs.2c04516.

Abstract

In recent years, organic light-emitting diodes (OLED) have rapidly grown in relevance due to their high color purity, mechanical flexibility, and energy efficiency making them attractive for application in the lighting and display industry, in smartphones, television, monitors, and wearable electronics. Especially the modeling of the electronically excited-state properties of emitters in OLED devices has become an essential part of the research and development pipeline, giving insights into the design, and making screening of next-generation organic optoelectronic materials possible. The accurate and efficient prediction of physical properties of OLED emitters is therefore of great importance for the advancement of OLED technology. This thesis addresses the limitations and challenges associated with emitter modeling via common computational methods, i.e., linear-response time-dependent density functional theory (TD-DFT), by presenting alternative state-specific excited-state ΔSCF approaches within the framework of Kohn-Sham density functional theory (KS-DFT). Specifically, I investigate the spin-unrestricted open-shell and two-determinant spin-restricted open-shell Kohn-Sham methods, herein called ΔUKS and ΔROKS respectively, for their accuracy in calculating singlet-triplet (ST) energy gaps and fluorescence energies in three different classes of emitters, namely donor-acceptor thermally activated delayed fluorescence (DA-TADF), multiresonance TADF (MR-TADF), and inverted singlet-triplet gap (INVEST) systems. Related open questions in the ΔDFT framework such as the state-targeting problem, best initial orbital guess, best density functional, most reliable ΔDFT-method and basis set combinations for the best cost-accuracy-tradeoff are addressed, with the goal to make the application and integration of ΔDFT methods as black-box as possible.

Starting with DA-TADF emitters, I compiled a new and diverse benchmark set of 27 TADF emitters (25 out of 27 are DA-TADF), in which the associated experimental ST gaps are derived in the most reliable and accurate way: from temperature-dependent measurement of the TADF rate or reverse intersystem crossing (rISC) rate. And despite the fact that the charge-transfer (CT) states in DA-TADF emitters are notoriously difficult to model, due to the difficulties of capturing orbital relaxation and solvation effects, both ΔUKS and ΔROKS combined with a simple equilibrium polarizable continuum model (PCM) achieved sub-chemical accuracy (MAD < 0.044 eV / 1 kcal/mol) in the reproduction of experimental adiabatic ST gaps. In comparison, TD-DFT calculations, which use a linear-response PCM solvation treatment, gave substantial errors for the ST gap (mean absolute deviation: 0.2 eV), establishing TD-DFT as unsuitable for modeling DA-TADF molecules.

Due to the exceptional performance of ΔDFT in describing excited-state energy differences (ST gaps), I further investigated the calculation of fluorescence energies of DA-TADF emitters for validating

the accuracy of ΔDFT methods. Therefore, I compiled the STGABS27-EMS benchmark set of fluorescence energies, extracted from experimental spectra, for the original 27 TADF emitters of the STGABS27 benchmark. Furthermore, a perturbative state-specific (ptSS) PCM for ΔDFT methods was developed by a collaborator, since the correct description of the solvent response for fluorescence energies necessitates the use of a nonequilibrium solvation model. Both ΔUKS and ΔROKS give accurate results close to chemical accuracy (MAD[OT-ωB97M-V]: 0.10 eV and 0.13 eV, respectively) for the calculation of fluorescence energies in the STGABS27-EMS benchmark, with little (ΔUKS) to no significant (ΔROKS) dependence on the underlying density functional approximation (DFA). In contrast, TD-DFT exhibits strong functional dependence with MADs ranging from 0.76 eV (worst DFA) to 0.19 eV (best DFA), and is in general less accurate than both ΔDFT approaches.

In both studies on DA-TADF, ΔDFT approaches performed well for electronically challenging systems, i.e., two MR-TADF emitters of the STGABS27 benchmark, encouraging us to examine more challenging cases, especially those where TD-DFT is unsuitable. One such class of compounds are INVEST emitters that feature an inversion of the singlet-triplet energy gap, which is not possible to model with conventional TD-DFT methods. To assess the capabilities of ΔDFT methods, I compiled two partially new benchmark sets: the INVEST15 benchmark, consisting of 14 INVEST plus 1 non-INVEST molecule for which state-of-the-art wavefunction theory reference data is available, and the NAH159 benchmark, consisting of 159 non-alternant hydrocarbons INVEST candidates for which I calculated accurate WFT references. Test calculations on the INVEST15 benchmark established ΔUKS as the superior ΔDFT approach, being able to not only qualitatively but also quantitatively reproduce high-level WFT reference results. In contrast, both TD-DFT and ΔROKS failed to produce inverted singlet-triplet energy gaps.

Finally, I investigate the performance of ΔDFT approaches for ST gaps and fluorescence energies of MR-TADF emitters, for which I observed large differences between ΔUKS and ΔROKS in the STGABS27 benchmark. On a literature benchmark of 35 MR-TADF emitters with experimental references, the accuracy of computed ST gaps was strong in favor of ΔUKS compared to ΔROKS yet again, cementing ΔUKS as the more reliable and robust state-specific excited-state method. ΔUKS-calculated ST gaps reached chemical accuracy against experimental data, whereas ΔROKS failed to accurately reproduce trends in the benchmark set (wrong for very large and very small ST gaps). In the context of fluorescence energies, both ΔUKS and ΔROKS performed well, with a slight edge in accuracy towards ΔUKS. Perhaps most important, I identified a hybrid functional, dubbed FX175-ωPBE, which in combination with ΔUKS displays excellent performance for ST gaps and fluorescence energies, across all previous benchmarks and systems, be it DA-TADF, MR-TADF, or INVEST emitter.

This work establishes ΔDFT methods, foremost ΔUKS, as a valuable computational tool for the calculation and modeling of photophysical properties of optoelectronic OLED materials. ΔUKS is therefore of significant importance for predicting the performance of OLED emitters, and enables efficient and fast screening for the discovery of novel DA-TADF, MR-TADF, and INVEST emitters. Overall, the presented investigations also provide a knowledge basis for further method development in the context of ΔDFT, i.e., the integration with semiempirical quantum mechanics methods and machine-learning-assisted property prediction.

Contents

CHAPTER 1

Introduction

Electronically excited states play a fundamental role in a wide array of phenomena and processes observed in nature. They are essential for understanding key processes in photochemistry[6–9] and photobiology,[10,11] such as ultraviolet radiation damage in DNA[12,13] and photosynthesis,[14,15] but also extend to fields including astrophysics[16,17] and astrochemistry,[18] photocatalysis,[19–22] solar energy conversion[23–25] (e.g. photovoltaics), optoelectronics[26–28] and photonics,[29,30] as well as are integral for medical applications, i.e. photodynamic cancer treatments,[31] medical diagnostics[32,33] and bioimaging.[34–36] Generally, electronically excited states govern all phenomena related to optical absorption and light emission, crucially relevant for spectroscopic analysis of the electronic structure in materials science.[37,38] In recent years, organic electronics have seen a resurgence in research and real-world applications, including advancements in organic field-effect transistors (OFETs),[39–41] organic solar cells (OSCs),[42–44] chemical sensing,[45–47] printed electronics,[48,49] but especially organic light-emitting diodes.[50–52]

Organic light-emitting diode (OLED) devices are designed to emit electromagnetic radiation, typically within the visible to infrared spectrum, via electroluminescence by applying an electric field, and using organic compounds in the emissive layer. The fundamental discoveries[53] for modern OLED technology date back to the early 1960s with the observation of delayed fluorescence in eosin (1961)[54] and two years later with the realization of electroluminescence in anthracene crystals (1963).[55] However, it was not until 25 years later that the first low-voltage OLED device was successfully built at Eastman Kodak.[56] Following this breakthrough, further advancements were made including the fabrication of the first polymer-based OLED (1990),[57] the development of phosphorescent OLEDs (1998),[58] and the introduction of an efficient purely organic emitter for OLED devices (2011).[59] Today, OLED technology has seen adoption across the display industry for televisions, computer monitors, car panels, smartphones,[60] but also for lightweight, thin-panel lighting solutions.[61]

A simplified representation of a conventional OLED device and an abridged mechanism for electroluminescence is presented in Figure 1.1. Positive charges (called holes) and negative charges (called electrons) are injected at the anode and cathode, respectively, and rapidly travel through the electron transport layer (ETL) and hole transport layer (HTL) to the emissive layer, to recombine into

excitons.[62] The HTL and ETL are tuned for efficient charge-transport to ensure that holes and electrons are readily available for the emissive layer.[63,64] The emissive layer often consists of a host-guest matrix with a low concentration (1-5 wt.%) of organic emitter (guest) to avoid concentration-induced quenching of excited states.[65,66] The host material is designed with a sufficiently wide electronic band gap to assure that electrons and holes recombine primarily on the organic emitter in the emissive layer to form an electronically excited state (exciton). Since, the excitons are generated by electrical excitation (charge recombination), excited states form in a ratio of one singlet to three triplet excitons, due to the statistics of the electronic spin states as described by Fermi.[67] Formed excited states quickly relax to the lowest excited state of the same spin multiplicity via internal conversion processes, where singlet excited states can then spontaneously decay to the electronic ground state, emitting a photon (light) in the process. The transition from triplet excited states to the electronic ground state are usually spin-forbidden. Additionally, both singlet and triplet excited states can decay without emitting a photon, i.e. non-radiative decay, where the energy of the singlet/triplet is released thermally in the form of vibrations.

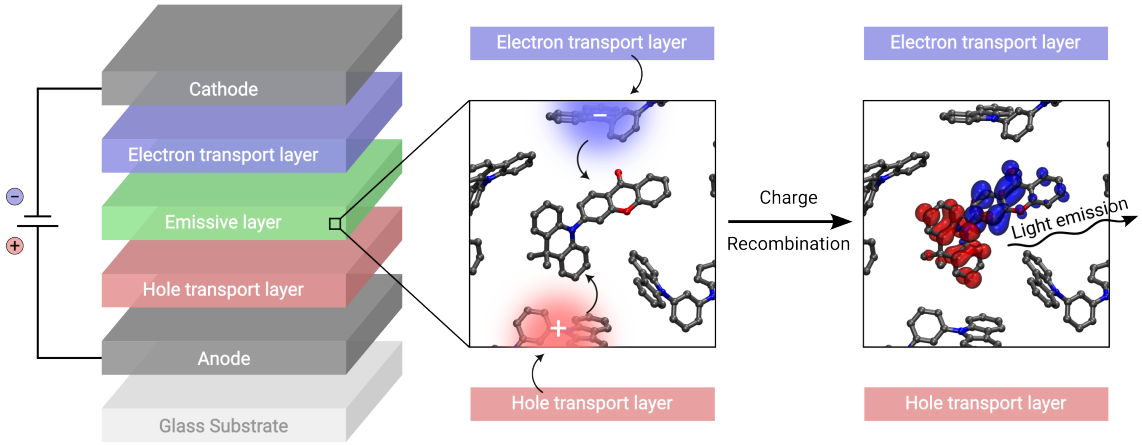

Figure 1.1: Simplified layer structure of an OLED device, schematic process of charge recombination and subsequent spontaneous light emission (electroluminescence).

OLED devices can be categorized by the type of emitter used, either a fluorescent or phosphorescent emitter.[68,69] Fluorescent emitters generate light through the radiative decay of singlet excitons (to the ground state), whereas in phosphorescent emitters light emission originates from triplet excitons (see Figure 1.2). Although emission from triplet excited states is generally spin-forbidden, therefore very slow, it can be accelerated by strong spin-orbit coupling between singlet and triplet excited states, e.g., by introduction of heavy-metal centers in the emitter structure. The internal quantum efficiency (IQE), defined as the ratio of the number of produced photons to the number of injected charges, is inherently limited in fluorescent emitters. Since only singlet excitons can be harvested for fluorescence, the IQE is restricted to a maximum of 25%, which severely harms their performance in OLED applications. In contrast, phosphorescent emitters can achieve up to 100% IQE due to intersystem crossing (ISC) processes, in which singlet excitons are converted into triplet excitons. However, despite their high theoretical efficiency, phosphorescent emitter face two siginificant challenges: Firstly, they are limited in their design to metal-organic molecules, as the heavy atom effect of rare heavy-metal atoms, e.g. Os, Ir, Pt, is necessary to realize strong spin-orbit coupling for efficient radiative relaxation from

the triplet excited state to the ground state. Secondly, it has proven difficult to engineer a long-term stable blue phosphorescent emitter, which hinders its use in display applications due to significantly reduced device lifetimes. Purely organic thermally activated delayed fluorescence (TADF) emitters have emerged as a promising alternative and are the focus of this thesis.

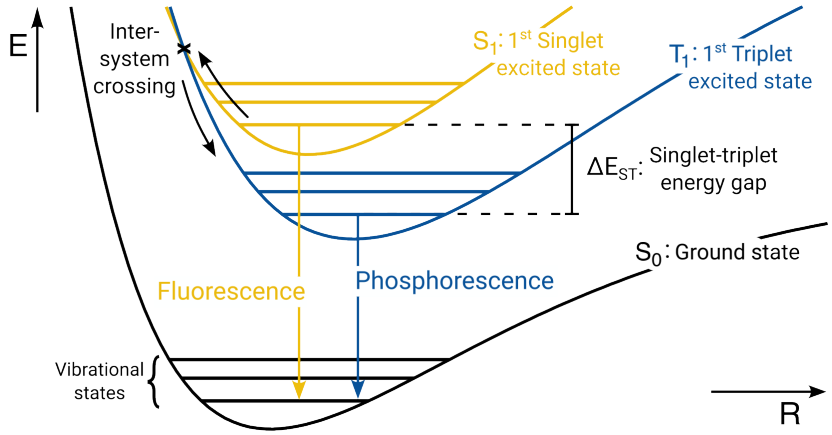

Figure 1.2: Potential energy surface diagram including the ground-state, lowest singlet S_1 and triplet T_1 excited state with the adiabatic singlet-triplet energy gap indicated. Radiative relaxation pathways are shown, i.e. fluorescence and phosphorescence, as well as a singlet to triplet conversion pathway called intersystem crossing.

Similar to phosphorescent emitters, TADF emitters are capable of harvesting up to 100% of generated excitons in an OLED device (see Figure 1.4 for an overview of emitter types). This is possible through a process called reverse intersystem crossing (rISC), that is, the conversion of triplet excitons into singlet excitons. This conversion is enabled by a small energy gap between the lowest singlet and lowest triplet excited state, called the singlet-triplet energy gap (ST gap). The rate of rISC is influenced by two key ingredients, the spin-orbit coupling between singlet and triplet excited state (the larger, the faster the rISC) and the size of the ST gap (the smaller, the faster the rISC). For efficient rISC, the size of the ST gap should be roughly on the order of the thermal energy at room temperature, but TADF emitters with ST gaps of >0.3 eV have been reported.[70] Balancing spin-orbit coupling and the ST gap, which depend oppositely on the overlap of electron and hole, while simultaneously retaining an appreciable oscillator strength is the main challenge of TADF emitter design. A near-vanishing electron-hole overlap is beneficial for achieving a small ST gap but leads to near-zero spin-orbit coupling, and vice versa.

A large majority of TADF emitters synthesized in the last decades fall into one of two categories: donor-acceptor type TADF (DA-TADF) or multiresonance TADF (MR-TADF) emitters (see Figure 1.3). DA-TADF emitters achieve a small ST gap by linking electron-accepting and electron-donating molecular moieties together and by structurally enforcing a dihedral twist between acceptor and donor moieties, spatially separating the highest occupied molecular orbital (HOMO, donor) and lowest unoccupied molecular orbital (LUMO, acceptor).[71] This arrangement of linked donor-acceptor structure leads to low-lying intramolecular charge-transfer (CT) excited states, while the dihedral twist ensures a small electron-hole overlap. CT states with small electron-hole overlap have a small

exchange integral, making the singlet and triplet CT state similar in energy, resulting in a small ST gap. Following a different design principle MR-TADF emitters achieve this by systematically doping aromatic extended π-systems with donor and acceptor atoms, such that HOMO and LUMO are localized on alternating atomic sites.[72] Upon a HOMO-LUMO excitation, charge shifts between alternating atomic sites, giving rise to so-called short-range charge-transfer (SRCT) states.

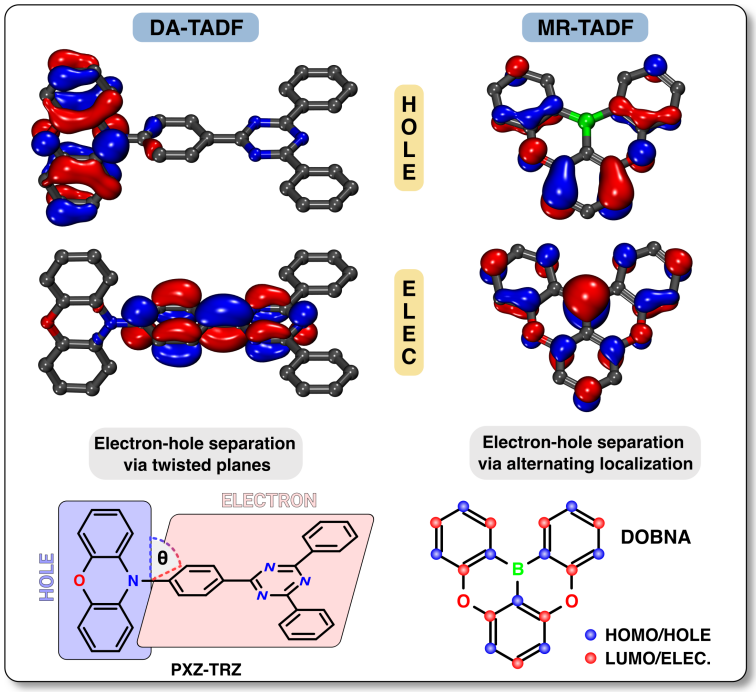

Figure 1.3: Exemplary hole and electron molecular orbitals for DA-TADF type and MR-TADF type emitters, with schematics highlighting both TADF types' key design feature.

A small electron-hole overlap is possible due to the alternating localization of electron and hole, ensuring a small ST gap. DA-TADF and MR-TADF emitters have different advantages and disadvantages: 1) very small ST gaps are more easily realized in DA-TADF emitters compared to MR-TADF emitters, 2) MR-TADF emitters show considerably narrower emission bands (better color purity) compared to DA-TADF emitters, and 3) rISC is often much faster in DA-TADF compared to MR-TADF emitters. Furthermore, recently a new class of TADF emitters were discovered, and are called inverted singlet-triplet energy gap (INVEST) emitters, which feature an inverted ordering of the lowest singlet and triplet excited state (breaking Hund's rule), and therefore a negative ST gap. INVEST emitters are particularly promising as the gap inversion may strongly facilitate rISC for more efficient emitters. However, thus far discovered INVEST emitters exhibit near-zero oscillator strengths (no emission) for the lowest singlet excited state and very low emission energies (in the visible red to near-infrared region). There are various challenges associated with the design of TADF emitters, particularly INVEST emitters, which necessitates the need for models and theories that can adequately describe the electronic structure of these molecules.

In the last decades, computational (quantum) chemistry has become an essential tool for understanding

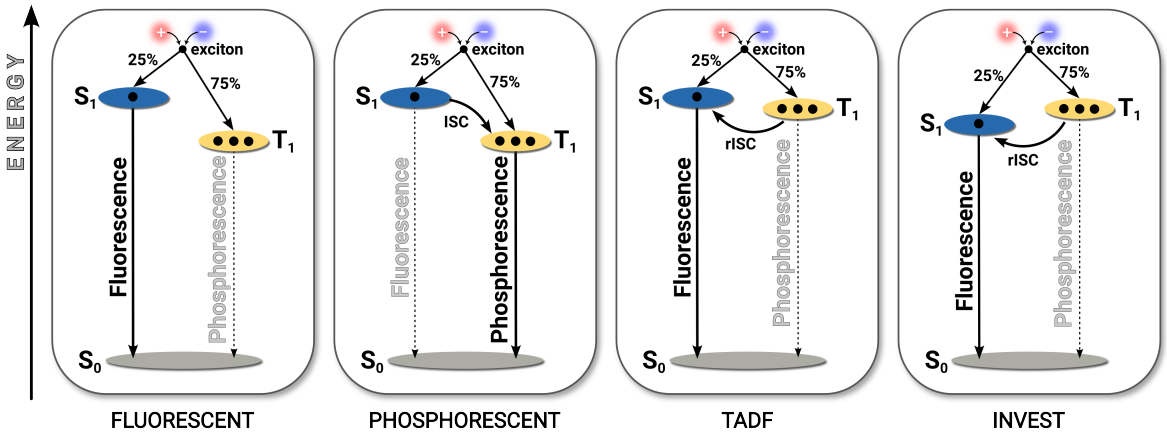

Figure 1.4: Overview of different emitter types: fluorescent, phosporescent, TADF and INVEST for application in OLED devices.

the electronic structure, properties, reaction thermodynamics and kinetics, excited states, and interactions in and inbetween molecules, aiding the design of new molecules and the modification of existing ones. Especially in OLED research, quantum chemistry can facilitate the design of novel and improved emitters, unravel structure-property relationships and elucidate the character and dynamics of excited states. By high-throughput computational screening of large candidate databases, it is possible to some degree predict properties and identify promising molecules without the need to synthesize each individual one. Computational screening can, therefore, greatly expedite the work of synthetic chemists, as well as reduce the amount of chemical waste and cut down on development time. For the research of new TADF emitters, possible properties of interest are the computation of fundamental gaps, HOMO and LUMO energy levels, fluorescence energies, oscillator strengths, as well as rISC-relevant properties such as spin-orbit coupling between singlet and triplet states and the singlet-triplet energy gap. However, modeling the electronic structure of systems, on which grounds such properties can be calculated, can become incredibly costly if very high accuracy is needed and it is the goal of quantum chemistry research to find good approximations to electronic structure methods. For obtaining meaningful results in a reasonable timeframe, it is, therefore, crucial to have efficient computational approximate methods with a favorable ratio of accuracy and robustness to computational cost (computational resources).

The foundation for quantum mechanics and electronic structure theory lies in the Schrödinger equation, which can describe the behavior and properties of the electronic states of physical systems. Solving the electronic Schrödinger equation provides information about the system in the form of the electronic wavefunction that encodes all relevant properties of interest. In principle, the theory for obtaining the exact many-electron wavefunction is known, full configuration interaction (FCI),[73] but is computationally incredibly demanding such that calculations become intractable for systems larger than roughly 16-18 electrons. Therefore, theoretical approximations are necessary for keeping the computational cost at a manageable level, while at the same time due to the approximations, errors are introduced. There are many theories with different associated cost and accuracy, but for the sake of brevity two particularly important ones shall be introduce here, coupled cluster theory (CC)[74] and Kohn-Sham density functional theory (KS-DFT, in following simply called DFT).[75,76] CC has been one of the most effective

theories for the computation of highly accurate results but with a high associated computational cost, while DFT can give decently accurate results in a much shorter timeframe. As a result, DFT established itself as the workhorse for quantum chemistry and the method of choice for computational studies. CC, on the other hand, has become the gold-standard for providing highly accurate reference values for benchmarking, for fitting lower-scaling computational models (i.e., DFT functionals) and anytime a definitive answer is sought, i.e, in cases where the accuracy of DFT results is called into question.

This is the case for the computation of ground-state, as well as excited-state properties, with the latter being the main focus of this thesis. Modeling electronically excited states is challenging, since not only one potential energy surface (PES; as in the ground-state case), but multiple PES's of excited states need to be considered. Additionally, the range of accessible types of electronically excited states is very diverse including valence, Rydberg, core-excited, and charge-transfer excited states, but also doubly excited, which are difficult to treat on an even level of accuracy. Many CC methods for electronically excited state have been developed, but similar to the ground-state case, the majority of excited-state quantum chemistry studies are conducted in the framework of linear-response time-dependent DFT (TD-DFT) due to its decent accuracy and low computational cost. Indeed, the accuracy of the low-cost CC methods, such as linear-response approximate second-order coupled-cluster (LR-CC2)[77] or equation-of-motion coupled cluster with singles and doubles (EOM-CCSD)[78] is often only a moderate improvement, making TD-DFT the natural choice for most practical applications. However, there are instances where TD-DFT has proven to fail dramatically, i.e. for charge-transfer excited states and excited states with double excitation character (also doubly excited states).[79] A general concern in linear-response and excitation-based quantum chemistry methods is also the appropriate inclusion of solvent interactions for the excited state, as the dielectric stabilization for, e.g., highly polar CT states is crucial for correct excitation energies and properties. Moreover, the typical accuracy of TD-DFT for well-behaved systems is around 0.2-0.4 eV, which might not be enough for certain applications. If high accuracy is required, usually only wavefunction theory methods with excitations up to third-order are computationally feasible and accurate enough, but even they are limited to systems with less than 30 non-hydrogen atoms due to computational cost and scaling.

A promising alternative family of excited-state methods are state-specific DFT (ΔDFT) approaches, in which excited states are targeted as higher roots of the self-consistent field (SCF) equations. Since ΔDFT methods shared the same foundational equations as ground-state DFT, the very good cost-to-accuracy ratio of ground-state DFT may also extend to ΔDFT, making it an attractive competitor to TD-DFT. Orbitals in ΔDFT are optimal for each calculated excited-state, whereas in TD-DFT ground-state orbital energies are used and excited-state specific orbital relaxation is only accessible via the single excitation (and deexcitations, relative to the ground state) approximation. This might manifest in an advantage for the accuracy of ΔDFT compared to TD-DFT for difficult excited states, such as doubly excited states (or states with double excitation character). Another factor in favor of ΔDFT is the relative ease by which equilibrium and nonequilibrium continuum solvation models can be adopted for state-specific excited-state SCF solutions.

ΔDFT methods used in this thesis, come in two flavors, unrestricted (ΔUKS) and restricted open-shell (ΔROKS) KS-DFT. Topic of this thesis is the assessment of both of these ΔDFT approaches and development of suitable workflows for the modeling of the excited states of DA-TADF, MR-TADF and INVEST emitters. In Chapter 3, both ΔUKS and ΔROKS are examined for the calculation of ST

gaps of a small benchmark set, STGABS27, of 27 (mostly) DA-TADF emitters in condensed matter, i.e. solution and thin-films. Chapter 4 tests ΔUKS and ΔROKS for the calculation of fluorescence energies of the STGABS27 DA-TADF emitters with focus on different density functionals and polarizable continuum solvation models. In Chapter 5 ΔUKS and ΔROKS approaches are applied in the modeling the ST gap inversion of INVEST emitters, and developments for black-box protocols for high-throughput screening via ΔDFT methods. In Chapter 6 ΔUKS and ΔROKS are tested for the calculation of ST gaps and fluorescence energies of MR-TADF emitters, with the focus on appropriate density functional approximations, solvation models and computation protocols. Finally, summary, concluding remarks and an outlook on ΔDFT approaches for modeling excited states are given in Chapter 7.

CHAPTER 2

Theoretical Background

In this chapter an overview of quantum chemical methods relevant for this thesis is given. The basics of electronic structure theory, Hartree-Fock, configuration interaction, coupled cluster and Møller-Plesset perturbation theory are based largely on refs. [80–82]. Density functional theory and time-dependent density functional theory essentials are based on refs. [79, 83, 84]. State-specific density functional theory via the maximum overlap method and via on a two-determinant restricted open-shell approach are based on refs. [85, 86] and [87, 88], respectively. Polarizable continuum models for solvation described herein, are based on ref. [89].

2.1 Electronic Structure Theory

2.1.1 The Molecular Hamiltonian

This introductory overview on the theoretical background of quantum chemistry is by no means exhaustive and is solely meant to explain key features of the models and methods used throughout this work. In-depth descriptions of the mathematical backgrounds can be found in the references (vide supra), while derivations of the foundational equations are available in the original works. For the following, all equations are given in atomic units, unless stated otherwise. The foundation for a majority of electronic structure theory methods is solving the nonrelativistic time-independent Schrödinger equation,

$$\hat{H}\Psi = E\Psi \tag{2.1}$$

which is a differential eigenvalue problem, where E, denotes the total energy, Ψ the wavefunction of a particular state and $\hat{H}$ the Hamiltonian operator. The Hamiltonian operator can be separated into components,

$$\hat{H} = \hat{T}_N + \hat{T}_e + \hat{V}_{NN} + \hat{V}_{eN} + \hat{V}_{ee} \tag{2.2}$$

the kinetic energy operator of the nuclei $\hat{T}_N$, the kinetic energy operator of the electrons $\hat{T}_e$, the nuclear-nuclear Coulomb potential operator $\hat{V}_{NN}$, the electron-nuclear Coulomb potential operator $\hat{V}_{eN}$ and the electron-electron Coulomb potential operator $\hat{V}_{ee}$. To reduce the complexity of the problem, the Born-Oppenheimer approximation is applied, treating the nuclei as fixed classical point charges and considering only the electrons as quantum-mechanical objects. This is a reasonable approximation since the nuclei, due to their much higher mass, move much slower than electrons. As a consequence, the nuclear kinetic energy term $\hat{T}_N$ can be neglected ($\hat{T}_N = 0$) and the nuclear-nuclear Coulomb potential $\hat{V}_{NN}$ becomes a constant (V_{NN}), leading to the Hamiltonian operator in the Born-Oppenheimer approximation.

$$\hat{H}^{BO} = \hat{T}_e + \hat{V}_{eN} + \hat{V}_{ee} + V_{\mathrm{NN}}(\mathrm{const.}) \tag{2.3}$$

A system of K nuclei and N electrons can be described by their coordinate vectors $\mathbf{r}_i$ and $\mathbf{R}_A$ (where i, j are subscripts for electrons and A, B for nuclei) and the corresponding nuclear charges Z_A. The nuclear-nuclear Coulomb potential, is then defined as

$$\hat{V}_{NN} = \sum_{A=1}^{K} \sum_{B>A}^{K} \frac{Z_A Z_B}{|\mathbf{R}_A - \mathbf{R}_B|} \Rightarrow V_{\mathrm{NN}}(\mathrm{const.}) \tag{2.4}$$

and becomes a constant in the Born-Oppenheimer Hamilton operator. The electronic kinetic energy operator $\hat{T}_e$ is defined by

$$\hat{T}_e = -\sum_{i=1}^{N} \frac{1}{2} \nabla_i^2 \tag{2.5}$$

with the Laplace operator ∇_i^2 acting on electron i. The electronic Coulomb potential operators $\hat{V}_{ee}$ and $\hat{V}_{eN}$ are defined as

$$\hat{V}_{ee} = \sum_{i=1}^{N} \sum_{j>i}^{N} \frac{1}{|\mathbf{r}_i - \mathbf{r}_j|} \tag{2.6}$$

$$\hat{V}_{eN} = -\sum_{i=1}^{N} \sum_{A=1}^{K} \frac{Z_A}{|\mathbf{r}_i - \mathbf{R}_A|} \tag{2.7}$$

It can be of use to rewrite the Hamiltonian operator in terms of one-electron $\hat{h}_i$ and two-electron operators $\hat{g}_{ij}$

$$\hat{h}_i = -\frac{1}{2} \nabla_i^2 - \sum_{A=1}^{K} \frac{Z_A}{|\mathbf{r}_i - \mathbf{R}_A|} \tag{2.8}$$

$$\hat{g}_{ij} = \frac{1}{|\mathbf{r}_i - \mathbf{r}_j|} \tag{2.9}$$

and as the nuclear-nuclear potential $V_{\mathrm{NN}}(\mathrm{const.})$ is completely decoupled from the electronic problem, one can define an electronic Hamiltonian $\hat{H}^{BO}_{elec}$ with $\hat{h}_i$ and $\hat{g}_{ij}$, such that

$$\hat{H}^{BO} = \sum_{i=1}^{N} \hat{h}_i + \sum_{i=1}^{N} \sum_{j>i}^{N} \hat{g}_{ij} \tag{2.10}$$

2.1.2 Hartree-Fock Theory

The molecular Hamiltonian as setup in eq. 2.10 is analytically solvable only for hydrogen-like atoms, i.e., systems with exactly one electron, without any electron-electron interactions. However, most real systems of interest are many-electron problems, where the electron-electron repulsion is not analytically solvable, therefore approximations for $\hat{V}_{ee}$ have to be made. One approximation, which to this day serves as the basis for many WFT methods, is the Hartree-Fock (HF) approximation. In HF theory, the many-electron potential ($\hat{g}_{ij}$) is replaced by an effective one-electron potential, the Hartree-Fock potential $\hat{v}_i^{HF}$, in which the ith electron experiences electron repulsion only from the average field that arises due to the presence of all other electrons. We define the Fock operator $\hat{f}$ as

$$\hat{f}_i = \hat{h}_i + \hat{v}_i^{HF}. \tag{2.11}$$

Before we explore the specifics of the Hartree-Fock potential, it is necessary to first define the wavefunction. In HF, the many-electron wavefunction is approximated by a single properly normalized Slater determinant (Φ) of orthonormal one-electron wavefunctions (ϕ_i)

$$\Psi \approx \Phi(1, 2, \ldots, N) = \frac{1}{\sqrt{(N!)}} \begin{vmatrix} \phi_1(1) & \phi_2(1) & \ldots & \phi_N(1) \\ \phi_1(2) & \phi_2(2) & \ldots & \phi_N(2) \\ \vdots & \vdots & \ddots & \vdots \\ \phi_1(N) & \phi_2(N) & \ldots & \phi_N(N) \end{vmatrix}. \tag{2.12}$$

The one-electron wavefunctions ($\phi_i(k)$) are called spin orbitals and consist of a spatial orbital part $\psi_i(k)$ and a spin function σ_i (designating spin up or spin down for the ith electron), which form a spin orbital according to $\phi_i(k) = \sigma_i \psi_i(k)$. In early works, Hartree set up many-electron wavefunctions as a product of spin orbitals, called Hartree product, where the symmetry of the wavefunction could only be handled by group-theoretical methods.[90,91] Later, Slater realized that the product wavefunction by Hartree is disadvantageous for describing the symmetry behavior of electrons and that instead one should use an antisymmetrized linear combination of Hartree products which properly reflects the anti-symmetric properties of the many-electron wavefunction.[92] The determinantal form of the wavefunction first proposed by Heisenberg[93] and Dirac,[94] today called Slater determinant, fulfils

this condition and displays the correct anti-symmetric behavior, therefore obeying Pauli's exclusion principle.

As such, for an interchange of spin and spatial coordinates of any two electrons in an electronic wavefunction, it must change its sign (behave antisymmetric), i.e., $\Psi(1,\ldots,i,j,\ldots,N) = -\Psi(1,\ldots,j,i,\ldots,N)$.

Now, we define the Hartree-Fock potential as

$$\hat{v}_i^{HF} = \sum_j^N (\hat{J}_j - \hat{K}_j) \tag{2.13}$$

and the Fock operator as

$$\hat{f}_i = \hat{h}_i + \sum_j^N (\hat{J}_j - \hat{K}_j) \tag{2.14}$$

with the Coulomb operator $\hat{J}_j$ and the exchange operator $\hat{K}_j$ defined by its effect on spin orbital $\phi_i(1)$

$$\hat{J}_j|\phi_i(1)\rangle = \langle\phi_j(2)|\hat{g}_{12}|\phi_j(2)\rangle|\phi_i(1)\rangle \tag{2.15}$$

and

$$\hat{K}_j|\phi_i(1)\rangle = \langle\phi_j(2)|\hat{g}_{12}|\phi_i(2)\rangle|\phi_j(1)\rangle. \tag{2.16}$$

In the effective one-electron Fock operator $\hat{F}_i$, $\hat{h}_i$ describes the kinetic energy of the electrons and the attraction of the electrons from the nuclei, while the electron-electron repulsion is described by $\hat{J}_j - \hat{K}_j$. The Coulomb operator $\hat{J}_j$ acting on $|\phi_i(1)\rangle$ can be interpreted as the classical Coulomb interaction of electron 1 with the charge distribution arising from an occupied spin orbital (electron 2). The exchange interaction represented by the exchange operator $\hat{K}_j$ acting on $|\phi_i(1)\rangle$ arises due to the antisymmetric nature of the determinantal wavefunction and is a purely quantum-mechanical effect. The exchange interaction primarily eliminates the self-interaction error (SIE), which arises from the Coulomb repulsion term due to the interaction of orbitals with themselves. For one-electron systems, the SIE is the Coulomb energy and cancels with the exchange interaction, although SIE is important for many-electron systems as well. Since Hartree-Fock includes exchange interaction, it is SIE-free. The working equation of Hartree-Fock is given by the eigenvalue problem

$$\hat{f}_i|\phi_i\rangle = \varepsilon_i|\phi_i\rangle \tag{2.17}$$

where ϕ_i denote the canonical molecular orbitals (MOs) and ε_i the corresponding MO eigenvalues. Summing over all $\hat{f}_i$ gives the zeroth-order Hamiltonian $\hat{H}_0$ as

$$\hat{H}_0 = \sum_i^N \hat{f}_i \tag{2.18}$$

and with the corresponding zeroth-order energy E_0 as

$$E_0 = \sum_i^N \varepsilon_i. \tag{2.19}$$

E_0 is, however, not the Hartree-Fock energy as it double counts the electron-electron repulsion terms and does not include the nuclear-nuclear repulsion energy V_{NN}. Correcting for the double counting and the inclusion of V_{NN}, gives the Hartree-Fock energy E_{HF} as

$$E_{\mathrm{HF}} = \sum_i^N \varepsilon_i - \frac{1}{2}\sum_i^N \sum_j^N (J_{ij} - K_{ij}) + V_{\mathrm{NN}} \tag{2.20}$$

with the Coulomb integrals J_{ij} and exchange integrals K_{ij}, according to

$$\begin{aligned} J_{ij} &= \langle \phi_j | \hat{J}_i | \phi_j \rangle \\ &= \int \frac{\phi_i^*(1)\phi_i(1)\phi_j^*(2)\phi_j(2)}{|\mathbf{r}_1 - \mathbf{r}_2|}\, d\mathbf{r}_1 d\mathbf{r}_2 \end{aligned} \tag{2.21}$$

and

$$\begin{aligned} K_{ij} &= \langle \phi_j | \hat{K}_i | \phi_j \rangle \\ &= \int \frac{\phi_i^*(1)\phi_j(1)\phi_j^*(2)\phi_i(2)}{|\mathbf{r}_1 - \mathbf{r}_2|}\, d\mathbf{r}_1 d\mathbf{r}_2. \end{aligned} \tag{2.22}$$

Solving the Hartree-Fock equations has to be done iteratively, until a stationary solution is found. This procedure is called the self-consistent field, requiring the final charge distribution and thus the generated field to be "self-consistent" with the assumed initial field/charge distribution. The self-consistent field equations for Hartree-Fock were obtained by applying the Rayleigh-Ritz energy variational principle to the determinantal electronic wavefunction.[95] Using a trial wavefunction the energy can be minimized by variation of the variables, since any trial wavefunction gives an upper-bound expectation value of the energy relative to the true ground-state energy. Making the energy stationary with respect to variations in the orbitals, therefore gives the best approximation to the true ground-state energy.

The self-consistent field Hartree-Fock equations are solved in practice by introducing a set of known basis functions (χ, see eq. 2.24) and conversion of the differential equations into a set of algebraic

matrix equations, called the Roothaan equations.[96]

$$FC = SC\varepsilon \tag{2.23}$$

By defining the Fock matrix F with elements $F_{ij} = \langle \chi_i(1)|\hat{f}(1)|\chi_j(1)\rangle$, the expansion coefficient matrix C (of the basis set expansion, see eq. 2.24, the overlap matrix S with elements $S_{ij} = \langle \chi_i|\chi_j\rangle$ and the matrix ε, which if diagonal, contains the energies of the molecular orbitals. The Roothaan equations are solved through repeated iteration of the same procedure:

1. diagonalization of S from which a transformation matrix X for orthogonalization is obtained,
2. obtain guess for the density matrix P,
3. form the Fock matrix F,
4. transform Fock matrix F via X to form F',
5. diagonalize F' to obtain C' and ε,
6. transform C' via X to get C,
7. build new density matrix P from C
8. check for convergence, in energy, density, etc.; if criteria are not met, repeat steps 2-7,
9. if SCF equations are converged, calculate the energy, properties, etc.

Since eq. 2.23 is a nonlinear equation, this simple procedure outlined above is not guaranteed to converge. There are many ways for building the initial guess for P, the simplest being the core-Hamiltonian guess where P is the zero matrix. In general, the initial guess is crucial for convergence of the SCF procedure, as a poor initial guess may cause to oscillatory behavior or even divergence. Today, reasonable initial guesses can be obtained (for the ground-state case) by semiempirical methods or superposition of precomputed atomic densities. Convergence algorithms have been proposed that can reliably converge the SCF equations for a very large majority of cases. The by far most popular convergence algorithm is the direct inversion of the iterative subspace (DIIS)[97] procedure, which significantly cuts down on the number of iterations and simultaneously is much more robust than what is outlined above. However, especially for difficult open-shell spin systems, i.e., transition metal complexes and excited state wavefunctions, converging the SCF is still nontrivial.

2.1.3 Basis Set Approximation

So far, we have only looked at the spin orbitals as general functions without giving them an explicit form. For solving the self-consistent field equations, we need to introduce a set of basis of known basis functions that aims to represent the set of spatial parts of the spin orbitals used in HF calculations. A particular spatial orbital $\phi_i(\mathbf{r})$ can be expanded as a linear combination of basis functions $\chi_u(\mathbf{r})$ with their expansion coefficients $c_{\mu i}$

$$\phi_i(\mathbf{r}) = \sum_{\mu=1}^{K} c_{\mu i}\chi_\mu(\mathbf{r}). \tag{2.24}$$

In theory, only an infinite set of basis function would give the exact spatial orbitals, but for all practical purposes a finite set must suffice. Great effort has been made to design basis sets for the purpose of giving the best (lowest energy for HF) energy with as few basis functions as possible. Today, the majority of molecular calculations use either Slater type functions of the form

$$\chi_{\mu}^{Slater}(\mathbf{r}-\mathbf{R}_A) = e^{-\alpha|\mathbf{r}-\mathbf{R}_A|} \tag{2.25}$$

for an orbital centered around some nucleus A, described by its nuclear coordinate $\mathbf{R}_A$ and with the basis function exponent α. Or Gaussian type basis sets, where usually contracted Gaussian functions (CGFs) are used, in which each basis function is formed from a fixed linear expansion (called contraction) of Gaussian functions (primitives), according to

$$\chi_{\mu}^{CGF}(\mathbf{r}-\mathbf{R}_A) = \sum_{p=1}^{L} d_{p\mu} g_p(\alpha_{p\mu}, \mathbf{r}-\mathbf{R}_A) \tag{2.26}$$

with the number of primitives L, the contraction exponents $\alpha_{p\mu}$ and contraction coefficients $d_{p\mu}$. Primitive Gaussian functions in the CGF have the form

$$g_p(\alpha_{p\mu}, \mathbf{r}-\mathbf{R}_A) = e^{-\alpha_{p\mu}|\mathbf{r}-\mathbf{R}_A|^2}. \tag{2.27}$$

Under the condition to reproduce the lowest energy with as few functions possible, STOs have the advantage, as they can reproduce the correct slope and cusp of the wavefunction with fewer basis functions than GTOs, see Figure 2.1.

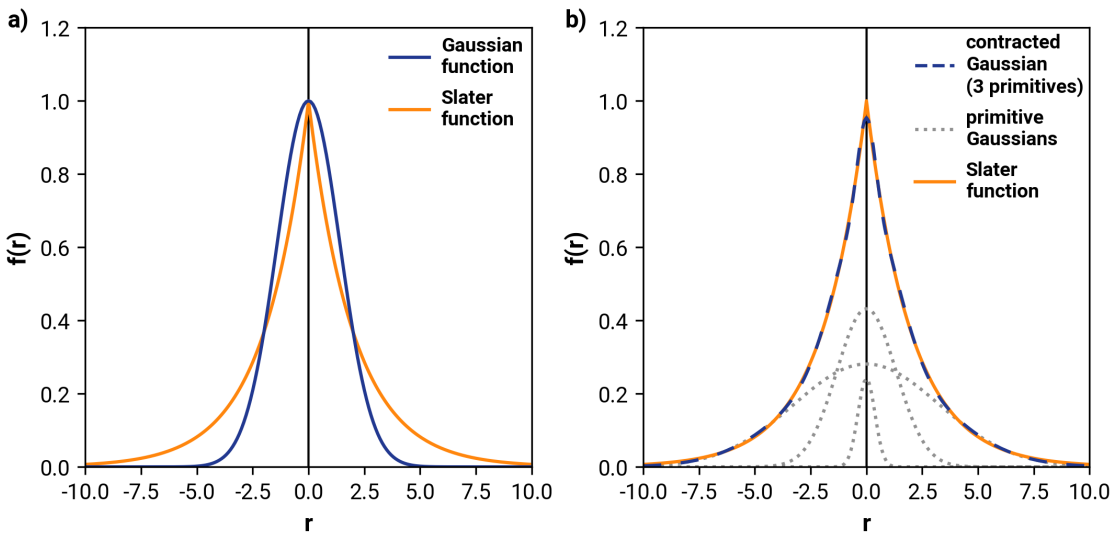

Figure 2.1: a) Comparison of a (primitive) Gaussian function (blue) against a Slater function (orange), b) comparison of a contracted Gaussian function (blue), with the corresponding primitives shown in grey, against a Slater function (orange).

However, GTOs have a much simpler integral evaluation than STOs, leading to a major advantage in computation time. It is noted at this point that the Slater and Gaussian functions, for the sake of a simple comparison, are shown without proper normalization, without radial part and without angular momentum part, necessary to form proper s, p, d, ..., orbitals. Molecular orbitals in quantum chemistry are expressed as a linear combination of atomic orbitals (LCAO), which in turn are expressed by a linear combination of basis functions (most often by CGF). The quality of a given basis set is indicated by its cardinal number, determined by, how many basis functions are used to represent a single physical (valence) atomic orbital. Basis set are categorized into split-valence or double-ζ basis sets for two basis functions per physical atomic orbital, triple-ζ for three basis functions per physical atomic orbital, etc. The lowest level are minimal basis sets, in which each atomic orbital (1s, 2s, $2p_x$, $2p_y$, ...) is represented a single CGF or Slater type basis function. Limiting the size of the basis set introduces an error to any quantum-chemical calculation, called the basis set incompleteness error (BSIE), and is defined as the difference between the energy in the finite basis and the energy in an infinitely large basis set (in praxis an extremely large basis set is used). Minimal basis set can give at most qualitative results, while quantitative results (converged with respect to the basis set limit) for uncorrelated methods are obtained at the earliest with a triple-ζ basis set (e.g., reaction energies may need up to quadruple-ζ basis sets to be considered converged).

2.1.4 Correlated Wavefunction Theory

The Hartree-Fock method plays an important role in quantum chemistry as the basis of molecular orbital theory, giving chemists a simplified picture for the electronic structure of matter. Additionally, the Hartree-Fock wavefunction serves as the starting point for a lot of high-level correlated *ab initio* wavefunction theories. The Hartree-Fock energy, even in the limit of an infinite basis, is higher than the exact nonrelativistic electronic ground-state energy (E, within the Born-Oppenheimer approximation). Their difference, the missing energy, is called correlation energy (E_{corr})

$$E_{\text{corr}} = E - E_{\text{HF}}. \tag{2.28}$$

The goal of post-Hartree-Fock methods is to improve upon the single-determinant theory, Hartree-Fock, by finding the most efficient and accurate way to incorporate the effect of multiple determinants in the total energy, recovering the missing correlation energy.

2.1.4.1 Configuration Interaction Theory

In principle, the exact form of the many-electron wavefunction is known, and can be described by a theory called full configuration interaction (FCI). In FCI, we represent the exact N-electron wavefunction (Ψ_{FCI}) by a linear combination of N-electron Slater determinants and apply the variational method, Ψ_{FCI} can then be expressed as

$$|\Psi_{\text{FCI}}\rangle = c_0|\Phi_0\rangle + \sum_{ar} c_a^r|\Phi_a^r\rangle + \sum_{\substack{a<b\\r<s}} c_{ab}^{rs}|\Phi_{ab}^{rs}\rangle + \sum_{\substack{a<b<c\\r<s<t}} c_{abc}^{rst}|\Phi_{abc}^{rst}\rangle + \dots \tag{2.29}$$

where $|\Phi_a^r\rangle$ are singly excited determinants relative to $|\Phi_0\rangle$ with the two spin orbitals a and r swapped, Φ_{ab}^{rs} are doubly excited determinants relative to Φ_0 with spin orbitals a and r swapped and s and b swapped, and so on. The indices $a, b, c, \ldots$ designate occupied spin orbitals and indices $r, s, t, \ldots$ designate virtual (unoccupied) spin orbitals, with c_a^r, c_{ab}^{rs}, and so on being the CI expansion coefficients which are variationally determined. The FCI wavefunction expansion goes up to N-tuply excited determinants for any N-electron wavefunction. While the energy of the FCI wavefunction in an infinite basis gives the exact nonrelativistic ground-state energy, it is impossible to compute in practice. Already in a finite minimal basis, the number of determinants grows rapidly with the system size, making computations on for more than a few electrons unsolvable on traditional computer hardware in a reasonable time frame due to the considerable associated computational cost.
In practice, it is necessary to truncate the FCI expansion, giving rise to a hierarchy of methods with increasing accuracy: CI with only singly excited determinants (CIS), CI with singly and doubly excited determinants (CISD), CI with singly, doubly and triply excited determinants (CISDT), and so on. The simplest and least costly CI method, CIS, unfortunately does not improve upon the energy calculated by HF theory, since, as stated by Brillouins theorem,[98] singly excited determinants $|\Phi_a^r\rangle$ do not couple directly with the Hartree-Fock reference determinant $\langle\Phi_0|\hat{H}|\Phi_a^r\rangle = 0$, meaning $E_{CIS} = E_{HF}$. Doubly excited determinants, Φ_{ab}^{rs}, are the only ones interacting directly with $|\Phi_0\rangle$, giving usually the largest contribution to the correlation energy in CI methods. Singly excited determinants can interact indirectly with $|\Phi_0\rangle$, via the doubly excited determinants according to $\langle\Phi_a^r|\hat{H}|\Phi_{de}^{tu}\rangle$. Indeed, any two determinants that differ by more than two spin orbitals do not interact directly with each other and, consequently, triply and quadruply excited determinants only interact indirectly with $|\Phi_0\rangle$ via the doubly excited determinants. Inclusion of higher excited determinants comes at a rapidly growing computational cost as each newly added excitation class beyond single excitations raises the exponential cost function by two, i.e., CISD scales with $O(N^6)$, CISDT scales with $O(N^8)$, CISDTQ scales with $O(N^10)$, with N being system size (number of basis functions).

There are two shortcomings of the hierarchy of CI methods that limit their applicability and utility in computational chemistry. Firstly, truncation of the CI expansion at any point (with the exception of CIS) leads to the loss of size extensivity and size consistency of the resulting method, which is unphysical since the energy of a system of two noninteracting molecules should equal the sum of energies of the individual molecular subsystems (size consistency), and because the many-electron wavefunction has to be size extensive. Secondly, the hierarchy of truncated CI methods, CIS, CISD, CISDT, etc., converges only slowly to the FCI limit, necessitating the inclusion of high-order excited determinants for recovering essential parts of the correlation energy.

2.1.4.2 Coupled Cluster Theory

A theorical model that solves both issues of CI methods and the *de facto* standard for highly accurate electronic structure calculations, is the coupled cluster (CC) method. Similarly to the CI wavefunction, CC is a wavefunction expansion using excited determinants, but contrary to CI uses an exponential wavefunction ansatz. For simplicity, we first rewrite the FCI wavefunction in terms of excitation operators $\hat{X}_a^r$, $\hat{X}_{ab}^{rs}$, $\hat{X}_{abc}^{rst}$, ..., which generate the Φ_a^r, Φ_{ab}^{rs}, Φ_{abc}^{rst}, ..., determinants according to

$$\hat{X}_a^r|\Phi_0\rangle = c_a^r|\Phi_a^r\rangle, \quad \hat{X}_{ab}^{rs}|\Phi_0\rangle = c_{ab}^{rs}|\Phi_{ab}^{rs}\rangle, \quad \hat{X}_{abc}^{rst}|\Phi_0\rangle = c_{abc}^{rst}|\Phi_{abc}^{rst}\rangle, \quad \dots \tag{2.30}$$

when acting on $|\Phi_0\rangle$ (the HF determinant) with the excitation operator including all possible excitation classes being

$$\hat{T} = \underbrace{\sum_{ar} \hat{X}_a^r}_{\hat{T}_1} + \underbrace{\sum_{\substack{a<b \\ r<s}} \hat{X}_{ab}^{rs}}_{\hat{T}_2} + \underbrace{\sum_{\substack{a<b<c \\ r<s<t}} \hat{X}_{abc}^{rst}}_{\hat{T}_3} + \dots . \tag{2.31}$$

$|\Psi_{\mathrm{FCI}}\rangle$ can then be expressed as

$$\begin{aligned} |\Psi_{\mathrm{FCI}}\rangle &= (1 + \hat{T})|\Phi_0\rangle \\ &= \left(1 + \hat{T}_1 + \hat{T}_2 + \hat{T}_3 + \hat{T}_4 + \dots\right)|\Phi_0\rangle \\ &= |\Phi_0\rangle + \hat{T}_1|\Phi_0\rangle + \hat{T}_2|\Phi_0\rangle + \hat{T}_3|\Phi_0\rangle + \dots \end{aligned} \tag{2.32}$$

showcasing the linear nature of the CI expansion, while the nonlinear CC expansion can be expressed as

$$\begin{aligned} |\Psi_{\mathrm{CC}}\rangle &= e^{\hat{T}}|\Phi_0\rangle \\ &= \left(1 + \hat{T}_1 + \hat{T}_2 + \frac{1}{2}\hat{T}_1^2 + \hat{T}_3 + \hat{T}_1\hat{T}_2 + \frac{1}{6}\hat{T}_1^3 + \dots\right)|\Phi_0\rangle \\ &= |\Phi_0\rangle + \hat{T}_1|\Phi_0\rangle + \left(\hat{T}_2 + \frac{1}{2}\hat{T}_1^2\right)|\Phi_0\rangle + \left(\hat{T}_3 + \hat{T}_1\hat{T}_2 + \frac{1}{6}\hat{T}_1^3\right)|\Phi_0\rangle + \dots \end{aligned} \tag{2.33}$$

where $e^{\hat{T}}$ is expanded as a Taylor series. Products of operators such as $\frac{1}{2}\hat{T}_1^2$, $\hat{T}_1\hat{T}_2$, $\hat{T}_1^2\hat{T}_2$, ..., are called disconnected doubles, triples, quadruples, ..., and ensure that the CC expansion is size-consistent and size-extensive at any truncation level. Analogous to CI, truncated CC methods are called, CCS for $\hat{T} = \hat{T}_1$, CCSD for $\hat{T} = \hat{T}_1 + \hat{T}_2$, and so on. The disconnected terms in the CC expansion have the additional benefit that the hierarchy of truncated CC methods converge faster to full CC limit, as the disconnected terms are capable of capturing the effects of higher-lying excitation classes.

The faster convergence of truncated CC methods is observable already for small systems, e.g., the dissociation of the Be_2H_2 molecule, see Figure 2.2.

There are two errors or missing parts of electron correlation (relative to FCI) that are historically classified, dynamic correlation and static correlation. Static correlation is important for systems, where more than a single reference configuration is necessary to correctly the describe the electronic structure of the system, often due to the presence of (near-)degeneracies. Dynamic correlation is always relevant,

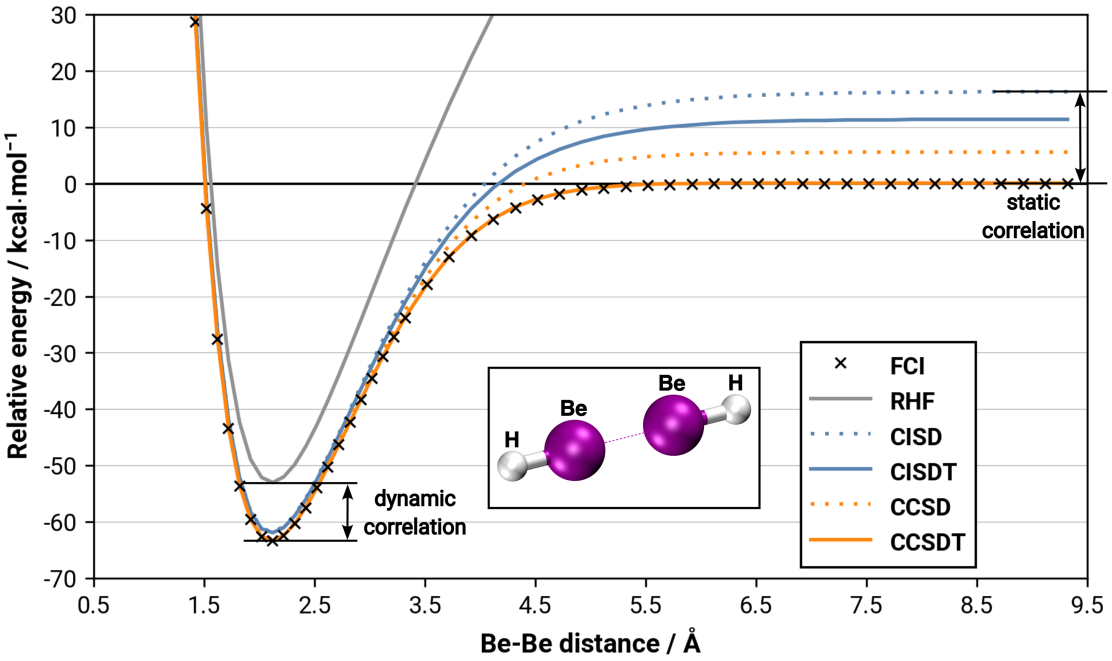

Figure 2.2: Dissociation curve for the Be_2H_2 molecule into BeH fragments for RHF, CISD, CCSD, CISDT, CCSDT, and FCI methods in the 6-31G basis set, Be-Be distances plotted from roughly 1.0-9.0Å, values in kcal/mol.

even in systems, where a single reference configuration is perfectly adequate. In the dissociation curve of Be_2H_2, near the equilibrium distance, a single reference configuration sufficient, while at large distances two reference configurations become equally relevant for the correct description of the system. Relative to FCI, both CISD and CISDT recover less dynamic correlation energy near the equilibrium distance (ΔE(CISDT-CCSDT) = 1.4 kcal/mol) than even CCSD, while at large distances static correlation contributions are consistently better incorporated by both CCSD and CCSDT. The static correlation error is visualized as the difference between CISD and FCI, although the error in the RHF curve at large distances is also due to missing static correlation (but is out of bounds of Figure 2.2).

CCSDT gives excellent accuracy for a large variety of systems, but becomes prohibitively expensive for chemically relevant system sizes (i.e., more than 20 atoms) due to CCSDT's steep scaling ($O(N^8)$) and iterative nature. As an approximation to CCSDT, CCSD(T) was developed which approximates the costly triple excitations noniteratively by perturbation theory (*vide infra*). CCSD(T) reaches quantitative agreement (error <1 kcal/mol) with experiment for a majority of systews, establishing itself as the gold-standard single-reference method of quantum chemistry.
Over the years many theories have been developed to further improve the scaling behavior, i.e., local-correlation methods such as the domain-based local pair natural orbital approximation (DLPNO-CCSD(T)), while explicitly correlated coupled cluster F12 theories have been invented to tackle the poor basis set convergence of conventional CCSD(T) approaches. The large improvements to speed via local correlation and explicit correlation made CCSD(T) the method of choice for high-level

quantum chemistry.

2.1.4.3 Møller-Plesset Perturbation Theory

Another successful post-Hartree-Fock *ab initio* correlated method is Møller-Plesset perturbation theory (MPPT). The starting point of MPPT is the zeroth-order wavefunction in Hartree-Fock theory, consequently making the zeroth-order Hamiltonian ($\hat{H}_0$, see eq. 2.18) the unperturbed Hamiltonian ($\hat{H}^{(0)}$). The zeroth-order problem can be written as

$$\hat{H}^{(0)}\Phi^{(0)} = E^{(0)}\Phi^{(0)} \tag{2.34}$$

with the corresponding unperturbed Hamiltonian

$$\hat{H}^{(0)} = \sum_i \hat{f}_i = \sum_i \hat{h}_i + \sum_{i,j}(\hat{J}_{ij} - \hat{K}_{ij}) \tag{2.35}$$

and the eigenvalue

$$E^{(0)} = \sum_i^{occ} \varepsilon_i \tag{2.36}$$

with the orbital energies ε_i of occupied orbital ("occ" represents the number of occupied orbitals) ϕ_i in HF, since $\Phi^{(0)} = \Phi_{HF}$. The idea of MPPT is to represent the exact Born-Oppenheimer Hamiltonian $\hat{H}$ as the sum of the unperturbed (zeroth-order) Hamiltonian and a perturbation operator $\hat{V}$

$$\hat{H} = \hat{H}^{(0)} + \hat{V} + V_{\mathrm{NN}} \tag{2.37}$$

with $\hat{V}$ being defined as the difference between the exact electron-electron interaction and the Hartree-Fock potential

$$\begin{aligned}\hat{V} &= \hat{H} - \hat{H}^{(0)} - V_{\mathrm{NN}} \\ &= \sum_{i=1}^{N}\hat{h}_i + \sum_{i=1}^{N}\sum_{j>i}^{N}\hat{g}_{ij} - \sum_i \hat{f}_i \\ &= \sum_{i=1}^{N}\sum_{j>i}^{N}\hat{g}_{ij} - \sum_{i=1}^{N}\hat{v}_i^{HF}.\end{aligned} \tag{2.38}$$

The nth-order correction energy $E^{(n)}$ to the zeroth-order energy is obtained from the equation

$$E^{(n)} = \langle\Phi^{(0)}|\hat{V}|\Phi^{(n-1)}\rangle, \quad n > 0 \tag{2.39}$$

giving rise to a series of successive energy corrections, reaching the exact energy of a system with $n \rightarrow \infty$

$$E_{exact} = E^{(0)} + E^{(1)} + E^{(2)} + E^{(3)} + \ldots \tag{2.40}$$

Truncating the expansion after the nth-order energy correction gives MPPT of nth order (MPn), with two noteworthy methods being MP1, as the equivalent to the HF energy expression

$$E_{\mathrm{MP1}} = E_{\mathrm{HF}} = E^{(0)} + E^{(1)} = \sum_{i}^{occ} \varepsilon_i + \frac{1}{2} \sum_{i,j}^{occ} \langle ij||ij \rangle + V_{\mathrm{NN}} \tag{2.41}$$

and MP2 as one of the most efficient expressions for (approximately) calculating the correlation energy of a system, where $\langle ij||ij \rangle$ follows the relation

$$\langle rs||tu \rangle = \langle \phi_r(1)\phi_s(2)|g_{12}|\phi_t(1)\phi_u(2) \rangle - \langle \phi_r(1)\phi_s(2)|g_{12}|\phi_u(1)\phi_t(2) \rangle. \tag{2.42}$$

The MP2 energy expression is given as

$$E_{\mathrm{MP2}} = E^{(0)} + E^{(1)} + E^{(2)} = E_{\mathrm{HF}} + \frac{1}{4} \sum_{i,j}^{occ} \sum_{a,b}^{virt} \frac{\langle ij||ab \rangle \langle ab||ij \rangle}{\varepsilon_i + \varepsilon_j - \varepsilon_a - \varepsilon_b} \tag{2.43}$$

where indices a, b denote virtual (unoccupied) orbitals and "$virt$" is the number of virtual orbitals. Investigations on the convergence of the series of MPn methods reveal it to become erratic or even divergent with growing m. Higher-order Møller-Plesset perturbation theory (n > 2) has little use cases, since more correlated wavefunction methods (CI/CC) exist at the same computational cost. A lot of effort went into improving upon MP2, i.e., spin-component scaling (improved molecular properties, energies, frequencies, etc.),[99] orbital optimization (improved description of open-shell species),[100,101] explicit correlation (accelerating basis set convergence),[102] and local correlation (improving scaling).[103] The most important application of MP2 is as part of so-called double-hybrid density functionals, a theory that combines density functional theory and MP2 (*vide infra*), resulting in a whole family of methods that are amongst the most cost-efficient today.

2.1.5 Density Functional Theory

,

Previously explored methods can be summarized under the umbrella term of wavefunction theory (WFT), that is, theories, where the main object of interest is the many-electron wavefunction. A different approach comes in the form of density functional theory (DFT), in which the main object of interest is the electron density. The foundations of DFT were formulated by Hohenberg and Kohn[75,76] in the form of two theorems called Hohenberg-Kohn theorems which state that: firstly, there exists a unique external potential which can be inferred by the ground-state electron density and vice versa,

meaning all ground-state properties of a system can be calculated from the electron density alone. Secondly, there exists an energy functional and minimizing the energy of this functional (by varying the ground-state electron density) will give the exact ground-state energy of a system. As of today, this exact universal energy functional of DFT is not known, but many (hundreds) of different functional forms have been proposed in the literature. Working in the Born-Oppenheimer approximation, the general energy functional ($F[\rho(\mathbf{r})]$) in DFT can be written as

$$F[\rho(\mathbf{r})] = T[\rho(\mathbf{r})] + V_{eN}[\rho(\mathbf{r})] + V_{ee}[\rho(\mathbf{r})] + E_{xc}[\rho(\mathbf{r})] \tag{2.44}$$

with

$$E_{xc}[\rho(\mathbf{r})] = E_x[\rho(\mathbf{r})] + E_c[\rho(\mathbf{r})] \tag{2.45}$$

where T gives the kinetic energy of the electrons, V_{eN} the electron-nuclear attraction, V_{ee} the electron-electron repulsion and E_{xc} the exchange-correlation term, and all terms are functionals of the electron density $\rho(\mathbf{r})$. For clarity, the coordinate dependence of the electron density is dropped for the functional terms, and it is always implied. The rather classical contributions in the density functional, are $V_{eN}[\rho]$ and $V_{ee}[\rho]$, given by

$$V_{eN}[\rho] = \sum_{A=1}^{K} \int \frac{Z_A \rho(\mathbf{r})}{|\mathbf{R}_A - \mathbf{r}|}\, d\mathbf{r} \tag{2.46}$$

and

$$V_{ee}[\rho] = \frac{1}{2} \int \frac{\rho(\mathbf{r}_1)\rho(\mathbf{r}_2)}{|\mathbf{r}_1 - \mathbf{r}_2|}\, d\mathbf{r}_1 d\mathbf{r}_2 \tag{2.47}$$

where Z_A is the nuclear charge of atom A, $\mathbf{R}$ the coordinate vector of an atom and $\mathbf{r}$ the coordinate vector of an electron. The term $V_{ee}[\rho]$ is nonzero for a one electron (1e) system and must be compensated by the exchange part E_x of E_{xc}, such that $V_{ee}[1e] - E_x[1e] = 0$. As the exact energy functional for E_{xc} is not known, the difference $V_{ee}[1e] - E_x[1e]$ is generally nonzero resulting in significant SIE in DFT, which becomes also apparent in many-electron systems (e.g., dissociation of charged systems). Another problematic part of DFT is the kinetic energy functional, which has to be approximated very accurately since the kinetic energy is one of the largest contributions to the total energy of the system. The Thomas-Fermi model[104] was one of the functional approximations for the kinetic energy (derived from the uniform electron gas (UEG)), and is given by

$$T^{\mathrm{UEG}}[\rho] = \frac{3h^2}{40m_e} \left(\frac{3}{\pi}\right)^{2/3} \int \rho(\mathbf{r})^{5/3}\, d\mathbf{r} \tag{2.48}$$

with h being Planck's constant and m_e the mass of an electron. Early calculations showed a poor performance for the kinetic energy of electrons using this functional (and a UEG-derived version of the exchange functional), as molecules were found to be unbound under this approximation. The

introduction of gradient corrections and nonlocality could improve only slightly, but even the best of approximations could only be applied to describe uniform systems such as periodic metals and alloys and failed to properly describe chemical bonds in molecules.[105] The poor performance of, what is today known as orbital-free DFT, for the kinetic energy led to the development of Kohn-Sham DFT, where the concept of the wavefunction in the form of a Slater determinant of orbitals were reintroduced into DFT framework.

2.1.5.1 Kohn-Sham Density Functional Theory

In the Kohn-Sham DFT scheme, the kinetic energy of the interacting system ($T[\rho]$) is replaced by the kinetic energy of a fictitious noninteracting auxiliary system (T_{KS}), while the (exact) electron density is the same for both the noninteracting and interacting case. The kinetic energy of the electrons in the fictitious systems is

$$T_{\mathrm{KS}} = -\frac{1}{2}\sum_{i=1}^{N}\langle\phi_i|\nabla_i^2|\phi_i\rangle \tag{2.49}$$

with orthonormal spin-orbitals ϕ_i and the electron density then given as

$$\rho(\mathbf{r}) = \sum_{i=1}^{occ}|\phi_i(\mathbf{r})|^2. \tag{2.50}$$

Inserting T_{KS} into the energy functional ($F[\rho]$) gives

$$F[\rho] = T_{\mathrm{KS}} + V_{eN}[\rho] + V_{ee}[\rho] + E_{xc}[\rho] \tag{2.51}$$

with the remaining term $T_c = T[\rho] - T_{\mathrm{KS}}$ being absorbed into the exchange-correlation functional. $E_{xc}[\rho]$, therefore, contains all nonclassical contributions to V_{ee} and T_{KS}. Taking the derivative of each functional with respect to the electron density ρ, we get the Kohn-Sham potential v_{KS} given as

$$v_{\mathrm{KS}}(\mathbf{r}) = \underbrace{v_{eN}(\mathbf{r})}_{\delta V_{eN}[\rho]/\delta\rho} + \underbrace{v_{ee}(\mathbf{r})}_{\delta V_{ee}[\rho]/\delta\rho} + \underbrace{v_{xc}(\mathbf{r})}_{\delta E_{xc}[\rho]/\delta\rho} \tag{2.52}$$

with the classical potential $v_{eN}(\mathbf{r})$ of the nuclei and Coulomb potential $v_{ee}(\mathbf{r})$, and the nonclassical exchange-correlation potential $v_{xc}(\mathbf{r})$. The working equations for KS-DFT are then given by

$$\underbrace{\left(-\frac{1}{2}\nabla^2 + v_{\mathrm{KS}}(\mathbf{r})\right)}_{\hat{h}_{\mathrm{KS}}}\phi_i = \varepsilon_i\phi_i \tag{2.53}$$

with the Kohn-Sham Hamiltonian operator $\hat{h}_{\mathrm{KS}}$, the Kohn-Sham orbitals ϕ_i and their corresponding orbital energies ε_i. From this result, it can be concluded that, firstly, the motion of interacting electrons can be described exactly by a system of independent particles and, secondly, the nonclassical electron-electron interactions can be described by the local Kohn-Sham potential $v_{\mathrm{KS}}(\mathbf{r})$. The only missing part is the explicit form of the exchange-correlation functional $E_{xc}[\rho]$. Exchange-correlation functionals are to this day a very active research area, with already hundreds of different exchange-correlation functionals published, some for particular properties and some intended as general-purpose functionals. In the following, the most successful and popular forms of exchange-correlation functionals and DFAs in general are discussed. The hierarchy of increasingly accurate DFAs in KS-DFT is called Jacob's ladder (see Figure 2.3), starting with local density approximation functionals.

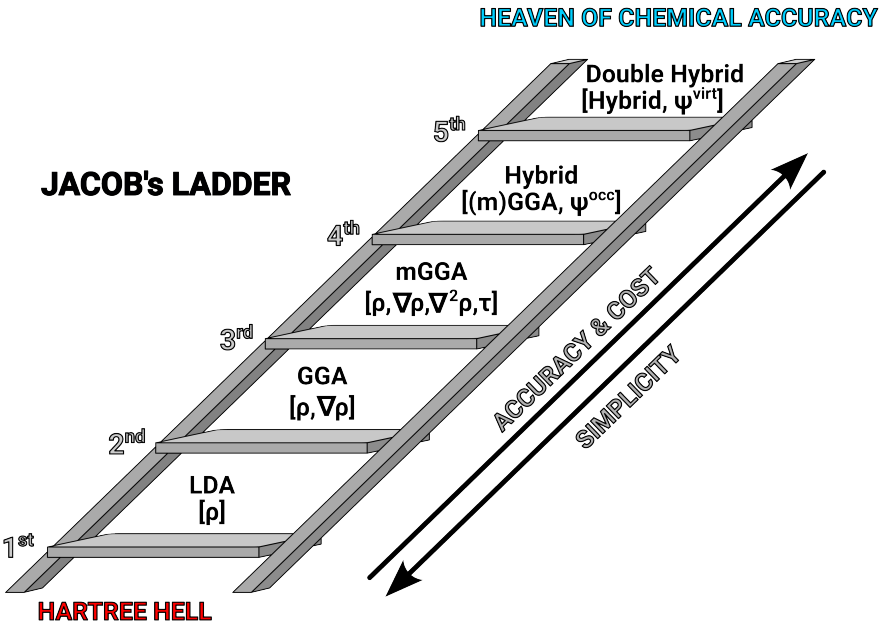

Figure 2.3: Jacob's ladder of density functional theory, with each rung (1^{st} to 5^{th}) accuracy increases and simplicity decreases.

2.1.5.2 Local (Spin-)Density Approximation (LDA/LSDA)

In the local density approximation (LDA), the exchange-correlation functional is local in the sense that its potential (functional derivative w.r.t. to the density) at some point in space only depends on the electron density at that point. Density functionals are usually constructed in the spin-polarized DFT formalism, where the exchange-correlation functional is dependent on the spin-densities ρ_α and ρ_β of the up-spin and down-spin electrons of the system, such that $\rho(\mathbf{r}) = \rho_\alpha(\mathbf{r}) + \rho_\beta(\mathbf{r})$, to treat materials and molecules with unpaired electrons correctly. In this case, LDA is more aptly known as the local spin-density approximation (LSDA/LSD), in which the main assumption is

$$E_{xc}^{\mathrm{LSDA}}[\rho_\alpha, \rho_\beta] = \int \rho(\mathbf{r})\, \varepsilon_{xc}(\rho_\alpha(\mathbf{r}), \rho_\beta(\mathbf{r}))\, d\mathbf{r} \tag{2.54}$$

with the exchange-correlation energy ε_{xc} per electron in the UEG. The LSDA exchange functional takes the form

$$E_x^{\mathrm{LSDA}}[\rho_\alpha, \rho_\beta] = -\frac{3}{2}\left(\frac{3}{4\pi}\right)^{1/3} \int \left(\rho_\alpha^{4/3}(\mathbf{r}) + \rho_\beta^{4/3}(\mathbf{r})\right) d\mathbf{r} \tag{2.55}$$

and is derived for the UEG. LSDA and the spin-unpolarized form, LDA, are equal for closed-shell systems (diamagnetic materials). Unfortunately, there does not exist a simple exact analytic form for the LSDA correlation functional, just different parameterizations fitted to accurate Quantum Monte Carlo data.[105] Many parametrizations for the LSDA correlation functional have been made, one successful and popular being by Vosko, Wilk and Nusair (VWN).[106] The resulting exchange-correlation functional is close to exact for the UEG system and gives reasonable results for simple metals (periodic mostly homogeneous systems), but is less accurate for properties of inhomogeneous systems, i.e., molecules. Overall, LSDA presents already a significant improvement over HF, especially for periodic systems and the condensed phase[107] but also for molecular energies, properties[107] and geometries.[105]

2.1.5.3 Generalized Gradient Approximation (GGA)

To overcome the shortcomings of the LSDA, a correction was devised to incorporate not only information of the local density at a point but also of the gradient of the density. Functionals dependent on the gradient of the density ($\nabla\rho$) follow the generalized gradient approximation (GGA), with the generic form

$$E_{xc}^{\mathrm{GGA}}[\rho_\alpha, \rho_\beta] = \int \rho(\mathbf{r})\, f\left(\rho_\alpha(\mathbf{r}), \rho_\beta(\mathbf{r}), \nabla\rho_\alpha(\mathbf{r}), \nabla\rho_\beta(\mathbf{r})\right) d\mathbf{r}. \tag{2.56}$$

Contrary to WFT, where the inclusion of more determinants into the wavefunction systematically improves the method, there does not exist a similar straightforward way to find or improve upon the form of f. Density functional approximation (DFA) development can be considered more of an artform than a craft. The two major ways (not mutually exclusive) to find DFA's, either via fitting against theoretical/experimental data or parameterizing the functional to fulfill the known physical bounds and conditions of the exact exchange-correlation functional. In the search for the exact denstiy functional a lot of different forms for f have been proposed, with a notable one being the PBE functional,[108] by Perdew, Burke and Ernzerhof in which all parameters (except in the LSDA expression) are derived from physical constants. Including more ingredients in the exchange-correlation functional, such as, the Laplacian of the up-spin (α) and down-spin (β) spin-densities $\nabla^2\rho_\alpha(\mathbf{r})$ and $\nabla^2\rho_\beta(\mathbf{r})$ and/or the kinetic energy densities $\tau_\alpha(\mathbf{r})$ and $\tau_\beta(\mathbf{r})$, with

$$\tau_\sigma(\mathbf{r}) = \frac{1}{2}\sum_i^{occ} |\nabla\phi_{i\sigma}|^2 \quad and \quad \sigma = \alpha, \beta \tag{2.57}$$

leads to so called meta-GGA (mGGA) functionals. Both GGA's and meta-GGA's are a significant step up in terms of accuracy compared to the LDA functionals; a more in-depth comparison is given in Chapter 2.1.5.8.

2.1.5.4 Global Hybrid (GH) Density Functionals

Global hybrid (GH) functionals are a combination of Hartree-Fock theory and Kohn-Sham DFT, where a part of the local exchange energy in the exchange-correlation functional (E_x^{DFT}) is replaced in part by nonlocal Fock exchange energy (E_x^{HF}). This mixing of theories is theoretically justified under the adiabatic connection formula, ensuring a smooth and continuous potential irrespective of mixing parameter (in the limits 0 and 1).[109–112] When this mixing of local functional exchange and nonlocal Fock exchange is constant for any electron-electron distance, such functional is called a global hybrid functional. Global hybrid density functionals (E_{xc}^{hybrid}) in the simple one-parameter variant have the generic form

$$E_{xc}^{\text{hybrid}} = (1-a)E_x^{\text{DFT}} + aE_x^{\text{HF}} + E_c^{\text{DFT}} \tag{2.58}$$

where a denotes the amount of Fock exchange mixed into the original density functional. Virtually any combination of LDA, GGA or meta-GGA with Fock exchange and also mixing between different exchange-correlation functionals is possible, leading to a vast ocean of combinations and also highly parametrized density functionals. From a (mostly) nonempirical perspective the PBE functional with 25% Fock exchange ($a = 0.25$),[113] a fraction based on a theoretical argument, gives a nearly optimal mixing, improving energies and properties across a large range of different chemical systems. In particular, the inclusion of Fock exchange into the density functional partially reduces, depending on the fraction of Fock exchange, the SIE of approximate functionals. HF theory is by construction SIE-free as the error in the Coulomb energy contribution, due to electron self interaction, is completely screened by the (100%) exchange part in the energy expression. Hybrid functionals perform for atomization energies, thermochemistry, ionization potentials, electron affinities, barrier heights, and geometries, on average better than their pure GGA/meta-GGA counterpart.[105,114] The frontier orbital energies of molecules, particular the HOMO energies, get partially corrected with increasing amount of Fock exchange; functionals of approx. 50% give the best agreement with experimental measurements.[115] However, since global hybrids use global mixing of Fock exchange, with admixtures less than 100%, they cannot completely eliminate SIE. This becomes particular apparent in charged species and separation of charged species, i.e., the dissociation curves of positively charged nobel gas dimers, for which global hybrids (and even more so LDA's/GGA's) produce huge errors.[116,117] Another problem of global hybrids is that the optimal amount (for best results of a particular property or relative energy) of global Fock exchange admixture is system-dependent. For example, transition metal complexes are best described with Fock exchange amounts of roughly 10-15% due to the large stabilization of high-spin states by Fock exchange, while reaction barrier heights are usually most accurate with larger amounts for Fock exchange 40-50%. This makes the search for a universally accurate hybrid functional, which uses linear mixing between Fock exchange and DF exchange, very challenging.

2.1.5.5 Range-Separated Hybrid (RSH) Functionals

Range-separated hybrid (RSH) functionals are the successor of global hybrid functionals and able to fix their shortcomings associated with linear mixing of Fock exchange and DF exchange. In RSH functionals, the amount of Fock exchange in the functional is dependent on the inter-electronic distance,

rather than being defined globally. To achieve this, the two-electron operator is split into a short-range (SR) and long-range (LR) part, according to

$$\frac{1}{r_{12}} = \underbrace{\frac{1-\left[b+c\cdot\mathrm{erf}(\omega r_{12})\right]}{r_{12}}}_{SR} + \underbrace{\frac{b+c\cdot\mathrm{erf}(\omega r_{12})}{r_{12}}}_{LR} \tag{2.59}$$

which is the generalized form for RSH functionals proposed by Handy and coworkers[118] and based on the original ideas of Hirao,[119] Savin,[120,121] and Gill.[122] ω is the range-separation parameter and adjusts the switching between SR and LR part, while the parameters b and c control the amount of fixed (independent of r_{12}) Fock exchange and fixed DFT exchange, respectively. In this generalized form any type of hybrid is accessible: global hybrids for $c = 0$ with the amount of Fock exchange b, long-range corrected hybrids for $b + c = 1.0$ and Coulomb-attenuated (CAM) functionals for $b + c \neq 1$.

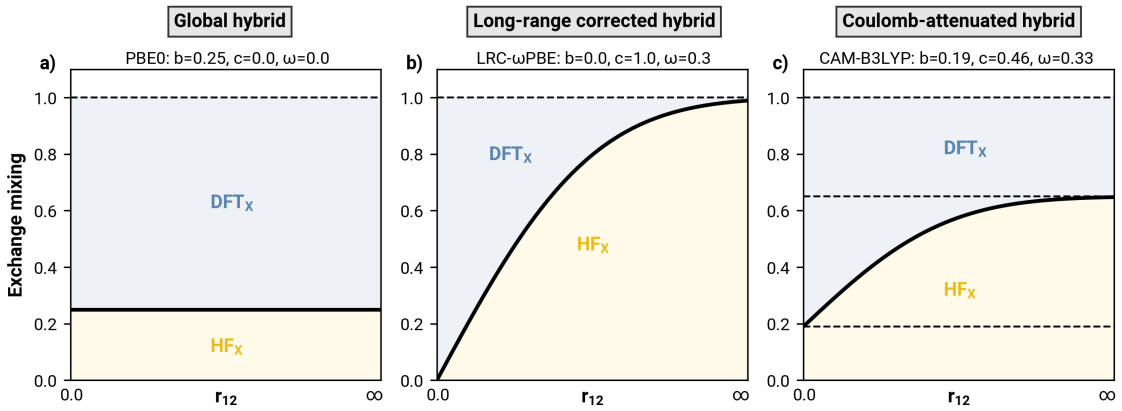

Figure 2.4: Comparison of exchange mixing of Fock exchange HF_X (yellow) and DFT exchange DFT_X (blue) (in dependence of the interelectronic distance r_{12}) in the energy functional for a) global hybrids, i.e. PBE0,[113,123] b) long-range corrected hybrids, i.e. LRC-ωPBE,[124] and c) Coulomb-attenuated hybrids, i.e. CAM-B3LYP.[118]

From the perspective of molecular chemistry, one major problem in global hybrids is choosing a reasonable tradeoff between semilocal DF exchange, which contains static correlation and is therefore important for an accurate short-range description, and Fock exchange, which is essential for eliminating the self-interaction error and getting the correct $1/r$-asymptotics of the exchange-correlation potential.[125] Via the more flexible design of RSH functionals you can get the best of both worlds: a good description of the short-range region, ideally dominated by semilocal exchange and a good description of the long-range region, ideally dominated by Fock exchange. RSH functionals generally significantly improved electronic properties, such as fundamental gaps, HOMO-LUMO gaps, 4s-3d interconfigurational energies, polarizabilities, reaction barriers and thermochemistry, and also improved Rydberg and charge-transfer excitation energies (more on excited states in Chapter 2.2.1).[114,119,125,126] Currently, one of the most cost-effective functionals for general main-group thermochemistry, kinetics and noncovalent interactions, is ωB97M-V,[127] a long-range corrected hybrid functional.

2.1.5.6 Optimal Tuning of the Range-Separation Parameter

In the description of the RSH functionals little detail was given on how to determine a reasonable value for the range-separation parameter ω, which sets the characteristic length scale for the mixing of the short-range to the long-range part. Indeed, for most RSH functionals the ω value is fitted empirically to best reproduce some property or energy of a specific benchmark set. Although, fixed ω values can be already a significant improvement over GH functionals, a similary problem to GH functionals still exists that some properties/energies are best reproduced with different values for ω. A way around this issue is to define an optimal molecules-specific ω value which should ideally be calculable from *ab initio* theories alone. The determination of the optimal ω value for a specific molecule is called optimal tuning[126,128,129] and is based around Koopmans theorem, which connects the frontier molecular orbitals energy of the HOMO (ε(HOMO)) with the molecular ionization potential (IP)) by

$$\varepsilon(\text{HOMO}) = -\text{IP} \;\Leftrightarrow\; \varepsilon(\text{HOMO}) + \text{IP} = 0. \tag{2.60}$$

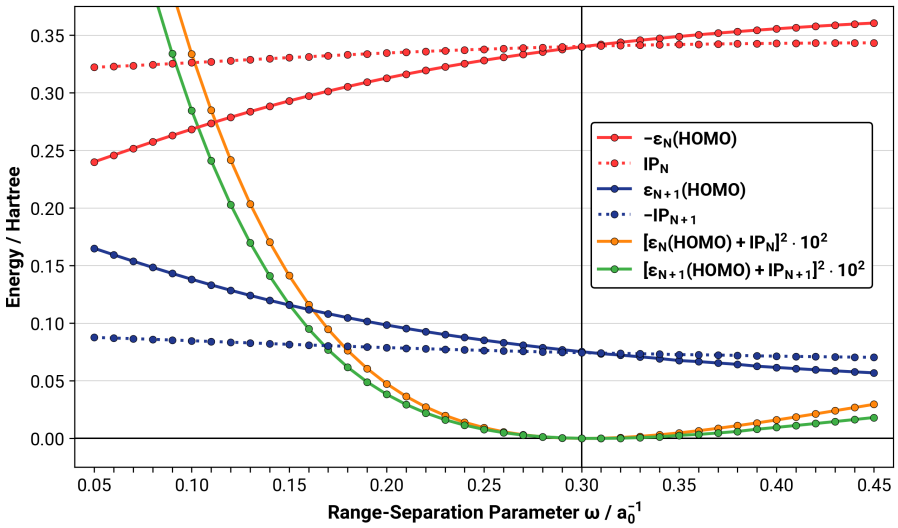

Figure 2.5: Parameters of the optimal tuning procedure of benzene for the ωB97 long-range corrected functional using the def2-SVP basis set, in the ω value range (0.05-0.45 a_0^{-1}). The subscripts N and $N+1$ refer to the neutral species and the anionic species (with one added electron) of benzene. a_0^{-1} is the Bohr radius.

Considering not only the neutral molecule species (with N electrons) but also the anionic species (with $N+1$), it is possible to tune both the HOMO and indirectly the LUMO energy (by tuning the HOMO of the anionic species) to fulfill Koopmans theorem. In practice, one defines a ω-dependent function $J^2(\omega)$ that becomes minimal for the optimal ω value:[130]

$$J^2(\omega) = \left[\varepsilon_N(\text{HOMO}) + \text{IP}_N\right]^2 + \left[\varepsilon_{N+1}(\text{HOMO}) + \text{IP}_{N+1}\right]^2 \tag{2.61}$$

As an example, Figure 2.5 shows the optimal tuning procedure for the long-range corrected ωB97 functional with benzene as the sample system. In this example, the optimal ω value for the ωB97 is

estimated to be around 0.30 a_0^{-1} (vertical line).

2.1.5.7 Double Hybrid Functionals

Double hybrid density functionals (DHDF) have been introduced in 2006 by Grimme,[131] and not only replace a part of semilocal exchange with Fock exchange but also replace semilocal correlation with correlation energy based on (in most cases) second-order perturbation theory (MP2). The expression for a (global) double hybrid functional mixing in, a part of correlation energy from Møller-Plesset perturbation theory can be written as

$$E_{xc}^{\text{double hybrid}} = (1-a)E_x^{\text{DFT}} + aE_x^{\text{HF}} + (1-d)E_c^{\text{DFT}} + dE_c^{\text{MP2}}. \tag{2.62}$$

The underlying Fock exchange mixing does not need to be of global hybrid type, but can, of course be a range-separated hybrid functional. The inclusion of a WFT-based expression for electron correlation significantly improves the capabilities of double hybrid functionals to accurately describe the electronic structure of molecules. Double hybrids are the highest rung on Jacob's ladder and include information about the virtual orbitals of the system via the (most often) perturbative correlation energy contribution. Additionally, the use of KS-DFT virtual orbitals instead of HF orbitals makes the correlation energy term more accurate and robust than the conventional MP2 correlation energy.[131] Double hybrids were also the first functionals to naturally capture long-range correlation effects, i.e., dispersion effects, which are near-impossible to capture with any LDA, GGA, mGGA, or hybrid functional without the use of additional corrections (*vide infra*). SIE in double hybrids is strongly reduced compared to most hybrids (with around 10-40% Fock exchange), since large amounts of Fock exchange (50-70%) are generally necessary for best accuracy with DHDF's. The computational cost of double hybrids is larger than for standard hybrid density functionals, due to the MP2 correlation term, and a scaling of $O(N^5)$ with system size is observed. The most recent modern double hybrid functionals have become remarkably accurate, reaching an accuracy between CCSD and CCSD(T), with a significantly reduced associated computational cost.

2.1.5.8 Practical Aspects of Density Functional Theory

Overall, inspection of the large general main group thermochemistry, kinetics and noncovalent interaction database, GMTKN55, shows that the proposition of Jacob's ladder is fulfilled and that the rung of a density functional roughly corresponds to its robustness and accuracy. LDA provides worst results making it uncompetitive and basically unusable for any calculations in molecular quantum chemistry (omitted from Figure 2.6). GGA functionals are a large step up in accuracy compared to LDA, based on the weighted mean absolute deviations (WTMAD-2), with associated WTMAD's in the range of 14 kcal/mol to 8 kcal/mol. The previously mentioned PBE functional (coupled with a good dispersion correction, see below for more on dispersion) performs reasonably well for a GGA, with an WTMAD-2 of roughly 8.3 kcal/mol. The next step on Jacob's ladder, meta-GGA functionals, improve only little upon GGA functionals with often similar WTMADs. A particular important mGGA is the strongly constrained and appropriately normed (SCAN) functional and its successor (regularized SCAN: r^{2}SCAN). The parameters of SCAN are in constrast to most functionals (which are often empirically fitted), motivated from known physical constraints for DFA, and simultaneously

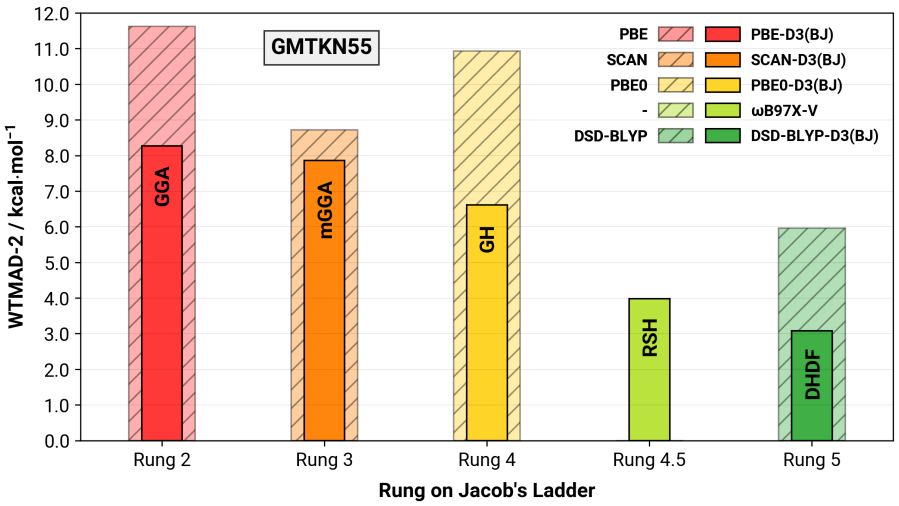

Figure 2.6: Weighted mean absolute deviations (WTMAD-2) of representative functionals of each rung of Jacob's ladder; rung 1 local density approximation (LDA, no data available), rung 2 generalized gradient approximation (GGA), rung 3 meta-generalized gradient approximation (mGGA), rung 4 global hybrid functionals (GH), rung 4.5 range-separated hybrids (RSH), rung 5 double hybrid functionals.

SCAN (with disp. correction) performs best of all at the time tested mGGA functionals. Going on to global hybrid functionals brings a moderate improvement over mGGA's and GGA's, with associated WTMADs roughly in the range of 11 kcal/mol to 5 kcal/mol. The PBE0 functional performs roughly 20-30% better than the PBE functionals through the inclusion of Fock exchange. More elaborate GH functionals like the Minnesota family of functionals, can reduce the WTMAD as low as 4.5 kcal/mol, but depending on the specific functional can contain dozens of empirical parameters and specifically fitted on similar large benchmark sets (as the GTMKN55). RSH functionals were split from global hybrid functionals for convenience and the associated rung 4.5 is for differentiation only, since no new ingredients are added in RSH functionals compared to GH functionals. The best-performing RSH functional is ωB97X-V incorporating dispersion corrections via a nonlocal density-dependent functional which is included in the empirical fit. ωB97X-V is still one of the most accurate and cost-efficient hybrid functionals, and a great choice as a general purpose functional. The overall best-performing functionals are double hybrids with the best WTMADs, roughly between 4 kcal/mol and 3 kcal/mol, with recently developed double hybrid functionals giving errors as low as 2.2 kcal/mol.[132]

Another important consideration of DFT calculations is the size of the basis set. Generally, DFT methods converge faster than WFT methods to the complete basis set (CBS) limit, meaning the BSIE is reduced with fewer basis functions and lower angular momentum basis functions compared the WFT. DHDFs, due to the MP2 correlation part, converge the slowest, most often somewhere inbetween MP2 and hybrid functionals. Additionally, in the calculation of noncovalent interactions (intermolecular and intramolecular, e.g., conformer energies), the presence of basis set superposition error (BSSE) should be kept in mind. BSSE originates from the incompleteness of the basis set, but manifest in the form of artificial energy lowering, due one atom borrowing the basis functions of other close atoms

of another molecule (intermolecular BSSE) or a different part of the same molecule (intramolecular BSSE)) to better represent its own electronic structure. This artifically lowers the total energy of the interacting system (i.e., noncovalently bound complexes or folded chain-like molecules), in relation to the noninteracting system (i.e., the fragments of the complex or the unfolded chain-like molecule). As a general rule, the results of density functional calculations should only be trusted with a basis set of at least triple-ζ quality, except for properties or energies where basis set convergence studies show that lower quality basis sets suffice.

A family of DFT composite methods which tackle the multiple shortcomings of the DFT, is the family of 3c-methods introduced by Grimme and coworkers.[133–137] In general benchmarking, calculations employ large basis sets to eliminate BSIE, to best represent a functionals performance and eliminate any biases and errors other than from the functional itself. These large basis set increase the cost of the DFT calculations significantly, such that, for very large systems (hundreds of atoms) even DFT becomes to costly. For very large systems and for very fast and accurate calculations, the family of 3c-methods were developed. Each 3c-method is designed a little differently, but generally they feature DFT-D dispersion corrections, a way to minimize the BSSE, often via the geometrical counterpoise correction (gCP), and come with an tailored basis set for the underlying functional. 3c-methods are as accurate or more accurate compared to calculations from the parent functional in a quadruple-ζ basis, at a fraction of the cost. Therefore, they are particularly suitable as general purpose methods for accurate and efficient DFT calculations.

2.1.5.9 Dispersion Corrections in DFT

One shortcoming of semilocal density functionals and also hybrid functionals is the inability to properly describe London dispersion interactions. London dispersion (in the following shortened to dispersion) is fundamentally of quantum-mechanical origin, stemming from long-range electron correlation effects.[138] For a model system with two fragments A and B, it arises from the interaction of two simultaneous virtual single particle-hole excitations local to A and B, respectively.[139] The transition densities associated with these virtual excitations induce dipole moments on the respective other fragment, though these processes happen instantaneous without the formation of any real measurable dipole moment. The interaction strength of two solely through dispersion effects bound atoms is relatively small in comparison to the strength of a chemical bonds (100-1000 times less) or even other noncovalent interactions such as hydrogen bonding (roughly 10x less). However, dispersion effects are present in all systems without exception and since the interaction strength roughly scales with the surface area and polarizability of two interacting molecules or fragments, dispersion interactions can outgrow the strength of other noncovalent interaction and become the dominant factor for bonding. Correctly capturing the effects of dispersion in DFT is important for the thermochemistry of both intermolecular interacting molecules (i.e., especially for liquids, molecular crystals and noncovalent complexes) and intramolecular interacting fragments (i.e., proteins and thermochemistry of molecules with bulky functional groups/ligands). Several methods exist to correct for the effect of dispersion in DFT, with the most popular two being, the family of DFT-D dispersion corrections[140–143] based on atomic dispersion coefficients and the family of nonlocal density-dependent functionals like the VV10.[144–146] The examination of 217 density functionals in the large GMTKN55[114] benchmark study showed clearly that the inclusion of dispersion corrections (irrespective of the type of correction,

DFT-D3 or VV10-type) improves calculated energies across the board (see examples in Figure 2.6). Even DHDF that naturally include long-range correlation (dispersion energy) via MP2 can benefit greatly from using dispersion corrections.[114,147] It is therefore always recommended to include some kind of dispersion correction in DFT calculations.

2.2 Electronically Excited States

2.2.1 Time-Dependent Density Functional Theory

The most popular and successful theory for computing the excitated states of molecules and solids is linear-response time-dependent density functional theory (LR-TD-DFT),[84,148] in the following used synonymous with TD-DFT. The central object of TD-DFT is the time-dependent one-electron density $\rho(\mathbf{r}, t)$, usually in the framework of KS-DFT. As is the case for time-independent DFT, the exact KS potential is unknown, and the first Runge-Gross theorem[149] (analogous to the first Hohenberg-Kohn theorem) states that there is a one-to-one mapping of the time-dependent potential and the time-dependent electron density of a system. And analogous to the variational principle in ground-state DFT, the exact time-dependent density makes the quantum-mechanical action A stationary

$$\frac{\delta A}{\delta \rho(\mathbf{r}, t)} = 0 \tag{2.63}$$

with

$$A = \int_{t_0}^{t_1} \langle \Psi(t) | i \frac{\partial}{\partial t} - \hat{H}(t) | \Psi(t) \rangle dt. \tag{2.64}$$

Additionally, the KS equations for the time-dependent case can be derived in the same manner as the ground-state case, in assuming the existence of a, now, time-dependent potential $v_{KS}(\mathbf{r}, t)$ for noninteracting particles which yields the exact same density as for the interacting particles, such that

$$\rho(\mathbf{r}, t) = \sum_{i=1}^{occ} |\phi_i(\mathbf{r}, t)|^2. \tag{2.65}$$

Minimizing the action under condition (2.65) leads to the time-dependent Kohn-Sham (TDKS) equations

$$\left(-\frac{1}{2}\nabla^2 + v_{KS}(\mathbf{r}, t) \right) \phi_i(\mathbf{r}, t) = i \frac{\partial}{\partial t} \phi_i(\mathbf{r}, t) \tag{2.66}$$

with

$$v_{KS}(\mathbf{r},t) = v(\mathbf{r},t) + \int \frac{\rho(\mathbf{r}_2,t)}{|\mathbf{r}_1 - \mathbf{r}_2|} d\mathbf{r}_2 + v_{xc}(\mathbf{r},t) \tag{2.67}$$

and

$$v_{xc}(\mathbf{r},t) = \frac{\delta A_{xc}[\rho]}{\delta\rho(\mathbf{r},t)} \tag{2.68}$$

where $A_{xc}[\rho]$ is the exchange-correlation action functional (analogous to the exchange-correlation functional $E_{xc}[\rho]$ in ground-state DFT). If the external potential varies slowly in time, $A_{xc}[\rho]$ reduces to $\int_{t_0}^{t_1} E_{xc}[\rho_t]dt$, which is called the adiabatic approximation. In the adiabatic approximation, the time-independent exchange-correlation functional can be simply applied in the TDKS equations and gives the time-dependent KS potential as

$$v_{xc}[\rho](\mathbf{r},t) = \frac{\delta A_{xc}[\rho]}{\delta\rho(\mathbf{r},t)} \approx \frac{\delta E_{xc}[\rho_t]}{\delta\rho_t(\mathbf{r})} = v_{xc}[\rho_t](\mathbf{r}). \tag{2.69}$$

Truly solving the TDKS equations in time, however, leads to a theory called real-time TD-DFT (RT-TD-DFT).[150] RT-TD-DFT is necessary in cases where the external perturbation is strong (strong laser fields, multi-harmonic generation, etc.), but is computationally demanding.

2.2.1.1 Linear-Response Formalism

A workaround to the real-time evolution of the TDKS equations was presented by Casida, where the excitation energies and oscillator strengths are extracted from pole structure of the dynamic polarizability of a system. The change in density ($\delta\rho$) as a response to a change in the external potential (δv^{KS}), can be related by

$$\delta\rho_i(\mathbf{r},\omega) = \sum_j \int \chi_{ij}^{KS}(\mathbf{r}_1,\mathbf{r}_2,\omega)\delta v_j^{KS}(\mathbf{r}_2,\omega)\, d\mathbf{r}_2 \tag{2.70}$$

for the KS system, with χ^{KS} being the linear density-density response function. χ^{KS} can be expressed in terms of unperturbed stationary ground-state Kohn-Sham orbitals (φ) as

$$\chi_{ij}^{KS}(\mathbf{r}_1,\mathbf{r}_2,\omega) = \lim_{\eta\to 0}\sum_{kl}^{\infty}(n_{li} - n_{ki})\frac{\varphi_{ki}(\mathbf{r}_1)\varphi_{ki}^*(\mathbf{r}_2)\varphi_{li}(\mathbf{r}_2)\varphi_{li}^*(\mathbf{r}_1)}{\omega - (\varepsilon_{ki} - \varepsilon_{li}) + \mathrm{i}\eta} \tag{2.71}$$

with the Kohn-Sham eigenvalues ε_{ki}, with the occupation number of the kth orbital n_k and the positive infinitesimal η. Through the exchange-correlation kernel f_{xc},

$$f_{xc}(\mathbf{r}_1,\mathbf{r}_2,\omega) = \frac{\delta v_{xc}(\mathbf{r}_1,\omega)}{\delta\rho(\mathbf{r}_2,\omega)} = \frac{\delta^2 E_{xc}(\omega)}{\delta\rho(\mathbf{r}_1,\omega)\delta\rho(\mathbf{r}_2,\omega)} \tag{2.72}$$

the exact response function χ can be related to the response function of the KS system via the Dyson-type equation

$$(\hat{1} - \chi^{KS}(\omega)\left[\frac{1}{|\mathbf{r}_1 - \mathbf{r}_2|} + f_{xc}(\omega)\right]\chi(\omega) = \chi^{KS}(\omega). \tag{2.73}$$

For an infinitesimally weak perturbation, the electronic transitions ω, can then be obtained from the non-Hermitian eigenvalue equation

$$\begin{pmatrix} \mathbf{A} & \mathbf{B} \\ \mathbf{B*} & \mathbf{A*} \end{pmatrix}\begin{pmatrix} \mathbf{X} \\ \mathbf{Y} \end{pmatrix} = \omega \begin{pmatrix} 1 & 0 \\ 0 & -1 \end{pmatrix}\begin{pmatrix} \mathbf{X} \\ \mathbf{Y} \end{pmatrix} \tag{2.74}$$

also known as the Casida equation, where $\mathbf{X}$ and $\mathbf{Y}$ are the solution vector to the single particle-hole (excitations) and single hole-particle (deexcitations) amplitudes

The matrix elements of $\mathbf{A}$ and $\mathbf{B}$ are given as

$$\begin{aligned} A_{ia,jb}(\omega) &= \delta_{ij}\delta_{ab}(\varepsilon_a - \varepsilon_i) + (ia|jb) + (ia|\hat{f}_{xc}(\omega)|jb) \\ B_{ia,jb}(\omega) &= (ia|bj) + (ia|\hat{f}_{xc}(\omega)|bj) \end{aligned} \tag{2.75}$$

with the two-electron integrals given in Mulliken notation as

$$(ia|\hat{f}_{xc}(\omega)|jb) = \int \varphi_i^*(\mathbf{r}_1)\varphi_a(\mathbf{r}_1)f_{xc}(\mathbf{r}_1, \mathbf{r}_2, \omega)\varphi_n^*(\mathbf{r}_2)\varphi_j(\mathbf{r}_2)\, d\mathbf{r}_1 d\mathbf{r}_2 \tag{2.76}$$

and

$$(ia|jb) = \int \varphi_i^*(\mathbf{r}_1)\varphi_a(\mathbf{r}_1)\frac{1}{|\mathbf{r}_1 - \mathbf{r}_2|}\varphi_b^*(\mathbf{r}_2)\varphi_j(\mathbf{r}_2)\, d\mathbf{r}_1 d\mathbf{r}_2 . w \tag{2.77}$$

The Casida equation in this form is applicable for so-called "pure" functionals, which are of LDA, GGA, or mGGA-type and do not employ an admixture of Fock exchange (c_{HF}, equal to a from eq. 2.58) or MP2 correlation energy. Corresponding matrix elements for $\mathbf{A}$ and $\mathbf{B}$ for global hybrid functionals are given by

$$\begin{aligned} A_{ia,jb}(\omega) &= \delta_{ij}\delta_{ab}(\varepsilon_a - \varepsilon_i) + (ia|jb) - c_{\mathrm{HF}}(ij|ab) + (1 - c_{\mathrm{HF}})(ia|\hat{f}_{xc}(\omega)|jb) \\ B_{ia,jb}(\omega) &= (ia|bj) - c_{\mathrm{HF}}(ib|aj) + (1 - c_{\mathrm{HF}})(ia|\hat{f}_{xc}(\omega)|bj). \end{aligned} \tag{2.78}$$

The Tamm-Dancoff approximation (TDA) is an approximation to the Casidas equation and completely neglects the $\mathbf{B}$ matrix, leading to the Hermitian eigenvalue problem

$$\mathbf{AX} = \omega\mathbf{X}. \tag{2.79}$$

Tamm-Dancoff approximated time-dependent density functional theory (TDA-DFT) is usually a very good approximation to TD-DFT, while cutting down cost by roughly a factor of two.[79] TD-DFT has quickly become the most prominent method for calculating excitation energies and transition moments for molecules and solids. Hundreds of different flavors of (ground-state) density functionals are available today, and by virtue of the adiabatic approximation have also been applied in the context TD-DFT. The accuracy of computed excitation energies in TD-DFT is typically in range of 0.1-0.4 eV, only slighly worse than much more expensive equation-of-motion CCSD. This reasonable accuracy is reached at a fairly low compuational cost, making the application of TD-DFT to very large molecules possible and explains the huge success and widespread adoption TD-DFT has received.

The accuracy of TD-DFT calculations is, however, also highly sensitive to the choice of density functional. The decent accuracy of TD-DFT can be traced back to the orbital energies on which matrix **A** depends. In KS-DFT, virtual orbital energies are determined for an N electron system, therefore can be interpreted as single-particle energies of an excited electron, a virtual particle sees N-1 electrons. Whereas in HF theory, virtual orbital energies are determined for an N+1 electron system, a virtual particle sees N electrons. This makes virtual KS orbitals decent approximations for excitation energies. Variations in excitation energies is therefore particularly high for different hybrid functionals, since the amount of Fock exchange in the underlying functional has a big influence on orbital energies. The percent of Fock exchange in TD-DFT calculations becomes the primary determining factor for a functionals accuracy, while the influence of the underlying LDA/GGA exchange and correlation functional are of lesser importance. For fitted functionals, i.e. functinals of the Minnesota family, this does not hold true, since the whole functional form (semilocal exchange, correlation and also Fock exchange) is fitted to produce the lowest error on variety benchmark data.

In benchmark calculations, global hybrid functionals with roughly 10-25% of Fock exchange perform best for valence excitation energies in medium-sized organic molecules.[151–154] For extended system or generally for excited states with (long-range) charge-transfer character (i.e., TADF emitters), functionals with higher amounts of Fock exchange are more accurate due to the wrong asymptotic potential in pure LDA/GGA and hybrid functionals with small amounts (<10-25%) Fock exchange.[155–157] Pure LDA/GGA functionals in particular show a large underestimation in charge-transfer excited states and exhibit the wrong 1/r dependence in potential energy curves of long-range CT states.[158] This is known as the charge-transfer failure of TD-DFT and leads to unphysical so-called ghost CT states in extended systems, if a LDA/GGA/mGGA functional is employed.[79,158] Increasing the amount of Fock exchange in the functional partially corrects this, but cannot entirely eliminates the wrong 1/r dependence. Long-range corrected (LRC) functionals have been successful in improving the charge-transfer error in TD-DFT, since LRC functionals only feature Fock exchange (correct for CT states) for large interelectronic distance. Still the accuracy of a RSH functional is in part determined by the ω value used for a specific system. Optimal tuning of RSH functionals offers a physically sound procedure to find the optimal ω value for a given system and in a study by Jacquemin[159] an optimally-tuned RSH functionals performed best for the calculation of 0-0 transition energies.
Problems with Ryberg excited states are also greatly reduced by RSH functionals, however, associated

errors are still larger compared to valence and CT excitations.[160] One of TD-DFT's biggest problems are states with significant double excitation character (and pure double excitations), since the linear-response formalism includes only singly excited states (excitations and deexcitations, relative to the electronic ground-state).[79,161] States with double excitation character are present in MR-TADF and INVEST emitters and it is therefore of great importance for research of OLED materials (MR-TADF/INVEST) to develop quantum-chemical methods which can describe double excitations.

2.2.2 ΔSCF Methods for Excited States

2.2.2.1 Open-Shell Wavefunctions

In the introduction to Hartree-Fock equations, the underlying wavefunction (Slater determinant) was introduced with spin orbitals $\phi_i(k) = \sigma_i\psi_i(k)$, where σ_i was the spin part and $\psi_i(k)$ the spatial part of the respective orbital. So far, only restricted closed-shell calculations were discussed, where the spatial part for a given MO is the same for the α (up-spin) and β (down-spin) spin orbitals. This restriction is reasonable for closed-shell systems, but not for open-shell systems with one or more unpaired electrons. In dealing with open-shell systems, two approaches have become common, using either unrestricted open-shell or restricted open-shell wavefunctions. Via either of these approaches the calculation of excited state energies becomes possible. For example, the lowest triplet excitation energy can be calculated, as the SCF energy difference (therefore ΔSCF methods) between singlet ground-state and lowest triplet "ground-state" energy.

2.2.2.2 Spin-Unrestricted Wavefunctions

The idea of unrestricted open-shell HF is rather simple. It splits the HF eigenvalue problem into two, such that α (ϕ_i^α) and β (ϕ_i^β) spin orbitals have different spatial parts, and redefines it as

$$\begin{aligned} \hat{f}_i^\alpha|\phi_i^\alpha\rangle &= \varepsilon_i^\alpha|\phi_i^\alpha\rangle \\ \hat{f}_i^\beta|\phi_i^\beta\rangle &= \varepsilon_i^\beta|\phi_i^\beta\rangle \end{aligned} \tag{2.80}$$

where the two Fock operators $\hat{f}_i^\alpha$ and $\hat{f}_i^\beta$ are defined by

$$\begin{aligned} \hat{f}_i^\alpha &= \hat{h}_i + \sum_j^{N^\alpha}(\hat{J}_j^\alpha - \hat{K}_j^\alpha) + \sum_j^{N^\beta}\hat{J}_j^\beta \\ \hat{f}_i^\beta &= \hat{h}_i + \sum_j^{N^\beta}(\hat{J}_j^\beta - \hat{K}_j^\beta) + \sum_j^{N^\alpha}\hat{J}_j^\alpha. \end{aligned} \tag{2.81}$$

The unrestricted exchange ($\hat{K}_j^\alpha$ and $\hat{K}_j^\beta$) and Coulomb operators ($\hat{J}_j^\alpha$ and $\hat{J}_j^\beta$) are analogously defined to the restricted ones, i.e., for the α case,

$$\hat{J}_j^\alpha |\phi_i^\alpha(1)\rangle = \langle \phi_j^\alpha(2)|\hat{g}_{12}|\phi_j^\alpha(2)\rangle |\phi_i^\alpha(1)\rangle \tag{2.82}$$

and

$$\hat{K}_j^\alpha |\phi_i^\alpha(1)\rangle = \langle \phi_j^\alpha(2)|\hat{g}_{12}|\phi_i^\alpha(2)\rangle |\phi_j^\alpha(1)\rangle. \tag{2.83}$$

While the wavefunction is still represented as a single Slater determinant, no restriction on the spin of the system is enforced. UHF solutions lead generally to the same or a lower energy than a respective RHF solution would give. In open-shell cases, α and β orbital energies usually differ significantly. For KS-DFT or more aptly, spin-density functional theory, the spin-unrestricted formalism is similar to UHF. The unrestricted Kohn-Sham (UKS) equations feature a different effective potential, eigenvalues and orbitals for the α and β electrons respectively,

$$\left[-\frac{1}{2}\nabla^2 + v_{\mathrm{KS}}^\alpha(\mathbf{r})\right] \phi_i^\alpha = \varepsilon_i^\alpha \phi_i^\alpha \tag{2.84}$$

and

$$\left[-\frac{1}{2}\nabla^2 + v_{\mathrm{KS}}^\beta(\mathbf{r})\right] \phi_i^\beta = \varepsilon_i^\beta \phi_i^\beta. \tag{2.85}$$

2.2.2.3 The Maximum Overlap Method (MOM)

The most common use case of unrestricted and restricted open-shell determinants is for the description of systems with open-shell ground states, i.e., radical systems and transition metal complexes. Standard SCF calculations follow the Aufbau principle, that is, filling the orbitals in ascending order of energy, which leads naturally to the ground-state configuration of an electronic state for a given spin multiplicity. It is, however, entirely possible to initialize an SCF calculation with a non-Aufbau electron configuration and then apply the SCF procedure. With a reasonably good convergence algorithm, such calculations still converge to the ground-state and not to an higher-order solution of the Schrödinger equation, which is called variational collapse to the ground-state. To prevent the collapse of the non-Aufbau configuration to the ground-state configuration, a constrain of the SCF algorithm is needed. In the maximum overlap method (MOM) a constrain is applied to the SCF procedure to maximize the overlap ($\mathbf{O}$) between new $\mathbf{C}^{\mathbf{new}}$ and old $\mathbf{C}^{\mathbf{old}}$ orbitals (coefficients) of each SCF step. A modified MOM approach was later developed to improve upon the standard MOM approach, called initial MOM (IMOM), in which the overlap between new orbitals and initial guess orbitals is maximized in the SCF.

$$\mathbf{O} = (\mathbf{C}^{\mathbf{old}})^\dagger \mathbf{S} \mathbf{C}^{\mathbf{new}} \quad \text{(MOM)} \tag{2.86}$$

$$\mathbf{O} = (\mathbf{C}^{\mathbf{initial}})^\dagger \mathbf{S} \mathbf{C}^{\mathbf{new}} \quad \text{(IMOM)} \tag{2.87}$$

In the case of a non-Aufbau electron configuration as initial orbital guess, the SCF targets an excited state solution of the Schrödinger equation. This enables the calculation of excited states in the HF and DFT frameworks. Since only a single determinant is used in both HF and DFT, singlet excited states obtained in this manner are not spin-pure with an expectation value $\angle S\rangle = 1.0$. An open-shell singlet determinant represents a mixed state of 50% singlet and 50% triplet, hence the spin expectation value should be 1.0. To correct this (i.e. $\angle S\rangle = 0$), a second complementary determinant (a multiconfigurational treatment) is necessary, where α and β spins of the singly occupied orbitals are swapped. Nonetheless, MOM and IMOM have been applied successfully for the calculation of excited states in DFT, resulting in excited-state specific optimized orbitals, which is why this method is also called orbital-optimized DFT (OO-DFT) or state-specific ΔSCF/ΔDFT. In principle, MOM/IMOM can be applied to either unrestricted or restricted open-shell wavefunctions, but usage of unrestricted wavefunctions is more common. To obtain a reasonable initial non-Aufbau configuration guess, it is common practice to start from a converged ground-state calculation and manually promoted an electron from an occupied to a virtual orbital, i.e., HOMO -> LUMO, or HOMO-2 -> LUMO+1. It is naturally also possible to promote multiple electrons and target, e.g., doubly excited states. The convergence of a MOM/IMOM calculation is to a significant extent dependent on how close the initial guess resembles the targeted excited state. In practice, IMOM often outperforms the original MOM approach in terms of convergence robustness.[86]

2.2.2.4 Two-Determinant Restricted Open-Shell Kohn-Sham

The restricted open-shell Kohn-Sham DFT approach explored in this thesis is a an approach specifically designed to target singlet excited states and aims to fix the spin-purity problem of one determinant singlet excited states (*vide supra*). Based on the vector-coupling approach of Roothaan, a spin-pure singlet excited state is constructed from two determinants, a restricted open-shell singlet determinant (also called mixed determinant) and a restricted open-shell triplet determinant. From these two determinants the spin-pure ROKS singlet excited state energy can be extracted as

$$E_S^{ROKS} = 2E_M[\{\psi_i\}] - E_T[\{\psi_i\}] \tag{2.88}$$

which is similar to the spin-purification scheme for one-determinant singlet wavefunctions. The defining factor of ROKS is that both open-shell determinants (mixed and triplet) are constructed from the same set of KS orbitals ψ_i. In a ROKS calculation, the spin-pure ROKS singlet excited state E_S^{ROKS} is obtained by variational minimization of the energy with respect to the KS orbitals for an unified eigenvalue problem. This makes the underlying variational minimization procedure more costly compare to UKS, but naturally produces a pure singlet excited state. A disadvantage of ROKS is its limited (restricted) variability of the wavefunction, leading to the lack of coupling to closed-shell double excitations, e.g., $HOMO^2$ -> $LUMO^2$.

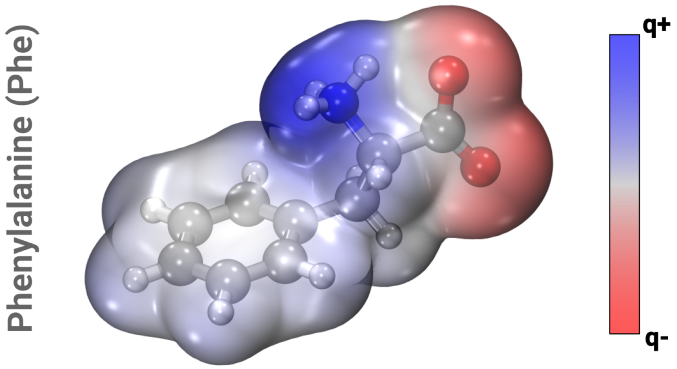

Figure 2.7: Electrostatic potential isosurface (blue regions -> pos. charge, red regions -> neg. charge) of the amino acid phenyalanin in its zwitterionic form (in the gas phase), calculated at an isodensity value of 0.003 e/Å^3, with the functional PBE0 in the def2-SVPD[162,163] basis set.

2.3 Solvation in Quantum Chemistry

2.3.1 Polarizable Continuum Solvation Models

Modeling the environment of a molecule via a dielectric continuum solvation model is an established way to calculate solvation energies and solvation effects on properties. Continuum solvation models are particularly efficient, since the many solvent molecules it would usually require to explicitly model the solvent environment, can be reduced to an implicit description via a dielectric continuum. Sampling over the solvents degree's of freedom is not necessary, as the averaging is included in the static (zero-frequency) dielectric constant ε_s, a parameter inherent to the solvent used. While extremely powerful and efficient in describing the effects of solvation, the shortcomings of continuum solvation models are easily apparent. Since, the interaction of solute and solvent is treated as an average interaction, strong specific noncovalent interactions, such as hydrogen-bonds are poorly described by continuum solvation models. Today, the term continuum solvation model is nearly completely synonymous with polarizable continuum models (PCMs) or more specifically apparent surface charge (ASC) models.

In these, a sharp solute-solvent surface boundary is defined, where the solute is placed inside a cavity, the quantum-mechanical (QM) region (treated by quantum mechanics), and the solvent is represented by the outside dielectric continuum. In the QM region, the Coulomb interaction between electrons is entirely described by the Schrödinger equation, therefore $\varepsilon(\mathbf{r}) = 1$, while for outside the cavity $\varepsilon(\mathbf{r}) = \varepsilon_s$. The fundamental assumption of continuum solvation models is that the electric response of a solvent can be described by the dielectric polarization of the solute potential. The central element for describing these effects, the Poisson equation, can be defined for a given charge density ($\rho(\mathbf{r})$) representing the solute (electrons and nuclei) and for a scalar function of the dielectric constant ($\varepsilon(\mathbf{r})$ as

$$\nabla \left[\varepsilon(\mathbf{r})\nabla\varphi(\mathbf{r})\right] = -4\pi\rho(\mathbf{r}) \tag{2.89}$$

where the electrostatic potential $\varphi(\mathbf{r})$ is related to the electric field $E(\mathbf{r})$ via $E(\mathbf{r}) = -\nabla\varphi(\mathbf{r})$. In

PCMs, the dielectric interface or discontinuity in the electric field results in a buildup of charge at this interface, called surface charge $\sigma(\mathbf{s})$, where $\mathbf{s}$ is a point on the solute cavity surface. With the outward-pointing unit vector $\mathbf{n_s}$ of point $\mathbf{s}$ at the interface, the surface-normal component of the electric field must satisfy

$$\varepsilon_{out}(\mathbf{n_s}\cdot\nabla)\varphi(\mathbf{s})|_{s=s^-} = \varepsilon_{in}(\mathbf{n_s}\cdot\nabla)\varphi(\mathbf{s})|_{s=s^+} \tag{2.90}$$

where s^- and s^+ denote one-sided derivatives, respectively, directly inside and outside the solute cavity surface. Denoting the normal derivative $\mathbf{n_s}\cdot\nabla$ as ∂_s, the surfaces charges at the dielectric interface can be expressed as

$$\sigma(\mathbf{s}) = \frac{1}{4\pi}\left(\frac{\varepsilon_{out}-\varepsilon_{in}}{\varepsilon_{out}}\right)\partial_s\varphi(\mathbf{s})|_{s=s^+} = \frac{1}{4\pi}\left(\frac{\varepsilon_{out}-\varepsilon_{in}}{\varepsilon_{out}}\right)\partial_s\varphi(\mathbf{s})|_{s=s^-} \tag{2.91}$$

showing that the surface charge is proportional to the normal electric field ($E_\perp(\mathbf{s})$) evaluated directly outside ($\partial_s\varphi(\mathbf{s})|_{s=s^+}$) or inside ($\partial_s\varphi(\mathbf{s})|_{s=s^-}$) the solute cavity surface. Choosing ε_{out} and ε_{in} based on $\varepsilon(\mathbf{r})$, and choosing the inside formalism to avoid problems with self-polarization of the solvent, results in the original formalism by Tomasi and coworkers[164–166]

$$\begin{aligned}\sigma(\mathbf{s}) &= \frac{1}{4\pi}\left(\frac{\varepsilon_s-1}{\varepsilon_s}\right)\left(\frac{\partial_s\varphi)}{\partial\mathbf{n}_s}\right)|_{s=s^-} \\ &= -\frac{1}{4\pi}\left(\frac{\varepsilon_s-1}{\varepsilon_s}\right)\underbrace{[E^\rho(\mathbf{s})+E^\sigma(\mathbf{s})]\cdot\mathbf{n_s}}_{E_\perp(\mathbf{s})}\end{aligned} \tag{2.92}$$

where $E^\rho = -\nabla\varphi^\rho$ is the electric field contribution associated with the electrostatic potential φ^ρ coming from the solute and $E^\sigma = -\nabla\varphi^\sigma$ is the reaction-field contribution coming from the surface charges with the corresponding electrostatic potential defined by $\varphi^\sigma(\mathbf{r}) = \int\frac{\sigma(s)}{|\mathbf{s}-\mathbf{r}|}d\mathbf{s}$. Eq. 2.92 is today known as the D-PCM. Defining the surface charges in terms of electrostatic potentials φ^ρ and φ^σ, where the normal derivative is evaluated at (and not near) the point $\mathbf{s}$, gives a generalized form of D-PCM

$$\sigma(\mathbf{s}) = \frac{f_\varepsilon}{2\pi}\partial_s\left[\varphi^\rho(\mathbf{s})+\varphi^\sigma(\mathbf{s})\right] \tag{2.93}$$

with the dielectric-constant-dependent prefactor

$$f_\varepsilon = \frac{\varepsilon_{out}-\varepsilon_{in}}{\varepsilon_{out}+\varepsilon_{in}}. \tag{2.94}$$

Assuming an ideal conductor as the medium ($\varepsilon_s = \infty$, one arrives at the conductor-like screening model (COSMO) or the conductor-like polarizable continuum model (C-PCM), for which the expression for

the surface charges simplifies to

$$\hat{S}\sigma(\mathbf{s}) = -f_{\varepsilon}(k)\varphi^{\rho}(\mathbf{s}) \tag{2.95}$$

with the single-layer potential operator $\hat{S}$, given by

$$\hat{S}\sigma(\mathbf{s}_1) = \int \frac{\sigma(\mathbf{s}_2)}{\parallel \mathbf{s}_2 - \mathbf{s}_1 \parallel} d\mathbf{s}_2 = \varphi^{\sigma}(\mathbf{s}) \tag{2.96}$$

and the dielectric-constant-dependent prefactor,

$$f_{\varepsilon}(k) = \frac{\varepsilon_s - 1}{\varepsilon_s - k} \tag{2.97}$$

where the parameter k depends on the model used:

$$k^{\mathrm{COSMO}} = 1/2 \quad \text{and} \quad k^{\mathrm{C-PCM}} = 0. \tag{2.98}$$

The scaling factor $f_{\varepsilon}(k)$ is introduced to account for the fact that ε_s is finite. For neutral solutes $k = 1/2$, has been found to work well, while for ions $k = 0$ produces better results.[89] A more modern approach and an exact solution to the classical continuum electrostatics problem is given by the integral equation formalism PCM (IEF-PCM) for which the working equation (this theory's equivalent to 2.93) takes the form

$$\left[\left(\frac{2\pi}{f_{\varepsilon}}\hat{1} - \hat{D}\right)\right]\hat{S}\sigma((s)) = \left(-2\pi\hat{1} + \hat{D}\right)\varphi^{\rho}(\mathbf{s}) \tag{2.99}$$

where $\hat{D}$ is the double-layer potential operator defined by

$$\hat{D}\sigma(\mathbf{s}) = \int \sigma(\mathbf{s}_2)\frac{\partial}{\partial \mathbf{n}_{\mathbf{s}_2}}\left(\frac{1}{\parallel \mathbf{s}_2 - \mathbf{s}_1 \parallel}\right) d\mathbf{s}_2. \tag{2.100}$$

The discretization of the solute cavity as well as the how-to of obtaining a reasonable smooth surface without adding significant computational cost are both important aspects of PCMs. How the cavity is constructed, i.e., from Van-der-Waals radii (which radii to take), the solvent excluded or solvent accessible surface algorithm, strongly influences the resulting solvation free energy. However, their discussion goes beyond the scope of this introduction to PCMs and can be found elsewhere.[89] Finally, the electrostatic solvation free energy (G_{solv}) for the solute can be computed via

$$G_{\mathrm{solv}} = \frac{1}{2}\int \varphi^{\rho}(\mathbf{s})\sigma(\mathbf{s})\, d\mathbf{s}. \tag{2.101}$$

Inclusion of any PCM in the SCF equations yields the self-consistent reaction field (SCRF) method,

where, simultaneous to the SCF iterations, the electrostatic solvation free energy is iterated to self consistency. The SCF solution for the QM region and the surface charges of the PCM (irrespective of exact formulation) are then in equilibrium with each other, which is why SCRF can also be called equilibrium PCM. Equilibrium PCMs can be applied to any SCF procedure which makes them trivially adoptable for the framework of ΔSCF methods, rendering state-specific fully equilibrated excited state energies easily accessible. For excitation-based methods such as TD-DFT, ADC(2), CC2, EOM-CCSD, but also *post*-Hartree-Fock methods in general, a state-specific PCM (SS-PCM) treatment is quite challenging to obtain, and not always accessible in quantum chemistry codes. Furthermore, for modeling the solvent response for electronic excitations and excited states, it is important to not only consider equilibrium solvation but also nonequilibrium solvation effects.

2.3.2 Nonequilibrium Solvation

How the solvent environment (continuum model) responds to a fast change in the solute electron density is exceedingly relevant for all electronic spectroscopies, such as absorption and emission from excited states, but also photoelectron spectroscopy in which electrons are removed from the solute. For equilibrium solvation treatments, the dielectric medium can be described entirely by its static permittivity (static dielectric constant ε_s, zero-frequency limit of $\varepsilon(\omega)$). However, for fast vertical electronic processes (excitations and ionizations), it is important to note that the dielectric constant is actually a frequency-dependent dielectric function $\varepsilon(\omega)$ and the solvation treatment has to be expanded for nonequilibrium solvation effects. In nonequilibrium solvation, the response of the environment is partitioned into a fast and slow component, where the fast response is related to the dielectric constant at optical frequencies ($\varepsilon(\omega)$, high-frequency limit being $\varepsilon_\infty = lim_{\omega\to\infty}\varepsilon(\omega)$ also called the optical dielectric constant) and the slow response related to both the static and optical dielectric constant. ε_∞ is generally greater than zero, which relates to the fact that there is always some part of the solvent polarization which is in phase with the applied field (electronic excitation). The slow polarization response, encapsulates frequency components which depend on $\varepsilon(\omega)$, but also vibrational contributions and orientational compontents (reorganization of the solvent environment) For a Franck-Condon process (fast vertical process), the nuclei remain at fixed positions and the solvent molecules cannot reorient, which limits the solvent response to its fast component that stays in equilibrium with the fast changes in electron density, whereas the slow component is determined solely by the equilibrium of solvent with the initial electronic state. In this framework, the frequency-dependent function $\varepsilon(\omega)$ is reduced to its limit values ε_s and ε_∞. ε_∞ is related to the solvents polarizability, but is in practice determined from measurements of the solvents' refractive index n, by the relation $n^2 = \varepsilon_\infty$. Optical dielectric constants ε_∞ typically range between 1.7 to 2.6, while static dielectric constants range from 2 to 110, a reflection of the fact that solvent are usually small molecule insulators with large band gaps, therefore similar polarizabilities.

In the continuum solvation framework, the nonequilibrium solvent response to electronic excitations can be computed by two different approaches, the state-specific (SS) and linear-response (LR) method.

2.3.2.1 State-Specific Approach

To obtain the nonequilibrium polarization in the state-specific approach, the slow susceptibility defined by $\chi_s = \left(\varepsilon_\infty - \varepsilon_s\right) / 4\pi$ is used to induce polarization for the initial state electron density (ρ_0) and the fast susceptibility defined by $\chi_f = \left(\varepsilon_\infty - 1\right) / 4\pi$ is used with the difference density $\Delta\rho = \rho_k - \rho_0$ to adjust the polarization in the final state (ρ_k, kth excited state). In PCMs this is realized by partitioning the surface charges $\sigma_0(\mathbf{s})$ arising from solving the ground-state equilibrium solvation problem (using ε_s) into fast and slow components

$$\begin{aligned} \sigma_0^s(\mathbf{s}) &= \left(\frac{\varepsilon_\infty - \varepsilon_s}{\varepsilon_s - 1}\right)\sigma_0(\mathbf{s}) \\ \sigma_0^f(\mathbf{s}) &= \left(\frac{\varepsilon_\infty - 1}{\varepsilon_s - 1}\right)\sigma_0(\mathbf{s}). \end{aligned} \tag{2.102}$$

$\sigma_0^s(\mathbf{s})$ are retained, while $\sigma_0^f(\mathbf{s})$ are replaced by surface charges induced by the excited state electron density ρ_k where ε_∞ is used. The electrostatic free energy E_k^{SS} of the final state k in the state-specific formalism can be derived from the Schrödinger equation

$$\underbrace{\left(\hat{H}_{vac} + \hat{R}_0^s + \hat{R}_k^f\right)}_{\hat{H}_k^{SS}} \Psi_k\rangle = E_k^{SS}|\Psi_k\rangle \tag{2.103}$$

where $\hat{H}_{vac}$ is the vacuum Hamiltonian, $\hat{R}_0^s$ is the slow component of the reaction-field operator originating from ρ_0 and χ_s, and $\hat{R}_k^f$ is the fast component of the reaction-field operator originating from the ρ_k and χ_f. Since $\hat{R}_k^f$ depends on the wavefunction of the kth excited state, the Hamiltonian H_k^{SS} is state-specific. The state-specific excited-state free energy ($G_k^{neq,SS}$) can be written as

$$G_k^{neq,SS} = E_k^{SS} - W_0^s - W_k^f + W_{0,k} \tag{2.104}$$

where W_k is the polarization work

$$W_k^n = \frac{1}{2}\langle\Psi_k|\hat{R}_k^n|\Psi_k\rangle = \frac{1}{2}\int \sigma_k^n(\mathbf{s})\varphi^{\rho_k}(\mathbf{s})\, d\mathbf{s} \tag{2.105}$$

and $W_{0,k}$ is

$$W_{0,k} = \frac{1}{2}\int \varphi^{\sigma_0^s}(\mathbf{s})\left[\sigma_k^f(\mathbf{s}) - \sigma_0^f(\mathbf{s})\right]\, d\mathbf{s} \tag{2.106}$$

and finally the excitation energy $\hbar\omega_{0,k}^{noneq,SS}$ can be expressed as

$$\hbar\omega_{0,k}^{neq,SS} = G_k^{SS} - G_0 = \Delta E_k^{SS} - \left(W_k^f - W_0^f\right) + W_{0,k}. \tag{2.107}$$

The nonequilibrium vertical excitation energy $\hbar\omega_{0,k}^{neq,SS}$ in the state-specific PCM (SS-PCM) framework is therefore, the difference between the ground- and excited-state eigenvalues (ΔE_k^{SS}) of the state-specific Hamiltonian, corrected by the difference in fast polarization work ($-(W_k^f - W_0^f)$) for each electronic state (0 and k). The term $W_{0,k}$ represents the Coulomb interaction between ground- and excited-state surface charges. However, converging the equations for the Hamiltonian defined in eq. 2.103 can be challenging and even if converged (by an iterative procedure), associated properties like oscillator strengths are formally wrong since the final-state wavefunctions are not orthogonal (due to different Hamiltonians).[89] A workarond is presented in the perturbative state-specific approach (ptSS-PCM) for nonequilibrium solvation, where $\hat{R}_k^f$ is treated as a perturbation to zeroth-order states which are eigenfunctions of H_0^{SS},

$$\hat{H}_0|\Psi_k^{(0)}\rangle = E_k^{(0)}|\Psi_k^{(0)}\rangle \tag{2.108}$$

where the eigenvalues $E_k^{(0)}$ are state energies in the presence of the ground-state reaction-field $\hat{R}_0$, such that eq. 2.104 can be rewritten as

$$G_k^{neq,ptSS} = E_k^{(0)} + W_0^{s+f} + W_{k-0}^f + W_{0,k}. \tag{2.109}$$

The terms W_{k-0}^f is given by

$$W_{k-0}^f = \frac{1}{2}\int \underbrace{\Delta\sigma_{k-0}^f(\mathbf{s})}_{\sigma_k^f(\mathbf{s})-\sigma_0^f(\mathbf{s})} \cdot \underbrace{\varphi^{\Delta\rho_{k-0}}(\mathbf{s})}_{\varphi_k(\mathbf{s})-\varphi_0(\mathbf{s})}\, d\mathbf{s} \tag{2.110}$$

where $\Delta\sigma_{k-0}^f$ is the difference in fast polarization charges for state k and 0, and $\varphi^{\Delta\rho_{k-0}}$ is the electrostatic potential associated with the difference density of state k and 0. For the nonequilibrium ptSS-corrected excitation energy $\hbar\omega_{k,0}^{neq,ptSS}$ the terms W_0^{s+f} cancel, which gives the form

$$\hbar\omega_{0,k}^{neq,ptSS} = G_k^{ptSS} - G_0 = \Delta E_k^{(0)} + W_{k-0}^f + W_{0,k}. \tag{2.111}$$

Both ptSS-PCM and SS-PCM approaches can be adopted for excitation-based excited-state methods (as mentioned previously), but can also be adopted for *post*-Hartree-Fock correlated wavefunction methods, since only a relaxed density for the initial and final states are required for the computation.

2.3.2.2 Linear-Response Approach

In contrast to the state-by-state approach in the (pt)SS-PCM framework, the linear-response approach is applicable only to linear-response (excitation-based) quantum chemistry methods (TD-DFT, CIS,

etc.), where the excitation energies are obtained from the poles of the frequency-dependent response to a perturbation. From a computational cost perspective, LR-PCM is more attractive than SS-PCM, since LR-PCM evaluation produces only negligible cost to a comparable gas-phase calculation, and free of the iterative nature of the full SS-PCM approach. For the formulation of the LR-PCM approach, the PCM electrostatic energy (G_{elst}) is given the form

$$G_{elst} = \frac{1}{2} \int \varphi(\mathbf{s}_1) \hat{Q}(\mathbf{s}_1, \mathbf{s}_2) \varphi(\mathbf{s}_2) \, d\mathbf{s}_1 d\mathbf{s}_2 \tag{2.112}$$

where $\hat{Q}(\mathbf{s}_1, \mathbf{s}_2)$ is the kernel ofthe solvent-response operator. With $\hat{Q}$ the linear-response PCM solvation-corrected excitation energy $\hbar\omega_{k,0}^{neq,LR}$ is given by

$$\hbar\omega_{k,0}^{neq,LR} = \hbar\omega_k^{(0)} + \langle \Psi_k | \hat{V} | \Psi_0 \rangle \, \langle \Psi_0 | \hat{Q}^f | \Psi_k \rangle \tag{2.113}$$

where $\langle \Psi_k | \hat{V} | \Psi_0 \rangle$ is the electrostatic potential arising from the transition density $\rho_{k,0}^{tr}$ (dependent on the transition dipole moment of the excitation), and $\langle \Psi_0 | \hat{Q}^f | \Psi_k \rangle$ the fast surface charge induced by $\rho_{k,0}^{tr}$. This dependence on the transition dipole moment is the most problematic aspect of the LR-PCM formalism, since the LR-PCM solvation correction vanishes for optically forbidden (dark) excited states. This inherent flaw, renders the application of LR-PCM for, e.g., TADF emitters, completely pointless since charge-transfer states can easily feature nearly vanishing oscillator strenghts/transition dipole moment, but should at the same time experience a very large dielectric stabilization from the solvent environment, which is in this case not recoverable in the LR-PCM framework.

CHAPTER 3

PCM-ROKS for the Description of Charge-Transfer States in Solution: Singlet-Triplet Gaps with Chemical Accuracy from Open-Shell Kohn-Sham Reaction-Field Calculations

Lukas Kunze,[†] Andreas Hansen,[†] Stefan Grimme,[†] Jan-Michael Mewes,[†]

Received: 16 July 2021
Published online: 27 August 2021

Reprinted in Appendix A (adapted) with permission[‡] from
L. Kunze, A. Hansen, S. Grimme, and J.-M. Mewes, *PCM-ROKS for the description of charge-transfer states in solution: Singlet-triplet gaps with chemical accuracy from open-shell Kohn-Sham reaction-field calculations*, J. Phys. Chem. Lett. **12** (2021) 8470, DOI: 10.1021/acs.jpclett.1c02299

Own contributions

- compilation of the benchmark set and data
- performing all quantum-chemical calculations
- statistical analysis and interpretation of the results
- first draft and co-writing of the manuscript

[†]Mulliken Center for Theoretical Chemistry, Clausius Institute for Physical and Theoretical Chemistry, University of Bonn, Beringstr. 4, 53115 Bonn, Germany
[‡]Permission requests to reuse material from this chapter should be directed to the American Chemical Society.

A small adiabatic energy gap between the lowest singlet and triplet excited state (ST gap) is one of the key characteristics of TADF emitters.[167–169] However, for DA-TADF emitters in particular the modeling of the adiabatic singlet-triplet is challenging via common computational methods such as TD-DFT,[84,148,149] due to two main reasons. Firstly, TD-DFT suffers from the well-known charge-transfer failure, which consequently is detrimental for the modeling of low-lying CT states in DA-TADF emitters.[79,158] Secondly, the popular LR-PCM[170,171] excited-state solvation model fails to capture the significant dielectric stabilization of CT states in solution due to their often vanishing transition densities.[89,169]

To address the limitations in modeling DA-TADF emitters, we tested two state-specific approaches: unrestricted Kohn-Sham (ΔUKS)[85,86] and restricted open-shell Kohn-Sham (ΔROKS)[88,172,173], combined with an equilibrium PCM,[89,174,175] for calculating the adiabatic ST gap of TADF emitters in solution. In order to assess our approach, we compiled the STGABS27 benchmark set, including 27 (mostly) DA-TADF emitters, for which accurate experimental adiabatic ST gaps are available. We focused on literature studies, in which the experimental ST gaps were obtained from temperature-dependent measurements of either the TADF rate or the rISC rate.[176] Molecular geometries were optimized for the lowest singlet and the triplet excited state of the TADF emitters in solution, via either UKS or ROKS, and the energy difference between singlet and triplet taken as the adiabatic ST gap. We tested three different RSH functionals, LC-ωPBE,[177] CAM-QTP(01),[178] and ωB97M-V,[127,179] in the double-ζ def2-SVP basis set,[162] and applied a global dielectric constant of $\varepsilon = 2.38$ (toluene) in the solvent model for all molecules. Optimal tuning[126,128,129] of the range-separation parameter ω was carried out for each RSH functional (denoted "OT-"), to get molecule-specific optimal ω values for each molecule-functional combination. Additionally, functional variants with average-tuned ω-values were assessed (denoted "FX"), where all molecule-specific optimal ω values (from OT) for a particular functional for the subset A of the STGABS27 benchmark were averaged.

In preliminary testing on a 15-molecule benchmark subset, we demonstrated that OT-LC-ωPBE, OT-ωB97M-V, and OT-CAM-QTP(01) perform all exceptionally well with mean absolute deviations (MADs) below 1 kcal/mol ($\approx$ 0.045 eV), indicating small functional dependence of ΔDFT methods. ΔROKS performs slightly better than ΔUKS independent of the functional with MADs for the best performer OT-ωB97M-V of 0.023 eV (ΔROKS) and 0.037 eV (ΔUKS), and mean deviations (MDs) of –0.009 eV (ΔROKS) and –0.019 eV (ΔUKS), respectively. Importantly, OT-functionals and FX-functionals performed nearly identical with differences in MADs and MDs between ST gaps of around 0.002 eV, well below the average errors. This is a significant finding, since the functional-specific averaged ω value can simply be used for all molecules without the considerable computational overhead of the optimal tuning procedure, which has roughly the cost of a full geometry optimization. Noteworthy, is also the small basis set dependence of the adiabatic ST gap, as the def2-SVP basis provides virtually converged results, which is most probably due to fortuitous error cancellation.

For the whole STGABS27 benchmark set, the combination of ΔROKS/OT-ωB97M-V achieves the best results (MAD: 0.022 eV, MD: –0.001 eV), with only few calculated ST gaps deviating more than ±0.05 eV from the experimental reference. Additionally, calculations for ΔUKS using the PBE0-D4 functional show very promising results (MAD: 0.029 eV, MD: –0.007 eV), and further underline the robustness of ΔDFT methods, since even the simple parameter-free PBE0 model can achieve exceptional accuracy. In contrast, Tamm-Dancoff[180,181] approximated TD-DFT calculations with the

OT-LC-ωPBE functional and LR-PCM give large errors (MAD: 0.205 eV, MD: 0.199 eV), making TDA/TD-DFT unsuitable for any predictive calculation of the ST gap involving CT states.

Overall, this work demonstrates the remarkable performance of both ΔROKS/PCM and ΔUKS/PCM for the calculation of adiabatic ST gaps for DA-TADF emitters in solution. Neither approach suffers from the CT failure of TD-DFT even for global hybrid functionals, and both approaches give accurate CT state descriptions via the inclusion of excited-state specific orbital relaxation. Since ΔDFT is state-specific, the dielectric stabilization excited-state arising from the solvent environment could be accurately modeled via a simple equilibrium PCM solvation approach.

CHAPTER 4

Benchmarking Charge-Transfer Excited States in TADF Emitters: ΔDFT Outperforms TD-DFT for Emission Energies

Thomas Froitzheim,[†¶] Lukas Kunze,[†¶] Stefan Grimme,[†] John M. Herbert,[‡] Jan-Michael Mewes[§]

Received: 21 January 2022
Published online: 4 April 2022

Reprinted in Appendix B (adapted) with permission[‖] from
T. Froitzheim, L. Kunze, S. Grimme, J. M. Herbert, and J.-M. Mewes, *Benchmarking charge-transfer excited states in TADF emitters: ΔDFT outperforms TD-DFT for emission energies*, J. Phys. Chem. A **128** (2024) 6324, DOI: 10.1021/acs.jpca.4c03273

Own contributions

- compilation of experimental emission data
- performing the ΔUKS and ΔROKS calculations
- statistical analysis of ΔUKS and ΔROKS calculations
- co-writing the manuscript

[†]Mulliken Center for Theoretical Chemistry, Clausius Institute for Physical and Theoretical Chemistry, University of Bonn, 53115 Bonn, Germany
[‡]Department of Chemistry and Biochemistry, The Ohio State University, Columbus, Ohio 43210, United States
[§]beeOLED GmbH, Niedersedlitzer Str. 75c, 01257 Dresden, Germany
[¶]These two authors contributed equally.
[‖]Permission requests to reuse material from this chapter should be directed to the American Chemical Society.

The fluorescence energy is a fundamental property of TADF emitters and important for their targeted design for use in electroluminescent applications including displays for televisions, smartphones, and computer monitors. Computational determination of the fluorescence wavelength can help speed-up the discovery of novel color-pure emitters, and can also be used to fine-tune the emission wavelength of existing ones via molecular modifications. In this study, we build on our previous work on the ST gap of TADF emitters, see Chapter 3, and extended our benchmark set to include experimental fluorescence (emission) energies, naming this new set STGABS27-EMS. We assess three density functional theory methods for the calculation of emission energies: TDA-DFT, ΔUKS, and ΔROKS, in combination with PCM solvation approaches. In our study on ST gaps, it was sufficient to apply an equilibrium state-specific polarizable continuum solvation model (SS-PCM),[171,182,183] since the singlet and triplet excited state could be assumed to be fully equilibrated with the solvent environment. However, the emission process (electronic transition) occurs on a shorter timescale than the geometric relaxation process of the solvent molecules, which invalidates the use of the equilibrium SS-PCM for the electronic ground-state. Therefore, a nonequilibrium solvation treatment for the electronic ground state, where only the fast (electronic) degrees of freedom of the solvent are relaxed, needs to be considered.

As part of this study, one of us (T. F.) implemented a nonequilibrium solvation model, the perturbative state-specific PCM (ptSS-PCM)[89,183] for ΔDFT methods in the Q-Chem program,[184] which we tested in combination with ΔUKS and ΔROKS. In all ΔDFT calculations the singlet excited-state was fully equilibrated with the environment via the equilibrium SS-PCM. Dielectric constants and optical dielectric constants, which scale the solvent response for the fast and slow relaxation in the ptSS-PCM approach, were chosen to reflect the experimental conditions as close as possible. We tested multiple density functionals: global hybrids with fixed amounts of Fock exchange (HFX), PBE0[123] (25% HFX) and PBE38[185] (37.5% HFX), and optimally tuned RSH functionals, OT-LC-ωPBE-D4,[140,142,143] OT-LRC-ωPBEh-D4[186] and OT-ωB97M-V. Fluorescence energies were calculated at the optimized excited-state geometries, as vertical transitions the electronic ground-state, neglecting (zero-point) vibrational contributions.

In the combinations with either the SS-PCM or the ptSS-PCM solvation model, ΔUKS and ΔROKS consistently outperformed TDA-DFT, with roughly 0.1 eV lower MADs, comparing best-performing functionals. Additionally, TDA-DFT exhibited a strong density functional dependence, with results ranging from the worst-performing PBE0-D4 (MAD: 0.76 eV) to the best-performing OT-LRC-ωPBEh-D4 (MAD: 0.19 eV). In contrast, ΔUKS significantly reduces functional dependence compared to TDA-DFT, while ΔROKS virtually eliminates it. For ΔUKS, OT-ωB97M-V performed best (MAD: 0.1 eV), while for ΔROKS several functionals, OT-ωB97M-V, PBE0-D4, and OT-LRC-ωPBEh-D4, showed similar performance with a MAD of 0.13 eV. One key factor for accuracy from a functional standpoint is the amount of HFX and if applicable the ω value of the functional. PBE38-D4 (37.5% HFX) is for all three methods either significantly better than PBE0-D4 (25% HFX)(TDA-DFT and ΔUKS) or about as good as PBE0-D4 (ΔROKS). Among optimally tuned RSH functionals and for all three computational methods, a fixed amount of HFX seems to generally work better (OT-LRC-ωPBEh-D4 20% fixed HFX, OT-ωB97M-V 15% fixed HFX) than none (OT-LC-ωPBE-D4 0% fixed HFX).

Moving on to solvation models, the LR-PCM for TDA-DFT fails recover the crucial dielectric stabilization of the involved singlet CT states, almost doubling the MADs in comparison to ptSS-PCM

(for OT-ωB97M-V, ptSS-PCM MAD: 0.21 eV and LR-PCM MAD: 0.37 eV). For ΔDFT methods, the difference to full equilibrium SS-PCM for both ground and excited state is less pronounced (for OT-ωB97M-V, ptSS-PCM MAD: 0.10 eV and SS-PCM MAD: 0.14 eV). This is, firstly, due to the fact that the SS-PCM at least correctly recovers the dielectric stabilization for the excited state, which TDA-DFT/LR-PCM lacks, and slightly overestimates solvent stabilization for the ground state. Secondly, for a large majority of cases the parameters for the solvation model which scale the slow solvent response (ε) and fast solvent response (n^2) are very similar, e.g, for toluene (ε = 2.37, n^2 = 2.25). For systems p-AC-DBNA and m'-AC-DBNA (in dichloromethane, ε=8.93, n^2=2.03), this is not the case and ptSS-PCM corrects the emission energies very well and gives much better fluorescence energy estimates than the same methods with equilibrium SS-PCM, see Fig. 4.

Overall, this study demonstrates the exceptional performance of ΔDFT approaches in calculating emission energies of CT states in the modeling of donor-acceptor type TADF emitters. In agreement with our previous results for ST gaps, ΔDFT consistently outperforms TDA-DFT-based approaches and reveal the unsuitability of nonequilibrium LR-PCM solvation approaches for modeling CT states in solution.

CHAPTER 5

ΔDFT Predicts Inverted Singlet-Triplet Gaps with Chemical Accuracy at a Fraction of the Cost of Wave Function-Based Approaches

Lukas Kunze,[†] Thomas Froitzheim,[†] Andreas Hansen,[†] Stefan Grimme,[†] and Jan-Michael Mewes[†‡]

Received: 3 June 2024
Published online: 31 July 2024

Reprinted in Appendix C (adapted) with permission[§] from
L. Kunze, T. Froitzheim, A. Hansen, S. Grimme, and J.-M. Mewes, *ΔDFT predicts inverted singlet–triplet gaps with chemical accuracy at a fraction of the cost of wave function-based approaches*, J. Phys. Chem. Lett. **15** (2024) 8065, DOI: 10.1021/acs.jpclett.4c01649

Own contributions

- compiling the INVEST15 benchmark set
- performing all LR-CC2 benchmark reference calculations
- performing all ΔDFT calculations
- statistical analysis and interpretation of the results
- first draft and co-writing of the manuscript

[†]Mulliken Center for Theoretical Chemistry, Clausius Institute for Physical and Theoretical Chemistry, University of Bonn, Beringstr. 4, 53115 Bonn, Germany
[‡]beeOLED GmbH, Niedersedlitzer Str. 75c, 01257 Dresden, Germany
[§]Permission requests to reuse material from this chapter should be directed to the American Chemical Society.

The reverse intersystem crossing (rISC) process of singlet into triplet excitons is dependent on the size of the singlet-triplet energy gap (ST gap) of the emitting molecule.[169] For inverted ST gap molecules (INVEST), the lowest singlet excited state (S_1) is lower in energy than the lowest triplet excited state. This gap inversion changes the typically unfavorable up-conversion rISC process into a thermally more favorable down-conversion process.[187] However, most known INVEST molecules exhibit no appreciable oscillator strength from the S_1, which severely limiting their application in OLEDs.[188] A solution to this challenge, lays in the exploration of the vast chemical space via theoretical screening methods, which could greatly expedite the discovery of INVEST molecules with non-zero oscillator strength from the S_1. Unfortunately, TD-DFT fundamentally lacks the ability to reproduce the ST gap inversion,[189] whereas high-level WFT approaches become impractically costly as system size increases.

In this study, we assessed the performance and viability of ΔUKS, ΔROKS, TDA-DFT, and WFT methods for the theoretical computation of ST gaps of INVEST molecules. We compiled the INVEST15 benchmark set, consisting of of 14 INVEST molecules plus 1 non-INVEST molecule (as a sanity check), for which state-of-the-art high-level coupled-cluster with single, double and triple excitations (CC3/CCSDT) vertical ST gap references are available.[190] After assessing the performance of our chosen methods on the INVEST15 set, we used a literature-known[191] significantly more extensive set comprised of 159 non-alternant hydrocarbon INVEST molecules to validate our best-performing screening approaches.

Starting with the computed vertical ST gap results for the INVEST15 set, WFT methods such as LR-CC2[77] and Mukherjee's multireference coupled-cluster of singles, doubles and approximate triples (Mk-MR-CCSD(T))[192–195] on a CAS(2,2) reference agree remarkably well with the TBE (MAD: 0.016 eV for LR-CC2, MAD: 0.031 eV for Mk-MR-CCSD(T)), with LR-CC2 having a slight edge in accuracy compared to Mk-MR-CCSD(T). Earlier studies[196] based on state-specific ΔCCSD(T)[197] calculations of INVEST molecules suggested that the ST gap inversion vanishes for larger basis sets (cc-pVTZ).[198,199] Our own calculations, however, do not support this finding, providing inverted ST gaps at both ΔCCSD(T)@UHF and ΔCCSD(T)@PBE0 level with the cc-pVTZ basis set for all but one system (3).

For all DFT-based methods, we tested the PBE, FX175-ωPBE,[1] PBE0, PBE38, PBE50,[200] and LC-ωPBE functional. With all these functionals, the ΔUKS method was able to reproduce the ST gap inversion, while yielding remarkably accurate results with functionals employing moderate amounts of Fock exchange (HFX, PBE0 and FX175-ωPBE). An optimal amount of HFX for global hybrids is reached at the PBE0 level (25% HFX), resulting in an impressive MAD of 0.035 eV, comparable to Mk-MR-CCSD(T). We suspect that ΔUKS via excited-state specific orbital relaxation is able to mimic the inclusion of doubly excited determinants and the consequential dynamic spin-polarization, the reason for the gap inversion.[201] This is indicated by the growing spin-contamination of the ΔUKS singlet excited state with increasing amounts of HFX. In contrast to ΔUKS, ΔROKS fails to reproduce the ST gap inversion and is unable to reproduce relative trends between inverted ST gaps in the INVEST15 set. Similar to ΔROKS, irrespective of the underlying functional, ST gaps computed via TDA-DFT are always positive for all molecules, caused by the lack of doubly excited determinants (relative to the ground-state). Inclusion of excited determinants beyond the single-excited determinants in TD-DFT by using double-hybrid functionals, i.e., a hybrid method of TD-DFT with the CIS(D) method, corrects the lack of gap inversion and overall improves results dramatically.[202,203] We noticed,

however, that the energy lowering of the S_1 is very systematic across the INVEST15 molecules. For example, TDA-PBE0 reproduces relative trends in the ST gap extremely well, reflected in the remarkably good standard deviation (SD: 0.075 eV), despite all ST gaps being positive. Indeed, shifting all TDA-PBE0 computed ST gap by –0.4 eV gives reasonable agreement (MAD: 0.055) with LR-CC2 reference values.

Aside from the outstanding performance of ΔUKS, calculated vertical ST gap show no significant basis set dependence, reaching sufficiently converged results with already def2-SVP basis set. The resulting method, ΔUKS/PBE0/def2-SVP, is two orders of magnitude faster than high-level WFT methods, i.e. LR-CC2/aug-cc-pVTZ, for a system of roughly 50 atoms.

After assessing theoretical methods on the INVEST15, we tested this exact approach, ΔUKS/PBE0/def2-SVP, for the diverse NAH159 set in a screening setting and compare to our own LR-CC2/aug-cc-pVTZ references of this benchmark set. To find the lowest excited states for ΔUKS in a black-box fashion, we calculate all singlet and triplet excited states including HOMO, HOMO-1, LUMO and LUMO+1, which is comparable to increasing the number of roots in, e.g., linear-response and excitation-based methods. We dubbed this approach PBE0@2x2, which in 83% of cases of the NAH159 computed the correct sign of the ST gap, reaching an excellent MAD of 0.053 eV.

Overall, this study establishes and showcases the great potential of the ΔUKS/PBE0 for use in screening applications for novel INVEST emitters. ΔUKS/PBE0 is robust and computationally efficient, overcoming fundamental limitations of conventional TD-DFT approaches, and opening new ways for the rational design of INVEST emitter for OLED applications.

CHAPTER 6

The Best of Both Worlds: ΔDFT Describes Multiresonance TADF Emitters with Wave-Function Accuracy at Density-Functional Cost

Lukas Kunze,[†] Andreas Hansen,[†] Stefan Grimme,[†] Jan-Michael Mewes,[†‡]

Received: 4 November 2025
Published online: 23 January 2025

Reprinted in Appendix D (adapted) with permission[§] from
L. Kunze, A. Hansen, S. Grimme, and J.-M. Mewes, *The best of both worlds: ΔDFT describes multiresonance TADF emitters with wave-function accuracy at density-functional cost*, J. Phys. Chem. Lett. **16** (2025) 1114, DOI: 10.1021/acs.jpclett.4c03192

Own contributions

- re-evaluation and compilation of experimental reference data
- performing all quantum chemical calculations
- statistical analysis and interpretation of results
- first draft and co-writing the manuscript

[†]Mulliken Center for Theoretical Chemistry, Clausius Institute for Physical and Theoretical Chemistry, University of Bonn, 53115 Bonn, Germany
[‡]beeOLED GmbH, Niedersedlitzer Str. 75c, 01257 Dresden, Germany
[§]Permission requests to reuse material from this chapter should be directed to the American Chemical Society.

Multiresonance thermally activated delayed fluorescence (MR-TADF) hold several advantages over DA-TADF emitters, exhibiting narrower emission bands, and higher quantum yields.[204] MR-TADF represent a bridge between INVEST and DA-TADF, encompassing features of both, which makes the theoretical modeling of these emitters challenging. Similar to INVEST emitters, TD-DFT struggles to accurately capture singlet excitation energies for MR-TADF emitters, rendering it unsuitable for computation of ST gaps and fluorescence energies. High-level WFT methods, e.g., LR-CC2 and EOM-CCSD[78] can accurately model the ST gap, but are ultimately limited in their scope due to their high computational cost and disadvantageous scaling with system size.

In this work, we put the state-specific ΔDFT approaches, ΔUKS and ΔROKS, and also TDA-DFT to the test in modeling the ST gap and fluorescence (emission) energies of MR-TADF emitters in solution. We use the systems from a benchmark study compiled by Hall and coworkers,[205] comprised of 35 MR-TADF emitters with a diverse set of doping and substitution patterns. For these 35 emitters, the experimental ST gaps were determined from the difference of the fluorescence and phosphorescence energy (estimated from the peak of the fluorescence and phosphorescence spectra). This is justified, because the emission spectra of MR-TADF emitters are very narrow and therefore should be reaonably accurate for the calculation of the ST gap, since vibrational components (between singlet and triplet excitation energies) are likely to cancel out. Our study, examines a variety of different density functionals, including PBE0, PBE38, PBE50, LC-ωPBE, ωB97M-V, LRC-ωPBEh, and RSHs, i.e., FX175-LC-ωPBE, FX155-ωB97M-V[1] and OT-LC-ωPBE. Early tests on the basis set dependence of the ST gap showed no substantial benefit for going beyond double-ζ quality, in our case def2-SVP.

Starting with vertical ST gaps calculated in the gas phase, we found ΔUKS to reproduce experimental ST gaps exceptionally well. Especially RSHs with a moderate ω value (around $0.2a_0^{-1}$) performed best (LRC-ωPBEh MAD: 0.026 eV) beating even spin-component scaled CC2 (SCS-CC2, MAD: 0.038).[205,206] Tuned RSHs (with smaller ω values, FX175-ωPBE and FX155-ωB97M-V) also gave very reasonable results (MADs around 0.03-0.04 eV) but underestimated larger ST gaps. Global hybrid functionals (PBE0, PBE38, PBE50) systematically underestimated the ST gaps by roughly 0.08 eV, clearly apparent due to the fact that –MAD=MD. However, especially PBE0 reproduced relative trends remarkably well, reflected in its SD (0.031 eV) being the lowest of all tested functionals. The key factor which determines a functionals accuracy for ST gaps proved to be the mixing of HFX and the ω value, while underlying DFA played usually a minor role. In contrast to this, in ΔROKS calculations all functionals performed very similarly, estimating the ST gap across all systems in the ballpark of 0.15 to 0.25 eV without reproducing relative trends between systems. This leads to reasonable MADs for most tested functionals ($\approx$ 0.05 eV), since the majority of experimental ST gaps in this benchmark are roughly of that size, but bad correlation with experimental ST gaps. Unexpectedly, TDA-DFT displays large errors with the best MAD (0.311 eV) for the B3LYP[207] functional. Still, we observed, similar to our previous study on INVEST systems, that the error in the ST gaps is very systematic for TDA-DFT. Application of a shift of roughly –0.4 eV corrects, e.g., TDA-FX155-ωB97M-V results substantially (MAD: 0.058).

Solvation effects (modeled by a PCM) on calculated ST gaps are minuscule with differences between gas-phase and condensed-phase gaps being –0.01 eV on average, with the largest changes seen in carbonyl-function-containing MR-TADF emitters. We reasoned that the absence of a significant impact of solvation effects arises from the small change in electric dipole moment upon excitation in

MR-TADF emitters.

The computation of emission energies needed different set-up requirements, hence we used the larger def2-TZVP(-f)[162] basis set, our previously (see Chapter 4) established ptSS-PCM nonequilibrium solvation model and optimized the geometry of the first singlet excited state. For emission eneriges, both ΔUKS and ΔROKS provided similarly good results, with ΔROKS's emission energies are consistently slightly lower than ΔUKS's. From our results, we determined that large amounts of HFX (and range-separation) in the functional are detrimental for the accuracy of emission energies (LRC-ωPBEh, MAD: 0.191 eV). On the flip side, too small amounts of HFX (and no range-separation) as in PBE0 are also damaging performance (–MAD=MD=0.155 eV), although PBE0's SD of only 0.071 eV is again remarkable. FX175-ωPBE sits in the middle and provides the best results with a MAD of 0.090 eV (ΔUKS), while working slightly worse in combination with ΔROKS (MAD: 0.105 eV). This makes ΔUKS, the only method for efficiently calculating fluorescence energies for MR-TADF emitters, since TD-DFT is systematically wrong and SCS-CC2 too computationally demanding to perform geometry optimizations in a reasonable timeframe.

Overall, we demonstrated that ΔUKS is able to provide outstandingly accurate results for both the ST gap and fluorescence energies of MR-TADF emitters at a fraction of the cost of high-level WFT methods. We also identified ways to cut cost in screening applications of ST gaps, i.e., by omitting the use of a solvation model and excited-state geometry optimization, since no accuracy or robustness is lost from their omission. We identify the FX175-ωPBE functional to work reasonably well across all tested systems of this and our previous works, delivering good estimates for ST gaps and excitation energies (emission energies) for DA-TADF, MR-TADF and INVEST systems. This work establishes ΔUKS as the best computational method in terms of accuracy-to-cost ratio for high-throughput screening applications of MR-TADF systems.

CHAPTER 7

Summary and Outlook

In nearly every field of chemistry, researchers are confronted with the challenge of exploring an almost limitless space of chemical compounds. Systematic exploration of this space via experimental means alone is impossible due to the associated enormous time, resource, and labor demands. Consequently, computational chemistry has emerged as a key tool for addressing this challenge, enabling the navigation of the vast chemical space by quantum chemical methods to screen for properties of interest in hypothetical compounds and selecting promising candidates for experimental evaluation. In the field of optoelectronic materials, the accurate quantum chemical description of excited state energies and properties is challenging, particularly for systems, in which the most prominent approach and workhorse of materials science, TD-DFT, is known to perform poorly. For instance, excited states with significant double excitation character as found in INVEST and MR-TADF emitters as well as charge-transfer excited states in DA-TADF emitters are difficult to accurately describe with TD-DFT (albeit due to different reasons). The efficacy of high-throughput screening workflows have been hindered so far, due to the inaccessibility of robust, accurate, and computationally efficient excited state methods for these types of emitters.

In this thesis, state-specific DFT approaches, namely spin-unrestricted Kohn-Sham (ΔUKS) and spin-restricted open-shell Kohn-Sham (ΔROKS), were assessed in their accuracy and robustness for calculating excited states of various DA-TADF, MR-TADF and INVEST emitters types in solution. Starting with the description of charge-transfer excited states, we compiled the STGABS27 benchmark set for assessing the accuracy of quantum mechanical excited-state methods in reproducing experimental singlet-triplet energy gaps (ST gaps) from reliable temperature-dependent references.[1] The STGABS27 benchmark set examines not only the accuracy and robustness of the employed excited-state method, but also tests the computational solvent model in these simulations. Thus, it serves as a complex stress test for combinations of excited-state electronic structure and environment models. We showed that both ΔDFT approaches give excellent results for adiabatic singlet-triplet gaps in solution (modeled by simple equilibrium PCMs), compared to the experimental references. Related studies employing TD-DFT on the STGABS27 benchmark set demonstrated that with self-consistent state-specific PCM solvation and optimally tuned range-separated hybrid functionals, TD-DFT still displays MADs roughly three times larger compared to ΔDFT.[208] Even TD-DFT with dielectrically screened range-separated

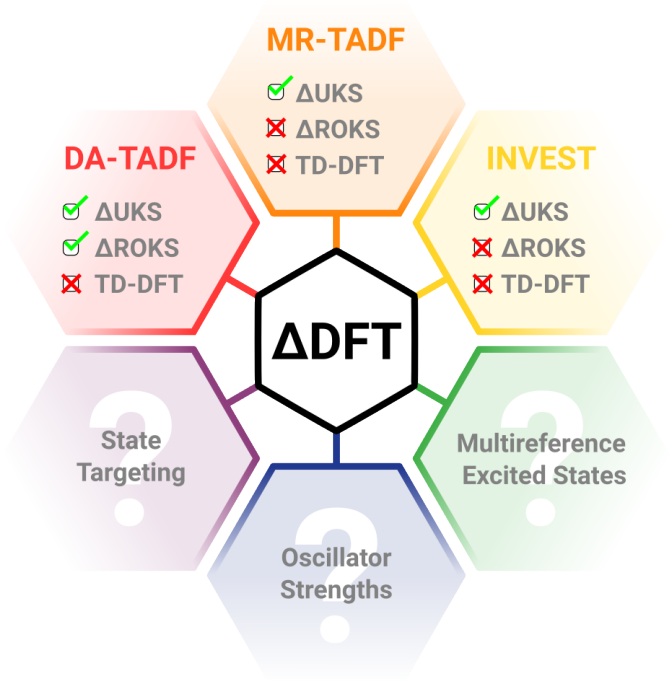

Figure 7.1: Overview of the capabilties and open questions of state-specific density functional theory (ΔDFT).

hybrid functionals which incorporate solvation contributions in the functional, displayed MADs two times larger than ΔDFT approaches for the STGABS27 benchmark.[209] This, in part, confirms our suspicion that the state-specific orbital relaxation is a major reason for the accuracy of ΔDFT approaches, which may also explain ΔDFT's relatively low dependence on the underlying density functional approximation (DFA). Low to moderate functional dependence was observed in the study on singlet-triplet gaps and fluorescence energies of DA-TADF emitters, but also in later studies for ST gaps of MR-TADF emitters. The only systems deviating significantly from this behavior are those with an inverted ST gap, INVEST emitters. Theoretical calculations on INVEST systems have been done previously, but the certain existence of a gap inversion was proven until Aizawa and coworkers showed the first experimental indications for an singlet-triplet inversion.[187] Later, Loos and coworkers confirmed the existence of inverted ST gaps from the side of theory via chemically accurate state-of-the-art WFT calculations.[190] In studying INVEST systems (and to a lesser degree in MR-TADF systems), we saw significant differences for ΔUKS and ΔROKS in accurately describing ST gaps. For ΔUKS, the amount of global and range-separated Fock exchange in the functional strongly affected the resulting ST gaps and excitations energies. The best agreement with the high-level references of Loos and coworkers, provided the PBE0 functional with 25% Fock exchange (HFX). Especially surprising was also the very good performance of the r^{2}SCAN functional,[210] since no other mGGA/GGA/LDA functional was close in accuracy for the modeling of inverted ST gap. In ΔUKS, the spin contamination (deviation from $\langle S^2 \rangle = 1.0$) of the singlet wavefunction increased roughly proportional to the amount of HFX in the functional, which indicates that HFX in state-specific DFT can mimic dynamic spin-polarization by state-mixing, which has been identified to be the underlying mechanism for the ST gap inversion.[201] ΔROKS completely failed to reproduce inverted ST gaps with

any of the tested functionals. We suspect the restricted nature of the two-determinant ROKS singlet wavefunction to be the reason, since ROKS produces spin-pure singlets, effectively eliminating the mechanism by which ΔUKS achieves inverted ST gaps. This failure showed the first indication that ΔUKS may be the overall more accurate theory compared to ΔROKS. In the context of TD-DFT, all functionals of rungs 1-4 of Jacob's ladder fail to reproduce the ST gap inversion, and a study of Derradji and coworkers[203] on double-hybrid functionals specifically tuned for INVEST systems show larger errors than ΔUKS/PBE0 at higher computational cost.

The character of the lowest singlet and triplet excited state of MR-TADF emitters displays similarities to both INVEST and DA-TADF emitters. In our study of 35 MR-TADF emitters, we confirmed our previously observed indications of shortcomings in the foundations of ROKS. ΔUKS provided very accurate ST gaps for the whole test set for many different functionals. Similar to the INVEST systems, ΔROKS performed worse than ΔUKS, especially in reproducing the relative trends in the ST gaps of the benchmark molecules. For ΔUKS, the tuned FX175-ωPBE and untuned LRC-ωPBE range-separated hybrids gave the best agreement with experimentally determined ST gaps. In contrast to DA-TADF emitters, for MR-TADF emitters the environment treatment and also the necessity for excited-state geometry optimization appeared to be negligible for obtaining accurate ST gaps. For ST gaps, ΔUKS presents as clearly superior to ΔROKS and can reproduce experimental and high-level WFT references of ST gaps for DA-TADF, MR-TADF and INVEST systems within chemical accuracy.

Although, the focus of most of our studies was the ST gap, we also examined the performance of ΔDFT approaches for fluorescence energies for DA-TADF emitters and MR-TADF, as well as vertical excitation energies for INVEST emitters. For the calculation of adiabatic ST gaps, an equilibrium PCM solvation model is sufficient and reasonable for accurately capturing the dielectric stabilization of CT states by the solvent environment. In contrast, for fluorescence energies a nonequilibrium PCM (ptSS-PCM) solvation model is necessary since the ground and excited state solvation response happens on different time scales. For the STGABS27 benchmark, the experimental fluorescence energies were compiled into the STGABS27-EMS set, and multiple functional and solvation model combinations tested with TD-DFT and ΔUKS/ΔROKS. Compared to TD-DFT, ΔUKS reduced the MAD of the best-performing functional with the ptSS-PCM solvation model by roughly half (0.2 eV (TD-DFT) to 0.1 eV (ΔUKS)). Additionally, we demonstrated that the commonly applied combination LR-PCM and TD-DFT displayed by far the largest errors (MAD: 0.37 eV), underlining the importance of appropriate (state-specific) solvation models for CT excited states. In the case of MR-TADF emitters, we used a triple-ζ basis set to optimize excited-state geometries and used the ptSS-PCM solvation model in the calculation of fluorescence (emission) energies. Emission energies computed by ΔUKS were in excellent agreement with experimental ones, with the best-performing functional being FX175-ωPBE. No other theoretical method is able to give accurate estimates of this accuracy for MR-TADF emitters, since TD-DFT is fundamentally wrong for reproducing MR-TADF emitters singlet excitation energies. Furthermore, accurate WFT approaches (LR-CC2) are too costly to perform excited-state geometry optimizations, while additionally a sufficient treatment of the solvation environment is difficult. For INVEST emitters, calculated vertical excitation energies were close to LR-CC2 reference values for PBE0 (best-performing functional), indicated by the MAD of roughly –0.2 eV to –0.15 eV for singlets and triplets respectively. Over all benchmark studies, excitation energies and fluorescence energies are reproduced by the ΔUKS approach with MADs of roughly 0.1-0.2 eV and confirms that the good performance of ΔUKS extends beyond the calculation of ST gaps. ΔROKS performs in most parts slightly worse or similar to ΔUKS (DA-TADF and MR-TADF) for excitation energies, but fails as

previously shown for INVEST emitters.

At this point, we note that across all our studies we observed different best-performers among the tested functionals for the particular properties of interest. However, functional differences were relatively small (exception INVEST) and the LCωPBE functional with an ω value of 0.175-0.200 a_0^{-1}, produced consistently accurate excited-state energies in all our studies, be it ST gaps or fluorescence energies. Especially noteworthy is also the mostly non-empirical PBE0 functional, which we applied in contrast to the tuned LC-ωPBE functionals unmodified in all studies. PBE0 produced reasonably good results for the ST gaps of DA-TADF emitters (with ΔUKS), INVEST emitters (best performer with ΔUKS) and MR-TADF emitters (lowest SD with ΔUKS of all functionals). This shows the validity of the PBE0 model, in which the functional parameters were determined based on physical reasoning alone, making it one of the few minimally empirical density functional approximation. One significant drawback of ΔDFT approaches, ΔUKS in particular, is their non-black box nature. Electron and hole orbitals have to be chosen beforehand, and when targeting, for example the lowest excited state, a HOMO-LUMO guess does not necessarily provide the lowest excited-state of the system in question. Finding the lowest excited state is practically a nonissue for triplet excited states, since the spin multiplicity constrains the SCF, and convergence algorithms exist to find global minima for SCF equations. ΔUKS singlet calculations are depend more on the quality and type of initial guess, from which the trial excited-state is manually constructed. The initial guess partially determines the type of final excited state and if the by MOM/IMOM-constrained SCF procedure reaches convergence. This is clear to see in any type of symmetric molecule, where a simple ground-state initial guess of course provides symmetric ground-state orbitals. The trial excited-state from such a guess is then also symmetric, which is enforced in the SCF via MOM/IMOM, even though a symmetry-broken SCF solution would provide a lower excited-state energy in such molecules. This issue is solved in a majority of cases by starting from a converged singlet ΔROKS calculation, as the "ground-state" of the two-determinant ROKS approach we used is an open-shell singlet. Another way to solve this, in the absence of two-determinant ROKS capabilities, and if an implementation of a spin-flip algorithm is accessible to use a converged triplet ΔUKS calculation as initial guess for the singlet calculations. This of course, only solves the problems for finding the lowest singlet and triplet excited states of a systems. Higher-lying excited singlet and also triplet states which display symmetry-breaking are still problematic to access in any case.

The performance of presented approaches for the calculation of excitation energies, vertical and adiabatic, and in particular for singlet-triplet energy gaps is remarkable. However, it is always important to know the limitations of computational methods. Thus it is crucial to know for which systems ΔDFT approaches struggle to give reasonably accurate excited-state energies, geometries and properties. Since, ΔUKS and ΔROKS differ significantly in their construction of the underlying wavefunction, single-determinant (ΔUKS) vs two-determinant (ΔROKS), large differences in their description of excited-states with significant multi-reference character is expected. Presumably, ΔUKS, due to its single-determinant nature, inherits the fundamental limitations of single-reference methods for the description of multi-reference excited states. We observed the largest errors for the calculation of ST gaps via ΔUKS/FX175-ωPBE in MR-TADF emitters with acene-like structures possibly due to this fundamental limitations of UKS. This potentially becomes problematic if ΔUKS is applied to TADF emitters with significant multi-reference character, e.g., emitters from a recent study based on a tetracene as core structure.[211] Therefore, it would be important to assess both approaches for their accuracy with respect to multi-reference excited states, i.e., at which percent of multi-reference

character ΔUKS/ΔROKS become unreliable.

Another venture for ΔDFT methods could be the extension to semi-empirical quantum mechanical (SQM) methods. SQM methods are several magnitudes faster than DFT methods, which accelerates the screening capabilities of simulations dramatically. Particularly, the extended tight-binding method for geometries, frequencies and non-covalent interaction (GFN-xTB/GFN2-xTB)[212,213] or the general-purpose extended tight-binding method (g-xTB)[214] are suitable for this endeavor, as the former has recently received a spin-polarized version (spGFN-xTB),[215] enabling the modeling of different spin multiplicities, while the latter features remarkable DFT-like accuracy and capabilities of range-separated hybrid functionals. Both spGFN-xTB and g-xTB offer huge speedups compared to standard DFT, and may be especially useful in the early steps of multilevel screening workflows. The extension of ΔDFT to semiempirical methods with a SCF procedure is simple as the maximum-overlap methods (MOM/IMOM) can be applied irrespective of the underlying Hamiltonian. With the large speedup that SQM methods offer, it would also become straightforward to study the electron dynamics of excited states via the robust ΔUKS method.

Overall, I demonstrate that state-specific DFT approaches are robust, efficient and accurate and a superior alternative compared to TD-DFT approaches in modeling the excited states of DA-TADF, MR-TADF and INVEST emitters. I identified computational protocols for dealing with the state targeting problem, to make ΔDFT approaches as black-box as possible, and determined density functional combinations with continuum solvation models to accurate account for equilibrium and nonequilibrium solvation effects for excited states. ΔDFT is a great addition in the toolbox of quantum chemistry approaches, where TD-DFT gives a lacking description of the excited state landscape of a system.

APPENDIX A

PCM-ROKS for the Description of Charge-Transfer States in Solution: Singlet-Triplet Gaps with Chemical Accuracy from Open-Shell Kohn-Sham Reaction-Field Calculations

Lukas Kunze,[†] Andreas Hansen,[†] Stefan Grimme,[†] Jan-Michael Mewes,[†]

Received: 16 July 2021
Published online: 27 August 2021

Reprinted in Appendix A (adapted) with permission[‡] from
L. Kunze, A. Hansen, S. Grimme, and J.-M. Mewes, *PCM-ROKS for the description of charge-transfer states in solution: Singlet-triplet gaps with chemical accuracy from open-shell Kohn-Sham reaction-field calculations*, J. Phys. Chem. Lett. **12** (2021) 8470, DOI: 10.1021/acs.jpclett.1c02299

Own contributions

- compilation of the benchmark set and data
- performing all quantum-chemical calculations
- statistical analysis and interpretation of the results
- first draft and co-writing of the manuscript

[†]Mulliken Center for Theoretical Chemistry, Clausius Institute for Physical and Theoretical Chemistry, University of Bonn, Beringstr. 4, 53115 Bonn, Germany
[‡]Permission requests to reuse material from this chapter should be directed to the American Chemical Society.

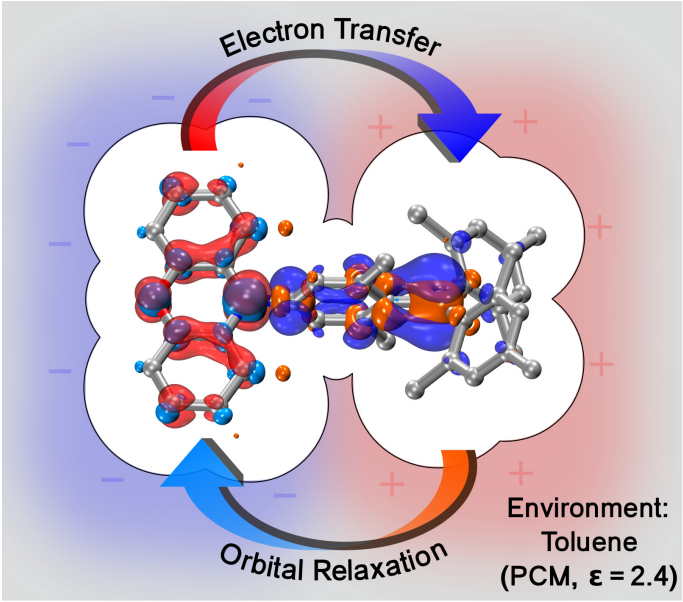

Figure A.1: Table of content graphic (ToC).

Abstract The adiabatic energy gap between the lowest singlet and triplet excited states ΔE_{ST} is a central property of thermally activated delayed fluorescence (TADF) emitters. Since these states are dominated by a charge-transfer character, causing strong orbital-relaxation and environmental effects, an accurate prediction of ΔE_{ST} is very challenging, even with modern quantum-chemical excited-state methods. Addressing this major challenge, we present an approach that combines spin-unrestricted (UKS) and restricted open-shell Kohn-Sham (ROKS) self-consistent field calculations with a polarizable-continuum model and range-separated hybrid functionals. Tests on a new representative benchmark set of 27 TADF emitters with accurately known ΔE_{ST} values termed STGABS27 reveal a robust and unprecedented performance with a mean absolute deviation of only 0.025 eV ($\approx$ 0.5 kcal/mol) and few deviations greater than 0.05 eV ($\approx$ 1 kcal/mol), even in electronically challenging cases. Requiring only two geometry optimizations per molecule at the ROKS/UKS level in a compact double-ζ basis, the approach is computationally efficient and can routinely be applied to molecules with more than 100 atoms.

A.1 Introduction

Materials for organic electronics and organic light-emitting diodes (OLEDs) have become very prominent research topics in recent years.[70,216,217] Central to the function of organic electronics is a transfer of charge in the form of electrons and holes. Accordingly, the study and computational modeling of charge-transfer (CT) excited states have attained great interest. In the mechanism of thermally activated delayed fluorescence (TADF), CT states and the energy gap between the lowest relaxed singlet and triplet states (ΔE_{ST}) are of particular relevance. Here, a recycling of excitons between the singlet and triplet manifolds via an intersystem crossing (ISC) and a reverse ISC (rISC) increases the maximum internal quantum yield fourfold – from 25% for fluorescent emitters to 100% for TADF emitters. For this exciton recycling to be fast and efficient, the molecules require a small

ΔE_{ST}, which exponentially governs the thermal upconversion rate

$$k_{\mathrm{rISC}} \propto \exp\left(-\frac{\Delta E_{\mathrm{ST}}}{k_B \mathrm{T}}\right). \tag{A.1}$$

Typically, for TADF emitters ΔE_{ST} is less than 0.2 eV, as this is necessary for rISC processes to become efficient, while lower values are always beneficial.[217,218] To predict the TADF rate with reasonable accuracy, the error in ΔE_{ST} should ideally be smaller than $k_B T$ at ambient conditions, which is ≈0.025 eV or 0.5 kcal/mol. Although it has in the meantime been established that this upconversion can be aided by spin-vibronic coupling mechanisms,[219–223] and, moreover, that a small gap alone is insufficient, the size of the ΔE_{ST} remains an important criterion. In addition to a small ΔE_{ST}, good emitters need significant a spin-orbit coupling (SOC) between the corresponding states and a large oscillator strength of the emitting singlet state, which are conflicting design goals.[70,217,224] This is because the electron-hole orbitals directly enter the exchange integral that governs ΔE_{ST} but also the integrals for oscillator strength and spin-orbit coupling.[217] A detailed discussion of these quantities and their connection in the framework of different electronic-structure approaches can be found in ref [225]. A comprehensive calculation of TADF and rISC rates for three emitters using a combination of self-consistent field (SCF)-based excited-state methods, time-dependent density functional theory (TD-DFT), and the correlated ab initio method ADC(2) has been presented in ref [169]. A recent study that explores the electronic structure of TADF emitters with state-of-the-art methods can be found in ref [226]. Here we exclusively focus on the quantitative prediction of ΔE_{ST} for a large set of emitters. We do this in part because of its direct relevance for TADF but also because this experimentally well-studied property constitutes a rigorous test of the description of CT states in dielectric environments.

The probably most popular method for studying TADF emitters and their respective singlet-triplet energy gap and, perhaps, also in general CT and materials for organic electronics is TD-DFT, typically in combination with the Tamm-Dancoff approximation (TDA-DFT).[148] This is despite the well-known CT failure of TD-DFT[79] and because more robust wave function-based approaches, like coupled-cluster (CC) or algebraic-diagrammatic construction (ADC), are computationally too demanding for all but the smallest systems of relevance.[79] As a result, they are employed mainly for small systems and testing purposes.[169,227,228] Besides the electronic structure method, also the description of the dielectric environment is crucial for highly polar CT states.[168,169] This is particularly important in TADF emitters, since their lowest triplet state is typically a CT with some admixture from local $\pi\pi^*$ contributions,[169] whose balance is very sensitive to the environment's polarizability. Although highly accurate wave function-based excited-state methods exist, they typically lack the ability to be combined with equilibrium-solvation approaches. Moreover, although most quantum-chemistry programs provide some kind of excited-state solvent method for TD-DFT, the by far most prominent one is the linear-response polarizable continuum model (LR-PCM),[170] which is known to fail in the description of CT states.[169,171,229,230] Only state-specific (also termed corrected LR, cLR)[231] solvent models recover the dielectric stabilization of CT states,[183] but they are, to the best of our knowledge, not available for excited-state optimizations due to a lack of gradients. A workaround for the LR-PCM formalism is to conduct an environment-specific optimal tuning of range-separated functionals.[168] Although this approach appears to mitigate some of the shortcomings of the LR-PCM method, it is not a rigorous model and moreover requires a significant number of additional calculations to obtain

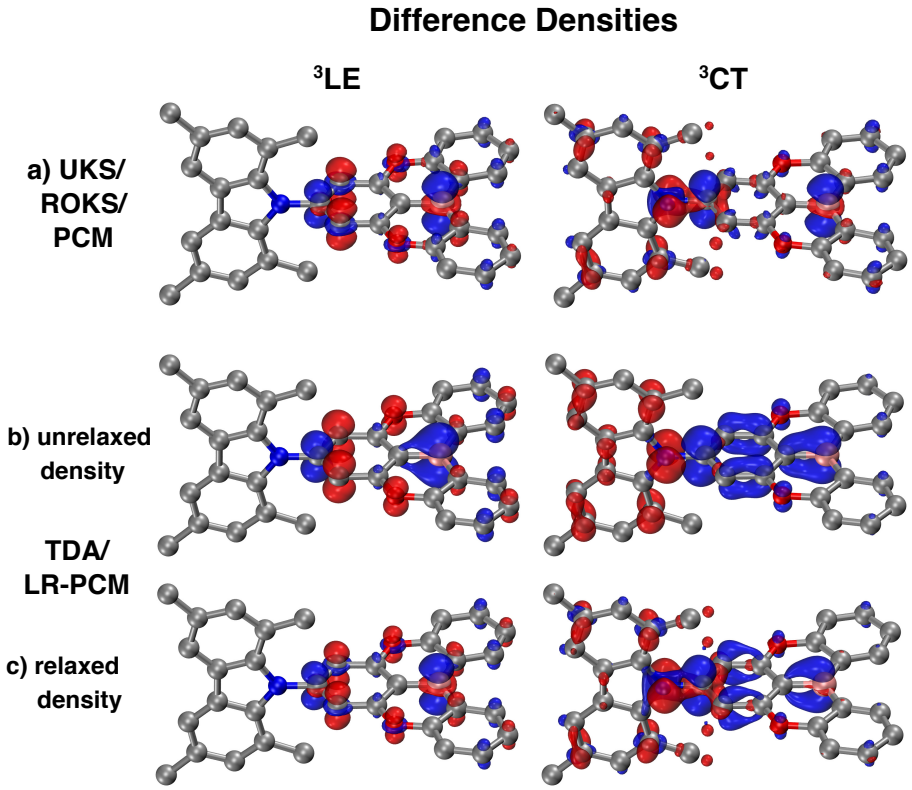

Figure A.2: Difference densities (increase blue, decrease red) of the lowest locally excited triplet (left, ^{3}LE) and the lowest triplet CT state (right, ^{3}CT) of the prototypical TADF emitter TMCz-BO in PPF thin film (ε = 3.5), calculated with (a) ROKS/PCM, (b) TDA-DFT/LR-PCM, and (c) TDA-DFT including orbital relaxation effects via the z-vector equations. Note that ROKS and UKS densities are identical to the eye. Moreover, the difference between the singlet CT (not shown) and triplet CT states is hardly noticable. Isodensity surfaces shown with isovalue of 0.0035 au. Visualization was performed with VMD 1.9.3,[233] difference-densities calculated with Multiwfn 3.7.[234] Calculations are conducted with the OT-LC-ωPBE-D3 functional and the def2-SVP basis set.

the range-separation parameter for each molecule/solvent pair. Furthermore, this approach has been shown to be problematic for CT states.[232]

Nevertheless, the quantitative prediction of ΔE_{ST} for a representative set of emitters has previously been attempted by several groups, for example, by Brédas and co-workers using TD(A)-DFT with optimally tuned (OT)[235] range-separated hybrid functionals (RSHs), the LR-PCM, and specific workflows to circumvent some of the problems, involving, for example, unrestricted Kohn-Sham (UKS)/CAM-B3LYP optimizations of triplet states with a PCM followed by single points with TD(A)-DFT.[167] The best-performing method in this study was the OT-LC-ωPBE functional, for which they reported a mean absolute deviation (MAD) of 0.09 eV, which reduced to 0.07 eV when the gaps were calculated in the vertical approximation, that is, at the ground-state geometry. Most notably, the LC-ωPBE[124,186] with the default range-separation parameter was among the worst performers in their study. While this illustrates the capability of optimal tuning to mitigate the CT-failure of TD-DFT, it at the same time reveals that the results are highly sensitive to those parameters, which must be determined for each system.

Also an SCF-based prediction of ΔE_{ST} has already been attempted by Hait and Van-Voorhis, who surveyed 27 compounds with four different functionals (PBE,[108] PBE0,[123] B3LYP,[207] and LC-ωPBE[124,186]) using spin-restricted open-shell Kohn-Sham (ROKS), yet without any solvent model.[172] They found that the B3LYP functional performed best with a mean deviation and root-mean-square deviation of 0.02 eV and 0.14 eV, respectively. Surprisingly, the RSH performed much worse with an MD/RMSD of 0.66/0.70 eV, which is presumably due to the lack of any solvent model in the calculation and optimal tuning (*vide supra*). Further recent attempts have been made with mixed success using the particle-particle random-phase approximation (ppRPA),[227] and second-order quasi-degenerate perturbation theory.[228]

Shee and Head-Gordon studied the performance of RSH functionals in combination with TD-DFT and solvent models for a set of 61 emitters, focusing on absorption and emission energies in the gas phase and different solvents rather than singlet-triplet gaps.[130] For the TADF emitter subset containing 21 compounds exhibiting CT character emission, they found that the optimally tuned LRC-ωPBE functional performed best with an MD, MAD and absolute maximum deviation (AMAX) of 0.11 eV, 0.18 eV, and 0.34 eV respectively. For four cases in which TD-DFT clearly failed, they reported that the ROKS approach leads to a much improved agreement.

In this work, we model the low-lying excited states of TADF emitters with ROKS[87,88,172,173,236] and unrestricted Kohn-Sham (UKS) calculations (often termed the ΔSCF approach) in combination with a polarizable-continuum model (PCM)[174,175,237,238] and modern (tuned, range-separated) hybrid functionals (RSHs)[124,186] as implemented in the Q-Chem 5 program.[239,240] As such, the approach explicitly accounts for orbital-relaxation effects (see Fig. A.2) and rigorously includes the interaction with a fully equilibrated dielectric environment (solvent) in a state-specific fashion via the "ground state" PCM.[169] We moreover present a practical workflow that combines the strengths and eliminates weaknesses of the ROKS and UKS approaches, building on the experience from an earlier study that employed the UKS/PCM approach together with the maximum-overlap method (MOM).[169] For the sake of comparability, we also report results obtained with the prominent but problematic TDA-OT-LC-ωPBE/LR-PCM approach.

Finally, we point out that, despite the focuses on the prediction of ΔE_{ST} of TADF emitters, the presented approaches are by no means limited to this application. Instead, ΔE_{ST} serves as a convenient, because experimentally well-investigated property to benchmark the performance for the description of CT states in dielectric environments. Moreover, ROKS/UKS/PCM is, to the best of our knowledge, the only practical approach that allows an optimization of structures of CT excited states in solution with a fully equilibrated solvent. The resulting structures are thus a valuable starting point for further calculations of transition properties with other methods such as TD-DFT/SS-PCM. As demonstrated in ref[169], such a combined approach (in this case TD-DFT//UKS/PCM) can provide TADF and rISC rates in good agreement with the experiment.

A.2 Benchmark Set

To thoroughly test the approach, we composed a representative set of structurally manifold TADF emitters. Key data of the selected molecules are summarized in Table A.1, while their structures are shown in Figure A.3.

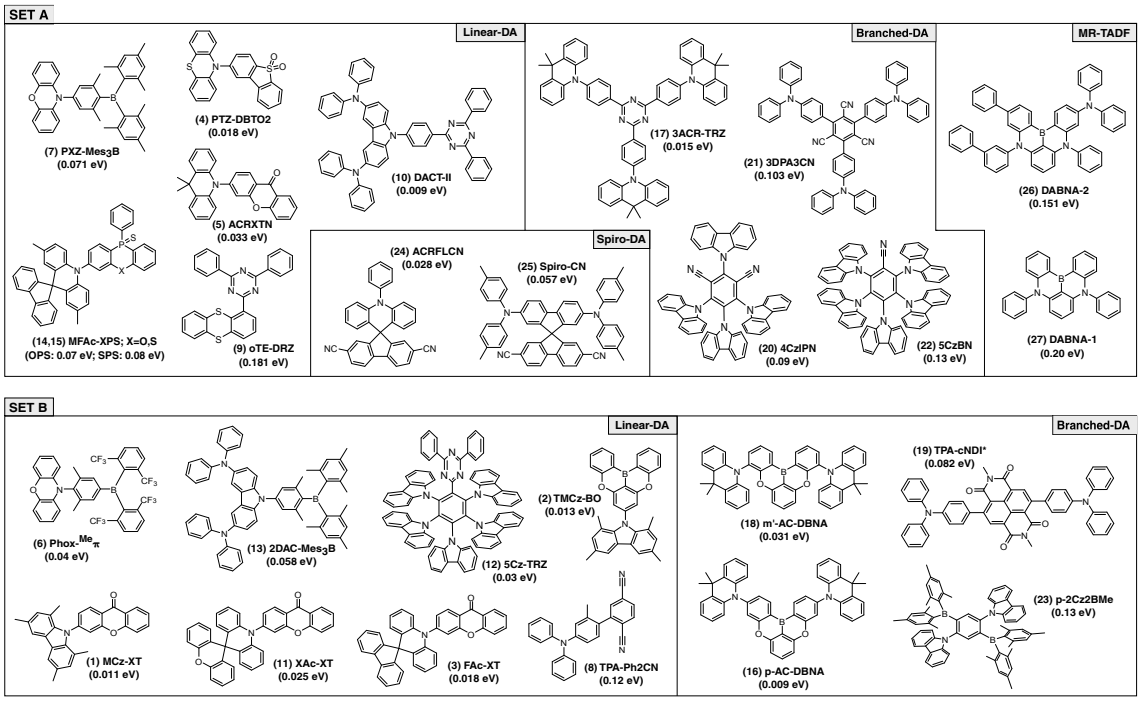

Figure A.3: Lewis structures, numbers, names, and experimentally determined singlet-triplet gaps of the TADF emitters contained in the STGABS27 test sorted by the type of the emitter.

A crucial aspect when compiling such a benchmark of singlet-triplet gaps with small absolute values (0.0-0.2 eV) is the accuracy and reliability of the experimental data. This can be illustrated using the above-mentioned work of Brédas and co-workers.[167] For the emitter ACRFLCN, their approaches predicted vertical and adiabatic gaps of 0.07 eV and 0.02 eV, respectively. While this deviates significantly from the experimental reference of 0.24 eV used in their study that is based on the peak of the phosphorescence and fluorescence spectra, their prediction agrees well with a more recent and more accurate reference for ACRFLCN of 0.03 eV obtained later *via* the Berberan-Santos method.[176,256] In our experience, estimates for ΔE_{ST} based on emission spectra are inherently unreliable, and we thus only consider emitters whose ΔE_{ST} values are determined with the Berberan-Santos or related methods, *i.e.*, from temperature-dependent measurements of the TADF or rISC rate.[176] Related methods refers to Adachi's approach to obtain ΔE_{ST} from quantum yields and excited state lifetimes, the experimental gaps ACRXTN and DABNA-1 were obtained this way.[259] We term this set of 27 adiabatic **s**inglet-**t**riplet energy **ga**ps from the **B**erberan-**S**antos method STGABS27.

The 27 molecules are split into two sets, namely, A and B. The first representative set A consists of 15 emitters and was subjected to a large series of tests, whose results guided the development of the protocol. The second set B consists of 12 further emitters, which were used to validate the computational protocol. Moreover, the emitters in both sets are grouped into subsets based on their molecular structures to check if there exists a connection with the accuracy of the method: (i) linear-DA with one (sDA) or multiple (mDA, e.g., DACT-II) donor groups linearly connected to one acceptor, (ii) branched-DA (BDA) with multiple donors connected to the same acceptor, (iii) donor and acceptor connected through a spiro-center; (iv) multiresonance (MR) TADF emitters in which

Table A.1: Names, types (explanations are provided in the text), details of the experimental ΔE_{ST} measurement, the experimental value (in eV), and literature references for all emitters of the STGABS27 set. Names were adopted from the original publications except for TPA-Ph2CN, for which no name was provided in the original work.

#	**Name**	Set, Type	Exp. Setup	ΔE_{ST}	Lit.
1	MCz-XT	B, sDA	5 wt%:PPF	0.011	[241]
2	TMCz-BO	B, sDA	30 wt%:PPF	0.013	[242]
3	FAc-XT	B, sDA	5 wt%:PPF	0.018	[241]
4	PTZ-DBTO2	A, sDA	5 wt%:Zeonex	0.018	[220]
5	ACRXTN	A, sDA	5 mol%:mCP	0.033	[224]
6	Phox-$^{Me}\pi$	B, sDA	10 μmol, tol.	0.04	[243]
7	PXZ-Mes_3B	A, sDA	16 wt%:CBP	0.071	[244]
8	TPA-Ph2CN	B, sDA	10 μmol, tol.	0.12	[245]
9	oTE-DRZ	A, sDA	neat film	0.181	[246]
10	DACT-II	A, mDA	6 wt%:CBP	0.009	[247]
11	XAc-XT	B, mDA	5 wt%:PPF	0.025	[241]
12	5Cz-TRZ	B, mDA	15 wt%:mCBP	0.03	[248]
13	2DAC-Mes_3B	B, mDA	16 wt%:DPEPO	0.058	[244]
14	MFAc-OPS	A, mDA	20 wt%:PPF	0.07	[249]
15	MFAc-SPS	A, mDA	20 wt%:PPF	0.08	[249]
16	*p*-AC-DBNA	B, BDA	5 wt%:BCPO	0.009	[250]
17	3ACR-TRZ	A, BDA	16 wt%:CBP	0.015	[251]
18	*m*'-AC-DBNA	B, BDA	5 wt%:BCPO	0.031	[250]
19	TPA-cNDI*†	B, BDA	1 wt%:Zeonex	0.082	[252]
20	4CzIPN	A, BDA	10 μmol, tol.	0.09	[253]
21	3DPA3CN	A, BDA	6 wt%:DPEPO	0.103	[254]
22	5CzBN	A, BDA	10 μmol, tol.	0.13	[253]
23	*p*-2Cz2BMe	B, BDA	10 μmol, tol.	0.13	[255]
24	ACRFLCN	A, Spiro	6 wt%:TPSi-F	0.028	[256]
25	Spiro-CN	A, Spiro	6 wt%:mCP	0.057	[257]
26	DABNA-2	A, MR	6 wt%:mCBP	0.151	[258]
27	DABNA-1	A, MR	1 wt%:mCBP	0.20	[72]

donor and acceptor are in the same plane. While MR emitters are known to be particularly challenging for electronic-structure theory and will thus provide a good account of the robustness of any tested method,[204,260] a comparison between sDA and mDA/BDA emitters may reveal possible issues with electron/hole (de)localization.

A.3 Workflow and Theory

Initial ground-state geometries were obtained with the PBEh-3c[134] composite method in the gas phase. Comprehensive conformer searches for the ground state were omitted since the molecules are typically not flexible and the most stable conformers are thus self-evident. This holds true even more for the CT excited states, in which the delocalization of the excited-electron/electron-hole on the acceptor/donor moieties strongly drives the respective π-systems to planarity.

PBEh-3c geometries served as input structures for the optimal tuning (OT)[235] procedure and as starting point for all further calculations. The OT was conducted using the Golden-section search method for the ω-dependent target function $J^2(\omega)$ (see the Supporting Information for details) for fixed structures in the gas phase.[130] Since the molecule-specific optimal ω values of each of the functionals turned out quite similar for all emitters of set A (standard deviation about 10%), we also consider the RSHs with fixed ωs averaged over subset A (prefix FX, 0.134 a.u. for CAM-QTP(01),[178] 0.155 a.u. for ωB97M-V,[127] and 0.175 a.u. for LC-ωPBE-D3)[124,186]. This simplification eliminates any molecule-specific parameters and the time-consuming OT step, which takes almost as long as one excited-state optimization and is, thus, particularly helpful in screening workflows.

With UKS, singlet excited states are obtained with the help of the maximum overlap method (MOM) as a single-reference solution,[85] which is formally inconsistent for the multireference open-shell singlet wave function (the resulting open-shell singlet is essentially a mixture of a triplet and a singlet wave function; see ref [173] for a detailed discussion). This problem is mitigated by the ROKS approach, which provides formally consistent wave functions at a slightly increased computational cost.[172,261] In a nutshell, ROKS is a two-determinant approach that achieves spin-pure singlet states by simultaneous optimization of both a triplet and mixed (broken-symmetry singlet) determinant sharing a common set of restricted open-shell orbitals $\{\phi_{\mathrm{ROKS}}\}$.[88,173] A variational minimization of the energy of the spin-adapted open shell singlet

$$E_S^{\mathrm{ROKS}} = 2E_M[\{\phi_{\mathrm{ROKS}}\}] - E_T[\{\phi_{\mathrm{ROKS}}\}] \,, \tag{A.2}$$

where E_M is the energy of the mixed (UKS-like) determinant, and E_T is the energy of the triplet, allows a spin adaption at the level of KS orbital optimization. For a detailed description of the theory and properties of ROKS the reader is referred to ref [173]. While previous studies report the resulting differences between ROKS and UKS singlet to be negligible for CT states,[86,169,172] we will demonstrate that ROKS significantly improves on UKS since the energy differences considered here are very small. In contrast, a simple post-SCF spin purification for UKS using Yamagushi's formula,[262] which essentially doubles the UKS gaps, substantially worsens the agreement with experiment in most cases (vide infra).

The adiabatic singlet-triplet gaps ΔE_{ST} are calculated consistently; that is, they correspond to the energy difference between fully relaxed singlet and triplet excited states in a toluene solution. Accordingly, all optimizations of the excited states are conducted with the integral equation formalism (IEF)-PCM solvation model with parameters for toluene, corresponding to a full equilibration of the solvent degrees of freedom. This is desirable to account for the microsecond time scale of the TADF process.[169]

Singlet states are optimized with ROKS and UKS, the latter in combination with the (initial) maximum-overlap method (MOM/IMOM) to avoid a variational collapse to the ground state.[85,86] In the UKS/IMOM calculations (in the following just UKS), the excited state must be targeted explicitly. This is realized through a manipulation of the initial guess orbitals in which one electron is moved from the highest occupied molecular orbital (HOMO) to lowest unoccupied molecular orbital (LUMO). ROKS optimizations do not need such a guess for the excitation vector. They reliably converge on the lowest excited singlet state, whereas the UKS optimizations occasionally converge on higher-lying solutions (ca. 30% of all cases). This issue arises when the localization of the HOMO-LUMO guess vector differs from the lowest-energy CT state, since any change of the (de)localization is effectively

prevented by IMOM (as it attempts to maximize the overlap with the first step/initial guess orbitals). Accordingly, the issue can be solved by using a properly (de)localized ROKS guess for the UKS/IMOM optimization.

Triplet states were optimized exclusively with the UKS approach, which converged onto the lowest excited triplet state much more reliably than ROKS. Accordingly, ROKS triplets were obtained from single point energy calculations on the UKS optimized structures, since the effect of re-optimizing the structure with ROKS was negligible (ΔE <1 meV, see SI). In summary, by combining ROKS optimizations of the singlet states with the ROKS//UKS approach for triplet states, no further user input is required to obtain the lowest singlet and triplet excited states. Input files with the respective fine-tuned SCF parameters that ensure a stable convergence are provided in the Supporting Information.

Excited-state characters (locally excited (LE) or CT) are derived from the SCF dipole moments (see the Supporting Information for all values) or, in ambiguous cases, from an inspection of the difference densities (see Figure A.2). This revealed that, already with parameters for toluene, the lowest singlet and triplet states of all but one emitter (No. 2, TMCz-BO) are dominated by a CT character (p-2Cz2BMe also has a near-zero dipole, but this is because the S1 and T1 are symmetric CT states, not LE states). In TMCz-BO, the triplet CT state is just 0.03-0.08 eV above the triplet LE state at the ROKS/PCM level (depending in the functional). However, already with PCM parameters for the more polar 2,8-bis(diphenylphosphoryl)dibenzo[b,d]furan (PPF) thin film (ε = 3.5), which has been used in the experiments, the ordering is inverted, and the triplet CT states turns out as the lowest state, approximately 0.04 eV below the LE state. Hence, our calculations confirm for a much larger set of emitters what has previously been established for a smaller set of three emitters:[169] The lowest excited states of (non MR) TADF emitters are dominated by the CT character if the molecular environment is properly included.

Note that we do not report any calculations in gas phase since this is not directly relevant for the problem at hand. Moreover, characters of the lowest excited state there are different in gas phase, often with multiple near-degeneracies, which makes it difficult to locate and converge the lowest states. For a detailed comparison of the excited states in the gas-phase and in various solvent environments for three emitters including PTZ-DBTO2 (No. 4) and ACRXTN (No. 5) from STAGBS27, we kindly refer the reader to ref [169].

A.4 Results and Discussion

Let us begin with few a statistical evaluations of the comprehensive results for the molecule set A. Figure A.4a displays mean deviations (MD) and mean absolute deviations (MAD) of the calculated (adiabatic) ΔE_{ST} for the three tested functionals (different colors), each of which is considered with the UKS and ROKS approaches (brighter and darker colors), and with molecule-specific optimally tuned ω values (prefix OT, left half) as well as fixed averaged ω values (averaged over set A, prefix FX, right half). Most importantly, the results show that all combinations provide ΔE_{ST} in excellent agreement with experimental values with MADs well below the chemical accuracy (0.05 eV or 1 kcal/mol). The very similar performance of the different functionals and ω values shows that the performance is robust with respect to the choice of the functional and the amount of exact exchange. To further explore this aspect, we recalculated set A with the (unaltered) global hybrid functional PBE0-D4 (not shown, see

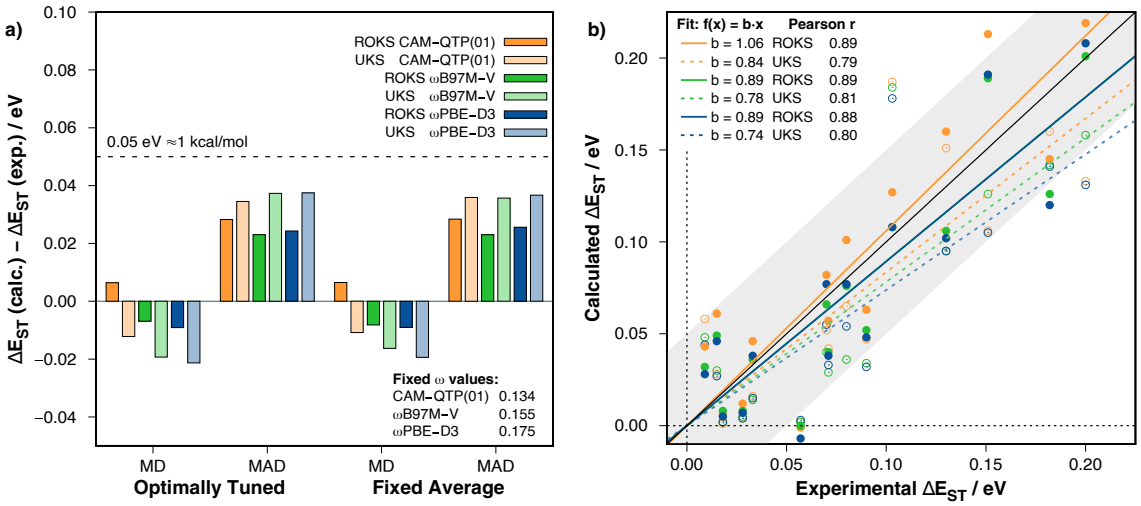

Figure A.4: (a) MD and MAD of the calculated ΔE_{ST} for three tested functionals with OT and fixed-average ω values (FX, averaged over Set A), (b) correlation plot of calculated and experimental ΔE_{ST} computed with OT/FX CAM-QTP(01), ωB97M-V, and LC-ωPBE comparing UKS and ROKS, all values given in electronvolts.

Supporting Information).[123,143,263] To our surprise, even this very general approach provides very accurate gaps with an MD/MAD of 0.018/0.037 eV in combination with ROKS and −0.021/0.037 eV in combination with UKS. This confirms that SCF-based methods like ROKS and UKS are much more robust than a TD-DFT based approach when it comes to the description of CT states.

While the choice of the density functional and details of the range-separation parameter ω (OT vs FX) exert only a minor influence, the difference between ROKS and UKS is substantial. From their direct comparison, the spin-restricted ROKS approach emerges with a distinct advantage: It achieves a more balanced MD and a lower MAD, while the UKS approach tends to a systematic underestimation of the ΔE_{ST} resulting in a larger MAD and more negative MD. This falls into place nicely considering the formal problems of the UKS approach. Since the single-reference treatment of the open-shell singlet leads to a state that is a 50:50 mixture of a singlet and a triplet, differences between the singlet and triplet states are systematically underestimated. However, in contrast to ROKS, Yamagushi's $\langle S^2 \rangle$-dependent post-SCF spin-purification does not improve the calculated gaps.[262] An application of this correction, which essentially doubles the gaps calculated with UKS, turns the slight systematic underestimation of UKS/OT-LC-ωPBE-D3 (MD = −0.021 eV, MAD = 0.037 eV) into a severe overestimation (MD = 0.042 eV, MAD = 0.058).

A further inspection of the results for set A in the form of a linear regression analysis is shown in Figure A.4b. Most notably, this analysis reveals that the UKS approach also exhibits a larger statistical error than that of ROKS: The Pearson coefficient is consistently larger by ≈0.1 for ROKS (0.88-0.89) than for UKS (0.79-0.81). Inspection of the slopes for the ROKS approach shows values relatively close to unity for CAM-QTP(01) (1.06), while LC-ωPBE-D3 and ωB97M-V (both 0.90) are a little worse, which is consistent with the MDs for the three functionals. Also the systematic underestimation of the gaps with UKS is reflected in their slopes, which are well-below unity (0.74-0.84). Note that all calculations presented here and in the following are conducted with Ahlrich's compact def2-SVP basis set.[162] Tests with the larger def2-TZVP basis set[162] were conducted, but no significant changes

were observed (the MAD between gaps calculated with SVP and TZVP is less than 0.005 eV; see the Supporting Information for details). This is consistent with previous studies and presumably the result of stable error compensation (basis-set effects cancel out for structurally and electronically very similar singlet and triplet CT states).[167,169]

Lastly, we discuss the influence of the parameters chosen for the dielectric environment. In a previous work,[169] some of us demonstrated that it is of utmost importance for the calculated gaps to include at least the electronic polarizability of the dielectric environment ($\varepsilon \approx 2$) since differences to the gas-phase are huge, whereas the differences between common non-polar and polar environments (ε(zeonex) $\approx$ 2, ε(mCP/PPF) $\approx$ 3.5)[168,169] are much smaller. On the basis of this experience and because we are designing an approach to predict gaps, we conducted all calculations with parameters for toluene (ε = 2.38), even if the experimental gaps were determined under different conditions (typically more polar environments). Note that this is a typical simplification in the theoretical modeling of ΔE_{ST}.[167] To explore the impact of small changes in the dielectric constant, we repeated the ROKS/OT-LC-ωPBE-D3 calculations for a subset (22 emitters) with the highest conceivable polarity of common thin-film environments, that is, ε = 3.5. Although these calculations show a small but systematic decrease of the calculated gaps (MD compared to toluene −0.016 eV), which moreover restores the agreement for the three largest overestimated gaps (vide infra), the effect averages out in the statistical evaluation (ΔMAD: 0.001 eV; see Figure S3 in the Supporting Information). This confirms that the use of parameters for toluene in all calculations gives a reasonable approximation. In future studies, a slightly higher dielectric of $\approx$ 3 could be better suited to account for the widespread use of polar thin-film environments (see Table A.1).

Having concluded the detailed analysis of subset A, let us now consider the complete STGABS27 set, that is, sets A and B, focusing on the performance for the different structural subsets and particularly challenging cases. For this, we employ two of the best-performing methods for set A, namely, ωB97M-V and LC-ωPBE-D3, both in combination with the ROKS approach. In addition, because of its surprisingly good performance for set A, we employ PBE0-D4 with the ROKS and UKS approaches to see if and how well its performance transfers to the larger set. Lastly, for the sake of comparison, we calculated all gaps with the TDA-OT-LC-ωPBE-D3/LR-PCM by optimizing the lowest singlet and triplet excites states. A visual comparison between absolute values of experimental gaps and results of the calculations sorted by the type of the emitters and size of the gaps is shown in Figure A.5, while a detailed statistical analysis is given in Table A.2.

Similar to set A, the results show that the performance of two OT RSHs ωB97M-V and LC-ωPBE-D3 is statistically indistinguishable (green and blue lines). In comparison, PBE0-D4 in combination with ROKS performs significantly worse as it tends to overestimate gaps (MD 0.026 eV, not shown). However, in combination with the UKS approach (yellow line), a fortuitous error cancellation between the systematic overestimation of PBE0-D4 and the systematic underestimation of the UKS approach leads to a very similar performance compared to ROKS/RSH. In contrast, TDA-OT-ωPBE-D3/LR-PCM systematically and substantially overestimates all gaps (MD $\approx$ MAD $\approx$ 0.20 eV). This can be traced back to the previously discussed CT failure of the LR-PCM solvation model, which does not recover the strong dielectric stabilization of CT states.[169,171,229,230] It bears pointing out that ROKS/PCM calculations are not only much more accurate but also 1.4-1.8 times faster than TDA-DFT/LR-PCM (UKS/PCM even more so with a factor of 3.2-4.8), and exhibit a more favorable scaling with system size (given are the timings per optimization step for the smallest and largest molecules of STGABS27;

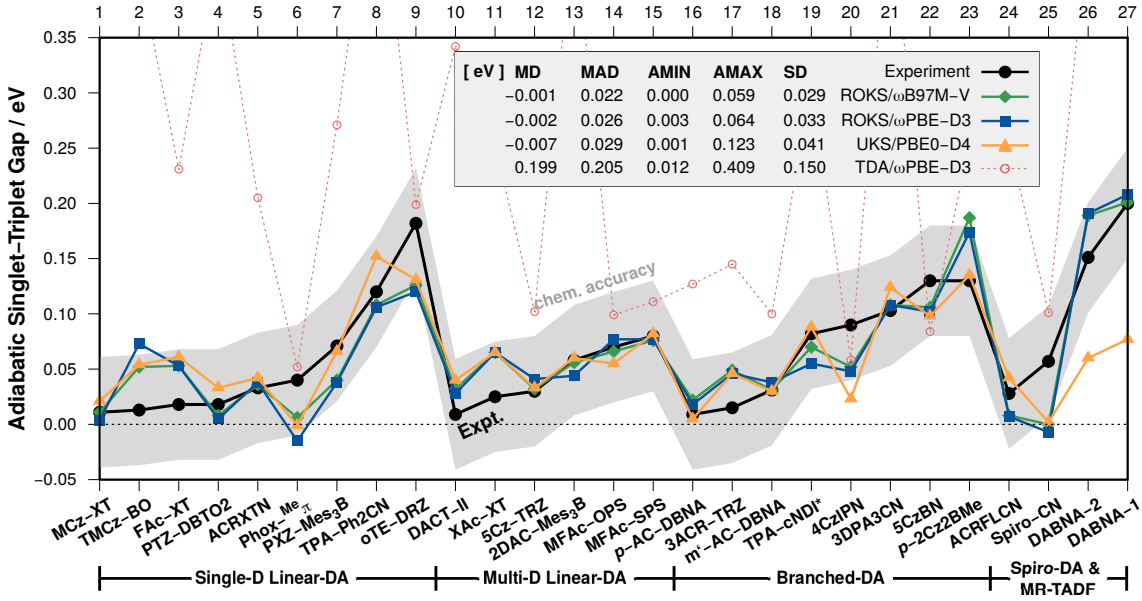

Figure A.5: Experimental (in black) ΔE_{ST} and calculated values for the whole STGABS27 set, categorized by their structure sorted by increasing gap size. Calculated values are shown for the most accurate methods, that is, ROKS/OT-ωB97M-V/PCM (green), ROKS/OT-LC-ωPBE-D3/PCM (blue), UKS/PBE0-D4/PCM (yellow, solid and dashed), and, for reference (and to serve as a warning), also for TDA-OT-LC-ωPBE-D3/LR-PCM (red, see the Supporting Information for further details). All calculations use the IEF-PCM with parameters for toluene and the def2-SVP basis set. All values given in electronvolts. All numerical values are provided in the Supporting Information.

see the Supporting Information for details).

An interesting observation is that all SCF-based methods, and, in particular, the ROKS/RSHs yield very similar patterns of deviations. Some striking examples of this are shown in Figure A.5 (from left to right), and they include the overestimation of the gaps of TMCz-BO, FAc-XT, and XAc-XT, as well as the underestimation of the gaps of Phox-$^{Me}\pi$, oTE-DRZ, 4-CzIPN, and spiro-CN. However, even in these seven worst cases, the deviation of the ROKS/RSH approach from experiment hardly ever surpasses the 0.05 eV defining "chemical accuracy". Because of the very similar pattern, we speculate that, in most of these cases, the deviation is due to a specific effect that is not included in the ROKS/RSH + PCM(toluene) approach. For example, an investigation of the influence of the polarity of the environment (see Figure S2 in the Supporting Information) revealed that all overestimated gaps mentioned above result from the larger polarity of the environment in the experiment (TMCz-BO, FAc-XT, and XAc-XT were studied in a PPF thin film with $\varepsilon \approx 3.5$) compared to the calculation using toluene parameters ($\varepsilon \approx 2.4$). Something that could also contribute but is much more difficult to assess are specific interactions (e.g., a structural confinement) within the thin-film environment that are absent in free optimizations with a dielectric continuum model. Assuming such as confinement constrains large-scale motions that reduce the ΔE_{ST} (but rotate freely in our optimizations), for example, the torsion around the donor-acceptor bond, this could explain the underestimation of the gaps particularly large bulky emitters (Phox-$^{Me}\pi$, oTE-DRZ, and 4-CzIPN). For oTE-DRZ, also the fact that experimental data was recorded in neat (pure) thin film could explain the observed deviation

Table A.2: Detailed statistical analysis for the two best-performing functionals OT-LC-ωPBE-D3 and OT-ωB97M-V in combination with the ROKS and PBE0-D4 in combination with ROKS and UKS for for all subsets and the complete STGABS27 (Set A + Set B). All values are given in electronvolts.

	MD	MAD	AMIN	AMAX	SD
Linear-DA (sDA and mDA)					
ωB97M-V	−0.001	0.020	0.000	0.056	0.027
LC-ωPBE-D3	−0.002	0.025	0.003	0.062	0.033
PBE0-D4	0.036	0.045	0.020	0.126	0.040
PBE0-D4(UKS)	0.008	0.023	0.002	0.051	0.028
Branched-DA (BDA)					
ωB97M-V	0.004	0.023	0.000	0.057	0.031
LC-ωPBE-D3	0.000	0.024	0.005	0.044	0.030
PBE0-D4	0.016	0.040	0.003	0.074	0.045
PBE0-D4(UKS)	−0.005	0.021	0.001	0.067	0.031
MR- & Spiro-DA					
ωB97M-V	−0.010	0.029	0.001	0.057	0.040
LC-ωPBE-D3	−0.009	0.033	0.008	0.064	0.044
PBE0-D4	0.008	0.032	0.002	0.052	0.043
PBE0-D4(UKS)	−0.064	0.070	0.014	0.123	0.039
Full Set					
ωB97M-V	−0.001	0.022	0.000	0.057	0.029
LC-ωPBE-D3	−0.002	0.026	0.003	0.064	0.033
PBE0-D4	0.026	0.042	0.002	0.126	0.042
PBE0-D4(UKS)	−0.007	0.029	0.001	0.123	0.041

as intermolecular interaction can play a role.

An orthogonal example with surprisingly good performance are the two MR-TADF emitters (DABNA-1 and DABNA-2), which are known to be particularly challenging for theoretical methods due to strong electron-correlation effects in their singlet excited state.[260] Here, all ROKS-based methods provide good agreement with the experimental gaps, while the UKS-based PBE0-D4 (and TDA-DFT) shows a large (huge) deviation. However, also the opposite can be observed, for example, for p-2Cz2BMe, whose gap is significantly overestimated by the ROKS based approaches, whereas UKS/PBE0-D4 is spot-on. However, this could as well be a coincidence due to the systematic underestimation of the gaps with UKS-based approaches.

Altogether, the results for the complete set allow three important conclusions about the presented ROKS/PCM and UKS/PCM approaches: (i) They are approximately an order of magnitude more accurate than that of the prominent TDA-DFT/LR-PCM approach and at the same time computationally more efficient and scale more favorably. (ii) The very similar performance of the three RSHs and the global hybrid confirms that the SCF-based methods are more robust with respect to the admixture of nonlocal Fock exchange than TD-DFT. As a result, ROKS can be used with fixed average ω values or even UKS with global hybrid PBE0 without losing much accuracy. (iii) As evident from the performance for DABNA-based multiresonant emitters, ROKS/PCM is also robust with respect to electronically challenging situations in which TD-DFT breaks down.[204,260] This is consistent with previous reports on the performance of ROKS and MOM/UKS for electronically challenging excited

states, for example, doubly excited states.[86,172,173] Accordingly, it can be used to reliably estimate ΔE_{ST} of all common types of TADF emitters with chemical accuracy.

A.5 Summary and Conclusions

We have presented an improved computational protocol for a rigorous and accurate description of charge-transfer (CT) states in solution and specifically tested it for the prediction of the adiabatic singlet-triplet gap ΔE_{ST} of TADF emitters. The method employs spin-unrestricted and restricted open-shell Kohn-Sham self-consistent field calculations in combination with a polarizable-continuum model. It was evaluated in conjunction with modern and well-established density functionals against a new and comprehensive set of experimental ΔE_{ST} values of 27 TADF emitters. This set is termed STGABS27 and includes only data from reliable temperature-dependent measurements. These tests demonstrated an accurate prediction of the ΔE_{ST} with an unprecedented mean absolute deviation of only 0.025 eV (0.5 kcal/mol) and few deviations greater than 0.05 eV (1 kcal/mol) for the ROKS/PCM approach with optimally tuned range-separated functionals. Importantly, the performance is nearly identical for electronically challenging cases like the multiresonant emitters DABNA-1 and DABNA-2, for which TD-DFT-based approaches fail.[204,260] Concerning the character of the lowest excited states of the TADF emitters, our calculations clearly showed that S_1 and T_1 are dominated by CT character if the environment is properly included, confirming a hypothesis from an earlier work that investigated three emitters.[169]

Moreover, the accuracy of ROKS/UKS/PCM was found to be surprisingly robust with respect to the choice of the density functional and details of the range-separation parameter. This allows a speeding up of the calculations by skipping the time-consuming optimal tuning step and instead using fixed ω-values without losing much accuracy. Values of 0.134, 0.155, and 0.175 for CAM-QTP(01), ωB97M-V, and ωPBE-D3, were recommended. Further pursuing the path of reducing empiricism, it was established that the (unaltered) global hybrid PBE0-D4 with ROKS/PCM shows only slightly larger deviations, and — due to a fortuitous error compensation — PBE0-D4 with UKS/PCM is almost as accurate as the best-performing schemes. This is particularly interesting, since UKS/PCM is the fastest and perhaps also most widely available of the methods tested herein. However, it also appears to be the least robust in electronically challenging situations.

Ultimately, we conclude that the robustness and accuracy of the ROKS/PCM approach results from combining an SCRF-based description for excited states, which (i) does not suffer from the CT failure of TD-DFT, which (ii) explicitly includes orbital relaxation effects and (iii) affords a rigorous state-specific treatment of the dielectric environment through the IEF-PCM. To the best of our knowledge, the presented approach and workflow constitute the most accurate practical computational protocol for the prediction of singlet-triplet gaps of TADF emitters and is presumably also, in general, very adept for the modeling of charge-transfer states of large molecules in dielectric environments. Because of its favorable scaling and efficiency, ROKS/UKS/PCM can routinely be applied to large systems with more than 100 atoms. An extension to compute transition properties is ongoing and will be presented in the near future.

A.6 Acknowledgment

Deutsche Forschungsgemeinschaft (DFG) is gratefully acknowledged for financial support in the framework of the Gottfried-Wilhelm Leibniz prize to SG. This project has been funded with support from the RTG-2591 "TIDE - Template-designed Organic Electronics".

A.7 Supporting Information

The Supporting Information is available free of charge at
https://pubs.acs.org/doi/10.1021/acs.jpclett.1c02299.
Detailed description of employed computational programs, methods, and workflows; theory of the applied optimal tuning procedure for range-separated hybrid functionals; tests for basis set convergence of ΔE_{ST}; geometry dependence tests of ROKS T1 energies; the effect of more polar dielectric media (ε = 3.5) on ΔE_{ST}; the effect of dispersion correction (DFT-D4) on ΔE_{ST}; walltimes comparison in geometry optimizations using UKS(IMOM), ROKS, or TDA-DFT; TDA-DFT/LR-PCM results for adiabatic ΔE_{ST}; the effect of Yamaguchi spin correction on ΔE_{ST} from UKS calculations; statistical measures and analysis of all data plotted in the manuscript and additional results; dipole moments for S1 and T1 excited states at the UKS and ROKS levels; example input files for UKS and ROKS geometry optimizations (Q-Chem 5.4 program); all optimized geometries at UKS and ROKS level are available in a .zip-archive file.

A.8 Conflicts of Interest

There are no conflicts to declare.

APPENDIX B

Benchmarking Charge-Transfer Excited States in TADF Emitters: ΔDFT Outperforms TD-DFT for Emission Energies

Thomas Froitzheim,[†¶] Lukas Kunze,[†¶] Stefan Grimme,[†] John M. Herbert,[‡] Jan-Michael Mewes[§]

Received: 21 January 2022
Published online: 4 April 2022

Reprinted in Appendix B (adapted) with permission[‖] from
T. Froitzheim, L. Kunze, S. Grimme, J. M. Herbert, and J.-M. Mewes, *Benchmarking charge-transfer excited states in TADF emitters: ΔDFT outperforms TD-DFT for emission energies*, J. Phys. Chem. A **128** (2024) 6324, DOI: 10.1021/acs.jpca.4c03273

Own contributions

- compilation of experimental emission data
- performing the ΔUKS and ΔROKS calculations
- statistical analysis of ΔUKS and ΔROKS calculations
- co-writing the manuscript

[†]Mulliken Center for Theoretical Chemistry, Clausius Institute for Physical and Theoretical Chemistry, University of Bonn, 53115 Bonn, Germany
[‡]Department of Chemistry and Biochemistry, The Ohio State University, Columbus, Ohio 43210, United States
[§]beeOLED GmbH, Niedersedlitzer Str. 75c, 01257 Dresden, Germany
[¶]These two authors contributed equally.
[‖]Permission requests to reuse material from this chapter should be directed to the American Chemical Society.

Abstract Charge-transfer (CT) excited states are crucial to organic light-emitting diodes (OLEDs), particularly to those based on thermally activated delayed fluorescence (TADF). However, accurately modeling CT states remains challenging, even with modern implementations of (time-dependent) density functional theory [(TD-)DFT], especially in a dielectric environment. To identify shortcomings and improve the methodology, we previously established the STGABS27 benchmark set with highly accurate experimental references for the adiabatic energy gap between the lowest singlet and triplet excited states (ΔE_{ST}).[1] Here, we diversify this set to the STGABS27-EMS benchmark by including experimental emission energies (E_{em}) and use this new set to (re)-evaluate various DFT-based approaches. Surprisingly, these tests demonstrate that a state-specific (un)restricted open-shell Kohn-Sham (U/ROKS) DFT coupled with a polarizable continuum model for perturbative state-specific nonequilibrium solvation (ptSS-PCM) provides exceptional accuracy for predicting E_{em} over a wide range of density functionals. In contrast, the main workhorse of the field, Tamm-Dancoff-approximated TD-DFT (TDA-DFT) paired with the same ptSS-PCM, is distinctly less accurate and strongly functional-dependent. More importantly, while TDA-DFT requires the choice of two very different density functionals for good performance on either ΔE_{ST} or E_{em}, the time-independent U/ROKS/PCM approaches deliver excellent accuracy for both quantities with a wide variety of functionals.

B.1 Introduction

The rise of computation-driven rational design in organic electronics and materials necessitates the robust and accurate prediction of optoelectronic properties.[70,169,216–218,264,265] Next-generation organic light-emitting diodes (OLEDs) based on thermally activated delayed fluorescence (TADF) are a prominent example. TADF emitters harvest both singlet and triplet excitons through the transfer of excitons via (reverse) intersystem crossing [(r)ISC]. Since the rate of population transfer depends exponentially on the adiabatic energy gap ΔE_{ST} between the lowest singlet (S_1) and triplet (T_1) excited states, it imposes a tight constraint on TADF emitter design. One way to achieve small singlet-triplet gaps on the order of the thermal energy ($k_B T \approx 0.025\,\text{eV}$) is by spatially separating electron and hole in charge-transfer (CT) excited states. Accordingly, the computational study of CT states and the accurate prediction of their relative energies have attracted great interest.

To assess the accuracy of commonly applied methods for the CT state of TADF emitters, some of us previously introduced the STGABS27 benchmark set,[1] consisting of 27 emitters with highly accurate experimental ΔE_{ST} values obtained from temperature-dependent measurements of the TADF rate.[176] Our work demonstrated that state-specific restricted or unrestricted open-shell Kohn-Sham density functional theory (ROKS or UKS)[85,86,88,236] combined with a polarizable continuum solvation model (PCM)[89,164] yields ΔE_{ST} with a remarkably small error of $\approx$0.5 kcal/mol, which we attributed to the full inclusion of orbital relaxation and dielectric screening in the method. Note that by UKS, ROKS, and generally ΔDFT, we refer to SCF-based non-aufbau methods applied to open-shell singlet excited states and (as is more common) triplet states. In UKS for open-shell singlets, ground-state orbitals are manually repopulated to form a non-aufbau determinant, and converged using the maximum overlap method (MOM) to avoid variational collapse[85]. ROKS improves on UKS by correcting the spin-state of the open-shell singlet determinant through the introduction of a second (triplet) determinant in the same orbitals.[173] The spin-adapted open-shell singlet state is then obtained as twice

the open-shell singlet minus the triplet. These methods provide result within chemical accuracy and remain remarkably stable across various density functionals from the classic PBE0-D4 (mean unsigned error, MUE: 0.029 eV) to the state-of-the-art optimally tuned (OT) range-separated hybrid (RSH) functional OT-ωB97M-V (MUE: 0.021 eV). In stark contrast, some of us showed in a recent paper[208] that the accuracy of time-dependent density functional theory in the Tamm-Dancoff approximation (TD(A)-DFT[149,180,266]) depends strongly on the chosen functional and solvation model. For most method combinations, outliers dominate the results, leading to deviations frequently exceeding the absolute ΔE_{ST} values. Only functionals with a small fraction of Fock exchange ($\approx$10%), applied in vertical approximation (i.e., using ground-state structures) and evaluated without a proper solvent model, approach the accuracy of ΔDFT/PCM (MUE: 0.042 eV), which we attributed to strong error-cancellation effects. Accordingly, the good performance of this approach comes at the expense of overly stabilized CT states, sometimes by up to 1 eV, reminiscent of the CT failure of pure (meta-)GGA functionals.[79,158] To better identify such unreliable error-compensation-based methods and improve the diversity of the STGABS27 benchmark, we decided to include experimental emission energies E_{em}, which probe the energy difference between the polar excited CT (S_1) and the nonpolar ground state (GS). As such, emission energies offer a complementary challenge to the energy difference between two similar CT states (S_1 and T_1) in the original set, in which error-cancellation effects are much less helpful.

Countless previous studies have explored theoretical methods for calculating transition energies from and to CT excited states. For the sake of conciseness, we limit the following discussion to the most relevant ones. Shee and Head-Gordon recently investigated TD-DFT with a perturbative (pt)SS-PCM solvation model for the absorption and emission energies of twisted intramolecular (TI)CT excited states, including some TADF emitters.[130] They found optimally tuned RSH functionals such as OT-LC-ωPBE perform particularly well. Nonetheless, limitations of single-excitation-based TD-DFT persist, especially for smaller systems, which they attribute to missing orbital relaxation. Although they demonstrated that state-specific ΔROKS mitigates these errors, their approach lacked a proper account for solvation (they were taken from the TD-DFT calculations). A series of benchmarks by Jacquemin *et al.* on realistically sized organic emitters underscores the advantages of (OT-)RSH functionals.[151,152,157,159,267] Moreover, they emphasize the critical role of a state-specific nonequilibrium solvation model for treating CT states accurately. In another work, Jacquemin *et al.* explored the influence of correlation within a set of theoretical reference data for 30 intramolecular CT transitions.[268] Unfortunately, the prohibitive computational cost of high-level calculations limited the system size to only the smallest CT systems, in which orbital relaxation and dielectric stabilization are less important. While an RSH functional (ωB97X-D[269]) is again the most accurate with pure TD-DFT, more sophisticated wavefunction-based methods such as second-order algebraic diagrammatic construction ADC(2)[270,271] or second-order approximate coupled cluster CC2[77] provide some improvements. These findings were recently corroborated by Mester and Kállay,[272] further suggesting a benefit from an accurate explicit description of orbital relaxation. In this work, we want to systematically expand the benchmarking of CT emission energies in solution to ΔDFT-based methods, including a complete nonequilibrium solvation model. To this end, we implemented nonequilibrium state-specific solvation for ΔDFT in the Q-Chem program.[184]

This work adheres to the following structure: In section B.2, we present the reference values for the expansion of the STGABS27 set. Sections B.3 and B.4 outline the theory and technical details necessary for calculating vertical emission energies with TDA-DFT and ΔDFT. Lastly, in

Table B.1: Names, measurement conditions, experimental E_{em} value (in eV), and literature references for all emitters of the STGABS27-EMS set.

No.	name	solvent[a]	E_{em}[h]	ref.
1	MCz-XT	5 wt %:PPF[b]	2.59	[241]
2	TMCz-BO	10 μmol, tol.[c]	2.78	[242]
3	FAc-XT	5 wt %:PPF	2.54	[241]
4	PTZ-DBTO2	dilute tol.	2.12	[220]
5	ACRXTN	5 mol %:mCP[d]	2.59	[224]
6	PHOX-$^{Me}\pi$	20 μmol, tol.	1.99	[243]
7	PXZ-Mes_3B	10 μmol, tol.	2.44	[244]
8	TPA-PH2CN	10 μmol, tol.	2.52	[245]
9	oTE-DRZ	10 μmol, tol.	2.35	[246]
10	DACT-II	6 wt %:CBP[e]	2.40	[247]
11	XAc-XT	5 wt %:PPF	2.58	[241]
12	5Cz-TRZ	dilute tol.	2.48	[248]
13	2DAC-MES_3B	10 μmol, tol.	2.51	[244]
14	MFAc-OPS	10 μmol, tol.	2.80	[249]
15	MFAc-SPS	10 μmol, tol.	2.73	[249]
16	p-AC-DBNA	10 μmol, DCM[f]	2.23	[250]
17	3ACR-TRZ	10 μmol, tol.	2.43	[251]
18	m'-AC-DBNA	10 μmol, DCM	2.18	[250]
19	TPA-cNDI	10 μmol, tol.	1.65	[252]
20	4CzIPN	10 μmol, tol.	2.45	[253]
21	3DPA3CN	tol.	2.45	[254]
22	5CzBN	10 μmol, tol.	2.64	[253]
23	p-2Cz2BMe	10 μmol, tol.	2.22	[255]
24	ACRFLCN	6 wt %:TPSi-F[g]	2.56	[256]
25	Spiro-CN	6 wt %:mCP	2.30	[257]
26	DABNA-2	20 μmol, DCM	2.64	[258]
27	DABNA-1	20 μmol, DCM	2.68	[72]

a) If no value for n^2 is known 2.25 (toluene)[273] is used.

b) 2,8-bis(diphenylphosphoryl)dibenzo[b,d]furan: ε = 5.0[274].

c) Toluene: ε = 2.37, n^2 = 2.25.

d) N,N'-dicarbazolyl-3,5-benzene: ε = 2.84.[275]

e) 4,4'-bis(carbazol-9-yl)biphenyl: ε = 3.5 (see SI)

f) Dicholoromethane: ε = 8.93, n^2 = 2.03.[273]

g) Triphenyl-(4-(9-phenyl-9H-fluoren-9-yl)phenyl)silane: ε = 2.5.[276]

h) Estimated accuracy ±0.02-0.06 eV in the given spectral region.

section B.5, we illustrate the specific emission energies and the statistical performance of various density functionals on the expanded STGABS27 set to derive general recommendations for treating solvated CT states.

B.2 Benchmark Set

To thoroughly judge the applicability of an excited state method for the CT states of TADF emitters, we extended the STGABS27 benchmark set with experimental emission energies E_{em} for all included systems. This new benchmark set shall be named STGABS27-EMS. Table B.1 summarizes the key data, including reference emission energies, experimental measurement conditions, and corresponding literature references.

In contrast to the singlet-triplet gaps in STGABS27 where careful consideration of the experimental method was crucial to ensure reliable data for the mostly tiny energy differences < 0.1 eV, the 10-20 times larger emission energies can be taken from standard fluorescence spectra reported in the original publications. We primarily rely on the peak maximum or photoluminescence wavelength λ_{PL}. Where λ_{PL} was not explicitly stated (molecules 4, 12, 20, 22, and 25), we extracted the maximum position from the reported fluorescence spectra. Since polar CT states present in all but the multiple resonance (MR-)TADF emitters DABNA-1 (27) and DABNA-2 (26) exhibit a large bandwidth for the fluorescence peaks, we assume a statistical uncertainty in the emission energy of up to 10 nm ($0.02 - 0.06$ eV in the spectral region between $440 - 750$ nm).

Further, we want to acknowledge that the fluorescence maximum typically does not directly correspond to the vertical emission energy at the optimized excited state geometry. Discrepancies arise from differences in zero-point vibrational energy (ZPVE) between ground and excited state or vibrational effects leading to deviations from strictly vertical transitions.[151,277] Unfortunately, the strong S_1 CT character prevents a more well-founded comparison to 0-0 transitions, as the required absorption peak is typically weak and broad.[278] Moreover, 0-0 transitions, i.e., equilibrium-to-equilibrium, are not suitable for testing nonequilibrium solvation corrections for state-specific ΔDFT, which is a side goal of this work. Thus, we will compare E_{em} to the fluorescence maximum, arguing that this still provides valuable insights since most donor-acceptor type TADF emitters are rather similar regarding their electronic and chemical structure, which should lead to rather systematic deviations. Facing the same issue, other authors assume an uncertainty of absolute vertical emission energies ranging between 0.1 and 0.2 eV, of which we chose the latter as a conservative estimate.[130,151,153,277,279]

B.3 Theory: Solvation for Vertical Transitions

In the following, we briefly introduce the theoretical background for calculating vertical transition energies in the presence of a dielectric continuum. We omit a comprehensive review of the underlying theory for polarizable continuum models (PCM) and instead refer the reader to relevant literature.[89,182,183,229,280–283] Throughout, we follow the notation established in ref [89], where a reaction field operator $\hat{R}_i$ of state $|\Psi_i\rangle$ polarizes the continuum and leads to the following state-specific Schrödinger equation

$$\left(\hat{H}^{\mathrm{vac}} + \hat{R}_i\right) |\Psi_i\rangle = E_i |\Psi_i\rangle. \tag{B.1}$$

Since electronic transitions occur on a much shorter timescale than the structural relaxation of the solute, the polarization response to the transition can be split into two parts, which can be regarded as

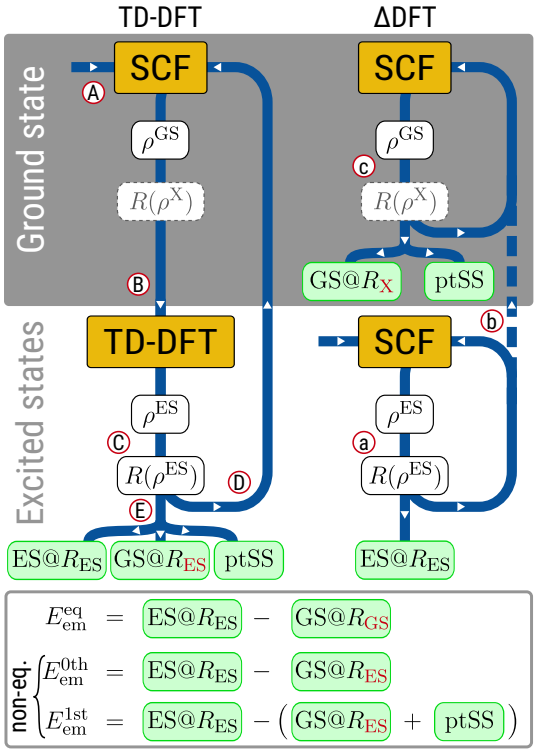

Figure B.1: Schematic overview for the calculation of emission energies with either TD-DFT (left) or ΔDFT (right) in solution. White boxes indicate intermediates (the dashed $R(\rho^{x})$ is replaced after the first iteration by the frozen excited state reaction field of the excited state), while green boxes indicate final results. Letters A-E in the TD-DFT and letters a-c in the ΔDFT procedure mark sections referenced in the text.

the application of the Frank-Condon principle to the solvent: On the one hand, there is a fast electronic response from the solvent electronic degrees of freedom (DOF) that can follow the changing charge distribution of the solute, and on the other a slow orientational and vibrational response of the solvent nuclear DOFs, which remain unchanged. Therefore, we need to partition the total reaction field ($\propto \varepsilon$) into a fast part ($\propto \varepsilon_\infty = n^2$, with the refractive index n), and a remaining slow part[284–288]

$$\hat{R} = \hat{R}^f + \hat{R}^s. \tag{B.2}$$

Accordingly, during a vertical transition from the equilibrium initial state fulfilling eq B.1 (e.g., some excited state for emission) to the nonequilibrium final state, only the fast component $\hat{R}^f$ relaxes. Consequently, the Hamiltonian of the final state depends on both the fast component of its own and the slow component of the initial reaction field

$$\hat{H}_{\mathrm{final}} = \hat{H}^{\mathrm{vac}} + \hat{R}^f_{\mathrm{final}} + \hat{R}^s_{\mathrm{initial}}. \tag{B.3}$$

The energy difference between the initial and final states defines the vertical emission energy E_{em}. However, the strict application of this scheme results in a computationally demanding iterative approach

and non-orthogonal states. To sidestep such complications, we avoid the interdependence between the initial and final states in the Hamiltonian by approximating the relaxation of $\hat{R}^f$ for the final state by perturbation theory (denoted ptSS-PCM[229], closely related to the corrected linear-response (cLR)-PCM[231]), using the usual perturbation expression

$$\hat{R}^f_{\text{final}} = \hat{R}^f_{\text{initial}} + \lambda \left(\hat{R}^f_{\text{final}} - \hat{R}^f_{\text{initial}} \right). \tag{B.4}$$

The clear advantage of the perturbative approach is that the 1st-order perturbative approximation of the fast response of the final state ($E^{1\text{st}}_{\text{em}}$, compare Figure B.1), can be obtained in a single step once the excited-state density is known.

B.3.1 Excitation- and ΔSCF-Based Procedures

Below, we detail the calculation of the initial excited and the final ground state with excitation- and ΔSCF-based methods, now integrated into the latest version of the Q-Chem program.[184]

In the state-specific (SS-)PCM formalism for excitation-based methods[182,183,231,281,289–295], such as configuration interaction (CI[73]), algebraic diagrammatic construction (ADC(n)[270,271]), equation-of-motion/linear-response coupled cluster (EOM/LR-CC[296,297]), or most relevant here TD(A)-DFT, the reaction field enters the calculation through the "solvated" ground state orbitals. Consequently, to equilibrate the initial excited state, its reaction field has to be coupled back into the ground state SCF. This is done in a procedure known as PerTurbation of Energy and Density (PTED) SS-PCM, illustrated on the left of Figure B.1.[183] It begins with a ground state SCF calculation, usually including a PCM (A) to produce initial orbitals for the excited state TD-DFT calculation (B). From the TD-DFT calculation, we obtain the excited state density used subsequently to polarize the continuum and yield the excited state reaction field (C). This reaction field enters unchanged (frozen reaction field) into the next ground state SCF (D), which produces an updated set of orbitals to return to step (B). Hence, at the high computational cost of repeated (iterative) calculation of the excited states, the PTED approach prepares both ground and excited states in the reaction field of the targeted excited state. Combined with the perturbative nonequilibrium approach described above (E), this allows the direct calculation of vertical emission energies.

For ΔSCF-based methods, the procedure depicted on the right of Figure B.1 is more straightforward than for excitation-based methods, which originates in the state-specific nature of the ΔSCF approach: The inherent separation of the ground and excited state calculations in two distinct SCFs enables the concurrent optimization of the excited-state reaction field and the excited-state density (a), i.e., without the need to repeat the entire ground- and excited-state computation until convergence. Since isolated calculations yield each state under equilibrium conditions, the converged reaction field of the initial excited state must enter the final ground state (b). Ultimately, only a single SCF in this frozen reaction field is necessary (c) for the final ground state and the ptSS-PCM correction.

Let us finish with a few words about the nomenclature used in the following:

- ptSS-PCM always refers to the first-order corrected nonequilibrium transition energy. In the case of absorption, this means the ground-state equilibrated PCM and a ptSS-PCM term for

relaxation in the the excited state, and, in the case of emission, it means the excited-state equilibrated PCM and a ptSS-PCM term for relaxation to the ground state ($E_{\mathrm{em}}^{\mathrm{1st}}$ in Figure B.1).

- SS-PCM refers to fully equilibrated state energies, i.e., the lack of any ptSS nonequilibrium corrections ($E_{\mathrm{em}}^{\mathrm{eq}}$). For this, excitation-based methods require an iterative solvent-field optimization for each state (left of Figure B.1), whereas full equilibration is the "natural" result in state-specific ΔDFT approaches. This would be the physically correct model for 0-0 transitions.
- Just "PCM" refers to calculations using the ground state reaction field, i.e., no excited states are considered for solvation (correct for absorption at zeroth-order, $E_{\mathrm{abs}}^{\mathrm{0th}}$). This is the "natural" result of excitation-based approaches (when using solvated orbitals), while it does not naturally occur in ΔDFT approaches. Even though such ground-state solvation is incorrect for emission calculations (TDA-DFT calculation for the excited state structure), it is the default solvation procedure in some quantum chemistry programs.
- Finally, the linear-response (LR-)PCM[170] is the default solvation model for TD-DFT in many programs also for excited-state optimizations, since analytical gradients are available. As known for a long time, however, LR-PCM fails to recover the strong polarization response of CT states (see below).[171,229,298,299]
- Correct conditions for an emission calculation with the reaction field fixed to the excited state ($E_{\mathrm{em}}^{\mathrm{0th}}$) require an SS-PCM calculation only for the initial state, termed $\mathrm{SS}^{\mathrm{initial}}$-PCM. While excitation-based methods with SS-PCM naturally yield the final ground state in the reaction field of the initial excited state, ΔDFT requires a specific frozen reaction field SCF.

B.4 Computational Details

All calculations were performed with a development version of the Q-Chem 5.4.2 program, containing the solvation model developments for TD(A)-DFT and ΔDFT described in section B.3. Emission energies were generally calculated in the vertical approximation at the relaxed structure of the first excited singlet state S_1, optimized at the same level of the theory. Since the state-specific PCM formalism for TDA-DFT lacks analytical nuclear gradients, geometry optimizations were carried out with TDA-DFT in the gas phase. Aside from exploratory calculations, all emission energies were calculated with state-specific PCM solvation with nonequilibrium effects added perturbatively via the ptSS-PCM (vide supra). The reaction field was divided into fast and slow components according to the Marcus partition,[300,301] with the required parameters ε and n for each solvent taken from the Minnesota Solvent Descriptor Database.[273]

Our selection of density functional approximations (DFAs) covers a range of global and optimally tuned[128,235] range-separated hybrid functionals mostly based on PBE[108]. For the global hybrids, the fraction a_x of admixed exact exchange varies between 10% for PBE10, 25% for PBE0,[123] and 37.5% for PBE38.[185] By interpreting a_x as a screening of electron-hole attraction in TDA-DFT calculations ($a_x = \frac{1}{\varepsilon}$),[129,225,302] these admixtures equate to dielectric screening factors between $\varepsilon = 10$ (10%) and 2.6 (37.5%). For the range-separated hybrid functionals, we selected the optimally tuned LC-ωPBE (OT-LC-ωPBE, with no short-range Fock exchange)[124] and LRC-ωPBEh (OT-LRC-ωPBEh, 20% short-range Fock exchange)[186] as well as the best performer for singlet-triplet gaps on the STGABS27

set, the optimally tuned ωB97M-V (OT-ωB97M-V, 15% short-range Fock exchange)[127] functional. We omit untuned RSH functionals, as extensive prior studies found that the standard ω values, typically optimized for ground state thermochemistry, are too large for excited state applications.[1,130,159] The optimally tuned range-separation parameters ω were taken from ref. [1]. All calculations employ the DFT-D4 dispersion correction,[142,143] using the same damping parameters for OT-RSHs as in the untuned functional.[303] Furthermore, all calculations employ the def2-SVP basis set[162,304] (see the Supporting Information for a detailed basis set study).

B.5 Results and Discussion

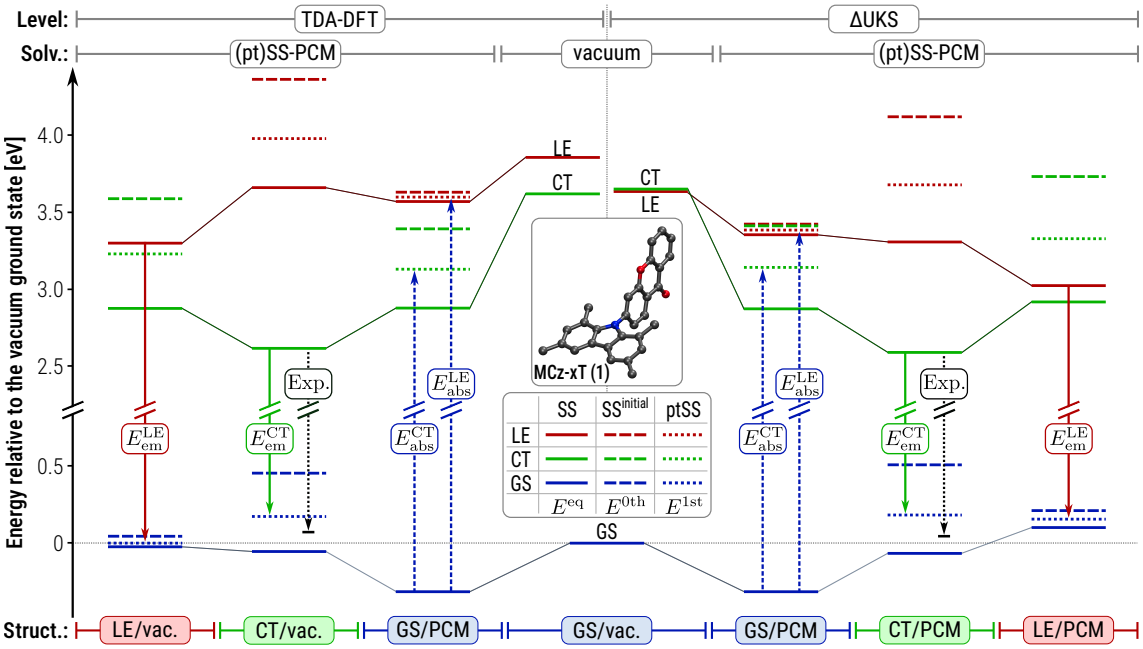

Figure B.2: Energy level diagram for the TDA-DFT (left) and ΔUKS (right) calculation of absorption (dashed arrows) and emission energies (solid arrows) for the lowest charge-transfer (CT, green) and locally excited (LE, red) states of MCz-XT (molecule 1) solvated in a PPF matrix (ε = 5.00, n^2 = 2.25). All calculations employ the OT-ωB97M-V functional. For each possible initial state [ground state (GS, blue), CT, and LE], geometries indicated at the bottom are optimized (for TDA-DFT without solvation due to the lack of analytical nuclear gradients for SS-PCM). At each geometry, all states are calculated under equilibrium solvation conditions (SS-PCM, solid levels), in the reaction field of the initial state (SS$^{\text{initial}}$-PCM, dashed levels), and under first-order nonequilibrium conditions (ptSS-PCM, dotted levels). For comparison, the experimental emission energies are drawn in black.

B.5.1 The Example of MCz-XT

Let us begin with an in-depth comparison of solvation effects at either the TDA-DFT or ΔDFT level, using 1,3,6,8-tetramethylcarbazole-xanthone (MCz-XT, molecule 1) as an example. Figure B.2 shows the energy shifts caused by the dielectric environment for the ground (GS, blue), as well as the

lowest CT (green) and LE (red) excited states of MCz-XT. Starting with MCz-XT in vacuum at the ground-state geometry (middle), both TDA-DFT and ΔUKS predict the CT and LE at around 3.7 eV, but with different ordering. TDA-DFT favors the CT state, while ΔUKS predicts a near degeneracy. For D-A TADF emitters containing extended π-systems, such as MCz-XT, near degeneracies between low-lying CT and LE states are common. Upon structural relaxation, either the CT or LE state can become the lowest one.

If we now include the dielectric environment, three distinct scenarios have to be considered, depending on the choice of the state for geometry optimization: (i) vertical absorption at the relaxed ground.state structure, as well as vertical emission at either (ii) the CT or (iii) LE excited-state structure. Let us begin with the optimized ground-state structure (i). Under equilibrium solvation conditions for each state (SS-PCM, solid levels), we find a consistent stabilization for all states with respect to the vacuum. The effect is more pronounced for the polar CT state (-0.69 or -0.86 eV) than in the less polar GS and LE state (-0.26 to -0.35 eV). Consequently, the CT state is invariably the lowest excited state. However, this is not as unambiguous under nonequilibrium conditions appropriate for modeling vertical absorption. Without any relaxation of the final excited-state reaction field (zeroth-order neq., $SS^{initial}$, dashed levels), the relative excited-state levels remain almost unchanged compared to the vacuum. In particular, the CT state experiences no special stabilization since the nonpolar GS only weakly polarizes the dielectric environment. Only the relaxation of the fast solvent DOFs to the specific excited state via the ptSS-PCM (first-order neq., dotted levels) drives the CT below the LE states and yields lower CT absorption energies ($E_{abs}^{1st,CT} < E_{abs}^{1st,LE}$). While the CT remains equal for TDA-DFT and ΔDFT, the absorption energies to the LE still reflect the initial gas phase energy discrepancy.

Moving on to the excited state structures of CT (ii) and LE (iii), we identify two main factors for the vertical emission energies of either state at its optimal geometry, namely, (a) the overall stabilization due to the dielectric environment, and (b) the nonequilibrium effect on the ground state. For factor (a), we begin again with equilibrium solvation conditions. Compared to the ground-state structure, both states experience an additional energy lowering after state-specific geometry optimization. This seems to be dominated by the geometric relaxation of the solute as both CT and LE states respond similarly (≈0.25-0.3 eV, with either TDA-DFT or ΔUKS).

As for vertical absorption, nonequilibrium solvation (b) plays a crucial role for E_{em}. Whereas nonequilibrium solvation effects increase vertical absorption energies, vertical emission energies are consistently decreased compared to treating all states in their respective equilibrium conditions. The polarized CT reaction field greatly destabilizes the nonpolar ground state (+0.4-0.6 eV for zeroth-order and +0.2-0.3 eV first-order solvation) while nonequilibrium effects for emission from the LE state are negligible (below 0.1 eV). This destabilization is mostly due to the polarization work, which amounts to half of the interaction energy of the initial state (here CT) with its self-induced polarization. Because the polar CT strongly polarizes the environment, the polarization work is large whereas the interaction with the nonpolar ground state is small. Together, this results in a pronounced destabilization of the GS.[183]

Combined, the CT emission energy $E_{em}^{1st,CT}$ is lower than $E_{em}^{1st,LE}$ by 0.62 and 0.79 eV for TDA-DFT and ΔUKS, respectively, confirming the assignment of the experimental emission to the CT state. Again, the nonequilibrium solvation effects for TDA-DFT and ΔUKS occur largely in parallel, yielding very similar emission energies for the CT state (E_{em}^{CT}=2.51 vs 2.48 eV). Both values agree excellently

with the experiment (2.59 eV), especially when compared with the calculation in vacuum or the popular TDA-DFT/LR-PCM (3.19 eV). These findings confirm that state-specific solvation, including appropriate nonequilibrium conditions for vertical transitions, cannot be neglected for either absorption or emission energies of competing low-energy CT and LE states.

B.5.2 TDA-DFT

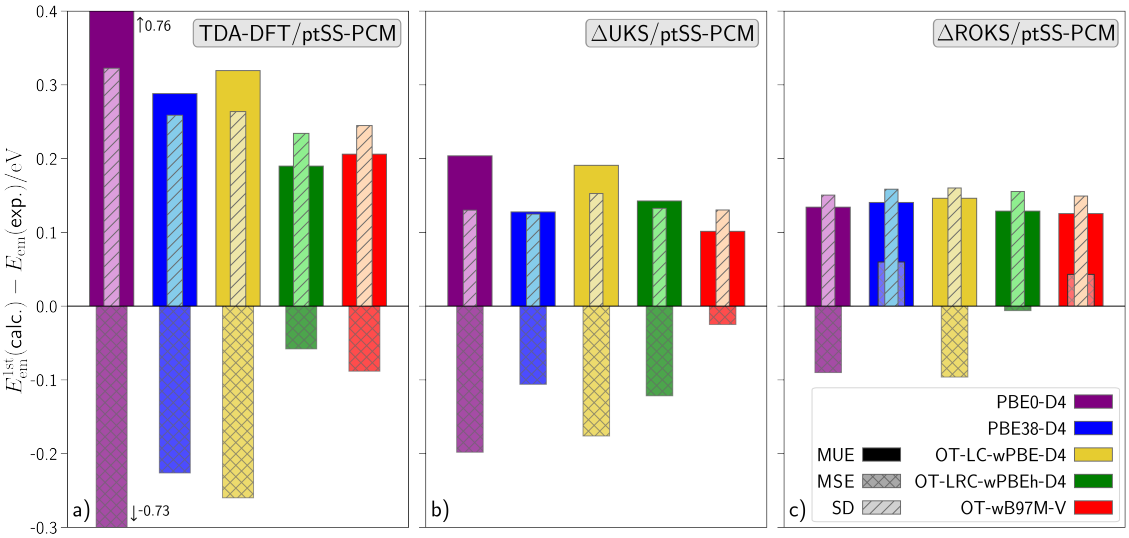

Figure B.3: Plots of the MUE (solid outer bar), MSE (hatched middle bar), and SD (dashed inner bar) for the calculated E_{em}, relative to the experimental reference. Values are shown for different functionals at the (a) TDA-DFT/ptSS-PCM, (b) UKS/ptSS-PCM, and (c) ROKS/ptSS-PCM level of theory. All calculations employ the S_1 optimized structures at the same level of theory (for TDA-DFT without solvation due to the lack of analytical nuclear gradients for SS-PCM).

Following our detailed analysis of MCz-XT, we continue with the statistical evaluation of the entire STGABS27-EMS benchmark set, beginning with the results for TDA-DFT. Figure B.3a presents the statistical measures for TDA-DFT/ptSS-PCM with various density functionals. These statistics include the mean unsigned error (MUE), mean signed error (MSE), and standard deviation SD; see the SI for definitions.

A striking initial observation is the strong functional dependence of E_{em}, which ranges from the promising accuracy of OT-LRC-ωPBEh-D4 (green) to a substantial underestimation with PBE0-D4 (purple, MSE $\approx -$MUE $= -0.73$ eV). The crucial factor influencing performance is the fraction of non-local Fock exchange within the functional incorporated either globally (global hybrids) or in a distance-dependent way (range-separated hybrids). Increasing the global admixture, e.g., from 25% in PBE0-D4 to 37.5% in PBE38-D4 (blue), reduces the MUE by more than a factor of two, primarily due to a decrease in the negative MSE accompanied by a minor reduction in SD. Among the optimally tuned RSHs, OT-LC-ωPBE-D4 (yellow, 0% short-range Fock exchange and 100% long-range Fock exchange) exhibits a similar error to PBE38-D4, while OT-LRC-ωPBEh-D4 (20% short-range Fock exchange and 100% long-range Fock exchange) and OT-ωB97M-V (red, 15% short-range Fock exchange and 100% long-range Fock exchange) are the most accurate. Interestingly, further analysis reveals a correlation

between performance and Fock exchange fraction effective at the relevant electron-hole distance, as we already reported in a previous work.[208] For OT-LRC-ωPBEh, this fraction rises already around 0.7 Å above the 37.5% of PBE38-D4 compared to 1 Å for OT-LC-ωPBE (see Figure 2 in ref [208]). To understand this curious trend of decreasing errors with increasing Fock exchange, we revisit our previous interpretation of the Fock exchange fraction as an effective dielectric screening between electron and hole ($\varepsilon \approx \frac{1}{a_x}$, see ref. [208] for details). Since the SS-PCM already accounts for screening due to the dielectric continuum, we suspect that only a limited further screening (large a_x) is required to mimic the effect of orbital relaxation. Notably, the opposite is true for predicting singlet-triplet gaps, where as little as 10% Fock exchange combined with an incomplete solvation model achieved the best performance with the help of a surprisingly stable error-compensation.[208] This highlights the need for comprehensive testing across different properties to avoid methods that work primarily due to fortuitous error cancellation. In general, the observed performance of TDA-DFT/ptSS-PCM is in line with previous studies, which reported MUEs between 0.2 and 0.3 eV for the emission from CT states of similar emitters.[130,157,167] Notably, these studies also reported benefits from both system-specifically optimally tuned RSHs and increased fractions of Fock exchange.

B.5.3 ΔDFT

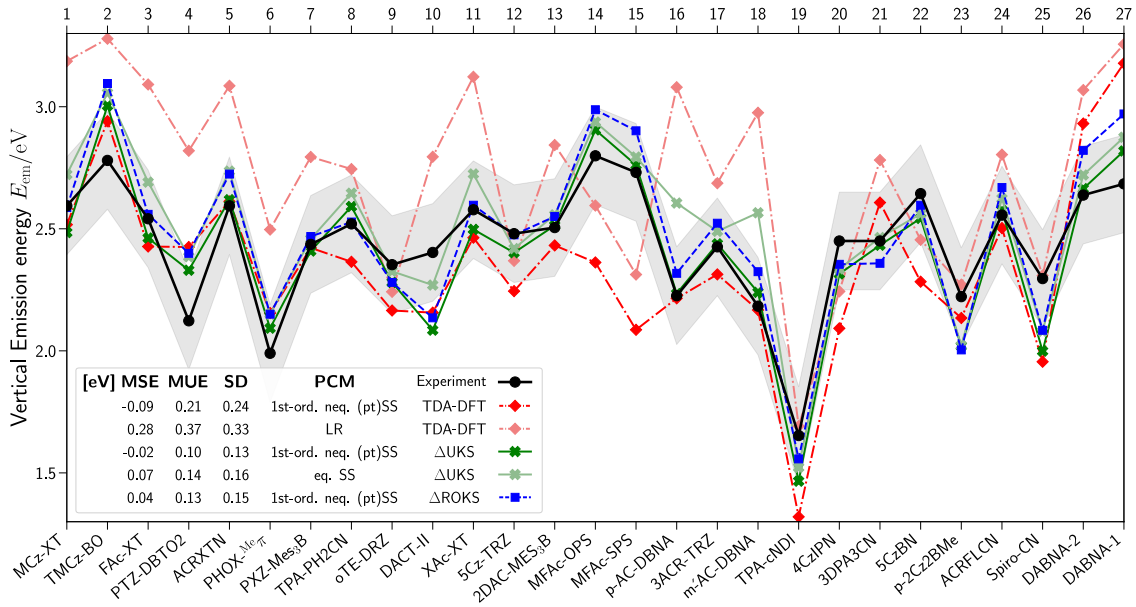

Figure B.4: Experimental (black) and calculated emission energies E_{em} for the emitters of the STGABS27 benchmark set. The calculated values are given for the OT-ωB97M-V functionals with TDA-DFT (red, dash-dotted), ΔUKS (green, solid), and ΔROKS (blue, dashed) at the consistently optimized S_1 geometry. Aside from 1st-order nonequilibrium state-specific solvation conditions (ptSS-PCM, full colors), TDA-DFT/LR-PCM (shaded red) and ΔUKS/SS-PCM under equilibrium conditions (shaded green) are plotted. ε and n^2 were chosen for the measurement-specific solvent (see Table B.1). An estimated uncertainty of ±0.2 eV for the experimental reference is marked by a gray band. MSE, MUE, and SD values for the set are tabulated.

After exploring the accuracy of TDA-DFT, we now turn to the ΔDFT-based methods. Figure B.3b and c illustrate the statistical analysis of the performance of ΔUKS/ptSS-PCM and ΔROKS/ptSS-PCM,

respectively. From the start, it is clear that both are more consistent and provide much-improved emission energies as compared to TDA-DFT. Across all tested functionals, the MUE and the magnitude of the MSE are consistently below 0.2 eV, with the best-performing ΔUKS/OT-ωB97M-V achieving exceptional accuracy. Notably, this improved accuracy extends to the statistical error as measured by the SD, which is nearly halved compared to even the best TDA-DFT/SS-PCM method. This improvement of both systematic and statistical errors confirms that ΔDFT not only removes a systematic bias between experimental and calculated E_{em} values but leads to an overall more accurate description of the vertical emission process.

This improvement is clearly evident from the plot of the absolute emission energies (E_{em}) against the experimental references depicted in Figure B.4 (see Supporting information for plots including all tested methods): For OT-ωB97M-V, inspection shows that ΔDFT/ptSS-PCM (UKS in solid green, and ROKS in dashed blue lines) faithfully reproduces the relative trends in emission energies with only a few cases beyond the error range of 0.2 eV, whereas TDA-DFT/ptSS-PCM (red, dash-dotted line) exhibits much larger deviations and more than a third of the cases at or clearly outside the 0.2 eV range. Selected examples include systems 14 and 15, where TDA-DFT underestimates the emission energies by over 0.5 eV, or 20, 21, and 22, which reverse their relative order, and all of which are accurately described by the ΔDFT-based methods. While seemingly acceptable in a benchmark considering mostly statistical performance, it should be noted that such severe deviations for several of the studied molecules can critically deteriorate the performance of screening and optimization tasks in material design.[305,306] In this respect, having no outliers > 0.3 eV is more important than eliminating small statistical deviations of ≈ 0.1 eV

Furthermore, we want to emphasize the remarkable robustness of the ΔDFT approaches regarding functional choice. In particular, the SD shows minimal variation across different functionals, regardless of the amount of admixed Fock exchange. Apart from a rather systematic shift toward smaller emission energies (negative MSE), most functionals provide almost identical, highly accurate values for E_{em}. A remarkable example is the simple PBE38-D4 functional with ΔUKS/ptSS-PCM, which shows the lowest SD (0.13 eV) among all tested methods. This is particularly advantageous since it allows screening workflows without a sophisticated RSH or the computationally demanding system-specific optimal tuning procedure.

Having established the generally superior performance of time-independent ΔDFT/ptSS-PCM compared to the more common TD-DFT approach, we now turn to the choice of reference wavefunction for the open-shell singlet state. In other words, is the formally correct ROKS approach so much better than UKS that the additional computational cost is justified? Comparing the emission energies for UKS (green) and ROKS (blue) with OT-ωB97M-V in Figure B.4, both curves run largely parallel to each other, with ROKS predicting slightly higher E_{em} values (between 0.07 and 0.17 eV increase in MSE). This systematic positive shift of ΔROKS (less negative MSE) holds for all tested functionals. We note that the singlet-triplet gap ΔE_{ST} displays a similar trend, where ROKS yields generally larger values than UKS due to a more destabilized singlet state.[307,308] The explanation lies in the inherent difference between UKS and ROKS wavefunctions. ROKS incorporates two determinants for proper spin-adaptation, avoiding the unwanted admixture of the energetically close but lower triplet state known as spin-contamination. Interestingly, the statistical measures suggest a slight benefit from the spin-contamination in UKS. This even extends to the statistical error (SD) indicating that UKS is more accurate despite its formally incorrect handling of open-shell singlets, at least for the CT states studied

herein. Hence, since the additional effort for ROKS offers no improvement in accuracy, the more widely available ΔUKS should be used for generally accurate emission energies of CT states.

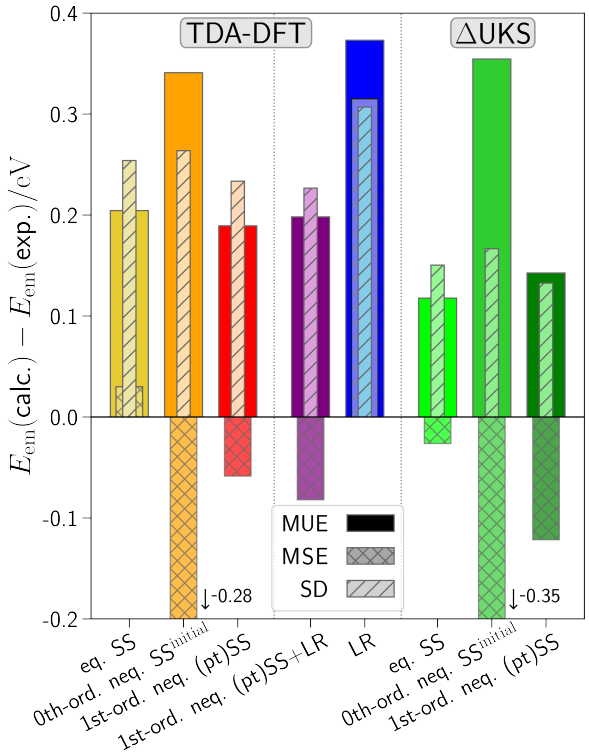

Figure B.5: Plots of the MUE (solid outer bar), MSE (hatched middle bar), and SD (dashed inner bar) for the calculated E_{em} relative to the experimental reference. Values are shown for TDA-DFT and ΔUKS with different solvation models. All calculations use the OT-LRC-ωPBEh-D4 functional and S_1 optimized structures (for TDA-DFT without solvation).

B.5.4 Solvation Models

After a detailed discussion of aspects of the electronic structure method applied to the solute, let us now examine the influence of the solvent model for the dielectric environment. Figure B.5 shows the statistical measures for TDA-DFT and ΔUKS with the OT-LRC-ωPBEh-D4 functional and different excited state solvation models. For TDA-DFT, there are several choices for the excited state solvation model: In addition to the physically complete LR-PCM or (pt)SS-PCM models, one may use the ground-state PCM or SS-PCM without first-order ptSS-corrections (SS^{initial}). Here, we begin with TDA-DFT/SS-PCM under equilibrium conditions for ground and excited states (E_{em}^{eq}, yellow bar), which marginally overestimates the emission energies. However, nonequilibrium effects must be considered to account for the limited duration of the vertical emission process (see scheme in Figure B.1). In the zeroth-order SS^{initial} approach (E_{em}^{0th}, orange bar), which neglects any solvent relaxation upon emission, E_{em} is systematically overestimated (negative MSE), as we already saw in the exemplary case of MCz-XT (vide supra). Balanced emission energies require the relaxation of the fast electronic solvent DOFs at first-order via the ptSS-PCM correction (E_{em}^{1st}, red bar). Notably, the ptSS-

PCM treatment also yields the lowest SD, which confirms the advantage of nonequilibrium solvation for vertical transitions. A similar trend emerges for the stepwise introduction of nonequilibrium solvation in the ΔUKS calculations, albeit at a substantially lower overall error (especially the SD). We can again compare the explicit emission energies predicted in the nonequilibrium (bright green) and equilibrium (shaded green) regimes displayed in Figure B.4. Accounting for nonequilibrium solvation generally reduces the emission energies, though not uniformly by the same amount. The differences arise from the specific solvent used during measurement. Only polar solvents, where the total (ε) and infinite-frequency (ε_∞) dielectric constants deviate substantially, such as DCM or PPF (Sys.: 1, 3, 11, 16, 18, 26, and 27), exhibit a significant nonequilibrium effect. Meanwhile, for nonpolar solvents dominated by fast polarization, such as toluene, equilibrium and nonequilibrium conditions deviate only negligibly.

Knowing that sophisticated nonequilibrium solvation with the SS-PCM model for TDA-DFT works well, we also investigated the more widely available and popular LR-PCM model. Benefits of LR-PCM compared to state-specific approaches include that the solvent response is treated for all states simultaneously, and analytical gradients are often available. However, a straightforward application of LR-PCM (blue bar) yields large errors stemming from a combined increase in the statistical error (larger SD) and a systematic overestimation of emission energies (positive MSE). This is also apparent from the E_{em} values plotted in Figure B.4 (dash-dotted shaded red line). The substantial error arises from the near-zero contribution in the transition-density-based LR-PCM model, which is clearly a result of the vanishing transition density of polar CT states. Consequently, the simultaneous use of LR- and nonequilibrium SS-PCM, as suggested in ref [229], also changes the results only slightly. Therefore, we conclude that any treatment of CT states with excitation-based models should include SS-PCM solvation since LR-PCM fails to recover the large dielectric stabilization of such states.

B.6 Conclusions

We presented an extension of the STGABS27 benchmark set for singlet-triplet gaps to experimental emission energies E_{em}, termed STGABS27-EMS. This new data complements the existing singlet-triplet gaps ΔE_{ST} for 27 TADF emitters, allowing a more robust test of excited-state methods. The combined benchmark data probes polar CT states not only relative to each other[1,208] but also relative to the nonpolar ground state, which allowed us to refine our recommendations for treating charge transfer states in solution. In particular, STGABS27-EMS enabled us to explore the nuances of functional choice and excited-state solvation for vertical transitions based on TDA-DFT and ΔDFT.

The primary result of this work is that ΔDFT/PCM-based approaches can predict emission energies of CT states of typical TADF emitters with higher accuracy and robustness than TDA-based approaches, as evident from the excellent mean unsigned errors of 0.10 eV and standard deviation of 0.13 eV for the best-performing OT-ωB97M-V with ΔUKS/ptSS-PCM. Such deviations fall within our assumed maximum uncertainty for the reference E_{em} values, suggesting our initial estimate of 0.2 eV might be too conservative. Moreover, the ΔDFT accuracy shows at least a four times smaller sensitivity to the functional choice than TDA-based approaches. Accordingly, the largest shift of the MSE between the tested functionals is 0.67 eV for TDA-DFT, whereas the respective shift is just 0.17/0.16 eV for UKS/ROKS. TDA-DFT introduces systematic shifts in the emission energies and the accuracy depends more on the functional. This is evident from the SD, which varies between 0.23 and 0.32 eV for

TDA, while it remains below 0.15/0.16 eV with UKS/ROKS. Hence, TDA-DFT calculations for CT require state-of-art range-separated hybrids in combination with optimal tuning and the sophisticated ptSS-PCM solvation model, whereas a ΔDFT calculation can employ any reasonable hybrid DFA, as evident from the good performance UKS/PBE38-D4. Clearly, the newly implemented nonequilibrium ptSS-PCM solvation for ΔDFT further improves the vertical emission energies, highlighting the general need for proper state-specific solvation.

In stark contrast, the most widely used excited-state method, TD-DFT or TDA-DFT with SS-PCM solvation, exhibits much larger deviations even with the best-performing OT-LRC-ωPBEh-D4 functional (MUE: 0.19 eV, SD: 0.23 eV). Unlike in our prior studies of singlet-triplet gaps, where a minimal admixture of $\approx$ 10% yields optimal error cancelation, emission energies require a large fraction (> 38%). Furthermore, we again confirmed the benefit of state-specific excited-state solvation, as the commonly employed linear-response variant yields only a negligible stabilization over the vacuum. Although the best TDA-DFT/ptSS-PCM approach provides reasonable errors below 0.2 eV, it is not generally reliable for CT states in TADF emitters.

In conclusion, the combined benchmarking of ΔE_{ST} and E_{em} strongly suggests that ΔDFT/PCM methods provide a generally robust and accurate account of polar CT states in solution. This success can be attributed to (i) the explicit account for orbital relaxation, (ii) an inherently state-specific treatment of solvation, and (iii) the avoidance of the long-range CT failure of TD-DFT.

B.7 Acknowledgments

T.F. acknowledges the Fonds der Chemischen Industrie (FCI) for funding under a Kekulé scholarship. This project has been funded with support from the RTG-2591 “TIDE-Template-designed Organic Electronics” by the DFG. J.M.H was supported by the U.S. National Science Foundation, grant no. CHE-1955282.

B.8 Supporting Information

The Supporting Information is available free of charge at
https://pubs.acs.org/doi/10.1021/acs.jpca.4c03273.
Detailed description of the computational workflow, methods, and used programs; complete plots of the emission energies for all used methods; investigationof basis set effects; definition of the used statistical measures. All optimized geometries of both singlet and triplet states, as well as all used input and output files for the presented results.

B.9 Conflicts of Interest

J. M. H. is part owner of Q-Chem and servers on its board of directors.

APPENDIX C

ΔDFT Predicts Inverted Singlet-Triplet Gaps with Chemical Accuracy at a Fraction of the Cost of Wave Function-Based Approaches

Lukas Kunze,[†] Thomas Froitzheim,[†] Andreas Hansen,[†] Stefan Grimme,[†] and Jan-Michael Mewes[†‡]

Received: 3 June 2024
Published online: 31 July 2024

Reprinted in Appendix C (adapted) with permission[§] from
L. Kunze, T. Froitzheim, A. Hansen, S. Grimme, and J.-M. Mewes, *ΔDFT predicts inverted singlet–triplet gaps with chemical accuracy at a fraction of the cost of wave function-based approaches*, J. Phys. Chem. Lett. **15** (2024) 8065, DOI: 10.1021/acs.jpclett.4c01649

Own contributions

- compiling the INVEST15 benchmark set
- performing all LR-CC2 benchmark reference calculations
- performing all ΔDFT calculations
- statistical analysis and interpretation of the results
- first draft and co-writing of the manuscript

[†]Mulliken Center for Theoretical Chemistry, Clausius Institute for Physical and Theoretical Chemistry, University of Bonn, Beringstr. 4, 53115 Bonn, Germany
[‡]beeOLED GmbH, Niedersedlitzer Str. 75c, 01257 Dresden, Germany
[§]Permission requests to reuse material from this chapter should be directed to the American Chemical Society.

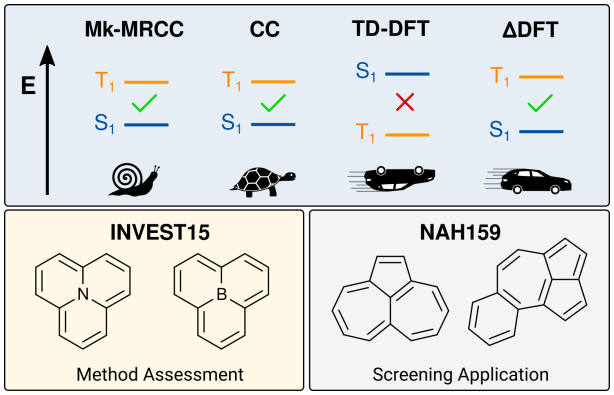

Figure C.1: Table of content graphic (ToC).

Abstract Efficient OLEDs need to quickly convert singlet and triplet excitons into photons. Molecules with an inverted singlet-triplet energy gap (INVEST) are promising candidates for this task. However, typical INVEST molecules have drawbacks like too low oscillator strengths and excitation energies. High-throughput screening could identify suitable INVEST molecules, but existing methods are problematic: The workhorse method TD-DFT cannot reproduce gap inversion, while wave function-based methods are too slow. This study proposes a state-specific method based on unrestricted Kohn-Sham DFT with common hybrid functionals. Tuned on the new INVEST15 benchmark set, this method achieves an error of less than 1 kcal/mol, which is traced back to error cancellation between spin contamination and dynamic correlation. Applied to the larger and structurally diverse NAH159 set in a black-box fashion, the method maintains a small error (1.2 kcal/mol) and accurately predicts gap signs in 83% of cases, confirming its robustness and suitability for screening workflows.

C.1 Introduction

Molecules with an inverted singlet-triplet energy gap (INVEST) have become a hot research topic as they would enable highly efficient emitters for organic light-emitting diodes (OLEDs).[187–189,309–317] In OLEDs, excited states (or excitons) are created by recombining electrons and holes.[318] According to Fermi-Dirac spin statistics, the ratio of singlet to triplet excited states generated via recombination is 1:3. Hence, any purely fluorescent emitter's internal quantum efficiency (IQE) is limited to 25%. Overcoming this limitation, modern emitters can thus harvest singlet and triplet excited states, either via phosphorescence in so-called PhOLEDs, or by upcycling triplets via reverse intersystem crossing (rISC) into light-emitting singlet excited states. The latter phenomenon is termed thermally activated delayed fluorescence (TADF) and has been intensively studied.[52,70,187,216,217,319–321]

A key property of TADF emitters is a small energy gap ΔE_{ST} between S_1 and T_1 states[70,216]

$$\Delta E_{ST} = E_{S_1} - E_{T_1} \,, \tag{C.1}$$

which is necessary to enable efficient triplet up-conversion. This is typically achieved by introducing

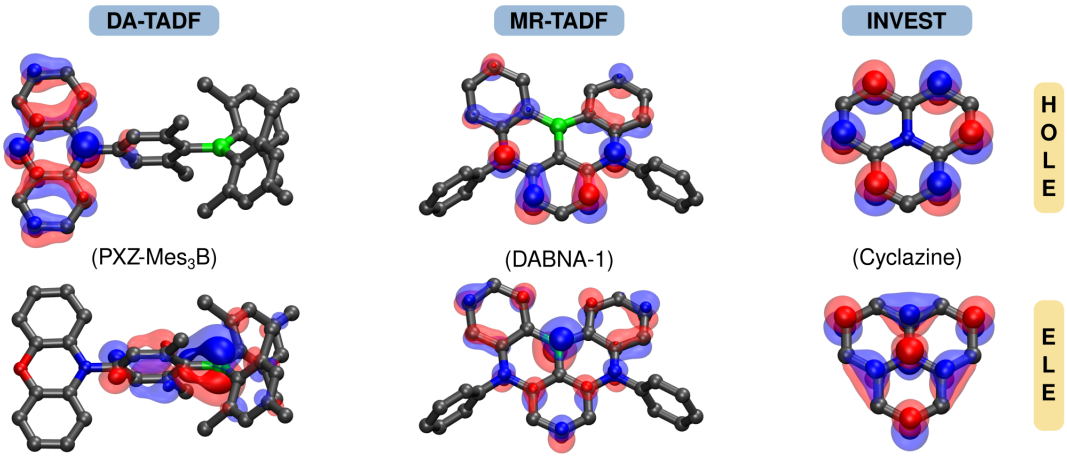

Figure C.2: Hole and electron molecular orbitals (MO) from a ΔUKS calculation with the FX175-ωPBE functional for a donor-acceptor type TADF emitter (DA-TADF), a multiresonance TADF emitter (MR-TADF) and an inverted singlet-triplet gap molecule (INVEST), isovalues of 0.08 Bohr^{-3} and 0.04 Bohr^{-3} were used for the inner (solid) and outer (transparent) isosurface, respectively.

a large spatial separation between the highest occupied molecular orbital (HOMO), located on a donor, and the lowest unoccupied molecular orbital (LUMO), located on the acceptor. A problem of this straightforward design is that small overlap also leads to vanishing spin-orbit coupling (SOC) and oscillator strength (f_{osc}) between the states of interest,[169] which negatively impacts (r)ISC and radiative decay rates. Additionally, such classical D-A-type TADF emitters exhibit the broad emission peaks characteristic of long-range charge-transfer (LRCT) states – the opposite of the desired sharp (color-pure) emission.[322]

In these regards, the discovery of multi-resonance TADF (MR-TADF) emitters changed the picture.[322] In contrast to the D-A architecture, MR emitters achieve a small electron-hole overlap by distributing the HOMO and the LUMO on alternating positions of an aromatic π-system.[204] Although this does not reduce electron-hole overlap as much as in D-A emitters and, in turn, leads to larger singlet-triplet gaps, other photophysical properties of MR-TADF emitter are more favorable: The emission spectrum of MR emitters is sharp and thus color pure and the transitions exhibit high oscillator strength and thus short lifetimes.[322,323] Because of these and further desirable properties, DABNA and its derivatives are used as fluorescent blue emitters in mass-produced OLED displays.[60]

Regarding their molecular and electronic structure, MR-type emitters can be regarded as a bridging element between classical D-A-type TADF emitters and INVEST-type emitters (cf.C.2). Analogous to MR-TADF emitters, INVEST emitters give up the spatial separation between donor and acceptor in favor of a strategy with alternating orbital lobes. The perhaps most prototypical examples for INVEST systems are cycl[3.3.3]azine and its derivatives, of which heptazine, a nitrogen-doped variant, has been experimentally shown to have properties that confirm an inverted ΔE_{ST}.[187] In a two-dimensional polymeric variant of heptazine, amorphous carbon nitride, Actis et al. observed in steady-state optical spectroscopy an inversion of singlet and triplet excitons by roughly 0.2 eV.[324] During the final stages of the preparation of this manuscript, another study reported the experimental determination of INVEST for a pentaazaphenalene (molecule #4 in our INVEST15 benchmark introduced below)

derivative.[325]

The special structure of these triangulene-like systems leads to an inversion of the singlet-triplet gap, meaning that in violation of Hund's rule, the S_1 is energetically lower than T_1. As a result, rISC changes from an uphill conversion process of triplet to singlet excitons in DA- and MR-TADF emitters to a downhill process in INVEST systems, which should translate into more efficient triplet harvesting and lower efficiency roll-off at high brightness. However, the inverted gap comes at a cost: the electronic structure that gives rise to an inverted gap causes poor photophysical properties, such as low oscillator strengths. Therefore, it is an essential task to identify INVEST emitters that combine an inverted gap with favorable emission properties.[188] Unfortunately, systematic high-throughput screenings are hindered by the reality that MR-TADF and INVEST emitters are only poorly described by time-dependent density functional theory (TD-DFT[149]), which is by far the most prominent and efficient workhorse in materials science. More specifically, it seems that the short-range charge-transfer (SRCT) states that emerge from the MR-TADF and INVEST scaffolds are poorly described by TD-DFT and its Tamm-Dancoff-approximated variant (TDA-DFT[180]), which predicts systematically too high singlet excitation energies and qualitatively wrong ΔE_{ST} (*vide infra*). In contrast to the shortcomings of TD-DFT with the description of the LRCT states and their dielectric embedding in classical TADF emitters,[2,208] the issues TD-DFT has with SRCT states can not be mitigated by using modern functionals and more complete solvation models, but are inherent to the underlying theory.

Previously, Hall and co-workers tested a variety of hybrid and range-separated hybrid functionals with different amounts of Fock exchange (FX) and range-separation parameters for MR-TADF emitters.[205] They attributed the imbalanced description of S_1 and T_1 with errors in ΔE_{ST} of up to 1.0 eV to the absence of doubly excited determinants in TD(A)-DFT, which affects the excited singlet states much more than the triplets.[225] In their recent study, which employed wave function-based correlated methods in addition to TD-DFT, Drwal et al. pointed out an implicit connection between doubly excited determinants and spin-polarization effects, which specifically stabilize the S_1 state out of a pair of singlet and triplet excited states involving the same molecular orbitals.[201] The spin-polarization balances the increasing electron-hole overlap and dynamical correlation, which together destabilize the S_1 relative to the T_1 state. Further works confirm the hypothesis that doubly excited determinants exert a large and selective influence on the energy of the singlet excited state.[189,306,312,326,327] This different impact of doubly excited configurations on singlet and triplet states explains why in wave function theory, highly correlated methods including at least up to triple substitutions are required for a balanced description of INVEST molecules (*vide infra*).

The conclusion derived by most authors is that computationally demanding correlated wave function-based approaches are necessary to describe the inversion of S_1 relative to T_1. For example, linear-response second-order approximate coupled cluster singles and doubles (LR-CC2[77]), second-order algebraic diagrammatic construction (ADC(2)[270,271]) and their spin-scaled variants[99,206] (SCS-CC2, SCS-ADC(2)), as well as state-averaged complete-active space self-consistent-field-based approaches (SA-CASSCF,[328] SC-NEVPT2,[329] and CASPT2[330,331]) are often used to study INVEST emitters because they include these effects at a manageable computational cost.[188,190,306,313,327] However, in face of the importance of doubly excited determinants, it is surprising that second-order methods like LR-CC2 or ADC(2) perform quite well for INVEST cases.

Further studies seek a more complete description that includes even higher-order correlation effects using state-specific coupled cluster with up to triple substitutions. Notably, Dreuw et al. reported a

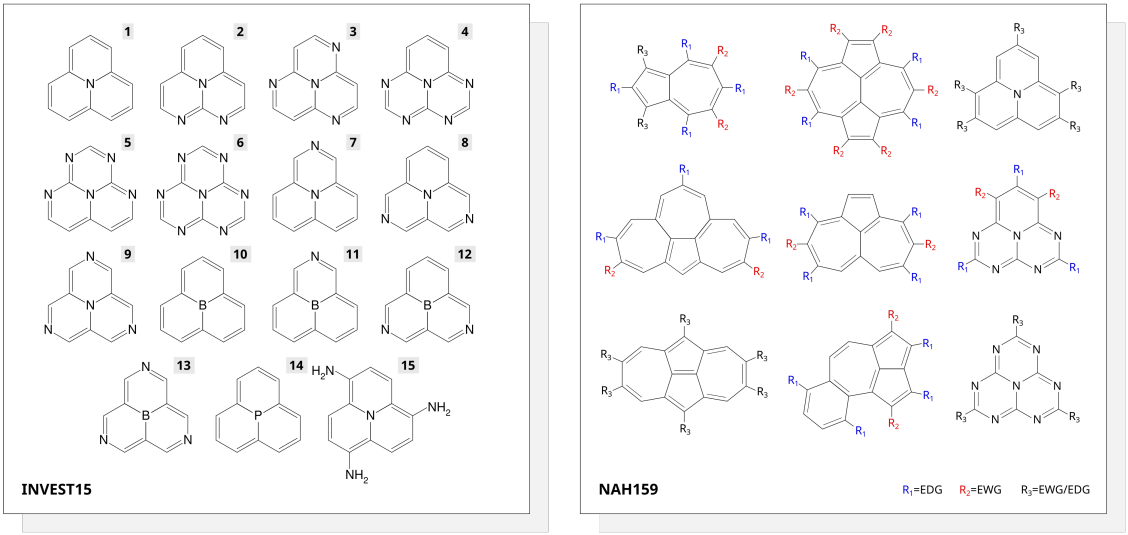

Figure C.3: INVEST15 benchmark set, a selection of 15 cyclazine derivates, differing in doping pattern and doping atoms and NAH159, a selection of substituted cyclazine derivates and non-alternant hydrocarbons, only an excerpt is shown with positions of electron-donating (EDG) and electron-withdrawing groups (EWG) colored blue and red, respectively.

decrease of the inverted gaps or even positive ΔE_{ST}-values for prototypical INVEST emitters when they systematically converged the level of theory by increasing basis set size and correlation treatment, questioning the existence of inverted ST-gaps.[196] Specifically, they used a state-specific coupled cluster approach with unrestricted Hartree-Fock reference wave functions [termed ΔCCSD(T)@HF[332]], as well as the ADC method of up to third order.[201] Meanwhile, a minimal CASSCF(2,2) reference in Mukherjee's MR-CC-formalism [Mk-MR-CCSD(T)@CAS(2,2)[193,194]] used by Drwal et al. tends to yield more negative gaps.[201]

Having established that various high-level single- and multireference methods agree with each other and can thus be considered converged, Loos and co-workers recently demonstrated that also the relatively efficient LR-CC2 and ADC(2) methods agree surprisingly well with EOM-CC3[333] and EOM-CCSDT[334].[190] Although this agreement has been traced back to error-cancellation effects, it means that INVEST systems can be modeled with widely available and relatively efficient (compared to MR-CC) ADC(2) or LR-CC2 methods. However, even these calculations take hours for typical INVEST molecules with converged, i.e., augmented triple-ζ basis sets, rendering them too costly to execute automatic screening workflows with thousands or even millions of molecules.

Addressing this major challenge, a recent work by Jorner and co-workers has presented a special-purpose semi-empirical quantum-chemical method focusing on the π-electrons (PPP theory).[305] Exploiting dynamic spin-polarization to recover the gap inversion, their PPP method shows a promising correlation with ADC(2) calculations after introducing several correction terms. While clear advantages of the method are its speed (less than a second per molecule) and robustness against technical issues (> 99.9% convergence in a test application), downsides are that it requires specialized software and, moreover, a clear separation between σ- and π-electrons, which excludes some functional groups.

This study presents a less approximate and thus slightly more costly (a few minutes per molecule) approach to predict ΔE_{ST} and absolute state energies accurately and reliably with standard quantum-chemical software packages. To this end, we use state-specific unrestricted Kohn-Sham DFT (here ΔUKS), targeting the respective singlet (and triplet) states directly, i.e., by converging a non-Aufbau initial guess. For the lowest excited states relevant to INVEST, this is typically a singly excited HOMO–LUMO determinant.

While targeting triplet excited states with ΔUKS is trivial via the multiplicity, converging open-shell singlet states requires generally non-standard SCF solvers. Here, we employ the (initial) maximum overlap method (IMOM/MOM), which avoids variational collapse to the ground-state via additional constraints.[85,86] A major advantage of such state-specific methods over excitation-based response methods like LR-CC2, ADC(2), or TD-DFT is that each excited state is calculated in its own optimal set of orbitals. As a result, orbital relaxation effects and higher (e.g., double) excitations are implicitly included in the description at a much lower cost than in comparably accurate response methods.[86,261] In addition to ΔUKS, we test the closely related restricted open-shell Kohn-Sham (here ΔROKS)[87,88,236] method, which improves on ΔUKS by providing a formally correct open-shell singlet with $\langle S^2 \rangle = 0$.[173,261]

For these state-specific ΔDFT methods, we explore the influence of the functional, focusing on the type and amount of exact exchange mixing, which strongly affects the computed gaps. The methods are evaluated in comparison to high-level reference values collected from the literature for a set of 15 INVEST molecules sharing the prominent cyclazine motif, as well as our own high-level calculations. We then rationalize the reliability of the ΔUKS approach by comparing it to state-specific post-SCF correlation methods. Finally, we apply the approach to a larger and structurally diverse validation set, where we explore the effect of the initial guess (HOMO–LUMO vs all excitations between HOMO-1, HOMO, LUMO, and LUMO+1). Eventually, we show that considering all these excitations by default mitigates many of the issues resulting from the state-specific nature of the approach and increases the method's robustness, as is desirable for an application in high-throughput screenings.

C.2 Benchmark Set and Reference Values

Based on recently published high-level calculations, we compiled the benchmark set INVEST15, which includes 15 INVEST emitters based on the cyclazine-scaffold, featuring various doping patterns and heteroatoms. Ten of the 15 molecules were taken from a recent work of Loos et al.,[190], in which they provided theoretical best estimates (TBE) using the most accurate methods affordable for those types of molecules, namely EOM-CC3 and EOM-CCSDT (with incremental corrections up to augmented triple-ζ basis set level). Five additional literature-known INVEST emitters, namely 3[306] and 10, 11, 14 and 15[188] originating from two papers of Ricci et al. were picked to diversify the test set and the doping patterns. System 15 was added as a sanity check to have at least one positive ΔE_{ST}. B97-3c optimized ground-state geometries were used for all INVEST15 systems, which showed fairly small root-mean-square deviations (RMSDs) compared to CCSD(T)/cc-pVTZ geometries (taken from Loos' benchmark set) typically around 0.005 Å.

The INVEST15 will serve as our test set for different functionals, basis sets, etc., while a second benchmark set by Garner et al.[191] will serve as our validation set (see Figure C.3). The second set

consists of substituted variants derived from systems 1, 4, and 6 of our INVEST15 benchmark set, as well as substituted variants of non-alternant hydrocarbons not part of INVEST15. In total, the validation set comprises 159 distinct systems, which we will refer to as NAH159 for simplicity.

In light of the fragmented reference data, we perform extensive tests of both state-specific coupled cluster approaches (namely ΔCCSD(T) and Mk-MR-CCSD(T)), as well as LR-CC2. We find that Mk-MR-CCSD(T) based on a reference wave function with only the two singly excited determinants (denoted $\langle\uparrow\downarrow| \pm \langle\downarrow\uparrow|)$[192,335] and LR-CC2 agree very closely with the TBE of Loos and co-workers (see Supporting Information for details). Therefore, we choose LR-CC2/aug-cc-pVTZ as the secondary reference method to provide consistent reference data for the larger NAH159 set.

To further investigate and rationalize the performance of the ΔUKS/PBE0 approach, we use the unrestricted Kohn-Sham wave function as a basis for ΔCCSD and ΔCCSD(T) calculations with Q-Chem,[74,332] and compare the results to those obtained with a canonical UHF reference similar to Dreuw and co-workers.[196] Recognizing the importance of spin-contamination (which refers to the deviation from the $\langle S^2\rangle$ expectation value of the wave function, e.g., 1.2 instead of 1.0) and spin-adaptation (by which we refer to changing the formally wrong $\langle S^2\rangle$ of a single-reference open-shell singlet of 1 to its correct value 0), we explored the impact of the Yamaguchi spin-correction based on the $\langle S^2\rangle$ expectation value from CCSD.[262] The underlying reason is that the singlet state obtained with UKS is usually a 50:50 mixture of singlet and triplet state exhibiting an ideal $\langle S^2\rangle = 1.00$. This is a direct result of the UKS approach using only a single determinant.

Finally, to eliminate any spin-related issues in wave function-based Δ approaches, we also considered a multireference level of theory with exactly two reference determinants. Namely, we calculated state-specific Mukherjee multireference coupled cluster with perturbative triple excitations [Mk-MR-CCSD(T)] on a reference wave function consisting of the required two singly excited determinants for proper spin-adaptation.[195] This level of theory is for a strict two-determinant state,[192,197,335] at least formally, the most highly correlated method used in this work, and presumably even superior to EOM-CCSDT of Loos and co-workers since excited states are targeted directly and no substitutions have to be spent to generate the excited states from the ground-state reference (see also SI).

C.3 Computational Details and Workflow

Several different programs were used throughout this study, including the Q-Chem program version 5.4.2[184] (for all ΔUKS, ΔROKS, ΔCC, and TDA-DFT[149,180] excited-state calculations), the ORCA program version 5.0.4[336] (for all DFT[75,76] ground-state geometry optimizations), the MRCC program[337] (for all single-reference correlated WFT calculations, mainly LR-CC2[77]), the NWChem program version 7.2.2[338,339] with the Tensor Contraction Engine[340] (for all multireference correlated WFT calculations), and the DALTON program version 2020.1[341,342] (for CC3[333] calculations). The ground-state geometry optimizations were carried out with the B97-3c[135] composite method. Symmetry constraints (C_{3h}) were enforced only for system 15, to be consistent with existing literature references. Comprehensive conformer searches for the ground-state geometries were omitted since the investigated molecules are rigid and planar, having only one self-evident low-energy structure.

For all excited-state energy calculations for the INVEST15 (ΔUKS, ΔROKS, ΔCC, Mk-MR-CCSD(T), LR-CC2, and LR-CC3), the B97-3c optimized ground-state geometries were used. In contrast to DA-

TADF emitters, the influence of the solvent is negligible (<0.02 eV for the best-performing ΔUKS/PBE0 approach in toluene, see Figure S6). Therefore, only gas phase calculations were considered. ΔUKS and ΔROKS methods were used in combination with the large Ahlrich's def2-TZVPP[162,304] basis set. All post-SCF ΔWFT calculations are conducted using Dunning-type basis sets up to cc-pVTZ.[198,199] The Mk-MR-CCSD(T) calculations adhere to a similar procedure as outlined by Drwal et al.[201] with a def2-TZVP basis set in the NWChem program (see SI for further details concerning basis-set and CC convergence).[338,339] LR-CC2 and LR-CC3 calculations employ the aug-cc-pVTZ[343] and cc-pVDZ basis sets, respectively.

The ΔUKS approach was used with the initial maximum-overlap method (IMOM)[85,86] as implemented in Q-Chem to prevent variational collapse to the ground-state. For the IMOM calculations, converged ground-state orbitals are used to generate the non-Aufbau initial guess by manually repopulating the orbitals (promoting an electron from an occupied to a virtual orbital for singlets, and for triplets also changing the spin of the electron, see SI for sample input files). MOM adds a constraint to the SCF solver, requiring the occupied orbitals to maximize overlap with those of the previous step (MOM) or the initial guess (IMOM).[85,86] Here, we exclusively use the more stable IMOM algorithm, which is comparable in speed to standard SCF (DIIS) iterations, while its convergence is only slightly less robust. For example, in the 1272 calculations of the structurally diverse NAH159 set at the PBE0/def2-SVP level of theory (including all possible excitations between HOMO-1, HOMO, LUMO, and LUMO+1), the ΔUKS/IMOM calculations achieved convergence after an average of just 22 cycles in 64 s. This is just twice as many as for the ground states, which converged on average after 10 cycles in 29 s. Moreover, only 1.8% of ΔUKS/IMOM calculations for this set failed to converge, which are mostly calculations targeting higher-lying states (14 failures out of 954 calculations), whereas those starting from a HOMO–LUMO guess converged even more robustly (only two failures out of 318 calculations or 0.6%, both are singlets and in both cases, the gap-sign is correctly predicted from higher-lying guesses). After convergence of the IMOM-SCF, excitation energies are calculated as the difference between the ground-state SCF energy and that of the open-shell singlet/triplet states. Singlet-triplet gaps correspond to the SCF energy differences between the energetically lowest open-shell singlet and triplet states. For a detailed explanation and theoretical background on MOM/IMOM, please refer to the provided references.[85,86]

For calculations on the validation set of 159 molecules, geometries optimized at the ωB97X-D[269]/def2-TZVP level were taken from a recent publication by Garner et al.[191] As reference for the NAH159 benchmark set, vertical singlet-triplet energy gaps were calculated at the LR-CC2[77,344]/aug-cc-pVTZ level, to be consistent with the references for the INVEST15 set. ΔUKS calculations for vertical singlet-triplet gaps of the validation set were carried out in the def2-SVP basis set with the PBE0 functional to simulate a screening application.

C.4 Results and Discussion

We begin our investigation by exploring the effect of the DFT functional on the ΔUKS approach, including results obtained with TDA-DFT and ROKS to complete the picture. Since the most important parameter in the DFT functional turned out to be the amount of Fock exchange (FX), we selected a hierarchy of PBE-based density functional approximations (DFAs) with increasing admixture of FX, namely PBE,[108] PBE0,[113,123] PBE38,[140] PBE50,[200] and LC-ωPBE,[177] as well as the tuned RSH

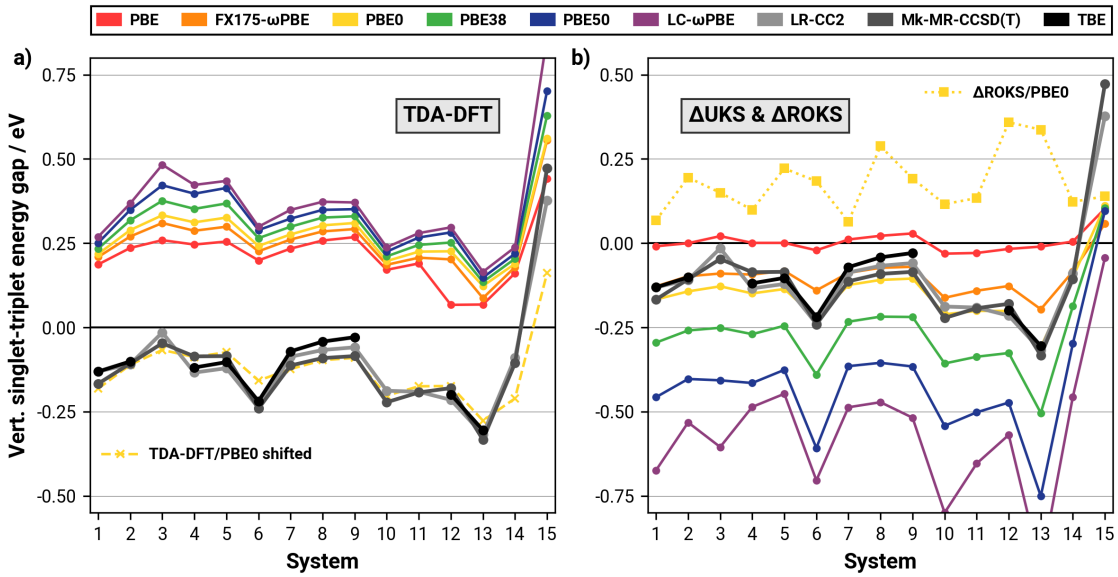

Figure C.4: Vertical singlet-triplet energy gap for investigated molecules calculated by **a)** TDA-DFT, ROKS/PBE0 and **b)** ΔUKS for various functionals of the PBE-family with different amounts of FX (increases from red to blue), all values in eV. The TBE is obtained from CC3/aug-cc-pVTZ + [CCSDT/6-31+G(d) – CC3/6-31+G(d)] for S_1 and CC3/aug-cc-pVDZ + [CCSD/aug-cc-pVTZ – CCSD/aug-cc-pVDZ] for T_1 as defined by Loos et al.[190] All TD-DFT and ΔDFT calculations use the def2-TZVPP basis set.

FX175-ωPBE with a ω value of 0.175 that was found to be most accurate for CT states of TADF and MR-TADF emitters in previous work.[1,208]

First, let us discuss the TDA-DFT results for the vertical ΔE_{ST} gaps shown in Figure C.4a. As expected, TDA-DFT yields positive ΔE_{ST} for all 15 molecules, irrespective of the amount and type of FX admixture. This can be rationalized by the lack of doubly excited determinants in TDA-/TD-DFT, which causes the respective S_1 state to be too high in energy.[161,345,346] Only for molecule 15, which has a positive singlet-triplet gap, TDA-DFT with the PBE functional agrees reasonably well with the reference. Generally, there is a clear systematic trend to larger gaps with an increasing amount of FX, which is the same for DA-type TADF emitters.[208] Moreover, despite this failure of TDA-DFT to reproduce absolute gaps, the relative trends between the INVEST15 systems are recovered rather well. These trends are also reflected in the Bessel-corrected standard deviation (SD) for TDA-PBE0 (see C.1), which is just 0.075 eV, compared to 0.381 eV for the mean absolute deviation (MAD), pointing at the systematic error of TDA. To illustrate this, we have added a dashed line with the TDA-PBE0 results down-shifted by −0.4 eV (MD vs TBE) in Figure C.4a). Inspection shows a reasonable agreement with the high-level references, indicating that the effect of double excitations on the singlet energy is rather consistent. However, one should be clear that this is based on error cancellation effects that are enabled by the structural similarity of the molecules in the INVEST15 set.

Therefore, let us move to the state-specific ΔDFT approaches, namely ΔUKS and ΔROKS, which account for doubly excited determinants via orbital optimization.[261] However, despite its state-specific nature and its principle ability to deal with double excited states, ΔROKS (Figure C.4b) is not more

accurate than TDA-DFT, which is in stark contrast to a recent benchmark for DA-type and MR-TADF emitters.[1] Similar to TDA-DFT, ΔROKS systematically overestimates gap sizes to an extent where it only provides positive gaps, which is true for all functionals (see Fig. S4 the SI). Moreover, in contrast to TDA-DFT, relative trends between the systems are worse, as shown by the SD of ΔROKS/PBE0 of 0.202 eV. The issue appears to be the missing doubly excited $LUMO^2$ singlet configuration (D_{CS}-type double excitation in ref.[347]) in the ROKS approach, which is responsible for the spin-polarization (the respective triplet-reference with two same-spin electrons in the LUMO which is required for ROKS spin-purification can not exist). Hence, we conclude that ΔROKS is unsuitable for application to INVEST systems, and presumably even more generally for D_{CS}-type doubly excited states.

In contrast to ROKS, the ΔUKS results shown in Figure C.4b all exhibit a trend similar to the various high-level reference methods, while the amount of FX appears to scale the gaps (the more FX, the more negative the gaps). With the RSH LC-ωPBE with a range-separation parameter of 0.175 (termed FX175-ωPBE, established to be optimal for TADF emitters in previous work)[1], and even with the common admixture of 25% of FX as in PBE0,[348] UKS provides exceptional agreement and virtually lies on top of the high-level references for all but two cases, namely system 3 (lacking uptick), and system 15 (too small positive gap). With even more FX as in PBE38, PBE50, or LC-ωPBE with the default range-separation parameter of 0.45, provides systematically too negative ST-gaps, while much or no FX as in the pure PBE functional provides too positive gaps. Note that the optimal amount of FX might vary with the functional.

Interestingly, modern pure functionals like the meta-generalized gradient approximation (meta-GGA) density functional r^2SCAN[210] (and to some extent also B97M-V)[179] remedy the shortcomings of PBE. r^2SCAN performs almost equal to UKS/PBE0 (MAD against LR-CC2 is 0.053 eV vs 0.046 eV for PBE0, cf. Table C.1) and becomes better if the outlier (*vide infra*) is removed (MAD 0.037 eV vs 0.049 eV for PBE0, cf. Figure S3 in the SI) albeit these differences are only borderline significant. However, there is also one issue, namely a systematic underestimation of nitrogen $n\pi^*$ states, which can artificially become S_1 or T_1, causing outliers, e.g., for molecule 13 (here the actual $\pi\pi^*$ states are S_2 and T_3, whose gap is spot-on (cf. Figure S3). Irrespective of those outliers, it appears that the exchange-functional of r^2SCAN mimics some properties of nonlocal FX, which has previously been reported in the context of self-interaction error.[348] Moreover, since pure functionals enable a substantial speedup over hybrids due to full exploitation of density-fitting,[348] they can offer an even faster screening for INVEST if $n\pi^*$ states could be automatically identified. We are currently exploring this possibility.

Statistical metrics for ΔUKS, ΔROKS, and TDA-DFT for the best-performing functionals PBE0 and FX175-ωPBE are given in Table C.1.

The best-performing method, ΔUKS/PBE0, shows a MAD of only 0.035 eV against the TBE, achieving chemically accurate (better than 1 kcal/mol ≈ 0.043 eV) results against a high-level WFT method. The nonzero MD of PBE0 provided in Table C.1 suggests that a slightly smaller fraction of FX of around 20% would render the MD closer to zero, further improving the MAD. However, it is questionable if such small changes for a limited number of molecules transfer to the bigger picture. The more modern tuned RSH FX175-ωPBE performs comparably well with an MAD and RMSD of 0.041 eV and 0.053 eV. Finally, we want to point out that the accuracy of the approach is retained even with a smaller basis set, as evident from the def2-SVP to def2-TZVPP RMSDs for PBE0 of only 0.016 eV (see SI for details). This enables much more efficient calculations, as the walltime with def2-SVP is

Table C.1: Statistical error metrics (formulas in the SI) for various tested methods against TBE and LR-CC2/aug-cc-pVTZ reference data, DFT calculations use the def2-TZVPP basis set, Mk-MR-CCSD(T) calculations use the def2-TZVP basis set. All values are given in eV.

Method	MD	MAD	RMSD	SD	AMAX
against TBE					
(excl. 3, 10, 11, 14, 15)					
LR-CC2	–0.016	0.016	0.018	0.009	0.030
Mk-MR-CCSD(T)	–0.017	0.031	0.034	0.031	0.056
ΔPBE0	–0.035	0.035	0.043	0.026	0.076
ΔFX175-ωPBE	0.023	0.041	0.053	0.051	0.114
Δr^2SCAN	0.007	0.052	0.088	0.093	0.263
against LR-CC2					
ΔPBE0	–0.041	0.046	0.079	0.070	0.266
ΔFX175-ωPBE	0.005	0.060	0.099	0.103	0.319
Δr^2SCAN	–0.007	0.053	0.100	0.103	0.276
ΔROKS/PBE0	0.284	0.315	0.344	0.202	0.655
TDA-PBE0	0.381	0.381	0.388	0.075	0.481
TDA-PBE0 (–0.4 eV)	–0.019	0.055	0.075	0.075	0.216

about 15-18 times shorter than with def2-TZVPP.

Another interesting observation is that system 15, the only one with a positive gap, steps out of line. Here the different functionals become much more similar, indicating that the strong dependence on the amount of FX vanishes for molecules with positive gaps. This is in line with our earlier study on the singlet-triplet gaps of TADF emitters, where ΔUKS and ΔROKS were much less sensitive to the amount of FX in the DFA than TD-DFT.[1] At the same time, this system shows the largest deviation between the best-performing ΔUKS approaches and the high-level references of around 0.3 eV, almost ten times the MAD.

After careful analysis of the gaps, let us now briefly consider the excitation energies of the S_1 and T_1, which are collected for the high-level references and the PBE0-based DFT methods in Table C.2 (for all methods, see Figure S1 and Figure S2 in the SI). Inspection shows highly systematic deviations between S_1 and T_1 excitation energies of the LR-CC2 reference and ΔUKS/PBE0, which leads to the previously established agreement for the gaps. For TDA-PBE0, the triplet energies are similar, whereas the deviation for the singlets is larger (by 0.4 eV) and of opposing sign. This can be rationalized by the aforementioned lack of doubly excited determinants (and spin-polarization). Further analysis of UKS results shows that the deviations strongly depend on the amount of FX (see SI), where the deviations for S_1 and T_1 cancel each other at around 25%. The relation between spin-contamination and excitation energy is also evident from Figure C.5b, which displays the $\langle S^2 \rangle$ expectation values of the S_1 excited states for the INVEST15 set (the respective data for the spin-adapted T_1 can be found in the SI): While intermediate amounts of FX found in FX175-ωPBE and PBE0 lead to some spin-contamination of S_1 with $\langle S^2 \rangle = 1.15$, going to pure HF leads to a highly contaminated state

Table C.2: Singlet and triplet excitation energies (EEs) of the LR-CC2 reference and deviations for the PBE0 functional using ΔUKS and TDA-DFT for the INVEST15 benchmark set, all values in eV.

	S_1	$\Delta^{S_1}_{CC2}$		T_1	$\Delta^{T_1}_{CC2}$	
mol.#	CC2	ΔUKS	TDA	CC2	ΔUKS	TDA
1	1.05	–0.15	0.25	1.18	–0.11	–0.10
2	1.61	–0.17	0.26	1.71	–0.14	–0.13
3	2.12	–0.27	0.16	2.14	–0.16	–0.19
4	2.21	–0.20	0.25	2.35	–0.19	–0.20
5	2.16	–0.19	0.27	2.28	–0.17	–0.18
6	2.75	–0.17	0.28	2.98	–0.19	–0.20
7	0.90	–0.16	0.26	0.99	–0.13	–0.11
8	0.76	–0.18	0.26	0.83	–0.14	–0.11
9	0.62	–0.19	0.26	0.68	–0.14	–0.11
10	0.85	–0.17	0.23	1.04	–0.15	–0.16
11	1.08	–0.17	0.25	1.27	–0.16	–0.17
12	1.32	–0.16	0.26	1.53	–0.17	–0.18
13	1.57	–0.13	0.28	1.89	–0.14	–0.16
14	1.27	–0.13	0.21	1.36	–0.12	–0.06
15	1.56	–0.50	–0.08	1.18	–0.23	–0.27

with $\langle S^2 \rangle > 2$.

Considering that dynamic spin-polarization, which is associated with certain doubly excited determinants, was previously identified as the driving mechanism for the singlet-triplet gap inversion,[201] we argue that the FX-dependent spin-polarization in ΔUKS mimics this effect. In orbital-optimized excited state methods like ΔUKS, double-excitation character manifests as mixing of HOMO and LUMO in both the alpha and beta spins, which, in turn, leads to a deviation of the $\langle S^2 \rangle$ from the ideal value (that is not strictly spin-contamination). As evident from Figure C.5b, the amount of FX in the functional governs this mixing, and the 25% of FX in PBE0 is "just right" to balance this effect. However, while this appears to be the working mechanism of hybrid functionals, it does not apply to semilocal functionals. Here, although no FX is admixed in the well-performing r^{2}SCAN functional, the spin polarization of the open-shell singlet state is nearly identical to that of PBE0 (see Figure S5 in SI), suggesting that a similar error-cancellation is possible with a semilocal exchange kernel.

Lastly, we want to point out that similar error-cancellation effects have been reported in a study on doublet excited states in structurally similar triangular molecules.[349] In their careful analysis of a comparison between single-reference (UKS/UHF, ROHF) and multireference methods, the authors demonstrated that spin-contamination in a UKS/UHF reference leads to negative contributions to the spin density that have the same impact as electron correlation in the MR reference calculation. In further analogy, the error cancellation worked best with small amounts of FX admixture for the spin-unrestricted wave function, but not for the spin-restricted ROHF. Hence, we speculate that the presence of this spin-polarization (*vide infra*) mechanism in the ΔUKS calculations explains the robustness of the approach.

Having explored the effect of mixing DFT and FX in unrestricted Kohn-Sham calculations, we now

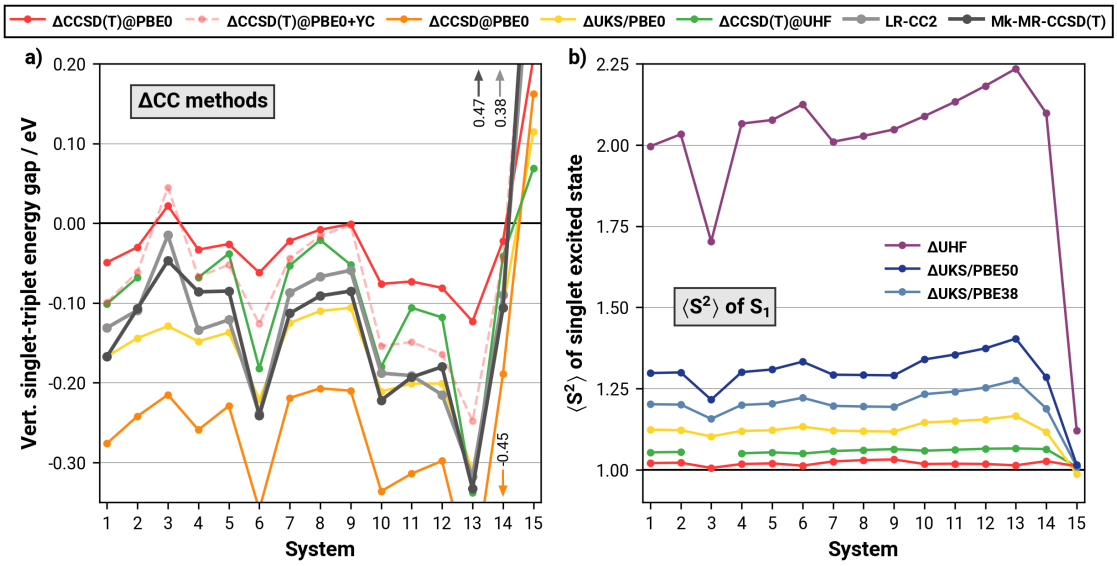

Figure C.5: a) ΔWFT (CCSD and CCSD(T)) results in cc-pVTZ basis for investigated molecules compared to ΔUKS/PBE0 and excitation-based WFT (LR-CC2, TBE*), all values in eV. Basis set effects are investigated in the SI. b) $\langle S^2 \rangle$ expectation values for different SCF and post-SCF methods. The respective plots for the triplet can be found in the SI.

systematically investigate the treatment of dynamic correlation beyond the Kohn-Sham correlation functional. For this purpose, we employ a set of increasingly sophisticated post-SCF correlation methods – namely CCSD and CCSD(T) – based on the unrestricted open-shell singlet and triplet reference wave functions from the ΔUKS/PBE0 calculations as well as on a (highly spin-contaminated) canonical Hartree-Fock reference. Inspection of Figure C.5a shows that while CCSD generally provides much too negative gaps (orange line), the "gold standard" CCSD(T) (red and green lines) provides too positive gaps. We argue that such a large effect of the (T) correction indicates that dynamical correlation strongly differs between the singlet and triplet states, hinting at a lack of error cancellation, and explaining why explicitly including triples is required for a balanced description of INVEST. Moreover, the resulting gaps depend strongly (by up to 0.15 eV or ≈3 kcal/mol) on the reference wave function (UHF vs PBE0). Analysis shows that this behavior is again related to the $\langle S^2 \rangle$ of the reference and CCSD wave functions depicted in Figure C.5b. With UHF (red line) both the open-shell S_1 and T_1 states suffer from substantial artificial spin-symmetry breaking ($\langle S^2 \rangle_{S_1} = 1.1 - 2.2$ and $\langle S^2 \rangle_{T_1} = 2.4 - 2.8$), while for ΔUKS/PBE0 (orange line) only the S_1 is weakly spin-polarized ($\langle S^2 \rangle_{S_1} = 1.0 - 1.1$ and $\langle S^2 \rangle_{T_1} = 2.0$). CCSD repairs this spin-contamination of both HF and PBE0 orbitals, as evident from Figure C.5b (green and red lines). However, since UHF starts much further away from the ideal value, the resulting $\langle S^2 \rangle$ values are distinctly closer to the ideal of 1.0 for a spin-broken S_1 with PBE0 orbitals than with HF orbitals (note that T_1 is generally much less contaminated and less interesting for this discussion). In line with our interpretation of the FX admixture to DFT, the removal of spin-polarization leads to a reduction in the magnitude of the inverted gaps compared to the reference wave function. Accordingly, the small remaining differences in $\langle S^2 \rangle$ values for ΔCCSD(T)@HF (green line) and ΔCCSD(T)@PBE0 (red line) explain the remaining

differences in ΔE_{ST}. We attribute this difference to the reduced flexibility in ΔCCSD(T)@HF to recover dynamic correlation when dealing with spin-contaminated references, which has recently been reported for in transition-metal complexes.[350] Accordingly, and in line with Drwal and Dreuw,[196,201] we observe that including more dynamic correlation in coupled-cluster calculations diminishes the magnitude of inverted gaps, which becomes evident when comparing ΔCCSD (orange line in Figure C.5a) to ΔCCSD(T).

Nevertheless, even the virtually spin-pure ΔCCSD(T)@PBE0 calculation still deviates significantly from the high-level references and ΔUKS/PBE0, which is surprising in light of the great performance of ΔUKS/PBE0 itself. To resolve this residual disagreement, it is necessary to adapt the formally wrong $\langle S^2 \rangle$ expectation value of the open-shell singlet (1 instead of 0) with the Yamaguchi correction. This yields the pale dashed red line in Figure C.5a, which is finally in reasonable agreement with the other highly correlated methods and ΔUKS/PBE0 for negative and positive ΔE_{ST}. It bears pointing out that the usefulness of the Yamaguchi correction for these coupled-cluster calculations is in contrast to its impact on ΔUKS/PBE0 itself (see SI), where it disrupts the previously discussed beneficial error cancellation.

To ultimately eliminate any issues resulting from spin-contaminated references, let us consider the ST gaps obtained with the properly spin-adapted two-determinant state-specific coupled cluster, Mk-MR-CCSD(T)@ $\langle\uparrow\downarrow| \pm \langle\downarrow\uparrow|$.Notably, this method predicts slightly more negative ST-gaps than the TBE (MD -0.02 eV, cf. Table C.1 and Figure C.4b) and distinctly more negative ST-gaps than the Yamagushi-corrected ΔCCSD(T)@PBE0. We attribute this disparity to the rudimentary nature of the Yamaguchi spin-correction, lacking the necessary optimization and subsequent stabilization of the spin-pure S_1 state, and the previously discussed high sensitivity of the ST-gap to the description of dynamical correlation (large impact of the (T) correction) when using spin-contaminated references. Consequently, even though relative errors between the methods are comparably small (below 0.2 eV between ΔCCSD(T)@PBE0, Mk-MR-CCSD(T), and the TBE), the lack of spin-adaptation precludes the use of ΔCCSD(T)@PBE0 for generating benchmark-quality reference values for ΔE_{ST}. Instead, spin-adapted Δ approaches like Mk-MR-CC or excitation-based methods like ADC or EOM-CC should be preferred. In this context, one advantage of the Mk-MR-CC approach (and state-specific methods in general) over excitation-based methods should be pointed out: Because no substitutions are required to generate the excited state from the reference ground state, the state-specific Mk-MR-CC approach includes more correlation for the singlet and triplet excites states than excitation-based CC methods. This becomes evident from the impact of the (T) correction on the gaps, which is virtually negligible in Mk-MR-CCSD(T) (see Figure S10 in the SI) compared to the substantial influence in EOM-CCSDT.[190] Also regarding the basis set, we find the Mk-MR-CC calculations to be essentially converged at a def2-TZVP level, as evident from the negligible effects of using def2-TZVPP (1 meV) or def2-TZVPD (3 meV) on the gap of heptazine (see Table S1 in the SI).

After extensive discussion of the INVEST15 set, we finally put the robustness of the ΔUKS/PBE0 approach to the test with the larger and structurally diverse NAH159 benchmark set. Further, simulating the conditions of high-throughput screenings, we employ a smaller def2-SVP basis set, avoid any molecule-specific parameters or manual guidance, and apply the approach in a black-box fashion. This brings up one shortcoming of state-specific excited state methods like ΔDFT: It is not known which occupied and virtual orbitals contribute to the lowest singlet and triplet excited states. While a large majority are HOMO–LUMO transitions, just using this guess leads to wrong gaps (not between S_1 and

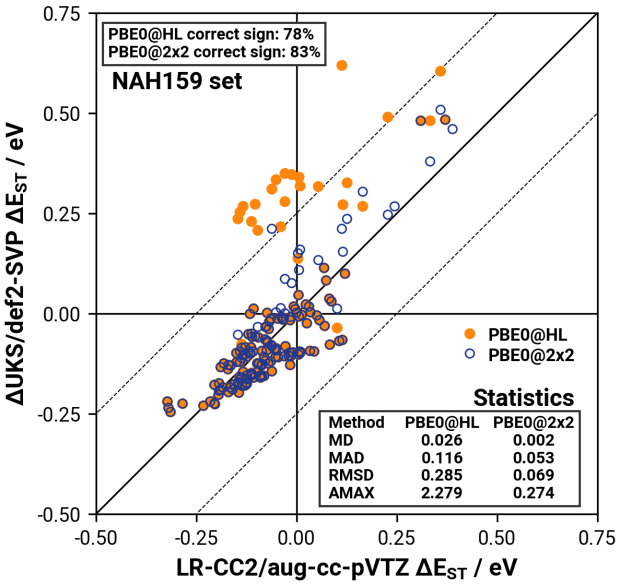

Figure C.6: Correlation plot for the vertical singlet-triplet energy gap calculated by ΔPBE0/def2-SVP and LR-CC2/aug-cc-pVTZ for the 159 molecules of the NAH159 benchmark set, for the PBE0@HL only the HOMO–LUMO excitation was modeled and for PBE0@2x2 all excitations between HOMO, HOMO-1, LUMO and LUMO+1 were considered to find the lowest singlet and triplet, dashed lines indicate deviations from reference of ±0.25 eV, all values in eV.

T_1) in 10 of 159 molecules of this set. Leveraging the low computational cost of UKS calculations, we mitigate the issue by considering all singlet and triplet states possible in a 2×2 orbital window, that is, transitions from HOMO-1 or HOMO to LUMO or LUMO+1, which has been suggested in the original MOM paper.[85] These states are converged with default settings and the gap is calculated between the lowest singlet and triplet excited states resulting from this protocol. Further increasing the orbital window did not improve the results for NAH159, which may be different for other classes of compounds.

The gaps obtained with this approach, termed PBE02 × 2 as well as with the exclusive HOMO–LUMO guess are plotted against the LR-CC2/aug-cc-pVTZ references in Figure C.6. Inspection shows a good correlation with no significant outliers for the 2×2 protocol. Further evaluation of the data confirms that in 83.0% of all cases (77.4% if only the HOMO–LUMO transition is considered), the sign of the gap is correctly predicted. The percentage of molecules with a negative gap according to LR-CC2 but a positive gap according to ΔUKS/PBE0 (false negatives) is only 7.5% (11.3% if only the HOMO–LUMO transition is considered). The percentage of molecules with a positive gap according to LR-CC2 but a negative gap according to ΔUKS/PBE0 (false positives) is only 9.4% (10.7% if only the HOMO–LUMO transition is considered). The overall MAD is 0.053 eV (0.116 eV if only the HOMO–LUMO transition is considered), and thus only slightly larger than for the much smaller and structurally less diverse INVEST15 set. This illustrates the usefulness of the 2×2 approach, which is further corroborated by the improvement in the Pearson correlation coefficient, which increases from 0.44 for the HOMO–LUMO approach to 0.87 for the 2×2 approach.

For completeness, we also report the performance of other methods that performed well on the smaller INVEST15 benchmark. Using the same 2×2 approach, the r^2SCAN functional performs slightly worse than PBE0, achieving an MAD of 0.063 eV, a Pearson coefficient of 0.7, and 80% correctly predicted gap signs. To our surprise, even TDA-PBE0 with the gaps shifted by 0.4 eV (*vide supra*) works surprisingly well, yielding an MAD of only 0.060 eV, with the same percentage of correctly predicted gap signs, 83.0%, as for ΔUKS/PBE0@2×2, while the computational cost is comparable. Plots and further statistical data for these approaches can be found in the SI.

During the final stages of the preparation of this manuscript, Kusakabe and co-workers reported an experimental measurement of an ST-gap for a molecule derived from #4 (termed 5AP-N$(C12)_2$) from the INVEST15 set and closely related to the molecules of the NAH159 set.[325] This second experimental conformation of molecular INVEST provided an ST-gap of -0.032 eV to -0.043 eV, which agrees reasonably well with the ΔUKS/PBE0/def2-SVP result of -0.02 eV (and furthermore with the SCS-CC2 calculations reported in the original manuscript).

In summary, the results for NAH159 demonstrate that a similar accuracy as in the INVEST15 benchmark can be achieved without human intervention at a tiny fraction of the computation cost of the LR-CC2 calculations. For example, the total walltime for all eight singlet and triplet states for the biggest molecule tested (46 atoms, 428 basis functions with def2-SVP) takes roughly 20 min on a quad-core Intel Xeon E3-1270 v5 @ 3.6 GHz compute node. The respective LR-CC2/aug-cc-pVTZ calculation including 10 singlet and 10 triplets (required to find the lowest states reliably) runs over 83 h on the same machine, which is about 250 times slower than ΔUKS. It should be noted that employing LR-CC2 with a smaller basis set reduces the advantage of ΔUKS to a factor of 80 and 5 for cc-pVTZ and cc-pVDZ, respectively. However, the computational cost difference between LR-CC2 and ΔUKS will increase substantially for larger systems, since even our largest test system is still relatively small (46 atoms, 24 non-hydrogen atoms). Moreover, similar performance optimizations can be done for the ΔUKS calculations, e.g., by using density-fitting for Coulomb and exchange integrals (particularly effective for semilocal functionals like r^2SCAN, which would be beneficial in Q-Chem), or by switching to the smaller 6-31G or 3-21G basis sets, which decrease the wall time by a factor of 5-7 compared to def2-SVP without affecting the accuracy too much (see Figure S11 in SI).

C.5 Summary and Conclusion

This study explored the accurate prediction of inverted singlet-triplet energy gaps (INVEST), focusing on efficient yet robust alternatives to computationally demanding wave function-based approaches. The main finding is that the intriguingly simple and computationally cheap ΔUKS/PBE0 approach with small basis sets shows a surprisingly robust performance (MAD 0.046 eV for INVEST15, 0.053 eV for NAH159) comparable to much more demanding wave function-based methods. Combining results from standard density functional theory (DFT) and sophisticated correlated (multireference) calculations, the performance of ΔUKS/PBE0 was traced back to a robust spin-polarization-based error-cancellation. Eventually, application of ΔUKS to the large and structurally diverse NAH159 benchmark set confirmed the robustness of the approach and suitability for screening workflows.

Further key findings from the study include:

- Role of Fock-Exchange: Including exact Fock exchange in ΔUKS calculations (i.e., using

hybrid functionals) is critical. The study demonstrates that a moderate amount of FX, as in PBE0 or tuned range-separated hybrids, provides the most reliable predictions. This is due to the effective handling of dynamic spin-polarization, which depends on the balance between spin contamination and dynamic correlation and is required for accurate gap predictions. An exception appears to be the r^{2}SCAN functional, which despite its meta-GGA nature predicts gaps with the same accuracy as PBE0 (MAD 0.053 eV for INVEST15, 0.061 eV for NAH159) except for a few outliers. meta-GGA functionals are interesting as they can fully exploit the density-fitting approximation, allowing for even faster calculations.

- State-Specific Post-SCF Correlation Methods: Advanced correlation methods such as CCSD(T) correct the spin contamination observed in simpler methods and improve the reliability of the predictions, though they require careful consideration of the reference wave function and spin state. An elegant solution is provided to use a spin-adapted two-determinant reference for the singlet, as evident from the superior performance of state-specific Mk-MR-CC, which is converged at the CCSD level in a triple-ζ basis set, where other excitation-based CC methods required at least perturbative triples for the same accuracy.

- High-Throughput Applications: In a test application of ΔUKS/PBE0 to a large and structurally diverse benchmark, the sign of the ST-gap was predicted in agreement with LR-CC2 in 83% of all cases, with less than 10% false positive and less than 8% false negatives, and only slightly worse error-statistics than for the smaller INVEST15 benchmark. For this, we considered all excitation from HOMO and HOMO-1 to LUMO and LUMO+1 to avoid issues with the state-specific method converging on higher-lying states. Since ΔUKS/PBE0 dramatically reduces the computational cost by two orders of magnitude compared to the wave function-based LR-CC2 reference (or the number of required LR-CC2 calculations if ΔUKS/PBE0 is used in a pre-screening), the reported method is a promising candidate for the high-throughput computational exploration of new INVEST materials.

Overall, this research sheds light on the effectiveness of hybrid density functionals and modern meta-GGA functionals in capturing the essential physics of singlet-triplet gap inversion in INVEST emitters. It also highlights the potential of ΔUKS in providing a computationally efficient alternative to more demanding methods, thus paving the way for rapid and reliable materials discovery in the field of organic electronics.

C.6 Acknowledgement

This project has been funded with support from the RTG-2591 "TIDE - Template-designed Organic Electronics". T.F. is most grateful to the “Fonds der Chemischen Industrie (FCI)” for financial support under a Kekulé scholarship. The authors gratefully acknowledge the granted access to the Marvin cluster hosted by the University of Bonn.

C.7 Supporting Information

The Supporting Information is available free of charge at
https://pubs.acs.org/doi/10.1021/acs.jctc.3c00617.
Detailed computational settings and workflows, singlet and triplet excitation energies for TDA-DFT results, singlet and triplet excitation energies for ΔUKS results, spin-expectation values for all singlet and triplet states for ΔUKS, the effect of solvation environment (modeled by a PCM) on the singlet-triplet gap calculated by ΔUKS, basis set convergence of the singlet-triplet gap results for ΔUKS and ΔCC methods, comparison of different WFT approaches for the singlet-triplet gap calculated by ΔCC, comparison of different MR-Mk-CC approaches for the calculation of the singlet-triplet gap, choice of the theoretical reference, further NAH159 set ΔUKS results, formulas for statistical measures, libreoffice spreadsheet of all relevant data points, geometries of all studied molecules in .xyz-file format (.zip-archive)

C.8 Conflicts of Interest

There are no conflicts of interest to declare.

APPENDIX D

The Best of Both Worlds: ΔDFT Describes Multiresonance TADF Emitters with Wave-Function Accuracy at Density-Functional Cost

Lukas Kunze,[†] Andreas Hansen,[†] Stefan Grimme,[†] Jan-Michael Mewes,[†‡]

Received: 4 November 2025
Published online: 23 January 2025

Reprinted in Appendix D (adapted) with permission[§] from
L. Kunze, A. Hansen, S. Grimme, and J.-M. Mewes, *The best of both worlds: ΔDFT describes multiresonance TADF emitters with wave-function accuracy at density-functional cost*, J. Phys. Chem. Lett. **16** (2025) 1114, DOI: 10.1021/acs.jpclett.4c03192

Own contributions

- re-evaluation and compilation of experimental reference data
- performing all quantum chemical calculations
- statistical analysis and interpretation of results
- first draft and co-writing the manuscript

[†]Mulliken Center for Theoretical Chemistry, Clausius Institute for Physical and Theoretical Chemistry, University of Bonn, 53115 Bonn, Germany
[‡]beeOLED GmbH, Niedersedlitzer Str. 75c, 01257 Dresden, Germany
[§]Permission requests to reuse material from this chapter should be directed to the American Chemical Society.

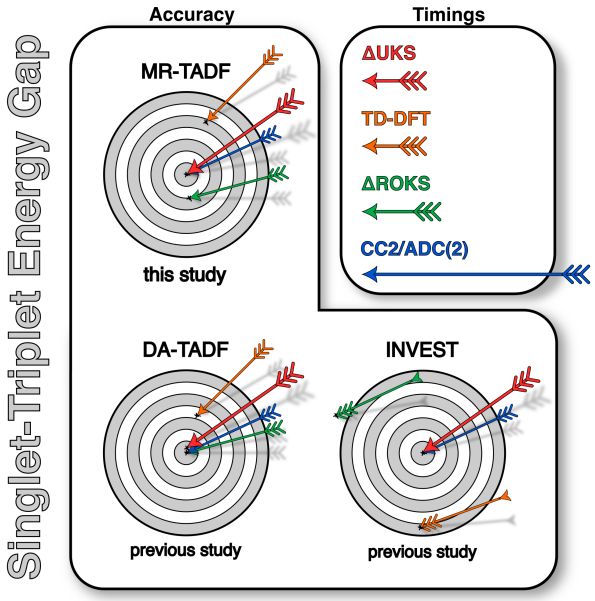

Figure D.1: Table of content graphic (ToC).

Abstract With their narrow-band emission, high quantum yield, and good chemical stability, multiresonance thermally activated delayed fluorescence (MR-TADF) emitters are promising materials for OLED technology. However, accurately modeling key properties, such as the singlet-triplet (ST) energy gap and fluorescence energy, remains challenging. While time-dependent density functional theory (TD-DFT), the workhorse of computational materials science, suffers from fundamental issues, wave-function-based coupled-cluster (CC) approaches, like approximate CC of second-order (CC2), are accurate but suffer from high computational cost and unfavorable scaling with system size. This work demonstrates that a state-specific ΔDFT approach based on unrestricted Kohn-Sham (ΔUKS) combines the best of both worlds: on a diverse benchmark set of 35 MR-TADF emitters, ΔUKS performs as good as or better than CC2, recovering experimental ST gaps with a mean absolute deviation (MAD) of 0.03 eV at a small fraction of the computational cost of CC2. When combined with a tuned range-separated LC-ωPBE functional, the excellent performance extends to fluorescence energies and ST gaps of MR- and donor-acceptor TADF emitters and even molecules with an inverted ST gap (INVEST), rendering this approach a jack of all trades for organic electronics.

D.1 Introduction

In the past decade, thermally activated delayed fluorescence (TADF) has established itself as an efficient mechanism to generate light in organic light-emitting devices (OLEDs).[320] In an electroluminescent device, excitons are generated by a recombination of electrons and holes, creating singlet and triplet excitons in a 1:3 ratio according to Fermi-Dirac spin statistics. This fundamentally limits the percentage of generated excitons converted into light, also called the internal quantum efficiency (IQE), to 25% in fluorescent emitters. Phosphorescent (PhOLED) and TADF emitters have overcome this limit by down-conversion of singlet into triplet excitons (PhOLED emitters) via intersystem crossing (ISC) or up-conversion of triplet into singlet excitons (TADF emitters) via reverse intersystem crossing

(rISC), respectively. The rISC process in TADF emitters requires a small energy gap between the lowest singlet (S_1) and lowest triplet (T_1) excited state, known as the singlet-triplet energy gap (ST gap).

$$\Delta E_{ST} = E_{S_1} - E_{T_1} \tag{D.1}$$

In donor-acceptor (DA-)TADF emitters, the small ST gap is achieved by structural means, i.e., by separating electron-donating and electron-accepting aromatic π-systems in space. This results in energetically low-lying singlet and triplet charge-transfer (CT) states that become close in energy due to the small electron-hole overlap.[320,351] However, DA-TADF emitters suffer from conflicting design goals: while a vanishing electron-hole overlap is beneficial for minimizing the ST gap, some electron-hole overlap is required for efficient rISC and fluorescence (via the S_1-T_1 spin-orbit coupling and S_1-S_0 oscillator strength).[169] Additionally, the emission spectra of DA-TADF are usually very broad, with poor color purity of the emitted light. In response to these issues, a new type of TADF emitter was introduced in 2015 by Hatakeyama and co-workers, later dubbed multiresonant or multiresonance TADF (MR-TADF) emitters.[72,352] In MR-TADF, systematic doping of electron-withdrawing and electron-donating elements in a conjugated π-system leads to a localization of the highest occupied molecular orbital (HOMO) and the lowest unoccupied molecular orbital (LUMO) on alternating atoms (e.g., DOBNA molecule, see Figure D.2). This resonance-driven separation between HOMO and LUMO gives rise to short-range charge-transfer (SRCT) states. These maintain a higher degree of electron-hole overlap than found in DA-TADF systems, which results in higher oscillator strengths but also larger ST gaps.[204] Due to the SRCT nature, the electron and hole are closer together than in DA-TADF emitters, leading to less polar excited states with hardly any solvatochromism and much more favorable, narrow emission bands.[72,204] Thus, MR-TADF emitters hold multiple advantages over DA-TADF emitters and are already being adopted for applications in the display industry.[60] It is therefore of great importance to have theoretical methods capable of efficiently predicting the ST gap and emission wavelength of a given sample molecule to accelerate the discovery of new and improved MR-TADF emitters.

The computational modeling of TADF emitters is challenging in almost every aspect. The workhorses of materials research, time-dependent density functional theory (TD-DFT) and its Tamm-Dancoff-approximated variant (TDA-DFT) struggle to accurately describe fundamental properties of MR- and DA-TADF emitters, albeit for different reasons.[1,148,180,205,208] Specifically for DA-TADF, the well-known failure of TD-DFT for CT states complicates the modeling.[79,208] While range-separated hybrid (RSH) functionals alleviate some problems of TD-DFT with CT states,[353] further issues result from the requirement to include the solvent environment in the excited-state description: for accurate state energies and character (CT vs locally excited), it is imperative to account for the substantial dielectric stabilization these highly polar CT states exhibit even in weakly polar environments.[1,169,208] However, the linear-response polarizable continuum model (LR-PCM), the default in many programs and thus perhaps the most prominent excited-state solvation model,[170] completely fails to recover the dielectric stabilization of CT states.[171,229,230] The state-specific (SS)-PCM can recover the dielectric stabilization for CT states but cannot provide gradients for excited-state optimizations.[1,169,183,208] While these issues of solvation and the CT failure are central for the polar states of DA-TADF emitters, where some progress has recently been made with dielectrically screened RSHs,[209] the less polar SRCT states of MR-TADF (and INVEST) emitters suffer from a lack of doubly excited determinants

in TD(A)-DFT.[3,201,205] Without these doubly excited determinants, the S_1 is systematically too high in energy compared to T_1, resulting in a large (yet very systematic)[3] overestimation of the ST gap.

Addressing these major challenges, we have been developing and testing an alternative state-specific excited-state method based on Kohn-Sham self-consistent field calculations (known as ΔSCF, orbital-optimized OO-DFT, or ΔDFT). To this end, we employ unrestricted Kohn-Sham (UKS) and a special two-determinant variant of restricted open-shell Kohn-Sham (ROKS) for open-shell singlet (OSS) states pioneered by Van Voorhis (also OSS-ROKS, herein termed ROKS).[88,173] While targeting the lowest triplet excited state is trivial with UKS via the multiplicity, the open-shell singlet and higher triplets require some technical help.[1,85,86,173] This help comes in the form of the maximum-overlap method of Gilbert and co-workers, which allows us to reliably converge a non-Aufbau configuration generated by repopulating converged ground state orbitals to resemble the desired excited state.[85] ΔUKS provides spin-pure triplets, while the resulting singlets are broken-symmetry solutions, i.e., a 50:50 mixture of a singlet and a triplet with $\langle S^2 \rangle = 1$. Spin-pure singlets ($\langle S^2 \rangle = 0$) can be obtained with the aforementioned two-determinant ROKS, which computes them as the difference between a broken-symmetry singlet and a triplet in the same set of orbitals.[88,173] Because of this construction, ROKS naturally converges to the lowest excited singlet state. However, similar to ΔUKS, higher lying roots can be targeted by manipulating the guess and converging with the help of the square-gradient minimization technique (SGM).[173] In this case, the ROKS approach can also be described as ΔROKS, where Δ generally indicates convergence on excited state and saddle points rather than the ground state and global minimum of the SCF equations. Since we also target higher-lying singlet and triplet states with both approaches (vide infra), we will consistently use the Δ. Finally, another advantage is that because both ΔUKS and ΔROKS are SCF-based, an inclusion of the dielectric environment (solvent) via the PCM is straightforward, as is the calculation of gradients and frequencies in the presence of a PCM.[1]

In our prior study of the 27 mostly DA-TADF (2 MR-TADF) emitters in the STGABS27 benchmark set, ΔUKS/PCM with PBE0 and in particular ΔROKS/PCM with optimally tuned ωB97X-V provided exceedingly accurate ST gaps with mean-absolute deviations (MADs) of 0.026 and 0.022 eV. Accordingly, while ΔROKS has a little edge over ΔUKS, both approaches are well within chemical accuracy (1 kcal/mol or 0.044 eV) and clearly superior to TD(A)-DFT.[1,208] In a recent follow-up, we extended the STGABS27 benchmark to include experimental emission energies, which we compared against TDA-DFT and ΔUKS/ΔROKS, all of which combined with a perturbative state-specific PCM (ptSS-PCM) to account for nonequilibrium solvation effects.[2] Again, ΔUKS and ΔROKS outperformed TDA-DFT, and, more importantly, the results with ΔUKS and in particular ΔROKS showed remarkably consistent performance with different density functionals. While this indicates that state-specific ΔDFT clearly outperforms any TDA-DFT approach in terms of accuracy and robustness for (DA-)TADF emitters, it is questionable how well the performance of ΔDFT translates to that of MR-TADF emitters.

Interestingly, for INVEST emitters, which share the SRCT excited-state character with MR-TADF, a different picture emerged: here, only ΔUKS is accurate in combination with certain functionals (depending on the amount of EXX), whereas ΔROKS cannot at all reproduce the gap inversion.[3] Specifically, ΔUKS with plain PBE0 and FX175-ωPBE (an RSH with the range-separation parameter tuned on the STGABS27 set) provides accurate inverted ST gaps with close to chemical accuracy for two diverse sets of 15 and 159 INVEST candidates (MAD 0.050 eV against coupled-cluster references).

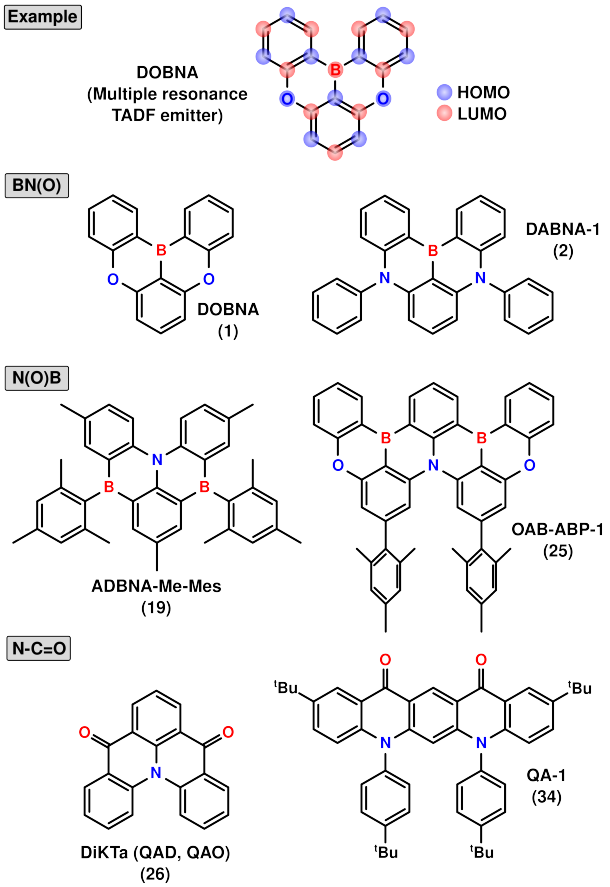

Figure D.2: Example illustration of the MR-TADF emitter, DOBNA, showcasing the alternating atomic site characteristic of the HOMO and LUMO as well as Lewis structure excerpts from the Hall benchmark set. Two example molecules are chosen for each subgroup (BN(O), N(O)B, N-C=O) of the benchmark. (A full overview is given in the Supporting Information).

The good performance of UKS was traced back to an implicit inclusion of doubly excited determinants via spin-polarization, which is missing at the spin-restricted ROKS level.[3] This large difference in the performance of ΔUKS, ΔROKS for DA-TADF, and INVEST motivated us to further explore their performance for a representative set of the important class of MR-TADF emitters, particularly because it has been speculated that double excitations contribute here as well (*vide infra*).[205]

To this end, we build on a previous study by Hall et al., who compiled a set of 35 literature-known MR-TADF emitters comprising experimental fluorescence and phosphorescence energies as well as ST gaps.[205] Their results confirm that TDA-DFT is systematically off, while correlated wave function theory (WFT), namely, spin-component scaled second-order coupled cluster (SCS-CC2/cc-pVDZ), performs well with an MAD of only 0.04 eV against experiment. While this rather small basis set for CC calculation is required to limit the computational effort, the authors demonstrated reasonable convergence of the ST gap for DOBNA, DABNA-1, and DiKTa by comparing to the larger cc-pVTZ basis (the largest change was from 0.27 eV to 0.24 eV for DiKTa). From the good agreement of SCS-CC2, the authors concluded that the inclusion of doubly excited determinants in the wave

function is crucial for the correct prediction of the ST gap in MR-TADF emitters. Further studies using double hybrids in TDA-DFT support this conclusion, since double hybrids significantly improve results (over standard hybrids) and give only slightly worse errors (MAD: 0.056 eV) compared to SCS-CC2.[202,354]

To the best of our knowledge, the only study exploring state-specific ΔDFT for MR-TADF emitters is by Sotoyama, who explored ΔUKS's performance for ST gaps of 13 different MR-TADF emitters, finding a performance of ΔUKS/B3LYP with an MAD of 0.041 eV similar to that of SCS-CC2 (yet for a different and smaller test set than in Hall et al.).[355] The present study aims to complete the picture by surveying the larger benchmark set of Hall and co-workers with several methods, namely ΔUKS, ΔROKS, and, for reference, also TDA-DFT and SCS-CC2 (using the results of Hall et al.). For the ΔDFT methods, we test several functionals (global hybrids, various flavors of RSHs with and without optimal tuning, and popular choices), and explore the impact of geometric relaxation, solvent models, and the basis set. Finally, we discuss the results for MR-TADF in the context of our previous works[1–3,208] and to conclude which flavor of ΔDFT is most accurate over all classes of organic electronic materials.

D.1.1 Benchmark Set

The structurally diverse benchmark set of 35 MR-TADF emitters is taken from Hall et al.,[205] including their grouping into BN(O), N(O)B, and N-C=O classes and their SCS-CC2/cc-pVDZ ST gaps and excitation energies. A representative excerpt of Lewis structures showing all motifs used for classification is given in Figure D.2 (all structures can be found in the Supporting Information). Since the work of Hall provides no geometry data, we conducted systematic conformer searches and optimizations for all 35 MR-TADF structures with the CREST/CENSO workflow,[356–358] which uses the r^{2}SCAN-3c composite method for final conformational energies.[136] All geometries used in this work are provided in the Supporting Information.

Regarding the experimental values for ST gaps, we found inconsistencies between the values provided by Hall and co-workers (ST gaps in their Table S1) and the ST gaps and emission energies provided in further tables (their Tables S2-S36). Thus, to ensure the consistency of the values used in this work, we revisited the original literature to re-extract and re-compile the emission energies and calculate the ST gap from these. Several of these articles provide experimental emission energies for several different solvents (or thin films) and temperatures. To compile consistent reference data, we prioritized using fluorescence and phosphorescence spectra obtained at a similar temperature, irrespective of the environment (solvent effects are small for MR-TADF, *vide infra*), with a second priority of using nonpolar solvents over polar solvents and finally solvent over thin-film environments. Further details are provided in the SI. The resulting ST gaps and S_1 emission energies we used in this work are provided in Table D.1, while a comparison to the ST gap provided by Hall and workers in Table S1 is given in the Supporting Information. Although most values agree with ours, there are minor differences (< 0.03 eV) for several molecules, and two molecules (**30** and **34**) show a deviation of about 0.05 eV.

Table D.1: Benchmark molecule names, their experimental singlet-triplet energy gap (ST gap), their experimental fluorescence energy (S_1^{em}), and the respective reference for the publications.

No.	Name	ST Gap	S_1^{em}	Ref.
1	DOBNA	0.18	3.08	[359]
2	DABNA-1	0.15	2.74	[72]
3	DABNA-2	0.15	2.71	[72]
4	*t*-DABNA	0.16	2.71	[360]
5	BN-DMAC	0.14	2.56	[361]
6	TABNA	0.21	3.11	[362]
7	B2	0.18	2.72	[363]
8	*v*-DABNA	0.02	2.64	[364]
9	α-3BNOH	0.31	3.12	[365]
10	DtBuCzB	0.13	2.52	[366]
11	DtBuPhCzB	0.10	2.44	[366]
12	2F-BN	0.16	2.51	[367]
13	3F-BN	0.08	2.48	[367]
14	4F-BN	0.11	2.50	[367]
15	*m*-Cz-BNCz	0.10	2.38	[368]
16	AZA-BN	0.19	2.38	[369]
17	BBCz-DB	0.13	2.66	[370]
18	R-BN	0.18	1.87	[371]
19	ADBNA-Me-Mes	0.19	2.58	[372]
20	ADBNA-Me-Tip	0.18	2.59	[372]
21	ADBNA-Me-Mes,MesF	0.19	2.55	[373]
22	ADBNA-Me-MesF	0.21	2.60	[373]
23	ADBNA-Me-Mes,MesCz	0.18	2.56	[373]
24	ADBNA-Me-MesCz	0.17	2.54	[373]
25	OAB-ABP-1	0.12	2.44	[359]
26	DiKTa	0.19	2.69	[374]
27	3-PhQAD	0.17	2.50	[375]
28	7-PhQAD	0.20	2.54	[375]
29	Mes_3DiKTa	0.20	2.62	[376]
30	DDiKTa	0.22	2.62	[377]
31	DQAO	0.19	2.66	[378]
32	OQAO	0.16	2.34	[378]
33	SQAO	0.16	2.23	[378]
34	QA-1	0.35	2.86	[379]
35	QA-2	0.22	2.79	[379]

D.2 Methods

Throughout this study, we used a development version of Q-Chem[184] 5.4.2 (all features for ΔUKS and ΔROKS calculations are available in the recent versions of Q-Chem 6), the ORCA[336] program package version 6.0.0 (for ground-state DFT geometry optimization and TDA-DFT calculations), and the CREST[356–358] program version 2.12 (for conformer sampling).

In the majority of cases, the geometry of the molecules is rigid such that the energetically lowest

conformer is self-evident (e.g., DOBNA, DiKTa, DABNA-1, see Figure D.2). For systems **5**, **8**, **16**, **18**, and **25**, we applied the CREST conformer search algorithm using the GFN-FF for the metadynamics part and the GFN2-xTB method for the subsequent optimizations and set the energy window to 6 kcal/mol.[213,380] The generated conformers were energetically reranked and optimized at the r^{2}SCAN-3c[136] level of theory with CENSO,[357] which provides excellent conformational energies.[348] The final ground-state geometries were verified to be true minima via frequency calculation (geometries are provided in the Supporting Information).

For the ΔUKS calculations, the initial maximum overlap method (IMOM)[85,86] was applied to prevent variational collapse to the ground-state. A converged ground-state calculation serves as an input guess, from which a non-Aufbau electron configuration is generated by promoting an electron from an occupied orbital to a virtual orbital (for triplets, the spin of the electron is changed). During the SCF, the IMOM algorithm constrains the occupied orbitals for the next SCF step to have the maximum overlap to the initial guess orbitals (the original MOM maximizes overlap with the previous SCF step). We exclusively used the IMOM algorithm, which, in our experience, is more stable than the MOM.

To find the lowest singlet and triplet excited states for all benchmark molecules with the least manual intervention, we calculated all single electron transitions in a 4×4 orbital window, including the HOMO, HOMO-1, HOMO-2, HOMO-3, LUMO, LUMO+1, LUMO+2 and LUMO+3 at the ΔUKS and ΔROKS with the PBE0[108,113,123] level, and used the lowest singlet and triplet states as starting points for the other tested functionals. In any case, we used the lowest S_1 and T_1 energies we could find (through orbitals windows, different initial guesses, etc.) to calculate the ST gap.

We explored a range of density functional approximations (DFAs) including PBE0,[108,113,123] PBE38,[140] PBE50,[200] LRC-ωPBEh,[186] LC-ωPBE,[177] ωB97M-V,[127] and fixed range-separation parameter variants of the RSH functionals. Molecule-specific optimal tuning of the range-separation parameter was carried out for the LC-ωPBE functional in vacuo[130,235] for r^{2}SCAN-3c-optimized ground-state structures. (For details, see the Supporting Information). We also tested the M06-2X[381], B3LYP,[382] and the CAM-B3LYP[118] functional as they are popular choices in the material science community and included B97M-V[179] as representative for a semilocal functional due to its good performance on the GMTKN55 benchmark set.[114,383]

In the excited-state calculations, we consider dispersion corrections only for ωB97M-V and B97M-V since they are included by design and take into account the electronic structure. For all other functionals, we omitted the (exclusively geometry-dependent) DFT-D4[142,143,263] dispersion correction, since it has no effect on the ST gap in the vertical approximation (same geometry for S_1 and T_1). Even for the adiabatic gaps discussed in the SI, including the D4 correction makes virtually no difference.

The basis set dependence was explored with the def2-SVP, def2-TZVP(-f) and def2-QZVP[162,304] basis sets. For this purpose, we calculated vertical ST gaps with ΔUKS on a small subset of 8 MR-TADF emitters (systems **1**, **2**, **26**, **27**, **28**, **31**, **32**, **33**) using the PBE0 functional. Against a PBE0/def2-QZVP reference, the basis sets def2-SVP and def2-TZVP(-f) show negligible MADs of 0.006 eV and 0.001 eV for ST gaps, while there is a slightly larger impact on emission energies (*vide infra*).

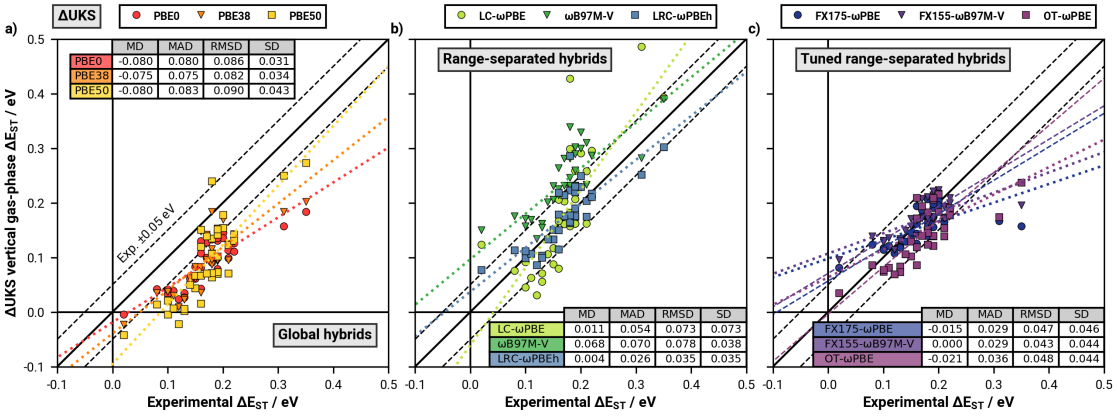

Figure D.3: Correlation plots between experimental references and vertical ST gaps calculated with ΔUKS/def2-SVP in the gas phase using the ground-state geometries . Tested functionals are grouped into a) global hybrids, b) range-separated hybrids, and c) tuned range-separated hybrids. Dashed black lines mark the range of ±0.05 eV around the references. Colored dotted lines are linear regressions including all points; colored dashed lines (only panel c) are fitted excluding the large-gap systems 9 and 34 (see discussion). All values given in eV.

D.3 Results and Discussion

D.3.1 Vertical Singlet-Triplet Gaps with ΔUKS

Let us begin the discussion with the ST gaps, focusing on state-specific ΔUKS and how the choice of the underlying functional affects the accuracy of calculated ST gaps in the vertical approximation; i.e., calculated as the energy difference between S_1 and T_1 at the ground-state equilibrium geometry. We tested three different classes of functionals with varying amount of exact exchange (EXX) and different range-separation parameters ω: a) global hybrids, b) (untuned) range-separated hybrids, and c) tuned range-separated hybrid functionals starting with ΔUKS; see Figure D.3. We have drawn linear regression lines for each functional to better visualize trends (for the parameters and details, see the Supporting Information).

An inspection of Figure D.3a shows that all global hybrid functionals systematically underestimate the ST gap, as evident from the negative mean deviation (MD) equal to the MAD. In the progression of PBE0 (25% EXX) to PBE38 (37.5% EXX) to PBE50 (50% EXX), the increase in EXX has little influence on the relative shift of the ST gaps, but it appears that in global hybrids a large amount of EXX is required to obtain the correct slope/trend. However, in conflict with the experiment, the large amount of EXX also causes some ST gaps to be inverted.

Moving to RSHs in panel b shows that the inclusion of range-separated EXX resolves the underestimation issue of the global hybrids. Here, the slope and size of the gaps agree much better with the experimental data, showing that an asymptotically correct treatment of EXX is helpful. The untuned RSH ωB97M-V (15-100% EXX, $\omega = 0.3\,a_0^{-1}$ with a_0 being the Bohr radius) overestimates the ST gap (positive MD) but reproduces the slope correctly, while LC-ωPBE (0-100% EXX, $\omega = 0.45\,a_0^{-1}$) gives balances gaps (MD $\approx$ 0) but yields a wrong slope. LRC-ωPBEh (20-100% EXX, $\omega = 0.2\,a_0^{-1}$) finds a good middle ground with the correct slope, a small systematic error (MD = 0.004 eV), and the lowest MAD so far (0.026 eV). It bears pointing out that this level of accuracy is almost twice better

than chemical accuracy (1 cal/mol, 0.045 eV), which becomes even more impressive considering that there is only one large error > 0.1 eV. We argue that the good performance of LRC-ωPBEh is due to its rather small range-separation parameter compared to ωB97M-V and LC-ωPBE. This difference, results from the fact that LRC-ωPBEh was designed by Rohrdanz and co-workers with a focus on excited states rather than performance for thermochemistry and kinetics.[186]

To further explore the influence of the range-separation parameter, let us move to the optimally tuned functionals and those with smaller non-default ω values ($0.175\,a_0^{-1}$ for LC-ωPBE and $0.155\,a_0^{-1}$ for ωB97M-V) determined to be optimal for the mostly DA-TADF emitters of the STGABS27 benchmark in a previous work.[1] The results displayed in panel c are interesting: while MAD and RMSD of the tuned RSHs are almost halved with compared to the default functionals, the slope is worse. Apparently, correctly reproducing such large gaps required large amounts of fixed EXX (PBE50), a large ω value (untuned LC-ωPBE), or a compromise between both (LRC-ωPBEh with $\omega = 0.2\,a_0^{-1}$ and 20% fixed EXX). However, as will become evident later, this comes at the cost of significantly worse performance for emission energies. In any case, there are only two molecules with ST gaps well above 0.2 eV (molecules **9**/QA-1 and **34**/α-3BNOH, see also Figure D.5), presumably because such large gaps are adversarial for good OLED performance (poor triplet harvesting). Eliminating those two molecules from the fit yields dashed lines whose slope shows a better correlation with the experiment. To illustrate the effect of varying ω, we added Figure S7 in the SI showing LC-ωPBE with values of $0.125\,a_0^{-1}$, $0.150\,a_0^{-1}$, $0.175\,a_0^{-1}$, $0.200\,a_0^{-1}$, $0.250\,a_0^{-1}$, and $0.300\,a_0^{-1}$. Depending on the class of the MR-TADF emitter, the best agreement is found for ω values between $0.175\,a_0^{-1}$ and $0.250\,a_0^{-1}$, with a global optimum closer to $0.200\,a_0^{-1}$ than to $0.175\,a_0^{-1}$. (All statistical measures and in particular the slope are better with $\omega = 0.2\,a_0^{-1}$ because it strongly improves the large gap systems, in particular when considering solvation effects.) However, since the difference between $0.175\,a_0^{-1}$, for which we have data across all benchmark sets, and $0.200\,a_0^{-1}$, for which we lack data for DA-TADF and INVEST sets, is rather small, we decided to select FX175-ωPBE for further tests. Nevertheless, we want to mention that preliminary calculations on the other sets indicate that a value of $0.200\,a_0^{-1}$ (FX200-ωPBE) performs at least as well as FX175 and will presumably be used as the new default in future studies.

In addition to the systematic variations of mostly PBE-based functionals, we also tested some popular functionals and one without EXX, namely, B97M-V (pure meta-GGA), B3LYP (20% EXX), M06-2X (54% EXX), and CAM-B3LYP (19-65% EXX) in combination with UKS. An analysis of the results depicted in Figure D.4 reveals that M06-2X and CAM-B3LYP achieve an accuracy comparable to that of tuned RSHs with an identical MAD of 0.033 eV (LRC-ωPBEh: 0.026 eV) and only a few deviations > 0.05 eV (LRC-ωPBEh: 1). The correlation with experiment as measured by their SD (M06-2X: 0.035 eV and CAM-B3LYP: 0.034 eV) is comparable to that of LRC-ωPBEh (0.035 eV). B97M-V as the only pure meta-GGA functional, performs worst with the largest MAD of all tested functionals, underlining the significance of EXX in the ΔUKS approach. The global hybrid B3LYP performs very similar to PBE0, which also has a similar EXX admixture (20% vs. 25%), emphasizing that the underlying GGA is less relevant than the amount of EXX. Interestingly, this is not the case for M06-2X, which despite a similar amount of EXX of 54% performs much better than PBE50. The explanation for this presumably lies in the 36 parameters of this empirical global meta-hybrid, which apparently compensate for the systematic downshift resulting from large amounts of fixed EXX (there is not a single negative ST gap with M06-2X), thus improving the description of ST gaps. As a result, M06-2X is the best global hybrid considered in this study. Surprisingly, its close relative M06 (not

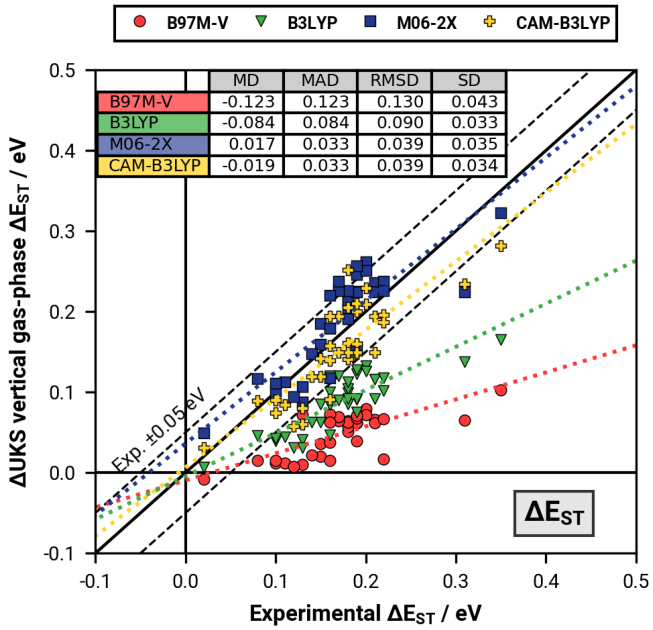

Figure D.4: Correlation plot between experimental references and vertical ST gaps calculated with ΔUKS in the gas phase using ground-state geometries. Colored dotted lines are linear regressions for the corresponding method. All values are provided in eV.

shown) with 27% EXX is not performing as well but is virtually identical to PBE0.

Overall, vertical ST gaps calculated by ΔUKS are remarkably accurate with various common functionals such as LRC-ωPBEh and M06-2X despite using the small def2-SVP basis set without any account of solvation or structural relaxation. In the PBE-based RSH functionals, a range-separation parameter of 0.200 appears to provide the best performance, surpassing even molecule-specific optimal tuning. Because of its simplicity (no excited-state optimizations required) and low computational cost (small basis set), this approach is particularly well suited for screening applications. However, it should be noted that the performance certainly profits from fortuitous error cancellation between the S_1 and T_1 excitation energies, which will become evident from the calculated emission energies (*vide infra*). Further, geometric relaxation and solvation effects are also presumably absorbed into the functional choice (amount of EXX). Nevertheless, from the good agreement over the whole structurally diverse benchmark, we may conclude that the aforementioned error cancellation is quite robust.

Finally, we want to point out that, as shown in the Supporting Information, explicitly accounting for geometric relaxation does not improve the calculated gaps but significantly worsens the agreement. This unexpected behavior is in stark contrast with the STGABS27 result, where ΔUKS/ΔROKS optimizations clearly improved the predicted gaps of (mostly) DA-TADF emitters.[1] However, it should be noted that in contrast to STGABS27, whose gaps are derived from the temperature dependence of the TADF rate, the gaps here are derived from vertical emission energies and thus not really adiabatic gaps.

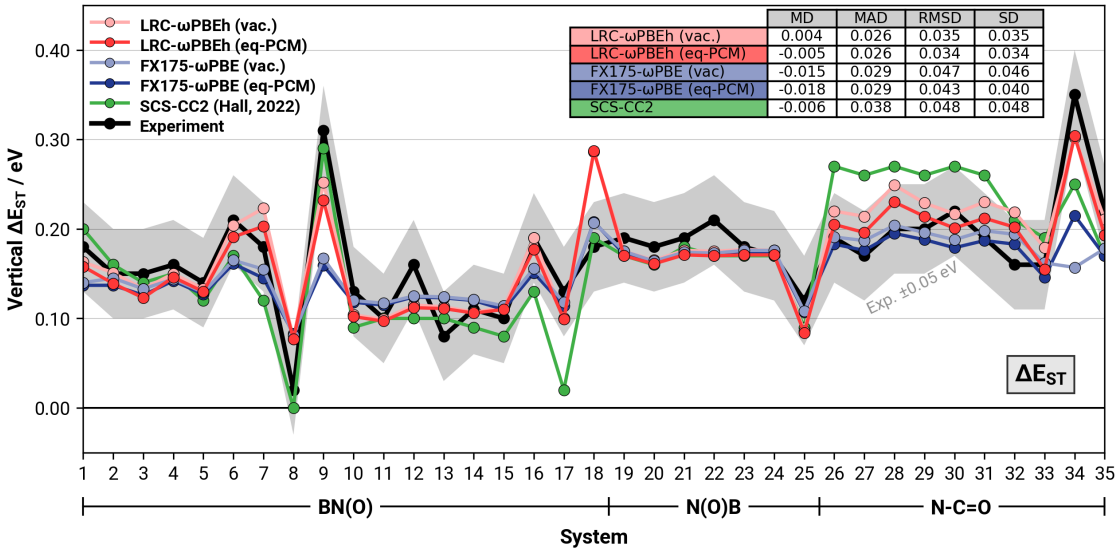

Figure D.5: Comparison of experimental (black) and SCS-CC2 (green) references against ST gaps from various ΔUKS methods. Vertical ST gaps were calculated with the LRC-ωPBEh (red) and the FX175-ωPBE (blue) functionals in the gas phase (vac., lighter color) and in solution (eq-PCM, darker color). SCS-CC2/cc-pVDZ results (gas phase) are taken from the study of Hall et al.[205] All values given in eV.

D.3.2 Influence of Solvent

Since SRCT excitations of MR-TADF are much less polar than the classical CT states of DA-TADF emitters, the impact of solvation is expected to be much smaller such that even gas-phase calculations can provide accurate ST gaps (vide supra). Nevertheless, we explore the influence of solvation on the ST gaps for the best-performing methods. To this end, we recalculate vertical ST gaps with full state-specific equilibrium solvation using the polarizable continuum model (PCM),[175,237,238] which can simply be combined with the ΔUKS approach. Specifically, we use the integral-equation formalism PCM (IEFPCM)[174] for modeling equilibrium solvation effects and a perturbative state-specific PCM variant (ptSS-PCM)[2] to model nonequilibrium solvation effects. The respective experimental conditions and associated solvent parameters, i.e., the dielectric constant and refractive index, used for the PCM can be found in Table S2 in the Supporting Information. For a detailed discussion of the theoretical background and practical limitations of the PCM, the reader is referred to refs [1] and [183]. For the analysis, we compare the MADs of the best-performing LRC-ωPBEh and FX175-ωPBE functionals, which are shown in Figure D.5 (see legend), while the absolute sizes of the ST gaps with and without solvation are plotted.

An inspection shows that for the complete set, statistical differences in the performance seem insignificant for both tested functionals (<0.005 eV). The absolute size of the ST gaps is slightly decreased in solution compared to in the gas phase, on average by –0.01 eV. However, a class-by-class analysis reveals that the impact differs depending on the type of molecule: while there are small effects for the majority of molecules, N-C=O-type MR-TADF emitters experience a notable shift of roughly −0.02 eV. For both functionals displayed in Figure D.5, accounting for solvation leads to a clear improvement for the N-C=O-type emitters. We speculate that this is due to the presence of

exposed carbonyl groups in these MR-TADF emitters, whose nonbonding orbitals are more strongly affected by the environment than the π-system of the other molecules. Despite the relatively small improvement here, we argue that including equilibrium solvation is advisable to increase the model's robustness at very little additional cost. For example, the discussed ΔUKS/FX175-ωPBE approach achieves sub 1 kcal/mol accuracy for ST gaps of DA-TADF, MR-TADF, and INVEST emitters only when combined with a PCM.[1,3] For ΔROKS and TDA-DFT discussed in the next section, solvation effects are similar and we therefore omit an explicit discussion.

D.3.3 ΔROKS and TDA-DFT

Results obtained with ΔROKS, TDA-DFT, and, for reference, SCS-CC2 are visualized in Figure D.6. While we tested the same functionals for ΔROKS as for ΔUKS, we show only the best-performing method FX155-ωB97M-V as all methods show the same basic deficiency (the other functionals can be found in the Supporting Information): Although ΔROKS yields ST gaps of approximately the right size, there is little correlation with the experimental values. Accordingly, the MAD of 0.046 eV ΔROKS/FX155-ωB97M-V is comparable to that of ΔUKS, whereas the SD of 0.064 eV is almost twice the ΔUKS value and the linear regression slope is close to zero (−0.02). We argue that this hints toward a fundamental issue with ΔROKS, namely, the lack of a description of double excitations. Although ΔUKS and ΔROKS can in principle describe doubly excited states,[173] previous work on INVEST molecules has shown that for the specific case of SRCT states, where doubly excited determinants (like $HOMO^2$ to $LUMO^2$) contribute to singly HOMO to LUMO excited S_1 and T_1 states, ΔUKS is superior.[3] For INVEST, the surprising performance of ΔUKS has been speculated to involve a mechanism by which dynamical spin polarization is mimicked by spin contamination of the UKS reference.[3] Since the spin-restricted ROKS method does not allow spin contamination, ROKS cannot describe the ST gap inversion in INVEST molecules and provides a poor correlation with experiment for MR-TADF.

The ST gaps obtained with TDA-DFT are, as expected, systematically too large, which is in line with previous studies.[205] Nevertheless, we note that TDA-DFT, specifically with FX155-ωB97M-V, reproduces some relative trends better than ΔROKS, resulting in a good slope and SD of 0.071 eV. (Other functionals like TDA-DFT/B3LYP, TDA-DFT/PBE0 and TDA-DFT/CAM-B3LYP have been tested and are all worse with SDs of 0.094 eV, 0.085 eV, and 0.080 eV; see the Supporting Information.) Again, this performance of TDA-DFT for MR-TADF is similar to that observed for INVEST systems, where the trend predicted by TDA-DFT agreed quite well with the high-level references apart from a constant shift of about 0.4 eV.[3] Albeit very systematic, the errors in TDA-DFT are still much larger than those obtained with ΔUKS or ΔROKS when using the same functional, as shown in Figure S8 in the Supporting Information displaying all methods in combination with PBE0.

Finally, out of all methods shown in Figure D.6 the SCS-CC2 results of Hall and co-workers exhibit a high correlation with the experiment, an MD close to zero, and MAD almost as low as for the best-performing ΔUKS methods. As pointed out by Hall, this is because SCS-CC2 explicitly includes doubly excited determinants (at zeroth order, i.e., only diagonal elements), which comes at the price of a much increased computational cost. However, although SCS-CC2 shows a robust performance for experimental ST gaps of MR-TADF emitters with excellent correlation, the statistical measures, in particular MAD, are not significantly better than for the much faster ΔUKS method with the

best-performing functionals.

D.3.4 Comparing SCS-CC2 and ΔUKS

To get a closer look at the two best-performing methods, namely ΔUKS and SCS-CC2, we plotted absolute values of ST gaps for the best-performing functional for MR-TADF (LRC-ωPBEh) as well as the most robust functional (FX175-ωPBE, also very accurate for DA-TADF and INVEST) next to SCS-CC2 in Figure D.5. For ΔUKS, we include results with SS-PCM equilibrium solvation (eq-PCM), as this physically more complete model improves the agreement for the N-C=O subset here and thus gives the overall best results (and is indispensable for DA-TADF). Inspection reveals that ΔUKS/LRC-ωPBEh stays consistently in the desired ±0.05 eV accuracy for all but one larger outlier for system **18** (error: +0.106 eV). With FX175-ωPBE, there are two more (previously mentioned) outliers > 0.1 eV for systems **9** and **34**, both of which have distinctly larger gaps and are the only MR-TADF emitters in the set that have a linear acene-like structure. The reduced EXX admixture (no fixed EXX and a smaller ω value) in FX175-ωPBE (compared to LRC-ωPBEh) decreases the ST gap of system **18**, giving a much better agreement with experiment. ST gaps calculated by LRC-ωPBEh and FX175-ωPBE are in most cases very similar, except for systems **26-35**, where the involvement of the carbonyl function in the aromatic system modulated the impact of the EXX admixture. Specifically for these systems, the inclusion of a solvent model in the ΔUKS approach improves the agreement substantially. Accordingly, the reason for the worse performance of SCS-CC2 for these molecules could be the lack of solvation effects.

Interestingly, in some cases, ΔUKS and SCS-CC2 are more consistent with each other than with the

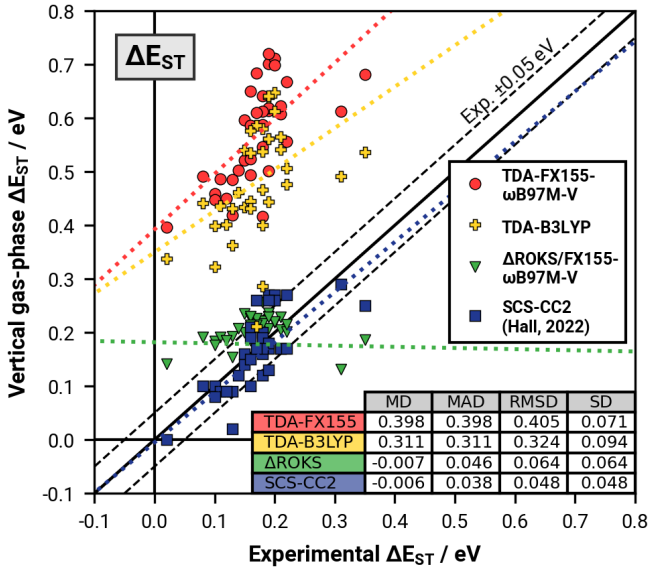

	MD	MAD	RMSD	SD
TDA-FX155	0.398	0.398	0.405	0.071
TDA-B3LYP	0.311	0.311	0.324	0.094
ΔROKS	-0.007	0.046	0.064	0.064
SCS-CC2	-0.006	0.038	0.048	0.048

Figure D.6: Correlation plot between experimental references and vertical ST gaps calculated in the gas phase using the def2-SVP basis set (DFT), and SCS-CC2/cc-pVDZ. Colored dotted lines are linear regressions for the corresponding method. SCS-CC2 values are taken from the study from Hall et al.[205] All values are given in eV.

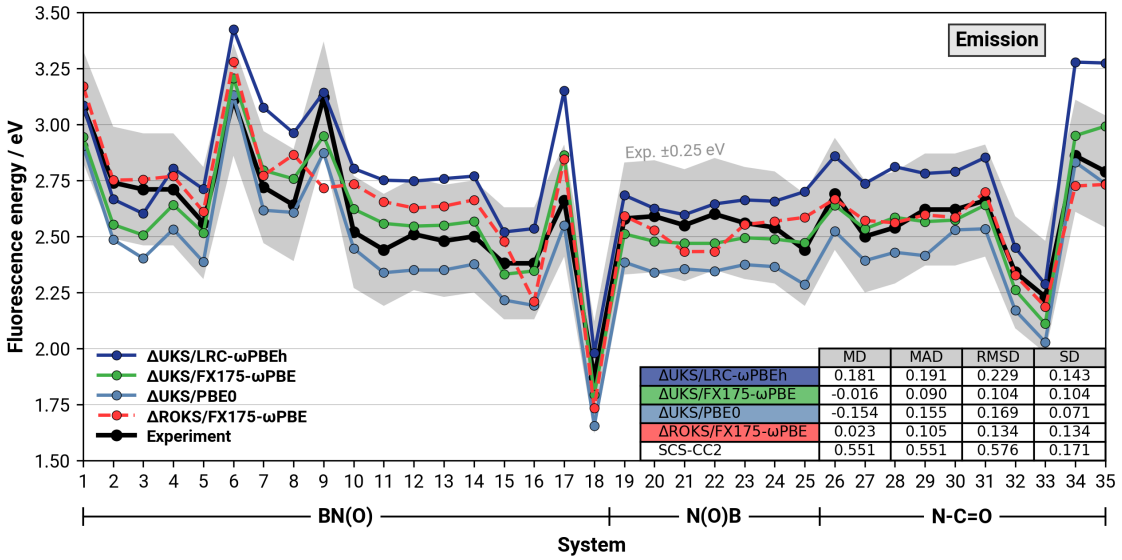

Figure D.7: Comparison of experimental fluorescence energies and ΔUKS/ΔROKS calculations with LRC-ωPBEh, FX155-ωB97M-V, FX175-ωPBE, and PBE0 using the def2-TZVP(-f) basis set, the ptSS-PCM for nonequilibrium solvation effects, and relaxed excited-state geometries. SCS-CC2 values (not shown in the graph) are vertical excitation energies (using ground-state geometries) taken from a study by Hall et al.[205] All values in eV.

experiment, agreeing within a few meV. Both methods agree very well on systems **12**, **13**, and **22**, where the experimental value deviates from all calculations by up to 0.05 eV. Accordingly, the MAD between SCS-CC2 and ΔUKS/LRC-ωPBEh is 0.029 eV and thus smaller than the respective MADs vs experiment. We speculate that this could hint toward problems with some experimental values, which are, in contrast to the STGABS27, not derived from more reliable temperature-dependent measurements but extracted from the spectra.[1] The issue with deriving gaps from fluorescence and phosphorescence spectra is caused by the presence of vibrational fine structure and different measurement temperatures, which can lead to ambiguities. Another hint in this direction is provided by the fact that the adiabatic ST gap compares worse to experiment than ST gaps calculated in the vertical approximation, as is shown in the Supporting Information.

In summary, the direct comparison of ST gaps of the best-performing methods showed that despite its much lower computational cost, ΔUKS is as accurate as or slightly more accurate than SCS-CC2 for the vertical gaps in the gas phase. When the environment is included via the PCM, ΔUKS becomes superior to SCS-CC2, in particular, for the class of N-C=O emitters. Regarding the computational cost, the explicit inclusion of doubly excited determinants causes SCS-CC2 to scale with N^5, where N is the system size, which is much less favorable than the effectively cubic N^3 scaling of ΔDFT (generally SCF) calculations in modern programs like ORCA[336] that include semi-numerical approximations for exchange.[384,385] In practice, i.e., for a typical MR-TADF emitter (system **29**) with roughly 90 atoms, the SCS-CC2/cc-pVDZ calculation takes roughly 40 h for eight singlet and triplet states (mrcc[337] (release August 2023) with a reduced-cost algorithm[344]), whereas the respective ΔUKS/def2-SVP calculation (3 × 3 orbital window or 9 states of each spin to be consistent with the 8 roots in the

SCS-CC2 calculation) takes only 2 h on the same hardware (Intel(R) Xeon(R) CPU E5-2660 v4 @ 2.00 GHz running in parallel on 28 cores/threads).

D.3.5 Fluorescence Energies

Having established the performance for ST gaps, we move on to the fluorescence energies. Here, geometric relaxation is much more important than for ST gaps; and therefore, we optimized the structure of each emitter for the energetically lowest singlet state using equilibrium solvation (PCM). In addition to the geometric relaxation, the basis set incompleteness error (BSIE) and (nonequilibrium) solvation effects also become important for fluorescence energies mostly because there is less error cancellation between S_1 and S_0 compared to S_1 and T_1. To reduce the significant BSIE (MAD def2-SVP vs def2-QZVP 0.100 eV), we employ the larger def2-TZVP(-f) basis set in the excited-state optimizations and emission energy calculations (MAD def2-TZVP(-f) vs def2-QZVP 0.003 eV). To account for nonequilibrium solvation effects, we fully equilibrate the S_1 excited state (fast and slow solvent response) with the environment and use the nonequilibrium limit (only the fast polarization component is relaxed) for the ground state using the ptSS-PCM scheme for emission with ΔDFT methods, as has recently been implemented and demonstrated for DA-TADF emitters.[2]

The emission energies calculated with this approach and the functionals PBE0, LRC-ωPBEh, FX155-ωB97M-V, and FX175-ωPBE (see the Supporting Information for the motivation of this choice) are visualized in Figure D.7. For reference, we added a statistical evaluation of the SCS-CC2 results which Hall and co-workers reported. (Note that the SCS-CC2 energies are systematically blue-shifted since the high cost of the approach forces them to use ground-state structures and the small cc-pVDZ basis set.)[205] Inspection shows that all four tested functionals can reproduce the relative trends in fluorescence energy reasonably well. PBE0 stands out with the smallest SD, but it systematically underestimates the fluorescence energy by roughly 0.15 eV, which is presumably a result of an EXX admixture that is too low (and fixed). Surprisingly, LRC-ωPBEh, the best-performing functional for ST gaps, shows the largest deviations for fluorescence energies: MD, MAD, and SD show that trends and absolute values are poorly reproduced. At least in part, this appears to be a result of an EXX admixture that is too high. Moreover, it means that the good performance of LRC-ωPBEh for the ST gaps results from a cancellation of errors between singlet and triplet excitation energies. Accordingly, FX175-ωPBE, with an EXX admixture in between PBE0 and LRC-ωPBEh, attains the lowest systematic (MD) and statistical (MAD) error, and the second best SD after PBE0. As evident from these results, the amount and type of EXX admixture are central parameters controlling the accuracy of the ΔUKS approach for MR-TADF emitters. This is a notable difference from DA-TADF, where the results for emission energies and ST gaps exhibit a small dependence on the EXX admixture.[2] We speculate that this is a result of the more prominent role of double excitations in MR-TADF (and INVEST). Nevertheless, despite these differences, the range-separation parameter of FX175-ωPBE, which was optimized for the STGABS27 set of DA-TADF emitters,[1] also shows the best overall performance for ST gaps and fluorescence energies of this set of MR-TADF emitters and was previously identified as one of the best methods for INVEST molecules (on par with PBE0).

ΔROKS performs similarly to ΔUKS with fluorescence energies being shifted to higher values by about 0.05 eV in comparison to those for ΔUKS (same functional). Hence, FX175-ωPBE retains the best performance for ΔROKS with an MAD of 0.105 eV. For a more detailed discussion on ΔROKS

for fluorescence energies, see the Supporting Information.

D.4 Summary and Conclusions

We have examined the performance of UKS- and ROKS-based ΔDFT approaches for the computation of singlet-triplet energy gaps (ST gaps) and fluorescence energies for a structurally diverse set of 35 MR-TADF emitters with known experimental reference values.[205] The results show that with a MAD below 0.03 eV, ΔUKS can be well within chemical accuracy (<1 kcal/mol or 0.044 eV) and is an order of magnitude faster than the similarly accurate spin-component-scaled second-order coupled-cluster calculations (SCS-CC2 with an MAD of 0.04 eV). While ΔUKS with the FX175-ωPBE functional is the most accurate and robust combination, the performance of ΔUKS for ST gaps is similar to that of any range-separated hybrid functional with 0-20% of the fixed exact exchange (EXX) and a range-separation parameter of $0.150-0.200\,a_0^{-1}$, like LRC-ωPBEh or CAM-B3LYP, and even with some global hybrids like M06-2X. In contrast, although ΔROKS also provides reasonably accurate estimates of the ST gaps, it predicts nearly uniform ST gaps (≈0.2 eV) across all systems, missing subtle differences that are captured by ΔUKS and SCS-CC2. We attributed this failure to a lack of a specific error compensation in the ROKS singlet wave function, which aligns well with a recently reported issue of ROKS with INVEST molecules.[3] In general, because of an apparently stable error cancellation between S_1 and T_1 energies covering nuclear relaxation and basis set effects, ST gaps can be efficiently predicted with a small (here def2-SVP) basis set in the vertical approximation (using ground-state geometries).

Regarding the influence of solvent, we found a much smaller influence than that for donor-acceptor (DA)-TADF emitters, which is in line with the much less polar nature of the excited states. Nevertheless, significant effects show up in the subset of polar N-C=O containing MR-TADF molecules (systems **26**-**35**) and some further cases, where including the solvent causes a systematic downshift of about −0.02 eV which systematically improves the agreement. We concluded that an application of solvation models is generally advisable to improve the robustness of the modeling (also, MR-TADF molecules can have donor and acceptor motifs giving rise to polar CT). Moreover, due to the state-specific nature of the ΔUKS approach, the inclusion of solvent is straightforward and computationally cheap, which is in stark contrast to excitation-based models like TD-DFT and CC2, where state-specific solvation results in a double-iterative procedure.[183]

Moving on to fluorescence energies, excited-state optimizations become paramount with an average shift of the excitation energy of ≈ 0.3 eV between the S_1 and S_0 optimized structures, and also the size of the basis set becomes important: while for the ST gaps def2-SVP agrees with def2-QZVP within < 0.01 eV, emission energies require the larger def2-TZVP(-f) basis set for similar convergence. In contrast to the ST gaps, ΔUKS and ΔROKS perform nearly on par with each other for emission energies. Another difference is that while several functionals provide accurate ST gaps with ΔUKS, only one of them, namely, FX175-ωPBE, also provides similarly accurate emission energies. Interestingly, the robustness of this specific combination appears to be more general: over all the different types of TADF emitters studied by us up to this point, i.e., ST gaps[1] and emission[2] of DA-TADF, gap inversion in INVEST molecules,[3] and MR-TADF (here), FX175-ωPBE exhibits a very consistent performance, making it the jack-of-all-trades functional for ΔUKS in organic electronics.

A remaining challenge for ΔUKS is the state-targeting problem, i.e., how to find the lowest singlet and triplet excited states reliably. Addressing this challenge, we have introduced a 4×4 approach, i.e., screening transitions between all orbitals between HOMO-3 and LUMO+3 and using the lowest energy states. However, while this mitigates the issue, it does not eliminate it. A particular problem with ΔUKS is the apparent inability of IMOM to reliably converge to symmetry-broken lower-energy solutions in symmetric oligomers (i.e., system **30**), which often requires manual intervention, preventing a black-box application of the method. Perhaps the best approach to automating this is to start the UKS calculations (for singlets) from the converged ROKS orbitals. This helps because ROKS readily finds symmetry-broken solutions if they are lower in energy. However, the trade-off for increased robustness of this mixed UKS//ROKS strategy is an about 3-fold increased cost (which is still well below that of CC2).

All in all, this study of a diverse set of MR-TADF emitters demonstrates the capabilities of ΔDFT methods, specifically ΔUKS, to predict the photophysical properties of MR-TADF emitters. When combined with the FX175-ωPBE functional and a PCM solvation model, the approach is as accurate for the highly polar CT states of DA-TADF emitter[1,2] and recovers the correlation-driven gap inversion in INVEST molecules with chemical accuracy.[3] Compared to similarly accurate and versatile wave function-based approaches like (SCS-)CC2 and ADC(2), ΔUKS holds the clear advantage of having a much lower computational cost and better scaling with molecular size, making it a valuable tool for the rational design design and discovery of new materials.

D.5 Acknowledgment

This project has been funded with support from the RTG-2591 "TIDE - Template-designed Organic Electronics".

D.6 Supporting Information

The Supporting Information is available free of charge at:
https://pubs.acs.org/doi/10.1021/acs.jpclett.4c03192.
Lewis structure overview for the whole set, optimal ω values of the OT-LC-ωPBE functional, experimental conditions and solvent parameters for polarizable continuum models, linear regression parameter singlet-triplet gaps, basis set convergence for singlet-triplet gaps and excitation energies tested on a small subset, TDA-DFT singlet-triplet gap results, ΔROKS singlet-triplet gap results, ΔUKS singlet-triplet gaps for LC-ωPBE with different ω values, vertical excitation energies for ground-state geometries (ΔUKS and ΔROKS), fluorescence energies calculated by ΔROKS, statistical measure formula, Q-Chem sample input files for ΔUKS and ΔROKS calculations, ORCA sample input files for ΔUKS calculations, and ground-state geometries (optimized at r^2SCAN-3c level). For better accessibility, geometries, experimental references, and supporting information are also provided in spreadsheet format.

Bibliography

[1] L. Kunze, A. Hansen, S. Grimme, and J.-M. Mewes,
PCM-ROKS for the description of charge-transfer states in solution: Singlet-triplet gaps with chemical accuracy from open-shell Kohn-Sham reaction-field calculations,
J. Phys. Chem. Lett. **12** (2021) 8470.

[2] T. Froitzheim, L. Kunze, S. Grimme, J. M. Herbert, and J.-M. Mewes,
Benchmarking charge-transfer excited states in TADF emitters: ΔDFT outperforms TD-DFT for emission energies, J. Phys. Chem. A **128** (2024) 6324.

[3] L. Kunze, T. Froitzheim, A. Hansen, S. Grimme, and J.-M. Mewes,
ΔDFT predicts inverted singlet–triplet gaps with chemical accuracy at a fraction of the cost of wave function-based approaches, J. Phys. Chem. Lett. **15** (2024) 8065.

[4] L. Kunze, A. Hansen, S. Grimme, and J.-M. Mewes, *The best of both worlds: ΔDFT describes multiresonance TADF emitters with wave-function accuracy at density-functional cost*,
J. Phys. Chem. Lett. **16** (2025) 1114.

[5] T. Jin, L. Kunze, S. Breimaier, M. Bolte, H.-W. Lerner, F. Jäkle, R. F. Winter, M. Braun, J.-M. Mewes, and M. Wagner, *Exploring structure–property relations of B, S-doped polycyclic aromatic hydrocarbons through the trinity of synthesis, spectroscopy, and theory*,
J. Am. Chem. Soc. **144** (2022) 13704.

[6] K. Rohatgi-Mukherjee, *Fundamentals of photochemistry*, New Age International, 1978.

[7] H. D. Roth, *The beginnings of organic photochemistry*,
Angew. Chem. Int. Ed. Engl. **28** (1989) 1193.

[8] K. Szaciłowski, W. Macyk, A. Drzewiecka-Matuszek, M. Brindell, and G. Stochel,
Bioinorganic photochemistry: Frontiers and mechanisms, Chem. Rev. **105** (2005) 2647.

[9] C. Förster and K. Heinze,
Photophysics and photochemistry with Earth-abundant metals–fundamentals and concepts,
Chem. Soc. Rev. **49** (2020) 1057.

[10] T. G. Truscott,
New trends in photobiology: The photophysics and photochemistry of the carotenoids,
J. Photochem. Photobiol. B **6** (1990) 359.

[11] G. Cilento and W. Adam, *Photochemistry and photobiology without light*,
Photochem. Photobiol. **48** (1988) 361.

[12] J. Eisinger and R. Shulman, *Excited electronic states of DNA*, Science **161** (1968) 1311.

[13] D. Markovitsi, *UV-induced DNA damage: The role of electronic excited states*, Photochem. Photobiol. **92** (2016) 45.

[14] G. R. Fleming and R. v. Grondelle, *The primary steps of photosynthesis*, Phys. Today **47** (1994) 48.

[15] C. König and J. Neugebauer, *Quantum chemical description of absorption properties and excited-state processes in photosynthetic systems*, ChemPhysChem **13** (2012) 386.

[16] W. A. Fowler, *Experimental and theoretical nuclear astrophysics: The quest for the origin of the elements*, Rev. Mod. Phys. **56** (1984) 149.

[17] E. Roueff and F. Lique, *Molecular excitation in the interstellar medium: Recent advances in collisional, radiative, and chemical processes*, Chem. Rev. **113** (2013) 8906.

[18] K. I. Oberg, *Photochemistry and astrochemistry: Photochemical pathways to interstellar complex organic molecules*, Chem. Rev. **116** (2016) 9631.

[19] L. Buzzetti, G. E. Crisenza, and P. Melchiorre, *Mechanistic studies in photocatalysis*, Angew. Chem. Int. Ed. **58** (2019) 3730.

[20] D. M. Arias-Rotondo and J. K. McCusker, *The photophysics of photoredox catalysis: A roadmap for catalyst design*, Chem. Soc. Rev. **45** (2016) 5803.

[21] J. Zhao, K. Xu, W. Yang, Z. Wang, and F. Zhong, *The triplet excited state of Bodipy: Formation, modulation and application*, Chem. Soc. Rev. **44** (2015) 8904.

[22] K. L. Skubi, T. R. Blum, and T. P. Yoon, *Dual catalysis strategies in photochemical synthesis*, Chem. Rev. **116** (2016) 10035.

[23] T. Markvart, *Light harvesting for quantum solar energy conversion*, Prog. Quantum Electron. **24** (2000) 107.

[24] V. Balzani, A. Credi, and M. Venturi, *Photochemical conversion of solar energy*, ChemSusChem **1** (2008) 26.

[25] T. F. Schulze and T. W. Schmidt, *Photochemical upconversion: Present status and prospects for its application to solar energy conversion*, Energy Environ. Sci. **8** (2015) 103.

[26] J. E. Kwon and S. Y. Park, *Advanced organic optoelectronic materials: Harnessing excited-state intramolecular proton transfer (ESIPT) process*, Adv. Mater. **23** (2011) 3615.

[27] Z. Shuai and Q. Peng, *Excited states structure and processes: Understanding organic light-emitting diodes at the molecular level*, Phys. Rep. **537** (2014) 123.

[28] O. Ostroverkhova, *Organic optoelectronic materials: Mechanisms and applications*, Chem. Rev. **116** (2016) 13279.

[29] P. Avouris, M. Freitag, and V. Perebeinos, *Carbon-nanotube photonics and optoelectronics*, Nat. Photon. **2** (2008) 341.

[30] R. Bhuyan, J. Mony, O. Kotov, G. W. Castellanos, J. Gómez Rivas, T. O. Shegai, and K. Börjesson, *The rise and current status of polaritonic photochemistry and photophysics*, Chem. Rev. **123** (2023) 10877.

[31] K. Plaetzer, B. Krammer, J. Berlanda, F. Berr, and T. Kiesslich, *Photophysics and photochemistry of photodynamic therapy: Fundamental aspects*, Lasers Med. Sci. **24** (2009) 259.

[32] W. Hu, P. N. Prasad, and W. Huang, *Manipulating the dynamics of dark excited states in organic materials for phototheranostics*, Acc. Chem. Res. **54** (2020) 697.

[33] J. A. Kim, D. J. Wales, and G.-Z. Yang, *Optical spectroscopy for in vivo medical diagnosis—a review of the state of the art and future perspectives*, Prog. Biomed. Eng. **2** (2020) 042001.

[34] H. M. Kim and B. R. Cho, *Small-molecule two-photon probes for bioimaging applications*, Chem. Rev. **115** (2015) 5014.

[35] O. S. Wolfbeis, *An overview of nanoparticles commonly used in fluorescent bioimaging*, Chem. Soc. Rev. **44** (2015) 4743.

[36] K. B. Bravaya, B. L. Grigorenko, A. V. Nemukhin, and A. I. Krylov, *Quantum chemistry behind bioimaging: Insights from ab initio studies of fluorescent proteins and their chromophores*, Acc. Chem. Res. **45** (2012) 265.

[37] T. Brixner, J. Stenger, H. M. Vaswani, M. Cho, R. E. Blankenship, and G. R. Fleming, *Two-dimensional spectroscopy of electronic couplings in photosynthesis*, Nature **434** (2005) 625.

[38] S. Mai and L. González, *Molecular photochemistry: Recent developments in theory*, Angew. Chem. Int. Ed. **59** (2020) 16832.

[39] G. Horowitz, *Organic field-effect transistors*, Adv. Mater. **10** (1998) 365.

[40] M. Muccini, *A bright future for organic field-effect transistors*, Nat. Mater. **5** (2006) 605.

[41] D. Braga and G. Horowitz, *High-performance organic field-effect transistors*, Adv. Mater. **21** (2009) 1473.

[42] H. Hoppe and N. S. Sariciftci, *Organic solar cells: An overview*, J. Mater. Res. **19** (2004) 1924.

[43] T. M. Clarke and J. R. Durrant, *Charge photogeneration in organic solar cells*, Chem. Rev. **110** (2010) 6736.

[44] P. Cheng and X. Zhan, *Stability of organic solar cells: Challenges and strategies*, Chem. Soc. Rev. **45** (2016) 2544.

[45] M. Schäferling, *The art of fluorescence imaging with chemical sensors*, Angew. Chem. Int. Ed. **51** (2012) 3532.

[46] S. W. Thomas, G. D. Joly, and T. M. Swager, *Chemical sensors based on amplifying fluorescent conjugated polymers*, Chem. Rev. **107** (2007) 1339.

[47] M. Van Bay, N. K. Hien, P. T. Quy, P. C. Nam, D. U. Van, and D. T. Quang, *Using calculations of the electronically excited states for investigation of fluorescent sensors: A review*, Vietnam J. Chem. **57** (2019) 389.

[48] C. Sekine, Y. Tsubata, T. Yamada, M. Kitano, and S. Doi, *Recent progress of high performance polymer OLED and OPV materials for organic printed electronics*, Sci. Technol. Adv. Mater. **15** (2014) 034203.

[49] J. S. Chang, A. F. Facchetti, and R. Reuss, *A circuits and systems perspective of organic/printed electronics: Review, challenges, and contemporary and emerging design approaches*, IEEE J. Emerg. Sel. Top. Circuits Syst. **7** (2017) 7.

[50] M. C. Gather, A. Köhnen, and K. Meerholz, *White organic light-emitting diodes*, Adv. Mater. **23** (2011) 233.

[51] Y. Tao, C. Yang, and J. Qin, *Organic host materials for phosphorescent organic light-emitting diodes*, Chem. Soc. Rev. **40** (2011) 2943.

[52] Y. Liu, C. Li, Z. Ren, S. Yan, and M. R. Bryce, *All-organic thermally activated delayed fluorescence materials for organic light-emitting diodes*, Nat. Rev. Mater. **3** (2018) 1.

[53] G. Hong, X. Gan, C. Leonhardt, Z. Zhang, J. Seibert, J. M. Busch, and S. Bräse, *A brief history of OLEDs—emitter development and industry milestones*, Adv. Mater. **33** (2021) 2005630.

[54] C. Parker and C. Hatchard, *Triplet-singlet emission in fluid solutions. Phosphorescence of eosin*, Trans. Faraday Soc. **57** (1961) 1894.

[55] M. Pope, H. P. Kallmann, and P. Magnante, *Electroluminescence in organic crystals*, J. Chem. Phys. **38** (1963) 2042.

[56] *S. A. VanSlyke, C. W. Tang, L. C. Roberts, Eastman Kodak Co, Electroluminescent device with organic luminescent medium. U.S. Patent US4720432A. 1987.*

[57] J. Burroughes, D. Bradley, and A. Brown, *Light-emitting diodes based on conjugated polymers*, Nature **347** (1990) 539.

[58] M. A. Baldo, D. F. O'Brien, Y. You, A. Shoustikov, S. Sibley, M. E. Thompson, and S. R. Forrest, *Highly efficient phosphorescent emission from organic electroluminescent devices*, Nature **395** (1998) 151.

[59] A. Endo, K. Sato, K. Yoshimura, T. Kai, A. Kawada, H. Miyazaki, and C. Adachi, *Efficient up-conversion of triplet excitons into a singlet state and its application for organic light emitting diodes*, Appl. Phys. Lett. **98** (2011) 083302.

[60] *Seifermann, S. Organic molecules for optoelectronic devices. U.S. Patent US11545632B2. January 3, 2023.*

[61] *M. Koden, Eastman Kodak Co, OLED displays and lighting, John Wiley and Sons, New York, 2016.*

[62] C. Adachi, S. Lee, T. Nakagawa, K. Shizu, K. Goushi, T. Yasuda, and W. J. Potscavage, "Organic light-emitting diodes (OLEDs): Materials, photophysics, and device physics," *Organic Electronics Materials and Devices*, Springer, 2015 43.

[63] A. P. Kulkarni, C. J. Tonzola, A. Babel, and S. A. Jenekhe, *Electron transport materials for organic light-emitting diodes*, Chem. Mater. **16** (2004) 4556.

[64] C. Giebeler, H. Antoniadis, D. D. Bradley, and Y. Shirota, *Influence of the hole transport layer on the performance of organic light-emitting diodes*, J. Appl. Phys. **85** (1999) 608.

[65] W. Z. Yuan, P. Lu, S. Chen, J. W. Lam, Z. Wang, Y. Liu, H. S. Kwok, Y. Ma, and B. Z. Tang, *Changing the behavior of chromophores from aggregation-caused quenching to aggregation-induced emission: Development of highly efficient light emitters in the solid state*, Adv. Mater. **22** (2010) 2159.

[66] S. Reineke, K. Walzer, and K. Leo, *Triplet-exciton quenching in organic phosphorescent light-emitting diodes with Ir-based emitters*, Phys. Rev. B— **75** (2007) 125328.

[67] E. Fermi, *Sulla quantizzazione del gas perfetto monoatomico*, Rend. Lincei **3** (1926) 145.

[68] D. J. Birch, Y. Chen, and O. J. Rolinski, "Fluorescence," *Photonics: Biomedical Photonics, Spectroscopy, and Microscopy*, Wiley Online Library, 2015 1.

[69] G. Baryshnikov, B. Minaev, and H. Ågren, *Theory and calculation of the phosphorescence phenomenon*, Chem. Rev. **117** (2017) 6500.

[70] Z. Yang, Z. Mao, Z. Xie, Y. Zhang, S. Liu, J. Zhao, J. Xu, Z. Chi, and M. P. Aldred, *Recent advances in organic thermally activated delayed fluorescence materials*, Chem. Soc. Rev. **46** (2017) 915.

[71] F. B. Dias, K. N. Bourdakos, V. Jankus, K. C. Moss, K. T. Kamtekar, V. Bhalla, J. Santos, M. R. Bryce, and A. P. Monkman, *Triplet harvesting with 100% efficiency by way of thermally activated delayed fluorescence in charge transfer OLED emitters*, Adv. Mater. **25** (2013) 3707.

[72] T. Hatakeyama, K. Shiren, K. Nakajima, S. Nomura, S. Nakatsuka, K. Kinoshita, J. Ni, Y. Ono, and T. Ikuta, *Ultrapure blue thermally activated delayed fluorescence molecules: Efficient HOMO-LUMO separation by the multiple resonance effect*, Adv. Mater. **28** (2016) 2777.

[73] C. David Sherrill and H. F. Schaefer, "The configuration interaction method: Advances in highly correlated approaches," *Advances in Quantum Chemistry*, ed. by P.-O. Löwdin, J. R. Sabin, M. C. Zerner, and E. Brändas, vol. 34, Academic Press, 1999 143.

[74] G. D. Purvis III and R. J. Bartlett, *A full coupled-cluster singles and doubles model: The inclusion of disconnected triples*, J. Chem. Phys. **76** (1982) 1910.

[75] P. Hohenberg and W. Kohn, *Inhomogeneous electron gas*, Phys. Rev. **136** (1964) B864.

[76] W. Kohn and L. J. Sham, *Self-consistent equations including exchange and correlation effects*, Phys. Rev. **140** (1965) A1133.

[77] O. Christiansen, H. Koch, and P. Jørgensen,
The second-order approximate coupled cluster singles and doubles model CC2, en,
Chem. Phys. Lett. **243** (1995) 409.

[78] J. F. Stanton and R. J. Bartlett,
The equation of motion coupled-cluster method. A systematic biorthogonal approach to molecular excitation energies, transition probabilities, and excited state properties,
J. Chem. Phys. **98** (1993) 7029.

[79] A. Dreuw and M. Head-Gordon,
Single-reference ab initio methods for the calculation of excited states of large molecules,
Chem. Rev. **105** (2005) 4009.

[80] A. Szabo and N. S. Ostlund,
Modern quantum chemistry: Introduction to advanced electronic structure theory,
Courier Corporation, 1996.

[81] T. Helgaker, P. Jorgensen, and J. Olsen, *Molecular electronic-structure theory*,
John Wiley & Sons, 2013.

[82] D. Cremer, *Møller–Plesset perturbation theory: From small molecule methods to methods for thousands of atoms*, Wiley Interdiscip. Rev. Comput. Mol. Sci. **1** (2011) 509.

[83] Á. Nagy, *Density functional. Theory and application to atoms and molecules*,
Phys. Rep. **298** (1998) 1.

[84] M. E. Casida, "Time-dependent density functional response theory for molecules,"
Recent Advances In Density Functional Methods: (Part I), World Scientific, 1995 155.

[85] A. T. Gilbert, N. A. Besley, and P. M. Gill,
Self-consistent field calculations of excited states using the maximum overlap method (MOM),
J. Phys. Chem. A **112** (2008) 13164.

[86] G. M. Barca, A. T. Gilbert, and P. M. Gill, *Simple models for difficult electronic excitations*,
J. Chem. Theory Comput. **14** (2018) 1501.

[87] M. Filatov and S. Shaik, *A spin-restricted ensemble-referenced Kohn-Sham method and its application to diradicaloid situations*, Chem. Phys. Lett. **304** (1999) 429.

[88] T. Kowalczyk, T. Tsuchimochi, P.-T. Chen, L. Top, and T. Van Voorhis,
Excitation energies and Stokes shifts from a restricted open-shell Kohn-Sham approach,
J. Chem. Phys. **138** (2013) 164101.

[89] J. M. Herbert, *Dielectric continuum methods for quantum chemistry*,
Wiley Interdiscip. Rev. Comput. Mol. Sci. **11** (2021) e1519.

[90] D. R. Hartree, "The wave mechanics of an atom with a non-Coulomb central field. Part I. Theory and methods," *Math. Proc. Camb. Philos. Soc.* Vol. 24,
Cambridge university press, 1928 89.

[91] D. R. Hartree, "The wave mechanics of an atom with a non-coulomb central field. Part II. Some results and discussion," *Math. Proc. Camb. Philos. Soc.* Vol. 24,
Cambridge University Press, 1928 111.

[92] J. C. Slater, *Note on Hartree's method*, Phys. Rev. **35** (1930) 210.

[93] W. Heisenberg, *Mehrkörperproblem und Resonanz in der Quantenmechanik*, Z. Phys. **38** (1926) 411.

[94] P. A. M. Dirac, *On the theory of quantum mechanics*, Proc. R. Soc. Lond. A **112** (1926) 661.

[95] V. Fock, *Näherungsmethode zur Lösung des quantenmechanischen Mehrkörperproblems*, Z. Phys. **61** (1930) 126.

[96] C. C. J. Roothaan, *New developments in molecular orbital theory*, Rev. Mod. Phys. **23** (1951) 69.

[97] T. P. Hamilton and P. Pulay, *Direct inversion in the iterative subspace (DIIS) optimization of open-shell, excited-state, and small multiconfiguration SCF wave functions*, J. Chem. Phys. **84** (1986) 5728.

[98] L. N. Brillouin, *La méthode du champ self-consistent*, Hermann & cie, 1933.

[99] S. Grimme, *Improved second-order Møller-Plesset perturbation theory by separate scaling of parallel-and antiparallel-spin pair correlation energies*, J. Chem. Phys. **118** (2003) 9095.

[100] U. Bozkaya, J. M. Turney, Y. Yamaguchi, H. F. Schaefer, and C. D. Sherrill, *Quadratically convergent algorithm for orbital optimization in the orbital-optimized coupled-cluster doubles method and in orbital-optimized second-order Møller-Plesset perturbation theory*, J. Chem. Phys. **135** (2011).

[101] J. Lee and M. Head-Gordon, *Regularized orbital-optimized second-order Møller–Plesset perturbation theory: A reliable fifth-order-scaling electron correlation model with orbital energy dependent regularizers*, J. Chem. Theory. Comput. **14** (2018) 5203.

[102] F. R. Manby, *Density fitting in second-order linear-r 12 Møller–Plesset perturbation theory*, J. Chem. Phys. **119** (2003) 4607.

[103] H.-J. Werner, F. R. Manby, and P. J. Knowles, *Fast linear scaling second-order Møller-Plesset perturbation theory (MP2) using local and density fitting approximations*, J. Chem. Phys. **118** (2003) 8149.

[104] L. H. Thomas, "The calculation of atomic fields," *Math. Proc. Camb.* Vol. 23, Cambridge University Press, 1927 542.

[105] N. Mardirossian and M. Head-Gordon, *Thirty years of density functional theory in computational chemistry: an overview and extensive assessment of 200 density functionals*, Mol. Phys. **115** (2017) 2315.

[106] S. H. Vosko, L. Wilk, and M. Nusair, *Accurate spin-dependent electron liquid correlation energies for local spin density calculations: A critical analysis*, Can. J. Phys. **58** (1980) 1200.

[107] J. Guan, P. Duffy, J. T. Carter, D. P. Chong, K. C. Casida, M. E. Casida, and M. Wrinn, *Comparison of local-density and Hartree–Fock calculations of molecular polarizabilities and hyperpolarizabilities*, J. Chem. Phys. **98** (1993) 4753.

[108] J. P. Perdew, K. Burke, and M. Ernzerhof, *Generalized gradient approximation made simple*, Phys. Rev. Lett. **77** (1996), erratum Phys. Rev. Lett. 78, 1396 (1997) 3865.

[109] J. Harris and R. Jones, *The surface energy of a bounded electron gas*, J. Phys. F: Met. Phys. **4** (1974) 1170.

[110] O. Gunnarsson and B. I. Lundqvist, *Exchange and correlation in atoms, molecules, and solids by the spin-density-functional formalism*, Phys. Rev. B **13** (1976) 4274.

[111] D. C. Langreth and J. P. Perdew,
Exchange-correlation energy of a metallic surface: Wave-vector analysis,
Phys. Rev. B **15** (1977) 2884.

[112] J. Harris, *Adiabatic-connection approach to Kohn-Sham theory*, Phys. Rev. A **29** (1984) 1648.

[113] K. Burke, M. Ernzerhof, and J. P. Perdew,
The adiabatic connection method: A non-empirical hybrid, Chem. Phys. Lett. **265** (1997) 115.

[114] L. Goerigk, A. Hansen, C. Bauer, S. Ehrlich, A. Najibi, and S. Grimme,
A look at the density functional theory zoo with the advanced GMTKN55 database for general main group thermochemistry, kinetics and noncovalent interactions,
Phys. Chem. Chem. Phys. **19** (2017) 32184.

[115] G. Zhang and C. B. Musgrave,
Comparison of DFT methods for molecular orbital eigenvalue calculations,
J. Phys. Chem. A **111** (2007) 1554.

[116] P. Mori-Sánchez, A. J. Cohen, and W. Yang,
Many-electron self-interaction error in approximate density functionals,
J. Chem. Phys. **125** (2006).

[117] O. A. Vydrov and G. E. Scuseria, *Assessment of a long-range corrected hybrid functional*,
J. Chem. Phys. **125** (2006).

[118] T. Yanai, D. P. Tew, and N. C. Handy, *A new hybrid exchange–correlation functional using the Coulomb-attenuating method (CAM-B3LYP)*, Chem. Phys. Lett. **393** (2004) 51.

[119] H. Iikura, T. Tsuneda, T. Yanai, and K. Hirao,
A long-range correction scheme for generalized-gradient-approximation exchange functionals,
J. Chem. Phys. **115** (2001) 3540.

[120] A. Savin and H.-J. Flad, *Density functionals for the Yukawa electron-electron interaction*,
Int. J. Quantum Chem. **56** (1995) 327.

[121] T. Leininger, H. Stoll, H.-J. Werner, and A. Savin,
Combining long-range configuration interaction with short-range density functionals,
Chem. Phys. Lett. **275** (1997) 151.

[122] P. M. Gill and R. D. Adamson, *A family of attenuated Coulomb operators*,
Chem. Phys. Lett. **261** (1996) 105.

[123] C. Adamo and V. Barone,
Toward reliable density functional methods without adjustable parameters: The PBE0 model,
J. Chem. Phys. **110** (1999) 6158.

[124] M. A. Rohrdanz and J. M. Herbert, *Simultaneous benchmarking of ground- and excited-state properties with long-range-corrected density functional theory*,
J. Chem. Phys. **129** (2008) 034107.

[125] T. Krzödörfer and J.-L. Brédas, *Organic electronic materials: recent advances in the DFT description of the ground and excited states using tuned range-separated hybrid functionals*,
Acc. Chem. Res. **47** (2014) 3284.

[126] S. Refaely-Abramson, R. Baer, and L. Kronik,
Fundamental and excitation gaps in molecules of relevance for organic photovoltaics from an optimally tuned range-separated hybrid functional, Phys. Rev. B **84** (2011) 075144.

[127] N. Mardirossian and M. Head-Gordon, *ωB97M-V: A combinatorially optimized, range-separated hybrid, meta-GGA density functional with VV10 nonlocal correlation*, J. Chem. Phys. **144** (2016) 214110.

[128] T. Stein, L. Kronik, and R. Baer, *Reliable prediction of charge transfer excitations in molecular complexes using time-dependent density functional theory*, J. Am. Chem. Soc. **131** (2009) 2818.

[129] S. Refaely-Abramson, S. Sharifzadeh, M. Jain, R. Baer, J. B. Neaton, and L. Kronik, *Gap renormalization of molecular crystals from density-functional theory*, Phys. Rev. B **88** (2013) 081204.

[130] J. Shee and M. Head-Gordon,
Predicting excitation energies of twisted intramolecular charge-transfer states with the time-dependent density functional theory: Comparison with experimental measurements in the gas phase and solvents ranging from hexanes to acetonitrile, J. Chem. Theory Comput. **16** (2020) 6244.

[131] S. Grimme,
Semiempirical hybrid density functional with perturbative second-order correlation, J. Chem. Phys. **124** (2006).

[132] G. Santra, N. Sylvetsky, and J. M. Martin,
Minimally empirical double-hybrid functionals trained against the GMTKN55 database: revDSD-PBEP86-D4, revDOD-PBE-D4, and DOD-SCAN-D4, J. Phys. Chem. A **123** (2019) 5129.

[133] R. Sure and S. Grimme, *Corrected small basis set Hartree-Fock method for large systems*, J. Comp. Chem. **34** (2013) 1672.

[134] S. Grimme, J. G. Brandenburg, C. Bannwarth, and A. Hansen, *Consistent structures and interactions by density functional theory with small atomic orbital basis sets*, J. Chem. Phys. **143** (2015) 054107.

[135] J. G. Brandenburg, C. Bannwarth, A. Hansen, and S. Grimme,
B97-3c: A revised low-cost variant of the B97-D density functional method, J. Chem. Phys. **148** (2018) 064104.

[136] S. Grimme, A. Hansen, S. Ehlert, and J.-M. Mewes,
r2SCAN-3c: A "Swiss army knife" composite electronic-structure method, J. Chem. Phys. **154** (2021) 064103.

[137] M. Müller, A. Hansen, and S. Grimme, *ωB97X-3c: A composite range-separated hybrid DFT method with a molecule-optimized polarized valence double-ζ basis set*, J. Chem. Phys. **158** (2023).

[138] S. Grimme, "Dispersion interaction and chemical bonding,"
The Chemical Bond: Fundamental Aspects of Chemical Bonding, Wiley Online Library, 2014 477.

[139] S. Grimme, A. Hansen, J. G. Brandenburg, and C. Bannwarth,
Dispersion-corrected mean-field electronic structure methods, Chem. Rev. **116** (2016) 5105.

[140] S. Grimme, J. Antony, S. Ehrlich, and H. Krieg,
A consistent and accurate ab initio parametrization of density functional dispersion correction (DFT-D) for the 94 elements H-Pu, J. Chem. Phys. **132** (2010) 154104.

[141] S. Grimme, S. Ehrlich, and L. Goerigk,
Effect of the damping function in dispersion corrected density functional theory,
J. Comp. Chem. **32** (2011) 1456.

[142] E. Caldeweyher, C. Bannwarth, and S. Grimme,
Extension of the D3 dispersion coefficient model, J. Chem. Phys. **147** (2017) 034112.

[143] E. Caldeweyher, S. Ehlert, A. Hansen, H. Neugebauer, S. Spicher, C. Bannwarth, and S. Grimme, *A generally applicable atomic-charge dependent London dispersion correction*,
J. Chem. Phys. **150** (2019) 154122.

[144] M. Dion, H. Rydberg, E. Schröder, D. C. Langreth, and B. I. Lundqvist,
Van der Waals density functional for general geometries, Phys. Rev. Lett. **92** (2004) 246401.

[145] O. A. Vydrov and T. Van Voorhis,
Nonlocal van der Waals density functional: The simpler the better, J. Chem. Phys. **133** (2010).

[146] K. Lee, É. D. Murray, L. Kong, B. I. Lundqvist, and D. C. Langreth,
Higher-accuracy van der Waals density functional, Phys. Rev. B **82** (2010) 081101.

[147] T. Schwabe and S. Grimme, *Double-hybrid density functionals with long-range dispersion corrections: Higher accuracy and extended applicability*,
Phys. Chem. Chem. Phys. **9** (2007) 3397.

[148] E. K. Gross and W. Kohn, *Time-dependent density-functional theory*,
Adv. Quantum Chem. **21** (1990) 255.

[149] E. Runge and E. K. U. Gross, *Density-functional theory for time-dependent systems*,
Phys. Rev. Lett. **52** (1984) 997.

[150] K. Yabana and G. Bertsch, *Time-dependent local-density approximation in real time*,
Phys. Rev. B **54** (1996) 4484.

[151] D. Jacquemin, V. Wathelet, E. A. Perpète, and C. Adamo,
Extensive TD-DFT benchmark: Singlet-excited states of organic molecules,
J. Chem. Theory Comput. **5** (2009) 2420.

[152] D. Jacquemin, A. Planchat, C. Adamo, and B. Mennucci,
TD-DFT assessment of functionals for optical 0–0 transitions in solvated dyes,
J. Chem. Theory Comput. **8** (2012) 2359.

[153] A. D. Laurent and D. Jacquemin, *TD-DFT benchmarks: A review*, en,
Int. J. Quantum Chem. **113** (2013) 2019.

[154] C. Suellen, R. G. Freitas, P.-F. Loos, and D. Jacquemin,
Cross-comparisons between experiment, TD-DFT, CC, and ADC for transition energies,
J. Chem. Theory Comput. **15** (2019) 4581.

[155] L. Goerigk and S. Grimme, *Assessment of TD-DFT methods and of various spin scaled CIS (D) and CC2 versions for the treatment of low-lying valence excitations of large organic dyes*, J. Chem. Phys. **132** (2010).

[156] C. Brückner and B. Engels, *Benchmarking ground-state geometries and vertical excitation energies of a selection of P-type semiconducting molecules with different polarity*, J. Chem. Phys. A **119** (2015) 12876.

[157] D. Jacquemin, I. Duchemin, and X. Blase, *0–0 energies using hybrid schemes: Benchmarks of TD-DFT, CIS(D), ADC(2), CC2, and BSE/GW formalisms for 80 real-life compounds*, J. Chem. Theory Comput. **11** (2015) 5340.

[158] A. Dreuw and M. Head-Gordon, *Failure of time-dependent density functional theory for long-range charge-transfer excited states: The zincbacteriochlorin-bacteriochlorin and bacteriochlorophyll-spheroidene complexes*, J. Am. Chem. Soc. **126** (2004) 4007.

[159] D. Jacquemin, B. I. Moore, A. Planchat, C. Adamo, and J. Autschbach, *Performance of an optimally tuned range-separated hybrid functional for 0–0 electronic excitation energies*, J. Chem. Theory Comput. **10** (2014) 1677.

[160] M. J. Peach, P. Benfield, T. Helgaker, and D. J. Tozer, *Excitation energies in density functional theory: An evaluation and a diagnostic test*, J. Chem. Phys. **128** (2008).

[161] D. J. Tozer and N. C. Handy, *On the determination of excitation energies using density functional theory*, Phys. Chem. Chem. Phys. **2** (2000) 2117.

[162] F. Weigend and R. Ahlrichs, *Balanced basis sets of split valence, triple zeta valence and quadruple zeta valence quality for H to Rn: Design and assessment of accuracy*, Phys. Chem. Chem. Phys. **7** (2005) 3297.

[163] D. Rappoport and F. Furche, *Property-optimized Gaussian basis sets for molecular response calculations*, J. Chem. Phys. **133** (2010).

[164] S. Miertuš, E. Scrocco, and J. Tomasi, *Electrostatic interaction of a solute with a continuum. A direct utilizaion of AB initio molecular potentials for the prevision of solvent effects*, Chem. Phys. **55** (1981) 117.

[165] S. Miertus and J. Tomasi, *Approximate evaluations of the electrostatic free energy and internal energy changes in solution processes*, Chem. Phys. **65** (1982) 239.

[166] J. Tomasi and M. Persico, *Molecular interactions in solution: An overview of methods based on continuous distributions of the solvent*, Chem. Rev. **94** (1994) 2027.

[167] H. Sun, C. Zhong, and J. L. Brédas, *Reliable prediction with tuned range-separated functionals of the singlet-triplet gap in organic emitters for thermally activated delayed fluorescence*, J. Chem. Theory Comput. **11** (2015) 3851.

[168] H. Sun, Z. Hu, C. Zhong, X. Chen, Z. Sun, and J.-L. Brédas, *Impact of dielectric constant on the singlet-triplet gap in thermally activated delayed fluorescence materials*, J. Phys. Chem Lett. **8** (2017) 2393.

[169] J. M. Mewes, *Modeling TADF in organic emitters requires a careful consideration of the environment and going beyond the Franck-Condon approximation*, Phys. Chem. Chem. Phys. **20** (2018) 12454.

[170] R. Cammi and B. Mennucci, *Linear response theory for the polarizable continuum model*, J. Chem. Phys. **110** (1999) 9877.

[171] S. Corni, R. Cammi, B. Mennucci, and J. Tomasi, *Electronic excitation energies of molecules in solution within continuum solvation models: Investigating the discrepancy between state-specific and linear-response methods*, J. Chem. Phys. **123** (2005) 134512.

[172] D. Hait, T. Zhu, D. P. McMahon, and T. Van Voorhis, *Prediction of excited-state energies and singlet-triplet gaps of charge-transfer states using a restricted open-shell Kohn-Sham approach*, J. Chem. Theory Comput. **12** (2016) 3353.

[173] D. Hait and M. Head-Gordon, *Orbital optimized density functional theory for electronic excited states*, J. Phys. Chem. Lett. **12** (2021) 4517.

[174] E. Cances, B. Mennucci, and J. Tomasi, *A new integral equation formalism for the polarizable continuum model: Theoretical background and applications to isotropic and anisotropic dielectrics*, J. Chem. Phys. **107** (1997) 3032.

[175] B. Mennucci, *Polarizable continuum model*, Wiley Interdiscip. Rev. Comput. Mol. Sci. **2** (2012) 386.

[176] M. N. Berberan-Santos and J. M. Garcia, *Advances in molecular quantum chemistry contained in the Q-Chem 4 program package*, Mol. Phys. **113** (2015) 184.

[177] E. Weintraub, T. M. Henderson, and G. E. Scuseria, *Long-range-corrected hybrids based on a new model exchange hole*, J. Chem. Theory Comput. **5** (2009) 754.

[178] Y. Jin and R. J. Bartlett, *The QTP family of consistent functionals and potentials in Kohn-Sham density functional theory*, J. Chem. Phys. (2016) 034107.

[179] N. Mardirossian and M. Head-Gordon, *Mapping the genome of meta-generalized gradient approximation density functionals: The search for B97M-V*, J. Chem. Phys. **142** (2015) 074111.

[180] S. Hirata and M. Head-Gordon, *Time-dependent density functional theory within the Tamm–Dancoff approximation*, Chem. Phys. Lett. **314** (1999) 291.

[181] A. L. Fetter and J. D. Walecka, *Quantum theory of many-particle systems*, Courier Corporation, 2012.

[182] R. Improta, V. Barone, G. Scalmani, and M. J. Frisch, *A state-specific polarizable continuum model time dependent density functional theory method for excited state calculations in solution*, J. Chem. Phys. **125** (2006) 054103.

[183] J.-M. Mewes, J. M. Herbert, and A. Dreuw,
On the accuracy of the general, state-specific polarizable-continuum model for the description of correlated ground- and excited states in solution,
Phys. Chem. Chem. Phys. **19** (2017) 1644.

[184] E. Epifanovsky, A. T. Gilbert, X. Feng, J. Lee, Y. Mao, N. Mardirossian, P. Pokhilko, A. F. White, M. P. Coons, A. L. Dempwolff, et al., *Software for the frontiers of quantum chemistry: An overview of developments in the Q-Chem 5 package*,
J. Chem. Phys. **155** (2021) 084801.

[185] L. Goerigk and S. Grimme, *A thorough benchmark of density functional methods for general main group thermochemistry, kinetics, and noncovalent interactions*,
Phys. Chem. Chem. Phys. **13** (2011) 6670.

[186] M. A. Rohrdanz, K. M. Martins, and J. M. Herbert, *A long-range-corrected density functional that performs well for both ground-state properties and time-dependent density functional theory excitation energies, including charge-transfer excited states*,
J. Chem. Phys. **130** (2009) 054112.

[187] N. Aizawa, Y.-J. Pu, Y. Harabuchi, A. Nihonyanagi, R. Ibuka, H. Inuzuka, B. Dhara, Y. Koyama, K.-i. Nakayama, S. Maeda, et al.,
Delayed fluorescence from inverted singlet and triplet excited states, Nature **609** (2022) 502.

[188] G. Ricci, J.-C. Sancho-García, and Y. Olivier, *Establishing design strategies for emissive materials with an inverted singlet-triplet energy gap (INVEST): A computational perspective on how symmetry rules the interplay between triplet harvesting and light emission*,
J. Mater. Chem. C **10** (2022) 12680.

[189] P. de Silva,
Inverted singlet-triplet gaps and their relevance to thermally activated delayed fluorescence,
J. Phys. Chem. Lett. **10** (2019) 5674.

[190] P.-F. Loos, F. Lipparini, and D. Jacquemin, *Heptazine, cyclazine, and related compounds: Chemically-accurate estimates of the inverted singlet-triplet gap*,
J. Phys. Chem. Lett. **14** (2023) 11069.

[191] M. H. Garner, J. T. Blaskovits, and C. Corminboeuf,
Enhanced inverted singlet-triplet gaps in azaphenalenes and non-alternant hydrocarbons,
Chem. Commun. **60** (2024) 2070.

[192] A. Balková and R. J. Bartlett, *Coupled-cluster method for open-shell singlet states*,
Chem. Phys. Lett. **193** (1992) 364.

[193] U. S. Mahapatra, B. Datta, and D. Mukherjee, *Development of a size-consistent state-specific multireference perturbation theory with relaxed model-space coefficients*,
Chem. Phys. Lett. **299** (1999) 42.

[194] U. S. Mahapatra, B. Datta, and D. Mukherjee, *A size-consistent state-specific multireference coupled cluster theory: Formal developments and molecular applications*,
J. Chem. Phys. **110** (1999) 6171.

[195] K. Bhaskaran-Nair, J. Brabec, E. Aprà, H. J. van Dam, J. Pittner, and K. Kowalski, *Implementation of the multireference Brillouin-Wigner and Mukherjee's coupled cluster methods with non-iterative triple excitations utilizing reference-level parallelism*, J. Chem. Phys. **137** (2012).

[196] A. Dreuw and M. Hoffmann, *The inverted singlet-triplet gap: A vanishing myth?* Front. Chem. **11** (2023) 1239604.

[197] Y. Damour, A. Scemama, D. Jacquemin, F. Kossoski, and P.-F. Loos, *State-specific coupled-cluster methods for excited states*, J. Chem. Theory Comput. **20** (2024) 4129.

[198] T. H. Dunning Jr, *Gaussian basis sets for use in correlated molecular calculations. I. The atoms boron through neon and hydrogen*, J. Chem. Phys. **90** (1989) 1007.

[199] D. E. Woon and T. H. Dunning Jr, *Gaussian basis sets for use in correlated molecular calculations. III. The atoms aluminum through argon*, J. Chem. Phys. **98** (1993) 1358.

[200] Y. A. Bernard, Y. Shao, and A. I. Krylov, *General formulation of spin-flip time-dependent density functional theory using non-collinear kernels: Theory, implementation, and benchmarks*, J. Chem. Phys. **136** (2012) 204103.

[201] D. Drwal, M. Matousek, P. Golub, A. Tucholska, M. Hapka, J. Brabec, L. Veis, and K. Pernal, *Role of spin polarization and dynamic correlation in singlet-triplet gap inversion of heptazine derivatives*, J. Chem. Theory Comput. **19** (2023) 7606.

[202] M. Kondo, *Singlet-triplet energy gap of multiresonant molecular systems: A double hybrid time-dependent density functional theory study*, Chem. Phys. Lett. **804** (2022) 139895.

[203] A. Derradji, D. Valverde, É. Brémond, Á. J. Pérez-Jiménez, Y. Olivier, and J. C. Sancho-García, *Searching the best double-hybrid density functional to correctly predict the singlet–triplet excited-state inversion in organic systems*, J. Phys. Chem. C **128** (2024) 18313.

[204] S. Madayanad Suresh, D. Hall, D. Beljonne, Y. Olivier, and E. Zysman-Colman, *Multiresonant thermally activated delayed fluorescence emitters based on heteroatom-doped nanographenes: Recent advances and prospects for organic light-emitting diodes*, Adv. Funct. Mater. **30** (2020) 1908677.

[205] D. Hall, J. C. Sancho-García, A. Pershin, G. Ricci, D. Beljonne, E. Zysman-Colman, and Y. Olivier, *Modeling of multiresonant thermally activated delayed fluorescence emitters – properly accounting for electron correlation is key!* J. Chem. Theory Comput. **18** (2022) 4903.

[206] A. Hellweg, S. A. Grün, and C. Hättig, *Benchmarking the performance of spin-component scaled CC2 in ground and electronically excited states*, Phys. Chem. Chem. Phys. **10** (2008) 4119.

[207] A. D. Becke, *Density-functional thermochemistry. III. The role of exact exchange*, J. Chem. Phys. **98** (1993) 5648.

[208] T. Froitzheim, S. Grimme, and J.-M. Mewes, *Either accurate singlet–triplet gaps or excited-state structures: Testing and understanding the performance of TD-DFT for TADF emitters*, J. Chem. Theory Comput. **18** (2022) 7702.

[209] R. Khatri and B. D. Dunietz, *Accurate singlet–triplet excited states energy gap can be mastered by time-dependent density functional theory calculations based on a dielectric-screened range-separated hybrid functional*, J. Phys. Chem. C **129** (2024) 436.

[210] J. W. Furness, A. D. Kaplan, J. Ning, J. P. Perdew, and J. Sun, *Accurate and numerically efficient r^2SCAN meta-generalized gradient approximation*, J. Phys. Chem. Lett. **11** (2020) 8208.

[211] J. Pimentel, J. Chagas, M. Pinheiro Jr, A. Aquino, H. Lischka, and F. Machado, *Thermally activated delayed fluorescence in B, N-substituted tetracene derivatives: A theoretical pathway to enhanced OLED materials*, J. Phys. Chem. A (2025).

[212] S. Grimme, C. Bannwarth, and P. Shushkov, *A robust and accurate tight-binding quantum chemical method for structures, vibrational frequencies, and noncovalent interactions of large molecular systems parametrized for all spd-block elements (Z= 1–86)*, J. Chem. Theory Comput. **13** (2017) 1989.

[213] C. Bannwarth, S. Ehlert, and S. Grimme, *GFN2-xTB – An accurate and broadly parametrized self-consistent tight-binding quantum chemical method with multipole electrostatics and density-dependent dispersion contributions*, J. Chem. Theory Comput. **15** (2019) 1652.

[214] T. Froitzheim, M. Müller, A. Hansen, and S. Grimme, *g-xTB: A General-Purpose Extended Tight-Binding Electronic Structure Method For the Elements H to Lr (Z= 1–103)* (2025).

[215] H. Neugebauer, B. Bädorf, S. Ehlert, A. Hansen, and S. Grimme, *High-throughput screening of spin states for transition metal complexes with spin-polarized extended tight-binding methods*, Journal of computational chemistry **44** (2023) 2120.

[216] F. B. Dias, T. J. Penfold, and A. P. Monkman, *Photophysics of thermally activated delayed fluorescence molecules*, Methods Appl. Fluoresc. **5** (2017) 012001.

[217] M. Y. Wong and E. Zysman-Colman, *Purely organic thermally activated delayed fluorescence materials for organic light-emitting diodes*, Adv. Mater. **29** (2017) 1605444.

[218] T. Huang, W. Jiang, and L. Duan, *Recent progress in solution processable TADF materials for organic light-emitting diodes*, J. Mater. Chem. C **6** (2018) 5577.

[219] M. K. Etherington, J. Gibson, H. F. Higginbotham, T. J. Penfold, and A. P. Monkman, *Revealing the spin-vibronic coupling mechanism of thermally activated delayed fluorescence*, Nat. Commun. **7** (2016) 1.

[220] R. S. Nobuyasu, Z. Ren, G. C. Griffiths, A. S. Batsanov, P. Data, S. Yan, A. P. Monkman, M. R. Bryce, and F. B. Dias, *Rational design of TADF polymers using a donor-acceptor monomer with enhanced TADF efficiency induced by the energy alignment of charge transfer and local triplet Excited States*, Adv. Opt. Mater. **4** (2016) 597.

[221] J. Gibson and T. Penfold, *Nonadiabatic coupling reduces the activation energy in thermally activated delayed fluorescence*, Phys. Chem. Chem. Phys. **19** (2017) 8428.

[222] I. Lyskov and C. M. Marian, *Climbing up the ladder: Intermediate triplet states promote the reverse intersystem crossing in the efficient TADF emitter ACRSA*, J. Phys. Chem. C **121** (2017) 21145.

[223] J. Gibson, A. P. Monkman, and T. J. Penfold, *The importance of vibronic coupling for efficient reverse intersystem crossing in thermally activated delayed fluorescence molecules*, ChemPhysChem **17** (2016) 2956.

[224] M. Inoue, T. Serevičius, H. Nakanotani, K. Yoshida, T. Matsushima, S. Juršenas, and C. Adachi, *Effect of reverse intersystem crossing rate to suppress efficiency roll-off in organic light-emitting diodes with thermally activated delayed fluorescence emitters*, Chem. Phys. Lett. **644** (2016) 62.

[225] P. Kimber and F. Plasser, *Toward an understanding of electronic excitation energies beyond the molecular orbital picture*, Phys. Chem. Chem. Phys. **22** (2020) 6058.

[226] Z. Pei, Q. Ou, Y. Mao, J. Yang, A. d. l. Lande, F. Plasser, W. Liang, Z. Shuai, and Y. Shao, *Elucidating the electronic structure of a delayed fluorescence emitter via orbital interactions, excitation energy components, charge-transfer numbers, and vibrational reorganization energies*, J. Phys. Chem. Lett. **12** (2021) 2712.

[227] R. Al-Saadon, C. Sutton, and W. Yang, *Accurate treatment of charge-transfer excitations and thermally activated delayed fluorescence using the particle-particle random phase approximation*, J. Chem. Theory Comput. **14** (2018) 3196.

[228] S. A. Servan, A. Ünal, B. Hamarat, and U. Bozkaya, *Assessment of the density-fitted second-order quasidegenerate perturbation theory for transition energies: Accurate computations of singlet-triplet gaps for charge-transfer compounds*, J. Phys. Chem. A **124** (2020) 6889.

[229] J.-M. Mewes, Z.-Q. You, M. Wormit, T. Kriesche, J. M. Herbert, and A. Dreuw, *Experimental benchmark data and systematic evaluation of two a posteriori, polarizable-continuum corrections for vertical excitation energies in solution*, J. Phys. Chem. A **119** (2015) 5446.

[230] Š. Budzák, P. Mach, et al., *Critical analysis of spectral solvent shifts calculated by the contemporary PCM approaches of a representative series of charge-transfer complexes between tetracyanoethylene and methylated benzenes*, Phys. Chem. Chem. Phys. **17** (2015) 17618.

[231] M. Caricato, B. Mennucci, J. Tomasi, F. Ingrosso, R. Cammi, S. Corni, and G. Scalmani, *Formation and relaxation of excited states in solution: A new time dependent polarizable continuum model based on time dependent density functional theory*, J. Chem. Phys. **124** (2006) 1.

[232] T. B. de Queiroz and S. Kümmel, *Charge-transfer excitations in low-gap systems under the influence of solvation and conformational disorder: Exploring range-separation tuning*, J. Chem. Phys. **141** (2014) 084303.

[233] W. Humphrey, A. Dalke, and K. Schulten, *VMD: Visual molecular dynamics*, J. Mol. Graphics **14** (1996) 33.

[234] T. Lu and F. Chen, *Multiwfn: A multifunctional wavefunction analyzer*, J. Comput. Chem. **33** (2012) 580.

[235] R. Baer, E. Livshits, and U. Salzner, *Tuned range-separated hybrids in density functional theory*, Annu. Rev. Phys. Chem. **61** (2010) 85.

[236] I. Frank, J. Hutter, D. Marx, and M. Parrinello, *Molecular dynamics in low-spin excited states*, J. Chem. Phys. **108** (1998) 4060.

[237] A. W. Lange and J. M. Herbert, *A smooth, nonsingular, and faithful discretization scheme for polarizable continuum models: The switching/Gaussian approach*, J. Chem. Phys. **133** (2010) 244111.

[238] A. W. Lange and J. M. Herbert, *Polarizable continuum reaction-field solvation models affording smooth potential energy surfaces*, J. Phys. Chem. Lett. **1** (2010) 556.

[239] Y. Shao, Z. Gan, E. Epifanovsky, A. T. Gilbert, M. Wormit, J. Kussmann, A. W. Lange, A. Behn, J. Deng, X. Feng, et al., *Advances in molecular quantum chemistry contained in the Q-Chem 4 program package*, Mol. Phys. **113** (2015) 184.

[240] E. Epifanovsky, A. T. B. Gilbert, X. Feng, J. Lee, Y. Mao, N. Mardirossian, P. Pokhilko, A. F. White, M. P. Coons, A. L. Dempwolff, et al., *Software for the frontiers of quantum chemistry: An overview of developments in the Q-Chem 5 package*, J. Chem. Phys. **155** (2021) 084801.

[241] J. Lee, N. Aizawa, M. Numata, C. Adachi, and T. Yasuda, *Versatile molecular functionalization for inhibiting concentration quenching of thermally activated delayed fluorescence*, Adv. Mater. **29** (2017) 1.

[242] J. U. Kim, I. S. Park, C. Y. Chan, M. Tanaka, Y. Tsuchiya, H. Nakanotani, and C. Adachi, *Nanosecond-time-scale delayed fluorescence molecule for deep-blue OLEDs with small efficiency rolloff*, Nat. Commun. **11** (2020) 1765.

[243] A. K. Narsaria et al., *Computationally guided molecular design to minimize the LE/CT gap in D-π-A fluorinated triarylboranes for efficient TADF via D and π-bridge tuning*, Adv. Funct. Mater. **30** (2020) 2002064.

[244] K. Suzuki, S. Kubo, K. Shizu, T. Fukushima, A. Wakamiya, Y. Murata, C. Adachi, and H. Kaji, *Triarylboron-based fluorescent organic light-emitting diodes with external quantum efficiencies exceeding 20 %*, Angew. Chem. Int. Ed. **54** (2015) 15231.

[245] G. A. Sommer, L. N. Mataranga-Popa, R. Czerwieniec, T. Hofbeck, H. H. Homeier, T. J. Müller, and H. Yersin, *Design of conformationally distorted donor-acceptor dyads showing efficient thermally activated delayed fluorescence*, J. Phys. Chem. Lett. **9** (2018) 3692.

[246] X. Cai, Z. Qiao, M. Li, X. Wu, Y. He, X. Jiang, Y. Cao, and S.-J. Su, *Purely organic crystals exhibit bright thermally activated delayed fluorescence*, Angew. Chem. **131** (2019) 13656.

[247] H. Kaji et al., *Purely organic electroluminescent material realizing 100% conversion from electricity to light*, Nat. Commun. **6** (2015) 1.

[248] L. S. Cui et al., *Fast spin-flip enables efficient and stable organic electroluminescence from charge-transfer states*, Nat. Photonics **14** (2020) 636.

[249] J. Lee, N. Aizawa, and T. Yasuda, *Molecular engineering of phosphacycle-based thermally activated delayed fluorescence materials for deep-blue OLEDs*, J. Mater. Chem. C **6** (2018) 3578.

[250] G. Meng, X. Chen, X. Wang, N. Wang, T. Peng, and S. Wang, *Isomeric bright sky-blue TADF emitters based on bisacridine decorated DBNA: Impact of donor locations on luminescent and electroluminescent properties*, Adv. Opt. Mater. **7** (2019) 1.

[251] Y. Wada, K. Shizu, S. Kubo, K. Suzuki, H. Tanaka, C. Adachi, and H. Kaji, *Highly efficient electroluminescence from a solution-processable thermally activated delayed fluorescence emitter*, Appl. Phys. Lett. **107** (2015) 183303.

[252] H. F. Higginbotham, P. Pander, R. Rybakiewicz, M. K. Etherington, S. Maniam, M. Zagorska, A. Pron, A. P. Monkman, and P. Data, *Triphenylamine disubstituted naphthalene diimide: Elucidation of excited states involved in TADF and application in near-infrared organic light emitting diodes*, J. Mater. Chem. C **6** (2018) 8219.

[253] H. Noda, X.-K. Chen, H. Nakanotani, T. Hosokai, M. Miyajima, N. Notsuka, Y. Kashima, J.-L. Brédas, and C. Adachi, *Critical role of intermediate electronic states for spin-flip processes in charge-transfer-type organic molecules with multiple donors and acceptors*, Nat. Mater. **18** (2019) 1084.

[254] M. Taneda, K. Shizu, H. Tanaka, and C. Adachi, *High efficiency thermally activated delayed fluorescence based on 1,3,5-tris(4-(diphenylamino)phenyl)-2,4,6-tricyanobenzene*, Chem. Commun. **51** (2015) 5028.

[255] H. Noda, H. Nakanotani, and C. Adachi, *Highly efficient thermally activated delayed fluorescence with slow reverse intersystem crossing*, Chem. Lett. **48** (2019) 126.

[256] G. Méhes, H. Nomura, Q. Zhang, T. Nakagawa, and C. Adachi, *Enhanced electroluminescence efficiency in a spiro-acridine derivative through thermally activated delayed fluorescence*, Angew. Chem. Int. Ed. **51** (2012) 11311.

[257] T. Nakagawa, S. Y. Ku, K. T. Wong, and C. Adachi, *Electroluminescence based on thermally activated delayed fluorescence generated by a spirobifluorene donor–acceptor structure*, Chem. Commun. **48** (2012) 9580.

[258] H. Nakanotani, T. Furukawa, T. Hosokai, T. Hatakeyama, and C. Adachi, *Light amplification in molecules exhibiting thermally activated delayed fluorescence*, Adv. Opt. Mater. **5** (2017) 1.

[259] Q. Zhang, H. Kuwabara, W. J. Potscavage Jr, S. Huang, Y. Hatae, T. Shibata, and C. Adachi, *Anthraquinone-based intramolecular charge-transfer compounds: Computational molecular design, thermally activated delayed fluorescence, and highly efficient red electroluminescence*, J. Am. Chem. Soc. **136** (2014) 18070.

[260] J. Sanz-Rodrigo, Y. Olivier, and J.-C. Sancho-García,
Computational studies of molecular materials for unconventional energy conversion: The challenge of light emission by thermally activated delayed fluorescence, Molecules **25** (2020).

[261] D. Hait and M. Head-Gordon,
Excited state orbital optimization via minimizing the square of the gradient: General approach and application to singly and doubly excited states via density functional theory,
J. Chem. Theory Comput. **16** (2020) 1699.

[262] K. Yamaguchi, F. Jensen, A. Dorigo, and K. Houk,
A spin correction procedure for unrestricted Hartree-Fock and Møller-Plesset wavefunctions for singlet diradicals and polyradicals, Chem. Phys. Lett. **149** (1988) 537.

[263] E. Caldeweyher, J.-M. Mewes, S. Ehlert, and S. Grimme,
Extension and evaluation of the D4 London-dispersion model for periodic systems,
Phys. Chem. Chem. Phys. **22** (2020) 8499.

[264] Q. Zhang, B. Li, S. Huang, H. Nomura, H. Tanaka, and C. Adachi, *Efficient blue organic light-emitting diodes employing thermally activated delayed fluorescence*, en,
Nat. Photonics **8** (2014) 326.

[265] P. K. Samanta, D. Kim, V. Coropceanu, and J.-L. Brédas,
Up-conversion intersystem crossing rates in organic emitters for thermally activated delayed fluorescence: Impact of the nature of singlet vs triplet excited states,
J. Am. Chem. Soc. **139** (2017) 4042.

[266] M. Petersilka, U. J. Gossmann, and E. K. U. Gross,
Excitation energies from time-dependent density-functional theory,
Phys. Rev. Lett. **76** (1996) 1212.

[267] T. Jaunet-Lahary, A. D. Laurent, C. Laurence, M. Medved', and D. Jacquemin,
Exploring the solvatochromism of betaine 30 with ab initio tools: From accurate gas-phase calculations to implicit and explicit solvation models, Chem. Eur. J. **23** (2017) 4108.

[268] P.-F. Loos, M. Comin, X. Blase, and D. Jacquemin,
Reference energies for intramolecular charge-transfer excitations,
J. Chem. Theory Comput. **17** (2021) 3666.

[269] J.-D. Chai and M. Head-Gordon, *Long-range corrected hybrid density functionals with damped atom–atom dispersion corrections*, en, Phys. Chem. Chem. Phys. **10** (2008) 6615.

[270] J. Schirmer, *Beyond the random-phase approximation: A new approximation scheme for the polarization propagator*, Phys. Rev. A **26** (1982) 2395.

[271] A. B. Trofimov and J. Schirmer,
An efficient polarization propagator approach to valence electron excitation spectra, en,
J. Phys. B: At. Mol. Opt. Phys. **28** (1995) 2299.

[272] D. Mester and M. Kállay, *Charge-transfer excitations within density functional theory: How accurate are the most recommended approaches?* J. Chem. Theory Comput. **18** (2022) 1646.

[273] P. Winget, D. Dolney, D. Giesen, C. Cramer, and D. Truhlar,
Minnesota solvent descriptor database, 1999.

[274] P. A. Vecchi, A. B. Padmaperuma, H. Qiao, L. S. Sapochak, and P. E. Burrows, *A dibenzofuran-based host material for blue electrophosphorescence*, Org. Lett. **8** (2006) 4211.

[275] E. Skuodis, O. Bezvikonnyi, A. Tomkeviciene, D. Volyniuk, V. Mimaite, A. Lazauskas, A. Bucinskas, R. Keruckiene, G. Sini, and J. V. Grazulevicius, *Aggregation, thermal annealing, and hosting effects on performances of an acridan-based TADF emitter*, en, Org. Electron. **63** (2018) 29.

[276] P.-I. Shih, C.-H. Chien, C.-Y. Chuang, C.-F. Shu, C.-H. Yang, J.-H. Chen, and Y. Chi, *Novel host material for highly efficient blue phosphorescent OLEDs*, en, J. Mater. Chem. **17** (2007) 1692.

[277] B. Lasorne, J. Jornet-Somoza, H.-D. Meyer, D. Lauvergnat, M. A. Robb, and F. Gatti, *Vertical transition energies vs. absorption maxima: Illustration with the UV absorption spectrum of ethylene*, Spectrochim. Acta A, Frontiers in molecular vibrational calculations and computational spectroscopy **119** (2014) 52.

[278] X. Tian, H. Sun, Q. Zhang, and C. Adachi, *Theoretical predication for transition energies of thermally activated delayed fluorescence molecules*, en, Chin. Chem. Lett. **27** (2016) 1445.

[279] C. Adamo and D. Jacquemin, *The calculations of excited-state properties with time-dependent density functional theory*, en, Chem. Soc. Rev. **42** (2013) 845.

[280] J. Tomasi, B. Mennucci, and E. Cancès, *The IEF version of the PCM solvation method: An overview of a new method addressed to study molecular solutes at the QM ab initio level*, J. Mol. Struct. THEOCHEM **464** (1999) 211.

[281] R. Improta, G. Scalmani, M. J. Frisch, and V. Barone, *Toward effective and reliable fluorescence energies in solution by a new state specific polarizable continuum model time dependent density functional theory approach*, J. Chem. Phys. **127** (2007) 074504.

[282] C. J. Cramer, D. G. Truhlar, C. A. Guido, B. Mennucci, G. Scalmani, and M. J. Frisch, *Practical computation of electronic excitation in solution: Vertical excitation model*, Chem. Sci. **2** (2011) 2143.

[283] C. A. Guido and S. Caprasecca, *On the description of the environment polarization response to electronic transitions*, en, Int. J. Quantum Chem. **119** (2019) e25711.

[284] E. G. McRae, *Theory of solvent effects on molecular electronic spectra. Frequency shifts*, J. Phys. Chem. **61** (1957) 562.

[285] E. Lippert, *Spektroskopische Bestimmung des Dipolmomentes aromatischer Verbindungen im ersten angeregten Singulettzustand*, Ber. Bunsenges. Phys. Chem. **61** (1957) 962.

[286] J. E. Brady and P. W. Carr, *An analysis of dielectric models of solvatochromism*, J. Phys. Chem. **89** (1985) 5759.

[287] A. Klamt, *Calculation of UV/Vis spectra in solution*, J. Phys. Chem. **100** (1996) 3349.

[288] Z. Q. You, J. M. Mewes, A. Dreuw, and J. M. Herbert, *Comparison of the Marcus and Pekar partitions in the context of non-equilibrium, polarizable-continuum solvation models*, J. Chem. Phys. **143** (2015) 204104.

[289] S. Yomosa, *Theory of the excited state of molecular complex in solution*, J. Phys. Soc. Jpn. **36** (1974) 1655.

[290] R. Bonaccorsi, R. Cimiraglia, and J. Tomasi, *Ab initio evaluation of absorption and emission transitions for molecular solutes, including separate consideration of orientational and inductive solvent effects*, de, J. Comput. Chem. **4** (1983) 567.

[291] R. Cammi, S. Corni, B. Mennucci, and J. Tomasi, *Electronic excitation energies of molecules in solution: State specific and linear response methods for nonequilibrium continuum solvation models*, J. Chem. Phys. **122** (2005) 104513.

[292] R. Fukuda, M. Ehara, H. Nakatsuji, and R. Cammi, *Nonequilibrium solvation for vertical photoemission and photoabsorption processes using the symmetry-adapted cluster–configuration interaction method in the polarizable continuum model*, J. Chem. Phys. **134** (2011) 104109.

[293] B. Lunkenheimer and A. Köhn, *Solvent effects on electronically excited states using the conductor-like screening model and the second-order correlated method ADC(2)*, J. Chem. Theory Comput. **9** (2013) 977.

[294] C. A. Guido, D. Jacquemin, C. Adamo, and B. Mennucci, *Electronic excitations in solution: The interplay between state specific approaches and a time-dependent density functional theory description*, J. Chem. Theory Comput. **11** (2015) 5782.

[295] B. Alam, H. Jiang, P. M. Zimmerman, and J. M. Herbert, *State-specific solvation for restricted active space spin–flip (RAS-SF) wave functions based on the polarizable continuum formalism*, J. Chem. Phys. **156** (2022) 194110.

[296] K. Emrich, *An extension of the coupled cluster formalism to excited states (I)*, Nucl. Phys. A **351** (1981) 379.

[297] H. Sekino and R. J. Bartlett, *A linear response, coupled-cluster theory for excitation energy*, en, Int. J. Quantum Chem. **26** (1984) 255.

[298] C. A. Guido, B. Mennucci, G. Scalmani, and D. Jacquemin, *Excited state dipole moments in solution: Comparison between state-specific and linear-response TD-DFT values*, J. Chem. Theory Comput. **14** (2018) 1544.

[299] S. Budzák, G. Scalmani, and D. Jacquemin, *Accurate excited-state geometries: A CASPT2 and coupled-cluster reference database for small molecules*, J. Chem. Theory Comput. **13** (2017) 6237.

[300] R. A. Marcus, *Electrostatic free energy and other properties of states having nonequilibrium polarization. I*, J. Chem. Phys. **24** (1956) 979.

[301] R. A. Marcus, *On the theory of oxidation-reduction reactions involving electron transfer. I*, J. Chem. Phys. **24** (1956) 966.

[302] B. Joo, H. Han, and E.-G. Kim, *Solvation-mediated tuning of the range-separated hybrid functional: Self-sufficiency through screened exchange*, J. Chem. Theory Comput. **14** (2018) 2823.

[303] M. Friede, S. Ehlert, S. Grimme, and J.-M. Mewes, *Do optimally tuned range-separated hybrid functionals require a reparametrization of the dispersion correction? It depends*, J. Chem. Theory Comput. **19** (2023) 8097.

[304] F. Weigend, *Accurate Coulomb-fitting basis sets for H to Rn*, Phys. Chem. Chem. Phys. **8** (2006) 1057.

[305] K. Jorner, R. Pollice, C. Lavigne, and A. Aspuru-Guzik, *Ultrafast computational screening of molecules with inverted singlet–triplet energy gaps using the Pariser–Parr–Pople semiempirical quantum chemistry method*, J. Phys. Chem. A **128** (2024) 2445.

[306] G. Ricci, E. San-Fabián, Y. Olivier, and J. C. Sancho-García, *Singlet-triplet excited-state inversion in heptazine and related molecules: Assessment of TD-DFT and ab initio methods*, en, ChemPhysChem **22** (2021) 553.

[307] A. D. Becke, *Singlet-triplet splittings from the virial theorem and single-particle excitation energies*, J. Chem. Phys. **148** (2018) 044112.

[308] P. Kimber and F. Plasser, *Energy component analysis for electronically excited states of molecules: Why the lowest excited state is not always the HOMO/LUMO transition*, J. Chem. Theory Comput. (2023).

[309] J. Ehrmaier, E. J. Rabe, S. R. Pristash, K. L. Corp, C. W. Schlenker, A. L. Sobolewski, and W. Domcke, *Singlet-triplet inversion in heptazine and in polymeric carbon nitrides*, J. Phys. Chem. A **123** (2019) 8099.

[310] F. Dinkelbach, M. Bracker, M. Kleinschmidt, and C. M. Marian, *Large inverted singlet-triplet energy gaps are not always favorable for triplet harvesting: Vibronic coupling drives the (reverse) intersystem crossing in heptazine derivatives*, J. Phys. Chem. A **125** (2021) 10044.

[311] R. Pollice, P. Friederich, C. Lavigne, G. dos Passos Gomes, and A. Aspuru-Guzik, *Organic molecules with inverted gaps between first excited singlet and triplet states and appreciable fluorescence rates*, Matter **4** (2021) 1654.

[312] A. L. Sobolewski and W. Domcke, *Are heptazine-based organic light-emitting diode chromophores thermally activated delayed fluorescence or inverted singlet-triplet systems?* J. Phys. Chem. Lett. **12** (2021) 6852.

[313] J. Sanz-Rodrigo, G. Ricci, Y. Olivier, and J.-C. Sancho-Garcia, *Negative singlet-triplet excitation energy gap in triangle-shaped molecular emitters for efficient triplet harvesting*, J. Phys. Chem. A **125** (2021) 513.

[314] L. Tučková, M. Straka, R. R. Valiev, and D. Sundholm,
On the origin of the inverted singlet-triplet gap of the 5th generation light-emitting molecules,
Phys. Chem. Chem. Phys. **24** (2022) 18713.

[315] S. Ghosh and K. Bhattacharyya,
Origin of the failure of density functional theories in predicting inverted singlet-triplet gaps,
J. Phys. Chem. A **126** (2022) 1378.

[316] J. Li, Z. Li, H. Liu, H. Gong, J. Zhang, Y. Yao, and Q. Guo,
Organic molecules with inverted singlet-triplet gaps, Front. Chem. **10** (2022) 999856.

[317] J. Terence Blaskovits, M. H. Garner, and C. Corminboeuf,
Symmetry-induced singlet-triplet inversions in non-alternant hydrocarbons,
Angew. Chem. Int. Ed. **62** (2023) e202218156.

[318] U. Mitschke and P. Bäuerle, *The electroluminescence of organic materials*,
J. Mater. Chem. **10** (2000) 1471.

[319] Q. Zhang, J. Li, K. Shizu, S. Huang, S. Hirata, H. Miyazaki, and C. Adachi,
Design of efficient thermally activated delayed fluorescence materials for pure blue organic light emitting diodes, J. Am. Chem. Soc. **134** (2012) 14706.

[320] Y. Tao, K. Yuan, T. Chen, P. Xu, H. Li, R. Chen, C. Zheng, L. Zhang, and W. Huang,
Thermally activated delayed fluorescence materials towards the breakthrough of organoelectronics, Adv. Mater. **26** (2014) 7931.

[321] S. Hirata, Y. Sakai, K. Masui, H. Tanaka, S. Y. Lee, H. Nomura, N. Nakamura, M. Yasumatsu, H. Nakanotani, Q. Zhang, et al.,
Highly efficient blue electroluminescence based on thermally activated delayed fluorescence,
Nat. Mater. **14** (2015) 330.

[322] J.-M. Teng, Y.-F. Wang, and C.-F. Chen,
Recent progress of narrowband TADF emitters and their applications in OLEDs,
J. Mater. Chem. C **8** (2020) 11340.

[323] K. R. Naveen, P. Palanisamy, M. Y. Chae, and J. H. Kwon, *Multiresonant TADF materials: Triggering the reverse intersystem crossing to alleviate the efficiency roll-off in OLEDs*,
Chem. Commun. **59** (2023) 3685.

[324] A. Actis, M. Melchionna, G. Filippini, P. Fornasiero, M. Prato, M. Chiesa, and E. Salvadori,
Singlet-triplet energy inversion in carbon nitride photocatalysts,
Angew. Chem. Int. Ed. **62** (2023) e202313540.

[325] Y. Kusakabe, K. Shizu, H. Tanaka, K. Tanaka, and H. Kaji,
An inverted singlet-triplet excited state in a pentaazaphenalene derivative (5AP-N(C12)$_2$),
Appl. Phys. Express **17** (2024) 061001.

[326] H. Kollmar and V. Staemmler, *Violation of Hund's rule by spin polarization in molecules*,
Theor. Chim. Acta **48** (1978) 223.

[327] T. Won, K.-i. Nakayama, and N. Aizawa,
Inverted singlet-triplet emitters for organic light-emitting diodes,
Chem. Phys. Rev. **4** (2023) 021310.

[328] B. O. Roos, P. R. Taylor, and P. E. Sigbahn, *A complete active space SCF method (CASSCF) using a density matrix formulated super-CI approach*, Chem. Phys. **48** (1980) 157.

[329] C. Angeli, R. Cimiraglia, S. Evangelisti, T. Leininger, and J.-P. Malrieu, *Introduction of n-electron valence states for multireference perturbation theory*, J. Chem. Phys. **114** (2001) 10252.

[330] K. Andersson, P. A. Malmqvist, B. O. Roos, A. J. Sadlej, and K. Wolinski, *Second-order perturbation theory with a CASSCF reference function*, J. Phys. Chem. **94** (1990) 5483.

[331] K. Andersson, P.-Å. Malmqvist, and B. O. Roos, *Second-order perturbation theory with a complete active space self-consistent field reference function*, J. Chem. Phys. **96** (1992) 1218.

[332] K. Raghavachari, G. W. Trucks, J. A. Pople, and M. Head-Gordon, *A fifth-order perturbation comparison of electron correlation theories*, Chem. Phys. Lett. **157** (1989) 479.

[333] H. Koch, O. Christiansen, A. M. Sanchez de Merás, T. Helgaker, et al., *The CC3 model: an iterative coupled cluster approach including connected triples*, J. Chem. Phys. **106** (1997) 1808.

[334] S. A. Kucharski, M. Włoch, M. Musiał, and R. J. Bartlett, *Coupled-cluster theory for excited electronic states: The full equation-of-motion coupled-cluster single, double, and triple excitation method*, J. Chem. Phys. **115** (2001) 8263.

[335] J. J. Lutz, M. Nooijen, A. Perera, and R. J. Bartlett, *Reference dependence of the two-determinant coupled-cluster method for triplet and open-shell singlet states of biradical molecules*, J. Chem. Phys. **148** (2018) 164102.

[336] F. Neese, F. Wennmohs, U. Becker, and C. Riplinger, *The ORCA quantum chemistry program package*, J. Chem. Phys. **152** (2020) 224108.

[337] M. Kállay, P. R. Nagy, D. Mester, Z. Rolik, G. Samu, J. Csontos, J. Csóka, P. B. Szabó, L. Gyevi-Nagy, B. Hégely, et al., *The MRCC program system: Accurate quantum chemistry from water to proteins*, J. Chem. Phys. **152** (2020) 074107.

[338] E. Apra, E. J. Bylaska, W. A. De Jong, N. Govind, K. Kowalski, T. P. Straatsma, M. Valiev, H. J. van Dam, Y. Alexeev, J. Anchell, et al., *NWChem: Past, present, and future*, J. Chem. Phys. **152** (2020) 184102.

[339] D. Mejia-Rodriguez, E. Aprà, J. Autschbach, N. P. Bauman, E. J. Bylaska, N. Govind, J. R. Hammond, K. Kowalski, A. Kunitsa, A. Panyala, et al., *NWChem: Recent and ongoing developments*, J. Chem. Theory Comput. **19** (2023) 7077.

[340] S. Hirata, *Tensor contraction engine: Abstraction and automated parallel implementation of configuration-interaction, coupled-cluster, and many-body perturbation theories*, J. Phys. Chem. A **107** (2003) 9887.

[341] K. Aidas, C. Angeli, K. L. Bak, V. Bakken, R. Bast, L. Boman, O. Christiansen, R. Cimiraglia, S. Coriani, P. Dahle, et al., *The Dalton quantum chemistry program system*, Wiley Interdiscip. Rev. Comput. Mol. Sci. **4** (2014) 269.

[342] *Dalton, a molecular electronic structure program, release Dalton2020.1 (2022), see http://daltonprogram.org*.

[343] R. A. Kendall, T. H. Dunning Jr, and R. J. Harrison,
Electron affinities of the first-row atoms revisited. Systematic basis sets and wave functions,
J. Chem. Phys. **96** (1992) 6796.

[344] D. Mester, P. R. Nagy, and M. Kállay, *Reduced-cost linear-response CC2 method based on natural orbitals and natural auxiliary functions*, J. Chem. Phys. **146** (2017) 194102.

[345] P. Elliott, S. Goldson, C. Canahui, and N. T. Maitra,
Perspectives on double-excitations in TDDFT, Chem. Phys. **391** (2011) 110.

[346] N. T. Maitra,
Double and charge-transfer excitations in time-dependent density functional theory,
Annu. Rev. Phys. Chem. **73** (2022) 117.

[347] M. T. Do Casal, J. M. Toldo, M. Barbatti, and F. Plasser,
Classification of doubly excited molecular electronic states, Chem. Sci. **14** (2023) 4012.

[348] M. Bursch, J.-M. Mewes, A. Hansen, and S. Grimme,
Best-practice DFT protocols for basic molecular computational chemistry,
Angew. Chem. Int. Ed. **61** (2022) e202205735.

[349] R. F. Spada, M. P. Franco, R. Nieman, A. J. Aquino, R. Shepard, F. Plasser, and H. Lischka,
Spin-density calculation via the graphical unitary group approach,
Mol. Phys. **121** (2023) e2091049.

[350] H. Neugebauer, H. T. Vuong, J. L. Weber, R. A. Friesner, J. Shee, and A. Hansen,
Toward benchmark-quality ab initio predictions for 3d transition metal electrocatalysts: A comparison of CCSD(T) and ph-AFQMC, J. Chem. Theory Comput. **19** (2023) 6208.

[351] H. Tanaka, K. Shizu, H. Miyazaki, and C. Adachi, *Efficient green thermally activated delayed fluorescence (TADF) from a phenoxazine–triphenyltriazine (PXZ–TRZ) derivative*,
Chem. Commun. **48** (2012) 11392.

[352] H. Hirai, K. Nakajima, S. Nakatsuka, K. Shiren, J. Ni, S. Nomura, T. Ikuta, and T. Hatakeyama,
One-step borylation of 1, 3-diaryloxybenzenes towards efficient materials for organic light-emitting diodes, Angew. Chem. **127** (2015) 13785.

[353] J. Neugebauer, O. Gritsenko, and E. J. Baerends, *Assessment of a simple correction for the long-range charge-transfer problem in time-dependent density-functional theory*,
J. Chem. Phys. **124** (2006) 214102.

[354] Sanyam, R. Khatua, and A. Mondal, *Cost-effective approach for modeling of multiresonant thermally activated delayed fluorescence emitters*, J. Chem. Theory Comput. **19** (2023) 9290.

[355] W. Sotoyama,
Simulation of low-lying singlet and triplet excited states of multiple-resonance-type thermally activated delayed fluorescence emitters by delta self-consistent field (ΔSCF) method,
J. Phys. Chem. A **125** (2021) 10373.

[356] S. Grimme, *Exploration of chemical compound, conformer, and reaction space with meta-dynamics simulations based on tight-binding quantum chemical calculations*,
J. Chem. Theory Comput. **15** (2019) 2847.

[357] P. Pracht, F. Bohle, and S. Grimme,
Automated exploration of the low-energy chemical space with fast quantum chemical methods,
Phys. Chem. Chem. Phys. **22** (2020) 7169.

[358] P. Pracht, S. Grimme, C. Bannwarth, F. Bohle, S. Ehlert, G. Feldmann, J. Gorges, M. Müller, T. Neudecker, C. Plett, et al.,
CREST – A program for the exploration of low-energy molecular chemical space,
J. Chem. Phys. **160** (2024) 114110.

[359] N. Ikeda, S. Oda, R. Matsumoto, M. Yoshioka, D. Fukushima, K. Yoshiura, N. Yasuda, and T. Hatakeyama, *Solution-processable pure green thermally activated delayed fluorescence emitter based on the multiple resonance effect*, Adv. Mater. **32** (2020) 2004072.

[360] S. H. Han, J. H. Jeong, J. W. Yoo, and J. Y. Lee, *Ideal blue thermally activated delayed fluorescence emission assisted by a thermally activated delayed fluorescence assistant dopant through a fast reverse intersystem crossing mediated cascade energy transfer process*,
J. Mater. Chem. C **7** (2019) 3082.

[361] P. Jiang, L. Zhan, X. Cao, X. Lv, S. Gong, Z. Chen, C. Zhou, Z. Huang, F. Ni, Y. Zou, et al., *Simple acridan-based multi-resonance structures enable highly efficient narrowband green TADF electroluminescence*, Adv. Opt. Mater. **9** (2021) 2100825.

[362] S. Nakatsuka, H. Gotoh, K. Kinoshita, N. Yasuda, and T. Hatakeyama,
Divergent synthesis of heteroatom-centered 4, 8, 12-triazatriangulenes,
Angew. Chem. **129** (2017) 5169.

[363] K. Matsui, S. Oda, K. Yoshiura, K. Nakajima, N. Yasuda, and T. Hatakeyama,
One-shot multiple borylation toward BN-doped nanographenes,
J. Am. Chem. Soc. **140** (2018) 1195.

[364] Y. Kondo, K. Yoshiura, S. Kitera, H. Nishi, S. Oda, H. Gotoh, Y. Sasada, M. Yanai, and T. Hatakeyama,
Narrowband deep-blue organic light-emitting diode featuring an organoboron-based emitter,
Nat. Photonics **13** (2019) 678.

[365] S. M. Suresh, E. Duda, D. Hall, Z. Yao, S. Bagnich, A. M. Slawin, H. Bässler, D. Beljonne, M. Buck, Y. Olivier, et al.,
A deep blue B, N-doped heptacene emitter that shows both thermally activated delayed fluorescence and delayed fluorescence by triplet–triplet annihilation,
J. Am. Chem. Soc. **142** (2020) 6588.

[366] Y. Xu, Z. Cheng, Z. Li, B. Liang, J. Wang, J. Wei, Z. Zhang, and Y. Wang,
Molecular-structure and device-configuration optimizations toward highly efficient green electroluminescence with narrowband emission and high color purity,
Adv. Opt. Mater. **8** (2020) 1902142.

[367] Y. Zhang, D. Zhang, J. Wei, Z. Liu, Y. Lu, and L. Duan, *Multi-resonance induced thermally activated delayed fluorophores for narrowband green OLEDs*,
Angew. Chem. Int. Ed. **58** (2019) 16912.

[368] Y. Xu, C. Li, Z. Li, Q. Wang, X. Cai, J. Wei, and Y. Wang, *Constructing charge-transfer excited states based on frontier molecular orbital engineering: Narrowband green electroluminescence with high color purity and efficiency*, Angew. Chem. Int. Ed. **59** (2020) 17442.

[369] Y. Zhang, D. Zhang, J. Wei, X. Hong, Y. Lu, D. Hu, G. Li, Z. Liu, Y. Chen, and L. Duan, *Achieving pure green electroluminescence with CIEy of 0.69 and EQE of 28.2% from an aza-fused multi-resonance emitter*, Angew. Chem. **132** (2020) 17652.

[370] M. Yang, I. S. Park, and T. Yasuda, *Full-color, narrowband, and high-efficiency electroluminescence from boron and carbazole embedded polycyclic heteroaromatics*, J. Am. Chem. Soc. **142** (2020) 19468.

[371] Y. Zhang, D. Zhang, T. Huang, A. J. Gillett, Y. Liu, D. Hu, L. Cui, Z. Bin, G. Li, J. Wei, et al., *Multi-resonance deep-red emitters with shallow potential-energy surfaces to surpass energy-gap law*, Angew. Chem. Int. Ed. **60** (2021) 20498.

[372] S. Oda, B. Kawakami, R. Kawasumi, R. Okita, and T. Hatakeyama, *Multiple resonance effect-induced sky-blue thermally activated delayed fluorescence with a narrow emission band*, Org. Lett. **21** (2019) 9311.

[373] J. A. Knöller, G. Meng, X. Wang, D. Hall, A. Pershin, D. Beljonne, Y. Olivier, S. Laschat, E. Zysman-Colman, and S. Wang, *Intramolecular borylation via sequential B- Mes bond cleavage for the divergent synthesis of B, N, B-doped benzo [4] helicenes*, Angew. Chem. Int. Ed. **59** (2020) 3156.

[374] Y. Yuan, X. Tang, X.-Y. Du, Y. Hu, Y.-J. Yu, Z.-Q. Jiang, L.-S. Liao, and S.-T. Lee, *The design of fused amine/carbonyl system for efficient thermally activated delayed fluorescence: Novel multiple resonance core and electron acceptor*, Adv. Opt. Mater. **7** (2019) 1801536.

[375] X. Li, Y.-Z. Shi, K. Wang, M. Zhang, C.-J. Zheng, D.-M. Sun, G.-L. Dai, X.-C. Fan, D.-Q. Wang, W. Liu, et al., *Thermally activated delayed fluorescence carbonyl derivatives for organic light-emitting diodes with extremely narrow full width at half-maximum*, ACS Appl. Mater. Interfaces **11** (2019) 13472.

[376] D. Hall, S. M. Suresh, P. L. dos Santos, E. Duda, S. Bagnich, A. Pershin, P. Rajamalli, D. B. Cordes, A. M. Slawin, D. Beljonne, et al., *Improving processability and efficiency of resonant TADF emitters: A design strategy*, Adv. Opt. Mater. **8** (2020) 1901627.

[377] D. Sun, S. M. Suresh, D. Hall, M. Zhang, C. Si, D. B. Cordes, A. M. Slawin, Y. Olivier, X. Zhang, and E. Zysman-Colman, *The design of an extended multiple resonance TADF emitter based on a polycyclic amine/carbonyl system*, Mater. Chem. Front. **4** (2020) 2018.

[378] S.-N. Zou, C.-C. Peng, S.-Y. Yang, Y.-K. Qu, Y.-J. Yu, X. Chen, Z.-Q. Jiang, and L.-S. Liao, *Fully bridged triphenylamine derivatives as color-tunable thermally activated delayed fluorescence emitters*, Org. Lett. **23** (2021) 958.

[379] H. Min, I. S. Park, and T. Yasuda, *cis-Quinacridone-based delayed fluorescence emitters: Seemingly old but renewed functional luminogens*, Angew. Chem. **133** (2021) 7721.

[380] S. Spicher and S. Grimme,
Robust atomistic modeling of materials, organometallic, and biochemical systems,
Angew. Chem. Int. Ed. **59** (2020) 15665.

[381] Y. Zhao and D. G. Truhlar,
The M06 suite of density functionals for main group thermochemistry, thermochemical kinetics, noncovalent interactions, excited states, and transition elements: Two new functionals and systematic testing of four M06-class functionals and 12 other functionals,
Theor. Chem. Acc. **120** (2008) 215.

[382] P. J. Stephens, F. J. Devlin, C. F. Chabalowski, and M. J. Frisch, *Ab initio calculation of vibrational absorption and circular dichroism spectra using density functional force fields*,
J. Phys. Chem. **98** (1994) 11623.

[383] A. Najibi and L. Goerigk, *DFT-D4 counterparts of leading meta-generalized-gradient approximation and hybrid density functionals for energetics and geometries*,
J. Comput. Chem. **41** (2020) 2562.

[384] F. Neese, F. Wennmohs, A. Hansen, and U. Becker,
Efficient, approximate and parallel Hartree–Fock and hybrid DFT calculations. A 'chain-of-spheres' algorithm for the Hartree–Fock exchange, Chem. Phys. **356** (2009) 98.

[385] B. Helmich-Paris, B. de Souza, F. Neese, and R. Izsák,
An improved chain of spheres for exchange algorithm, J. Chem. Phys. **155** (2021) 104109.

List of Figures

List of Tables

APPENDIX E

Acknowledgements

Throughout my Ph.D. studies many people have supported and inspired me, and I would like to take the opportunity to thank them and express my gratitude for making this thesis possible. First, I want to thank my supervisor, Stefan Grimme, for hosting me over seven years in his working group with financial and professional support, from my bachelor all the way to my Ph.D. He gave me the opportunity to learn and work in the field of quantum chemistry, opening doors for me to join the TIDE doctoral training program and visiting various conferences. A huge thanks goes to Jan-Michael Mewes for being my mentor since my Master's thesis. I learned an incredible amount from Jan, both professionally and on a personal level, and his support throughout every of my projects has been invaluable to me. I want to give special thanks to Andreas Hansen, who has co-supervised me alongside Jan and Stefan, supported me in every way possible and helped me overcome personal challenges. His encouragement and advice made this Ph.D. thesis possible. Likewise I want to thank Arne Lützen who supported and helped me in my personal and professional challenges, as well as for being third reviewer of my thesis. Big thanks goes also to Thomas Bredow and Gregor Hagelüken for being the second and fourth reviewer of this thesis. Thanks goes also to Markus Bursch who taught me a lot during my bachelor thesis project and beyond.

I want to thank all members of the TIDE doctoral program, supervisors and doctoral students, but especially its organizers Klaus Meerholz and Arne Lützen. Special thanks also to coordinators Ann-Christin Schmädicke, Steffi Meißner, Hanna Krikcziokat, for taking a huge part of the organisational burden from our (the doctoral students) shoulders. Further thanks goes to my supervision committee Stefan Grimme, Andreas Hansen and Arne Lützen. And of course thanks to all TIDE members for a great time at events, retreats and meetings, especially thanks to, Wing-Si Li, Marvin Schumacher, Simon Rickert, Anja Sutorius, Rita Tomar, Julia Kohn, and Nora Gildenmeister. For the welcoming and warm atmosphere I thank all the current and former colleagues from the Grimme group, especially Markus Bursch, Hagen Neugebauer, Benedikt Bädorf, Christian Hölzer, Julia Kohn, Jeroen Koopman, Jan-Michael Mewes, Sarah Löffelsender, Marvin Friede, Christoph Plett, and Marc de Wergifosse, Big thanks also to Thomas Froitzheim for helpful and interesting discussions and collaborations.

From the scientific community and the collaborators outside the Grimme group, I want to thank Tao

Jin, and Matthias Wagner (Goethe-Universität Frankfurt), as well as Dirk Laux, Sebastian Hütgens, and Arne Lützen (Rheinische-Friedrich-Wilhelms-Universität Bonn) for fruitful, interesting, and enlightening collaborations. I additionally want to thank Jan-Michael Mewes and Andreas Hansen for proofreading parts of this thesis. For all the administrative help and technical support, I want to thank Claudia Kronz and Jens Mekelburger. I want to thank my family and all my friends for their continuous loving support over the many years at the university, for always being there, helping and encouraging me to move forward.